Laboratory Medicine

March 2024 Vol 55 No 2 Pgs 109-250

labmedicine.com

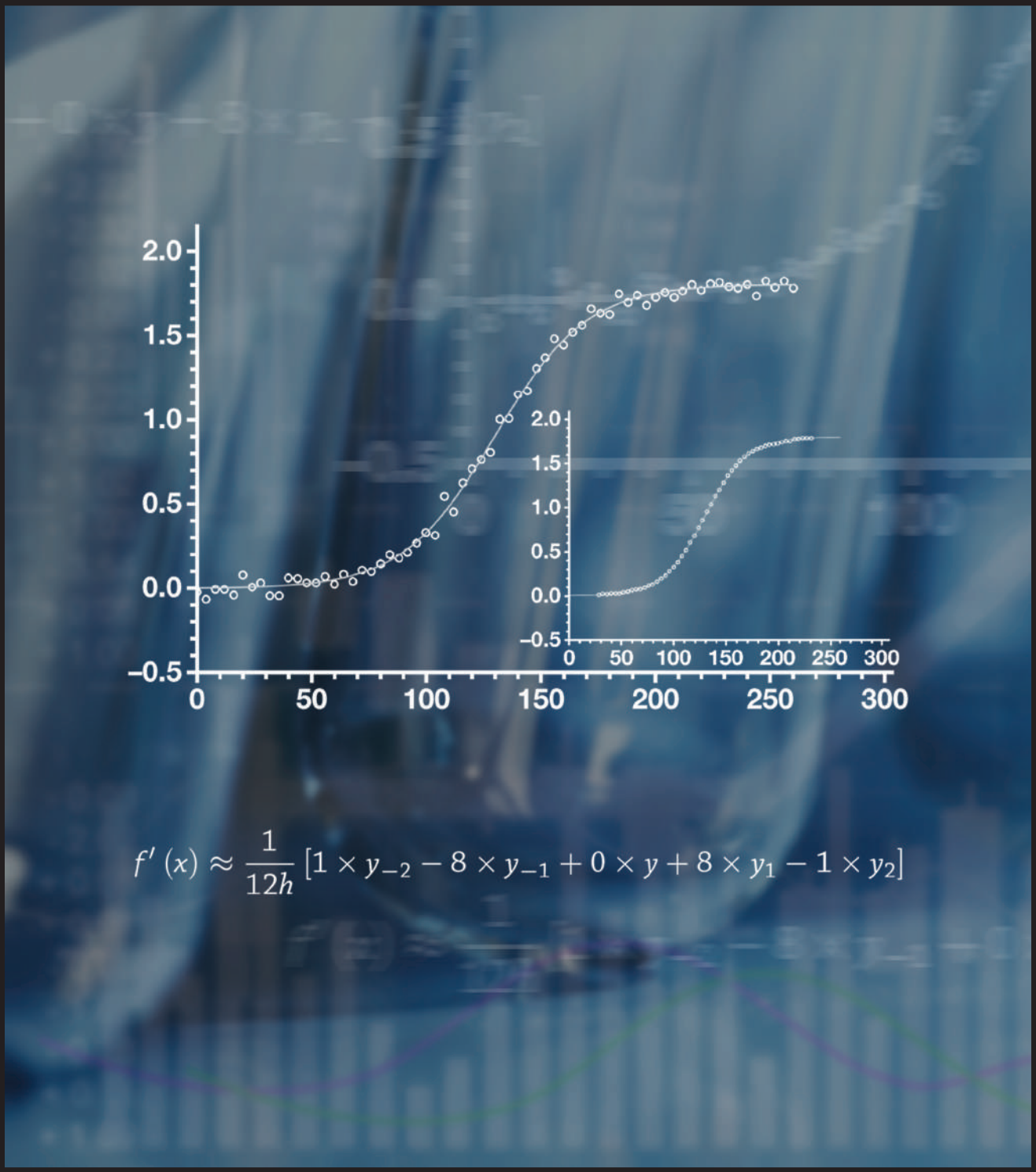

Laboratory Medicine (ISSN 0007-5027), is published 6 times per year (bimonthly). Periodicals Postage paid at Chicago, IL and additional mailing offices. POSTMASTER: Send address changes to *Laboratory Medicine*, Journals Customer Service Department, Oxford University Press, 2001 Evans Road, Cary, NC 27513-2009.

SUBSCRIPTION INFORMATION: Annually for North America, $182 (electronic) or $241 (electronic and print); single issues for individuals are $32 and for institutions $71. Annually for Rest of World, £118/€167 (electronic) or £154/€220 (electronic and print); single issues for individuals are £21/€30 and for institutions £44/€63. All inquiries about subscriptions should be sent to Journals Customer Service Department, Oxford Journals, Great Clarendon Street, Oxford OX2 6DP, UK, Tel: +44 (0) 1865-35-3907, e-mail: jnls.cust.serv@oup.com. In the Americas, please contact Journals Customer Service Department, Oxford Journals, 4000 CentreGreen Way, Suite 310, Cary, NC 27513, USA. Tel: 800-852-7323 (toll-free in USA/Canada) or 919-677-0977, e-mail: jnlorders@oup.com.

MEMBERSHIP INFORMATION: The ASCP membership fees for pathologists are as follows: fellow membership is $399; fellow membership plus 1-year unlimited online CE is $529; 2-year fellow membership is $749; and 2-year fellow membership plus 2-year unlimited online CE is $1009. The ASCP membership fees for laboratory professionals are as follows: young professional membership is $59; annual membership is $119; annual membership plus 1-year unlimited online CE is $158; 3-year membership is $389. All inquiries about membership should be sent to American Society for Clinical Pathology, 33 West Monroe Street, Suite 1600, Chicago, IL 60603, Tel: 312-541-4999, e-mail: ascp@ascp.org.

CLAIMS: Publisher must be notified of claims within four months of dispatch/ order date (whichever is later). Subscriptions in the EEC may be subject to European VAT. Claims should be made to Laboratory Medicine, Journals Customer Service Department, Oxford University Press, 4000 CentreGreen Way, Suite 310, Cary, NC 27513, USA, Tel: 800-852-7323 (toll-free in USA/Canada) or 919-677-0977, e-mail: jnlorders@oup.com.

Laboratory Medicine is published bimonthly by Oxford University Press (OUP), on behalf of the ASCP, a not-for-profit corporation organized exclusively for educational, scientific, and charitable purposes. Devoted to the continuing education of laboratory professionals, *Laboratory Medicine* features articles on the scientific, technical, managerial, and educational aspects ofthe clinical laboratory. Publication of an article, column, or other item does not constitute an endorsement by the ASCP of the thoughts expressed or the techniques, organizations, or products described therein. *Laboratory Medicine* is indexed in the following: MEDLINE/PubMed, Science Citation Index, Current Contents—Clinical Medicine, and the Cumulative Index to Nursing and Allied Health Literature.

Printed in the USA

ASCP
Laboratory Medicine
33 West Monroe Street, Suite 1600
Chicago, IL 60603

T: 312-541-4999
F: 312-541-4750

Laboratory Medicine

March 2024
Vol 55, No 2
Pgs 109-250

ON THE COVER: Analytical chemistry methods generally involve measurement of a signal (gravimetric, spectrophotometric, potentiometric, chemiluminescent, etc) that varies in proportion to the concentration of analyte (Europeans prefer the term, "measurand"). The relationship between the signal and analyte concentration is often linear within certain limits of concentrations that define the "linear range" of the method. Deviations from linear behavior may occur at very low and very high concentrations. However, in some analytical methods—most notably immunoassays, where ligand concentration is measured by its relationship to the relative amounts in the bound and free fractions—the association between signal and analyte concentration is nonlinear and requires mathematical tools appropriate for fitting nonlinear calibration data. In this issue of *Laboratory Medicine*, Peter McPherson of Ulster University in the UK reviews the medical laboratory applications of nonlinear mathematical curve fitting to enzyme-linked immunosorbent assays.

EDITORIAL

The FDA's proposed rule on laboratory-developed tests: what happens next?

Jonathan R. Genzen, MD, PhD,[1,2] *Karen A. Moser, MD*[1,2]

[1]Department of Pathology, University of Utah Health, Salt Lake City, UT, US; [2]ARUP Laboratories, Salt Lake City, UT, US. Corresponding author: Jonathan R. Genzen; jonathan.genzen@aruplab.com

Key words: laboratory-developed tests; Food and Drug Administration; federal regulations; Clinical Laboratory Improvement Amendments

Laboratory Medicine 2024;55:109-110; https://doi.org/10.1093/labmed/lmae001

On December 4, 2023 , the public comment period for the US Food and Drug Administration's (FDA) proposed rule to regulate laboratory-developed tests (LDTs) as medical devices closed, with approximately 6700 comments submitted.[1,2] The Biden Administration subsequently indicated an April 2024 potential timeline for a final rule in its unified agenda,[3,4] and while the FDA is not bound by this schedule, it is consistent with recent actions to proceed expeditiously. Concordantly, the FDA denied numerous requests for an extension of the public comment period,[5] and it has not signaled any plans to host public hearings or workshops on the proposed rule.

As described in an Office of the Federal Register guide to rulemaking, a federal agency should "base its reasoning and conclusions on the rulemaking record, consisting of the comments, scientific data, expert opinions, and facts accumulated during the pre-rule and proposed rule stages."[6] Several organizations (including our own) submitted comments emphasizing that there are material errors in both the economic and clinical assumptions used within the FDA's regulatory impact analysis on which many of the conclusions and cost benefit analyses are based.[7-9] Will the regulatory impact analysis be reconsidered and corrected? Will the FDA incorporate common sense practices—such as grandfathering of existing tests and allowing for common test modifications under CLIA—or will it stick with a manufacturer-oriented regulatory approach that is ill-suited to clinical environments?

It is also likely that any final rule will be challenged in court. Given that LDTs are not mentioned in the Medical Device Amendments of 1976,[10] it is possible that the FDA's final rule may not withstand judicial scrutiny, particularly in the context of a Supreme Court that is increasingly resistant to broad claims of administrative authority.[11] Legal challenges could take years to resolve, during which laboratories may face difficult decisions to potentially discontinue patient care activities if anticipated compliance costs exceed available financial resources. Most importantly, if the rule is finalized and survives judicial review, what would be the future impact to patient care?

Laboratory-developed tests have often filled gaps in commercially available FDA-cleared assays, particularly in the setting of rare diseases. Examples include the serotonin release assay for diagnosis of heparin-induced thrombocytopenia and ADAMTS13 activity for diagnosis of thrombotic thrombocytopenic purpura. These tests are considered standard of care and are required for rapid diagnosis to prevent potentially fatal thrombotic complications,[12,13] yet FDA-cleared alternatives are not available. If the financial and administrative burdens stemming from additional regulations are too high, the proposed rule may limit patient access to essential diagnostic testing—a concerning prospect in any clinical scenario, especially for conditions that may be clinically urgent.

The proposed rule would create numerous other problems for clinical laboratories and patients. For example, if the number of laboratories offering a given assay decreases, patients may not be able to obtain testing from a local or regional laboratory, thus leading to delays in testing and decreased laboratory integration into local health systems. Decreased integration may limit laboratory contributions to local quality improvement and patient safety initiatives, which are an important principle of laboratory practice. Market consolidation is also likely to result from the proposed rule,[14] and industry consolidation typically leads to increased prices as well as amplification of supply chain risk. Finally, loss of LDTs could contribute to erosion in longitudinal expertise and training in clinical laboratories. In a profession already challenged by staffing shortages,[15] it would be more difficult to ensure that the technical knowledge required to develop and maintain complex assays is passed on to the next generation of laboratory professionals in local and academic laboratories.

In conclusion, we anticipate numerous challenges to clinical laboratories resulting from the FDA's proposed rule for regulation of LDTs. We are encouraged by the skill, dedication, and compassion for patients exhibited daily by our clinical laboratory colleagues, and we hope that the FDA pauses its efforts and more thoroughly evaluates the likely negative impacts of the proposed rule on patient care in the United States.

REFERENCES

1. Medical Devices; Laboratory Developed Tests. A proposed rule by the Food and Drug Administration. October 3, 2023. *Docket No. FDA-2023-N-2177*. Accessed December 20, 2023. https://www.federalregister.gov/documents/2023/10/03/2023-21662/medical-devices-laboratory-developed-tests
2. Medical Devices; Laboratory Developed Tests. Rulemaking Docket. *Docket ID FDA-2023-N-2177*. Accessed December 20, 2023. https://www.regulations.gov/docket/FDA-2023-N-2177
3. Medical Devices; Laboratory Developed Tests. US General Services Administration and the Office of Management of Budget. RIN: 0910-AI85. Accessed December 20, 2023. https://www.reginfo.gov/public/do/eAgendaViewRule?pubId=202310&RIN=0910-AI85
4. FDA targets April 2024 for laboratory developed test (LDT) final rule. *JDSupra*. December 11, 2023. Accessed December 20, 2023. https://www.jdsupra.com/legalnews/fda-targets-april-2024-for-laboratory-9745228/
5. FDA won't extend LDT rule comment period. *Regulatory Focus*. October 31, 2023. Accessed December 20, 2023. https://www.raps.org/news-and-articles/news-articles/2023/10/fda-won%E2%80%99t-extend-ldt-rule-comment-period
6. A guide to the rulemaking process. *Office of the Federal Register*. Accessed December 20, 2023. https://www.federalregister.gov/uploads/2011/01/the_rulemaking_process.pdf
7. Laboratory Developed Tests Regulatory Impact Analysis (Proposed Rule). Accessed December 20, 2023. https://www.fda.gov/about-fda/economic-impact-analyses-fda-regulations/laboratory-developed-tests-regulatory-impact-analysis-proposed-rule
8. ARUP Laboratories public comment on the FDA's proposed rule on laboratory-developed tests. November 28, 2023. Accessed December 20, 2023. https://www.aruplab.com/files/resources/ARUP%20Public%20Comment%20Letter%20on%20LDTs.pdf
9. American Clinical Laboratory Association's comments on FDA's proposed regulation of laboratory developed tests and medical devices. December 4, 2023. Accessed December 20, 2023. https://www.acla.com/aclas-comments-on-fdas-proposed-regulation-of-laboratory-developed-tests-as-medical-devices/
10. "Medical Device Amendments of 1976." (PL 94 - 295, May 28, 1976) United States Statutes at Large, 90 (1976):539-583. Accessed December 20, 2023. https://www.gpo.gov/fdsys/pkg/STATUTE-90/pdf/STATUTE-90-Pg539.pdf
11. Supreme Court of the United States. West Virginia v Environmental Protection Agency. Accessed December 20, 2023. https://www.supremecourt.gov/opinions/21pdf/20-1530_new_l537.pdf
12. Cuker A, Arepally G, Chong BH, et al. American Society of Hematology 2018 guidelines for management of venous thromboembolism: heparin-induced thrombocytopenia. *Blood Adv*. 2018;2(22):3360-3392.
13. Zheng XL, Vesely SK, Cataland SR, et al. ISTH guidelines for the diagnosis of thrombotic thrombocytopenic purpura. *J Thromb Haemost.* 2020;18(10):2486-2495.
14. Bonislawski A. FDA oversight of LDTs likely to drive further consolidation within lab industry. *360Dx*. December 19, 2023. Accessed January 3, 2024. https://www.360dx.com/clinical-lab-management/fda-oversight-ldts-likely-drive-further-consolidation-within-lab-industry
15. Garcia E, Kundu I, Kelly M, Soles R. The American Society for Clinical Pathology 2022 vacancy survey of medical laboratories in the United States. *Am J Clin Pathol*. 2023. Accessed January 3, 2024. https://doi.org/10.1093/ajcp/aqad149

About the Authors

Jonathan Genzen, MD, PhD, is a professor at the University of Utah Department of Pathology. He serves as chief medical officer and senior director of government affairs at ARUP Laboratories, a not-for-profit enterprise of the University of Utah. He is a medical director in ARUP's chemistry division and is medical director of ARUP's laboratory automation team. His clinical and research focus is on automated clinical chemistry, process improvement initiatives, and clinical laboratory regulations.

Karen Moser, MD, is an associate professor at the University of Utah Department of Pathology. She serves as medical director of the hemostasis/thrombosis laboratory at ARUP Laboratories. Her primary research interests are in laboratory hemostasis and thrombosis testing and pathology education, with a focus on undergraduate medical education.

OVERVIEW

Approaches to nonlinear curve fitting in laboratory medicine

Peter A. C. McPherson, PhD

Ulster University, School of Pharmacy & Pharmaceutical Science, Coleraine, UK.
Corresponding author: Peter A. C. McPherson; p.mcpherson@ulster.ac.uk

Key words: clinical chemistry; informatics; chemistry; immunology; toxicology; basic science.

Abbreviations: ELISA, enzyme-linked immunosorbent assay; SSE, sum of squares error; AICc, Akaike's information criteria; LM, Levenberg and Marquardt; GRG2, generalized reduced gradient

Laboratory Medicine 2024;55:111-116; https://doi.org/10.1093/labmed/lmad069

ABSTRACT

Nonlinear curve fitting is an important process in laboratory medicine, particularly with the increased use of highly sensitive antibody-based assays. Although the process is often automated in commercially available software, it is important that clinical scientists and physicians recognize the limitations of the various approaches used and are able to select the most appropriate model. This article summarizes the key nonlinear functions and demonstrates their application to common laboratory data. Following this, a basic overview of the statistical comparison of models is presented and then a discussion of important algorithms used in nonlinear curve fitting. An accompanying Microsoft Excel workbook is available that can be used to explore the content of this article.

Introduction

A fundamental step in any analytical process is selecting an appropriate function to describe the observed data. In its simplest form, the relationship between an independent (x) and dependent (y) variable can be described as $y = f(x)$ where the function, f, can, in principle, have any form such as a logarithmic, exponential, trigonometric, or higher-order function. In the context of laboratory medicine, diagnostic assays are often designed to produce a linear response to changes in the independent variable; in this case, we see that the function is based on the well-known linear regression relationship, $y = mx + c$. However, some assays, particularly those using antibodies or enzymes, can display a nonlinear response to changes in the independent variable, and so a more complex model is required.

The first step in interrogating a plot of 2-dimensional data involves constructing a line that intersects most points. In all but the most trivial of cases, this will involve least squares analysis. In this method, values that satisfy the coefficients (parameters) of a best fit curve are selected so that when x-axis values are substituted into the best fit equation, the square of the differences between the calculated and observed y-values is minimized. The a priori assumption in this method is that all errors are incurred in the y-axis values. These errors are most likely to be indeterminate in nature—for example, Johnson–Nyquist noise.[1] In practice, determinate errors are also likely in x-axis values, particularly in the preparation of standards for a calibration curve.

The selection of an appropriate equation to fit experimental data is often a "black box" exercise, with software analyzing data and offering potential options. However, these options can vary widely in their form and function, and it is therefore important to understand the advantages and limitations of nonlinear least squares analysis. This is complicated to some extent by the range of commercial software that is available, each with their own idiosyncrasies that can be challenging for those new to the field. For example, Galitzine and co-workers used an open-source R package, MSstats, to perform nonlinear fits to mass spectrometry data.[2] Even without importing MSstats (or similar), the R program is well suited to nonlinear regression,[3] although there can be a steep learning curve until one becomes familiar with the input language used in R. In this article, I discuss the main nonlinear equations, their statistical comparison, and the underlying algorithms that are used in the analysis. Unlike many established approaches, I highlight the usefulness of Microsoft Excel in analyzing such data and have provided an Excel workbook in the Supplementary Materials. This will allow readers to explore the impact of the curve fitting parameters on the nonlinear fit using a platform, which is in all likelihood more familiar to them.

Hyperbolic Functions

From elementary biochemistry, most will be familiar with nonlinear functions as applied to enzyme kinetics (the Michaelis–Menten curve) or ligand-receptor binding (the Hill–Langmuir plot). These functions usually follow the form of a rectangular hyperbola and can be described by the general equation

$$y = \frac{ax}{z + x} \quad (1)$$

where a corresponds to the upper asymptote and z is the value of x that is equal to $0.5a$. Originally, the nonlinear nature of these functions was addressed by transformation into linear forms and then treated under the framework of linear regression. However, the use of linear transformations such as Lineweaver–Burk and Scatchard plots is now largely obsolete due to the availability of curve fitting software.[4] This can be viewed as a significant advantage, as in some instances Hill–Langmuir plots do not follow a rectangular hyperbola but instead adopt an S-shaped appearance. Such relationships are not readily linearizable and instead are more appropriately modeled using a family of equations based on the logistic function. The importance of nonlinear curves for enzyme-based assays was recently highlighted by Pant.[5] In that case report, the result for a creatine kinase measurement was initially underreported due to a failure to inspect the progress curve (absorbance vs time) for the analysis. Had this been done, it would have been clear that the substrate was depleted much more rapidly than the linearity of the assay permits. Had the progress curve been presented in its raw form (ie, a hyperbolic plot), the issue would not have been resolved, as the substrate depletion would have been hidden within the clustered data points close to the origin. For this reason, all clinical chemistry analyzers that operate in kinetic mode will seek to transform data to avoid clustering of data points. Similar issues can present with creatine kinase measurement in icteric samples, where substrate is rapidly consumed due to supraphysiological levels of the enzyme.[6]

The Logistic Function

The logistic function forms the foundation of many nonlinear equations and can be regarded as an admixture of an exponential and a power function. It was first proposed by Adolphe Quetelet and his student, Pierre-François Verhulst, in 1838 as a means of modelling population growth.[7,8] The most common presentation of the logistic function is

$$f(x) = \frac{a}{1 + \exp[-b(x-c)]} \tag{2}$$

where a is an upper limit that no value exceeds (the supremum), b is the gradient of the curve, and c is the x-value at the point of inflection. In the special case of eqn (2), where $a = 1$, $b = 1$, and $c = 0$, we obtain the general logistic function (**FIGURE 1**, solid line):

$$f(x) = \frac{1}{1 + \exp(x)} \tag{3}$$

and from this we see that as x changes, the function increases monotonically between its lower and upper bounds. Such functions are characterized by an initial lag, followed by an exponential increase, and finally, a plateau and are often styled as being S-shaped or sigmoidal in their appearance. The first derivative of eqn (3) is readily obtained,

$$f'(x) = \frac{\exp(x)}{[1 + \exp(-x)]^2} = f(x)[(1 - f(x)] \tag{4}$$

which produces a density function that is symmetrical, with a maximum corresponding to the point of inflection on the associated distribution curve (**FIGURE 1**, dashed line). Identifying the point of inflection is an important step in nonlinear curve fitting, as the corresponding value on the x-axis can be used as an initial guess for the c parameter. Approaches to obtaining an approximate first derivative are discussed at the end of this article. Such nonlinear functions are

FIGURE 1. Plot of the logistic function (solid line) and its first derivative (dashed line). Note how the maximum of the first derivative corresponds to the inflection point of the sigmoid curve.

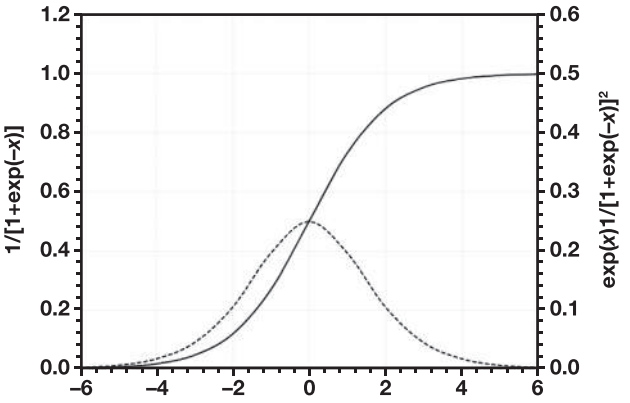

ubiquitous in nature and can be used to model (inter alia) the baroreceptor reflex,[9] lipoprotein oxidation,[10] microbial growth,[11] and the spread of infection.[12]

The Verhulst equation can be expanded by including additional parameters, creating a family of nested functions.[13] In eqn (5), a fourth parameter, d, has been added that specifies the lower asymptote:

$$y = a + \frac{d - a}{1 + \exp[-b(x-c)]} \tag{5}$$

A limitation of eqns (4) and (5) is that there is an inherent assumption that the functions are symmetrical about the point of inflection. In these cases, the midpoint value and point of inflection are indistinguishable (ie, $c = x_i$), which can be of benefit when providing initial guesses for curve fitting algorithms. However, with improvements in assay design, we often see that the trade-off for increased sensitivity and reduced signal-to-noise ratio is a more asymmetric calibration curve.[14] For this reason, the fit of visibly asymmetric curves can be improved by introducing a fifth parameter, g, which governs on which side of the inflection point the slope will be greatest. For a symmetrical function, $g = 1$:

$$y = a + \frac{d - a}{\{1 + \exp[-b(x-c)]\}^g} \tag{6}$$

Common Calibration Curve Functions

Given that there cannot be a known standard at every possible concentration of analyte, one of the most common applications of nonlinear functions can be found in establishing calibration curves. As an example, consider the measurement of an analyte by ELISA in which standards are prepared in the range 1 – 1000 pg/mL. An initial plot of signal vs antigen concentration is shown in **FIGURE 2**. At first glance, the inexperienced could be forgiven for assuming that a hyperbolic relationship exists between signal and concentration and that eqn (1) could be applied. Indeed, the correlation between the measured and calculated curve is good ($R^2 = 0.9631$), but when we plot the 95% CIs, we see that there is a significant deviation from the measured data. We also note

FIGURE 2. **Plot of sandwich ELISA data fitted by eqn (1) with 95% CI (gray shading). Curve fitting parameters: a = 4.350; z = 88.06. Insert: Semilogarithmic plot highlighting sigmoid shape of the curve.**

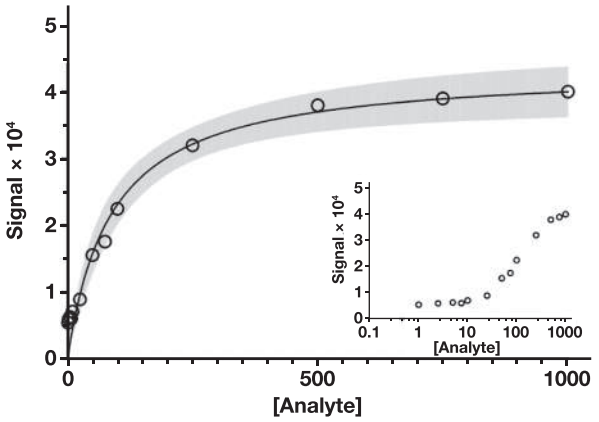

FIGURE 3. **Plot of sandwich ELISA data fitted by eqn (7) with 95% CI (gray shading). Curve fitting parameters: a = 4.00; b = 1.841; c = 5.065.**

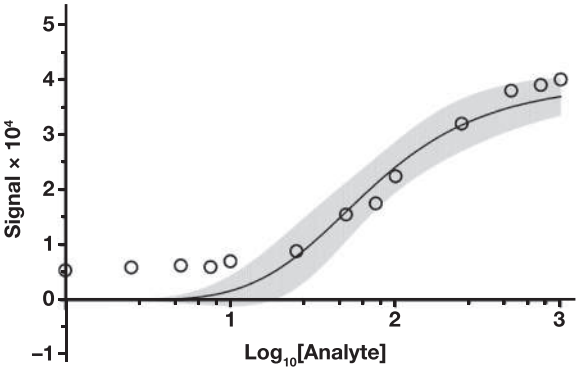

that at the lower end of the curve, the data points are tightly clustered. When we view the same data on a semilogarithmic plot (**FIGURE 2** insert), we see that the calibration curve takes on a sigmoid appearance, which suggests that logistic functions would be better suited to fit this data. Note that logarithmic transformation of x-values does not affect the curve fitting process, as this is based on vertical y-distances of the curve from the measured data points. Viewed another way, this example highlights a key assumption about nonlinear curve fitting: the data must be truly nonlinear. There are situations that can arise in which outliers can make linear data appear nonlinear.

Although eqns (2), (5), and (6) could be used for this calibration curve, it is customary to take the natural log of the denominator to produce a new family of nested functions, eqns (7) through (9), the simplest of which is the 3-parameter logistic function:

$$y = \frac{a}{1 + \left(\frac{x}{c}\right)^{-b}} \tag{7}$$

When we apply eqn (7) to the ELISA calibration curve, we obtain the line of best fit shown in **FIGURE 3**. We see in this case that the 3-parameter logistic function does not adequately model the lower and upper ends of the curve and has wide 95% CIs, despite having an acceptable R^2 (see **TABLE 1**). The performance of eqn (7) can be improved by the inclusion of the d-parameter,[15] producing the 4-parameter logistic equation

$$y = a + \frac{d - a}{1 + \left(\frac{x}{c}\right)^{b}} \tag{8}$$

When this is applied to our data, we obtain **FIGURE 4**, from which we see a significantly improved fit with much narrower 95% CI. Although the calibration curve does not appear particularly asymmetric, it can be worthwhile using eqn (9), often known as the Richard's equation,[16] to verify whether an additional parameter is required:

$$y = a + \frac{d - a}{\left[1 + \left(\frac{x}{c}\right)^{b}\right]^{g}} \tag{9}$$

The fit of this equation to the ELISA data is shown in **FIGURE 5**. On visual inspection, there appears to be no real difference between the 4- and 5-parameter functions (apart from a very slight improvement in 95% CI), and so in this case we would rely on interpretation of statistical tests to compare the 2 functions (see later). However, as has been noted elsewhere, if a curve is truly asymmetrical about its inflection point, the 4-parameter equation can in some instances provide a better fit.[17] This is because the benefits of using a 5-parameter equation are dependent on having a large amount of high-quality data; otherwise, the CIs can be wide and any increased precision is lost.

Statistical Considerations

The likelihood that the curve fitting parameters will produce a curve that is identical to the true curve can be evaluated by computing the weighted sum of squares error (SSE):

$$\text{SSE} = \sum_{i=1}^{N} \frac{1}{\sigma^2}(y_i - \hat{y}_i)^2 \tag{10}$$

where σ is the standard deviation of the observed data, y_i is an observed value, and $\hat{y}_i$ is the corresponding value predicted by the model. The difference, $y_i - \hat{y}_i$, is often referred to as the residual, a plot of which (vs fitted values) should give a random spread of points following a horizontal plane. By including a weighting, the curve fitting parameters are adjusted to make the predicted curve closest to the y_i value with the smallest variance (ie, the most certain points), and looser around those with the largest variance.

In principle, the predicted curves can be compared against the observed data using any suitable statistical test. In most cases, assuming that the data observes a normal distribution (which can be verified via the D'Agostino K^2 test), the SSE can be considered analogous to the χ^2 statistic with degrees of freedom equal to the number of curve points minus the number of parameters. However, the χ^2 test should be used with caution, as it depends on how accurately the standard deviation is known. For small data sets, this is unlikely, and so interpretation of the χ^2 statistic can be misleading; that is, is the P value due to differences in the measured vs calculated data, or is it due to an inaccurate standard deviation?

The Pearson coefficient of correlation (R^2) is extensively used in linear regression functions, but many authors caution against its use for nonlinear functions.[18] A suitable compromise is the adjusted R^2,

$$\text{Adjusted } R^2 = 1 - \frac{\sum_{i=1}^{N}(y_i - \hat{y}_i)^2/(N-k)}{\sum_{i=1}^{N}(\bar{y}_i - y_i)^2/(N-1)} \tag{11}$$

TABLE 1. Summary statistics for curve fitting using eqns (1) and (7) through (9) for the ELISA data

Equation	df	Sy.x	R^2	Adjusted-R^2	AICc
(1)	11	0.2790	0.9631	0.9597	−26.69
(7)	11	0.4258	0.9140	0.9062	−15.71
(8)	9	0.0683	0.9982	0.9976	−56.01
(9)	8	0.0723	0.9982	0.9973	−48.66

AICc, Akaike's information criteria; df, degrees of freedom; R^2, Pearson correlation coefficient; Sy.x, standard deviation of the residuals.

FIGURE 4. Plot of sandwich ELISA data fitted by eqn (8) with 95% CI (gray shading). Curve fitting parameters: *a* = 4.195; *b* = 1.342; *c* = 2.066; *d* = 0.5546.

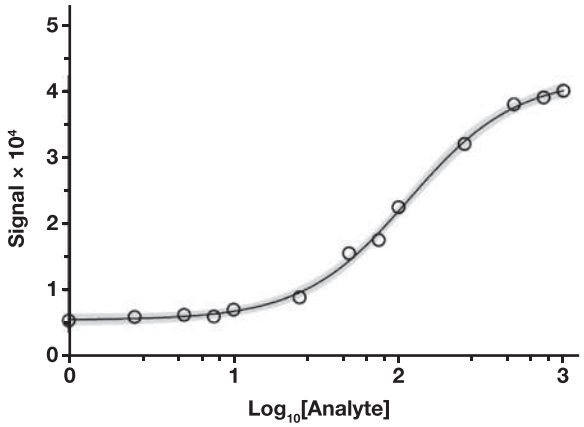

FIGURE 5. Plot of sandwich ELISA data fitted by eqn (9) with 95% CI (gray shading). Curve fitting parameters: *a* = 4.226; *b* = 2.071; *c* = 1.269; *d* = 0.5639; *g* = 1.161.

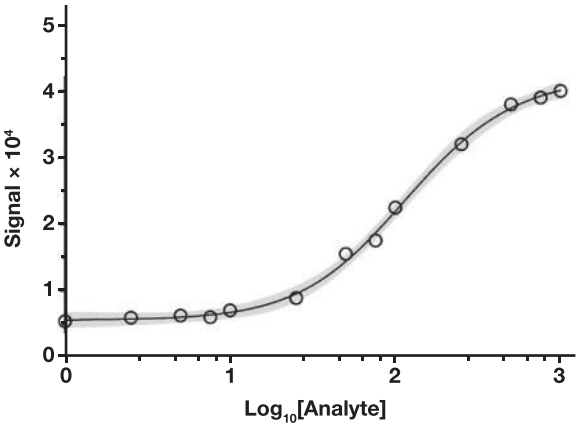

where N is the number of data points and k is the number of parameters. Interpretation of the adjusted R^2 follows the same principle as the standard correlation coefficient: the calculation returns $0 \le R^2 \le 1$ and as the value approaches unity, the stronger the correlation. Often we must rely on the third or fourth digit of a correlation coefficient to discern any difference, which is in itself problematic.

If 2 nonlinear models are nested, the F-test can be used to select which provides a better fit for the data. It is computed as

$$F = \frac{(\mathrm{SSE}_2 - \mathrm{SSE}_1)\,/\,(\mathrm{df}_2 - \mathrm{df}_1)}{\mathrm{SSE}_1/\mathrm{df}_1} \tag{12}$$

where df is the degrees of freedom (as previously described) and the subscripts 1 and 2 relate to the function with the least and greatest number of parameters, respectively. For comparison to the F-distribution, $df_1 - df_2$ and df_2 degrees of freedom are used. If models are not nested, then alternative goodness-of-fit criteria, such as the second-order variant of Akaike's information criteria (AICc) should be used:

$$\mathrm{AICc} = \left[N \ln\left(\frac{\mathrm{SSE}}{N}\right) + 2k\right] + \frac{2k\,(k+1)}{N-k-1} \tag{13}$$

where N is the number of data points and k is the number of parameters. This approach has its foundation in information theory, whereby it seeks to estimate the amount of information lost by the modeling process.[19] It is not associated with probabilities or statistical significance in the same way as other comparisons. However, if 2 functions are being compared that are not nested, then only the information criterion approach can be used. In this case, the lower the value for AICc, the better the fit of the model.

If we apply these statistical approaches to eqns (8) and (9) used for the ELISA calibration data (**TABLE 1**), we see that the R^2 values are equivocal, and that for the adjusted R^2 we need to rely on the fourth decimal place, which is in itself unreliable. Using the F-test to compare these 2 nested models, in which the null hypothesis is that the simpler model is more favorable, we obtain $F = 0.0601$ ($F_{crit} = 0.0042$; $P > .05$, $\alpha = .05$), which confirms that eqn (8) provides the more reliable fit, although the curve is slightly asymmetrical (g-parameter = 1.161). If we were comparing 3 or more nested models, a 1-way analysis of variance would be more efficient.

Curve Fitting Algorithms

The most technically demanding step in curve fitting is adjusting the parameters so that the SSEs are sufficiently minimized. Commercial curve fitting software such as SigmaPlot, GraphPad, and those preloaded onto instruments such as microplate readers, use the Levenberg and Marquardt (LM) method to optimize the parameters.[20] This is based on 2 separate numerical minimization algorithms. The first is the gradient descent method, which iteratively reduces the SSEs by changing the parameters so that the gradient is minimized (ie, it reaches a local minimum). The second algorithm is the Gauss-Newton method, which assumes a quadratic relationship for the SSEs and seeks to minimize this quadratic. As the LM method requires the use of partial derivatives of the function at each data point, this approach cannot be easily replicated in generic software such as Microsoft Excel; however, more sophisticated software, such as *Mathematica*, has preloaded code for implementation of this method. Likewise, editable Python scripts are readily available from online repositories, such as GitHub, for those with some experience of coding.[21]

For general use, a simpler alternative to the LM method is the generalized reduced gradient (GRG2) algorithm, which is available in Microsoft Excel via the Solver Add-in (see Supplementary Material). This process uses Newton–Raphson iterations to determine the root of the gradient of a function and as such uses numerical differentiation.[22] In general, the greater the number of parameters, the more likely the GRG2 algorithm is to experience difficulty in arriving at acceptable solutions. This is due to a statistical phenomenon referred to as ill-conditioning; when the SSE has virtually an infinite minima, the algorithm cannot distinguish between local and global minima. In other words, the region where the SSE is truly at a minimum is surrounded by an area where SSE is almost constant. For example, if a 5-parameter logistic equation is used and it is found that $a > d$, then $b < 0$ and the data will fall within the lower asymptotic region. When the algorithm attempts to find solutions, the iterations continue until a and c become so large that a completely unacceptable fit is obtained. In this case, it would be preferable to use a model with fewer parameters.

Being able to locate the point of inflection with precision is a crucial step in fitting a logistic function, as it is often one of the curve fitting parameters. In most cases, the first derivative cannot be determined analytically, and so it is approximated by taking finite differences, for example, using the 5-point stencil formula:

$$f'(x) \approx \frac{1}{12h}\left[-f(x+2h) + 8f(x+h) - 8f(x-h) + f(x-2h)\right] \quad (14)$$

For a function f, eqn (14) calculates the gradient on either side of a point x in increments of h. If the data are relatively noise free, then this approach is fairly robust, although inevitably some accuracy is lost due to loss of significant digits on numeric subtraction. This is particularly problematic when the 2 numbers being subtracted are approximately equal. Another common approach to numerical differentiation is to use a Savitzky-Golay filter, for example,

$$f'(x) \approx \frac{1}{12h}\left[1 \times y_{-2} - 8 \times y_{-1} + 0 \times y + 8 \times y_1 - 1 \times y_2\right] \quad (15)$$

This is based on a set of convolution coefficients that are obtained from low-degree polynomials.[23] Another feature of the Savitzky-Golay filter is that it can be used for smoothing data. To highlight this useful feature, **FIGURE 6** shows a plot of experimental data to which random Gaussian noise of unit standard deviation and zero mean has been added. This has then been processed by a 15-point Savitzky-Golay filter using the convoluting coefficients –78, –13, 42, 97, 122, 147, 162, 167, 162, 147, 122, 87, 42, –13, –78, and a normalizing factor of 143.[24] As we can see from the second plot in **FIGURE 6** (insert), the filtered data has significantly less noise. The obvious disadvantage of the Savitzky-Golay filter is that it truncates the data at each end of the curve.

Conclusion

If Occam's razor were applied to nonlinear curve fitting, it would lead us to conclude that the simplest function is most likely the best option. As was demonstrated for the sandwich ELISA, it is easy to mistake the simplest function (a hyperbolic equation) for the most accurate, eqn (8). However, that aside, it remains true that the simplest accurate function should be used; functions with fewer parameters are more stable with respect to least squares analysis, and statistically there are more degrees of freedom, which is important when the measured data set is small. This highlights the need for careful consideration of accompanying statistics when viewing nonlinear relationships. If these are not automatically provided by commercial software, they are easily computed using spreadsheets such as Microsoft Excel, or even by hand.

FIGURE 6. Sigmoid curve (solid line) with added Gaussian noise (open circles). Inset: Curve after application of Savitzky-Golay filter.

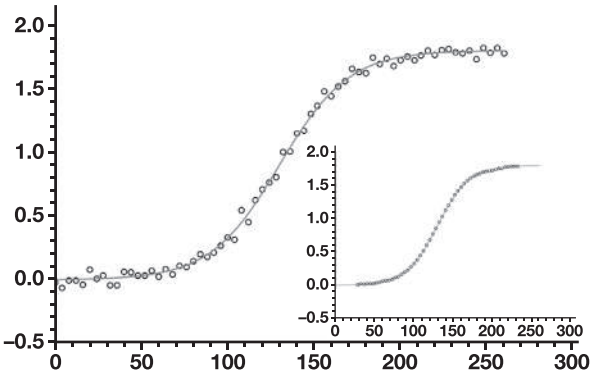

Supplementary Material

Supplementary material is available at *Laboratory Medicine* online.

Conflict of Interest Disclosure

The author has nothing to disclose.

REFERENCES

1. Fellgett PB, Usher MJ. Fluctuation phenomena in instrument science. *J Phys E Sci Instrum.* 1980;13(10):1041-1046. https://doi.org/10.1088/0022-3735/13/10/001
2. Galitzine C, Egertson JD, Abbatiello S, et al. Nonlinear regression improves accuracy of characterization of multiplexed mass spectrometric assays. *Mol Cell Proteomics*. 2018;17(5):913-924.
3. Baty F, Ritz C, Charles S, Brutsche M, Flandrois JP, Delignette-Muller ML. A toolbox for nonlinear regression in R: the package nlstools. *J Stat Softw*. 2015;66(5):1-21.
4. Grant GA. The many faces of partial inhibition: revealing imposters with graphical analysis. *Arch Biochem Biophys.* 2018;653:10-23. https://doi.org/10.1016/j.abb.2018.06.009
5. Pant V. Importance of observing the progress curve during enzyme assay in an automated clinical chemistry analyzer: a case study. *EJIFCC*. 2022;33(1):56-62.
6. Nanda SK, Dinakaran A, Ray L. Is dilution important: factitious total creatine kinase in case of rhabdomyolysis? *J Clin Diagnostic Res*. 2016;10(10):BD01.
7. Cramer JS. The early origins of the logit model. *Stud Hist Philos Sci Part C: Stud Hist Philos Biol Biomed Sci.* 2004;35:613-626.
8. Gesztelyi R, Zsuga J, Kemeny-Beke A, Varga B, Juhasz B, Tosaki A. The Hill equation and the origin of quantitative pharmacology. *Arch Hist Exact Sci.* 2012;66(4):427-438. https://doi.org/10.1007/s00407-012-0098-5
9. McDowall LM, Dampney RA. Calculation of threshold and saturation points of sigmoidal baroreflex function curves. *Am J Physiol Heart Circ Physiol.* 2006;291(4):H2003-H2007.

10. McPherson PA, Bole A, Cruz KA, Young IS, McEneny J. A curvilinear approach to the kinetic analysis of linoleate peroxidation in aqueous liposomes by 2, 2′ azobis (2-amidoinopropane) dihydrochloride. *Chem Phys Lipids.* 2012;165(6):682-688. https://doi.org/10.1016/j.chemphyslip.2012.07.004
11. Simon L, Karim MN. Probabilistic neural networks using Bayesian decision strategies and a modified Gompertz model for growth phase classification in the batch culture of *Bacillus subtilis*. *Biochem Eng J.* 2001;7(1):41-48.
12. Zarin R. Numerical study of a nonlinear COVID-19 pandemic model by finite difference and meshless methods. *Partial Differ Equ Appl Math*. 2022;6:100460.
13. Lipovetsky S. Double logistic curve in regression modeling. *J Appl Statist.* 2010;37(11):1785-1793. https://doi.org/10.1080/02664760903093633
14. Wild D. *The Immunoassay Handbook. Theory and Applications of Ligand Binding, ELISA and Related Techniques*. 4th ed. Elsevier; 2013.
15. Rodbard D, Frazier G. Statistical analysis of radioligand assay data. In: *Methods in Enzymology*. Vol 37. Academic Press; 1975:3-22.
16. Prentice R. A generalization of the probit and logit methods for dose response curves. *Biometrics.* 1976;32:761-768.
17. Cumberland WN, Fong Y, Yu X, Defawe O, Frahm N, De Rosa S. Nonlinear calibration model choice between the four and five-parameter logistic models. *J Biopharm Stat.* 2015;25(5):972-983. https://doi.org/10.1080/10543406.2014.920345
18. Ratner B. The correlation coefficient: its values range between + 1/– 1, or do they? *J Target Meas Anal Mark*. 2009;17:139-142.
19. Glatting G, Kletting P, Reske SN, Hohl K, Ring C. Choosing the optimal fit function: comparison of the Akaike information criterion and the F-test. *Med Phys.* 2007;34(11):4285-4292. https://doi.org/10.1118/1.2794176
20. Sauer T. *Numerical Analysis*. 2nd ed. Pearson; 2012.
21. Bogan A. Levenberg-Marquardt Method. Accessed November 14, 2022. https://github.com/abnerbog/levenberg-marquardt-method
22. Fylstra D, Lasdon L, Watson J, Waren A. Design and use of the Microsoft Excel Solver. *Interfaces.* 1998;28(5):29-55. https://doi.org/10.1287/inte.28.5.29
23. Barak P. Smoothing and differentiation by an adaptive-degree polynomial filter. *Anal Chem.* 1995;67(17):2758-2762. https://doi.org/10.1021/ac00113a006
24. De Levie R. *Advanced Excel for Scientific Data Analysis*. Oxford University Press; 2004.

SPECIAL REPORT

Long-term alliance for pathology equipment and technology acquisition: a paradigm shift for improved quality and efficiency

Gurmukh Singh, MD, PhD, MBA[1], Kellie A. Vinson, FACHE, MT(ASCP)SH, MBA[2], Kari Jones, MSM[3], Brandy Gunsolus, DCLS, MLS(ASCP)[CM4], Jeremy Keever, ThM, BS[5], Brooks A. Keel, PhD, HCLD (ABB)[6]

[1]Shepeard Chair in Clinical Pathology, Department of Pathology, [2]Pathology Services, [3]Alliance, AU Medical Center, [4]Medical College of Georgia at [6]Augusta University, Augusta, GA, US, [5]Danaher Corporation, Brea, CA, US. Corresponding author: Gurmukh Singh; gurmukhsinghmdphd@yahoo.com

Key words: laboratory budget; efficiency; long-term agreement; alliance with a single vendor; equipment acquisition; laboratory stewardship; pathology graduate medical education

Abbreviations: AU, Augusta University; CHOG, Children's Hospital of Georgia; DCLS, Doctorate in Clinical Laboratory Sciences; POC, point of care; AACC, American Association for Clinical Chemistry; FTE, full-time equivalent; HLA, human leukocyte antigens

Laboratory Medicine 2024;55:117-126; https://doi.org/10.1093/labmed/lmad071

ABSTRACT

Objective: Personnel costs are the largest single budget item in the clinical laboratory, other major expenses being equipment, analyzers, blood and blood components, and cost of day-to-day consumables. This report describes our experience with developing a long-term relationship with a single major vendor as a paradigm shift from the traditional multiple vendors, multiple contracts, and recurrent extended negotiations. Our objective was to develop a long-term approach for replacement of effete equipment and upgrades to operations in a pathology and laboratory medicine department in collaboration with vendors providing equipment and services.

Methods: Major vendors were invited to visit the department to analyze the workload and workflow and suggest integrated solutions to meet the goals of the department. Multiple iterations of the proposals were evaluated, and a recommendation made to the medical center leadership. The vendor, the medical center, and the department jointly developed a 15-year partnership plan to improve the operations of pathology services. The agreement encompasses a range of management and performance criteria for both sides. The salient items discussed were laboratory staffing, turnaround time, workload change, test insourcing, reference laboratory costs, and scholarly productivity and teaching.

Results: The agreement reduced laboratory staffing by 21%, eliminated stat tests by reducing the turnaround time for routine tests to less than 45 minutes for 90% of tests, with an increase of 9.1% in the number of tests, Cost avoidance in salary and reference laboratory costs was $3,424,136/year against an expected target of $2 million in total savings, despite not including cost avoidance from promoting appropriate use of laboratory testing for inpatients and increase in revenue from increase in ambulatory testing. Vizient score in laboratory utilization improved from the 94th to 76th percentile. Scholarly output increased by more than 100%.

Conclusion: This model of a long-term alliance with a chosen vendor led to improvements in quality and efficiency.

Introduction

Years of declining reimbursement have put enormous fiscal pressure on pathology and laboratory medicine services. The passage of the Patient Access to Medicare Act and the resulting changes to the Clinical Laboratory Fee Schedule were projected to reduce Medicare reimbursement for high-volume laboratory testing by 50% over the next 5 years, threatening profit margins and the survival of many laboratories.[1,2] The choices can be particularly stark for smaller laboratories as well as tertiary care academic medical centers, which already carry a disproportionate share of costs for nonreimbursed medical care while having to continuously invest in evolutionary and revolutionary technologies as part of their educational and research mandates.[3,4] The ability to reduce operating costs by 15% to 20% in a sustainable fashion may be essential for long-term health and mission fulfillment for academic clinical and anatomic pathology laboratories.[5]

The national shortage of clinical laboratory scientists has affected our ability to provide quality care in a timely manner. The shortage of laboratory personnel provides an added incentive to improve efficiency of operations, through promotion of optimal utilization of laboratory services, automation, and consolidation of functions.

The formation of strategic partnerships between health care organizations and industry vendors has long been suggested as an approach

to improve the quality of patient care while lowering costs.[6] The application of such a model to pathology and laboratory medicine services presents challenges and opportunities, as various divisions of services are usually supplied and equipped by multiple vendors using a variety of arrangements, such as purchase, lease, reagent rental agreements, etc. This entails a continuing struggle to ensure the most current test modalities and technology and constantly upgrading platforms and instruments due to attrition or changes in technology. It is often impractical to coordinate these efforts with multiple vendors, each of which may present varying timelines for contract dates, upgrades, replacement of instruments and introduction of new technologies. An added difficulty includes coordination with medical center leadership and procuring funding in competition with other departments. Strategic multispecialty partnerships in the laboratory space have been reported before, but not in the context of a tertiary academic center.[7] Potential drivers for total laboratory cost and cost-per-test savings can stem from the multiple factors listed in **TABLE 1**.

Pathology and Laboratory Medicine at Augusta University Health

The Department of Pathology serves the two hospitals of Augusta University (AU) Health, namely AU Medical Center (hospital for adult patients) and Children's Hospital of Georgia (CHOG). The adult hospital has 478 beds and serves as the level 1 trauma center for a 13-county region and CHOG supports 154 beds. There are 88 outreach clinics. During the period of pathology alliance implementation, the number of beds and total inpatient discharges remained constant at 632 beds and about 20,000 discharges per year. The medical centers perform 18,000-20,000 surgeries per year. However, with the implementation of outreach clinics, the number of visits increased by 21.3%

The Department of Pathology is part of the Medical College of Georgia at AU. The Medical College of Georgia operates 2 campuses and enrolls 260 new medical students per year. The department has 2 conventional major divisions, Anatomic Pathology and Clinical Pathology/Laboratory Medicine. The Clinical Pathology Division is staffed by 4 full-time equivalent pathologists, 2 Doctorate in Clinical Laboratory Sciences (DCLS) advanced practitioners, and 122 technical and administrative personnel. Twelve to 14 residents and fellows are in training at a given time.

The Pathology and Laboratory Medicine Department at AU Health has over 400 different analyzers and supporting equipment such as chemistry and immunochemistry analyzers, hematology, coagulation and flow cytometry analyzers, water baths, centrifuges, refrigerators, an automation line, point-of-care (POC) instruments, tissue processors, microbial culture and sensitivity analyzers, molecular testing, microscopes, apheresis equipment, and the like. Keeping all these items in top working condition and current with changing technologies through interactions with multiple vendors is a logistical challenge.

AU Health previously negotiated a long-term alliance with Philips Corporation to provide consulting services, medical technology purchases, and maintenance for imaging and other related tasks. This model was modified and applied to pathology and laboratory medicine.

TABLE 1. Potential drivers of cost savings

Standardization of instrumentation and middleware
Reducing the number of workstations
Eradication of obsolescence and end-of-life problems
Savings in service and maintenance issues
Reduction in expensive reference laboratory use
Reduction in reagent and supply chain costs
Elimination of cyclical major capital expenses and need for emergency capital
Continuous performance improvement programs, maximization of automation, and innovation

Methods

Innovation in Process

The Department of Pathology and Laboratory Medicine, in collaboration with AU Health, explored innovative ways to address the issue of replacement of outdated analyzers, the automation line, laboratory middleware, and introduction of new technologies. We did not follow any formal model for change but relied on our collective experience.

Much before this opportunity presented itself, the laboratory leadership developed a rapport with the staff by listening, formal recognition of their achievements at the monthly quality management meeting, taking all new employees to off-campus lunches, funding celebration parties after important events such as College of American Pathologists inspection, and celebrated national holidays such as Independence Day and year-end holidays. When the opportunity came for a transformational change, laboratory managers, supervisors, and bench CLS personnel were consulted from the beginning. They attended the vendor presentation, provided input for the selection of the vendor and instruments, were part of the site visit teams to evaluate the 2 finalists, and worked with the architects for design of the laboratory. The bench personnel and supervisors evaluated the new design through dry runs and "spaghetti diagraming" to ensure an efficient operation. The final product was their creation and was recognized at formal presentations by the departmental, medical center, medical school, and university leaders.

The laboratory leadership has continued similar cordial interactions with the staff after the activation of the renovated core laboratory. A particularly noteworthy act during COVID-19 exigency and the additional staff shortages was performed by the administrative director by taking on bench work duties, especially for the night shift in microbiology, to address the added workload for processing COVID-19 tests. Even the medical director made a token contribution to COVID-19 testing benchwork.

The department invited major vendors of equipment and services to assess its current state and present their proposals for a comprehensive, multiyear agreement to renovate, upgrade, and maintain the equipment and software. All the vendors were provided equal access to the department, data, and facilities and given the same goals. The key goals are listed in **TABLE 2**.

Within the department and medical center, there was an understanding that the improvement in efficiency of operations would not result in reduction in force, that is, layoffs. There would be reduction in manpower through attrition and duties of the staff may be revised as needed. This commitment to the staff, in addition to the abovementioned participation by the laboratory personnel in this transformation, were critical to obtaining the buy-in for such a change and efficient execution of the process for the change.

The aging of chemistry instruments and the need for replacement of these items was the key driver for the project. The initial intent was to

TABLE 2. Key goals presented to vendors

Address all sections of the department.
Reduce the number of workstations by at least 30%.
The turnaround time for all routine tests should be less than 45 minutes for more than 90% of the samples so that the need for stat tests could be eliminated.
Reduce the cost of operations by at least 10%.
Present a plan for the transition to the new state.
Develop a plan to have a long-term agreement lasting up to 15 years.

renovate the core sections of Clinical Pathology, that is, hematology and chemistry only. The medical and administrative directors of clinical pathology services sought to expand the scope of the renovation to include all sections of Clinical Pathology in a phased process. As the process evolved, Anatomic Pathology and informatics issues were added.

At the outset, it was expected that the core section of Clinical Pathology would undergo renovation in its existing space and the vendors were advised to include the cost of construction or structural alterations, modifications of swing space, and related logistical issues in their proposals. About a year after the process began, the medical center made new space available in an adjoining building. The new space, on the third (top) floor of an old building, had been gutted to the studs and sufficient space was available to accommodate all sections of Clinical Pathology. The transformation was expected to be executed in 3 phases.

In phase 1, the core laboratory, consisting of clinical chemistry, hematology, coagulation, urinalysis, immunology, toxicology, POC, and reference laboratory testing, was the initial target for change. Initial funding was limited to renovation for the core laboratory only.

In phase 2, the next step was expected to be the relocation of the microbiology and human leukocyte antigens (HLA) laboratories to space contiguous to the core laboratory, with extension of the automation line to microbiology. The space vacated by the microbiology and HLA laboratories was expected to allow accommodation of histology and cytology laboratories and bring these functions from a different building to space adjacent to other anatomical pathology functions.

In phase 3, the blood bank, apheresis services, and offices for medical and administrative leadership were expected to be relocated next to the core laboratory in 1 large open space. The configuration was expected to allow cross coverage among different sections and make 24-hour coverage of microbiology functions possible. The space vacated by transfusion medicine services was to be used for expansion of operating rooms, emergency medicine, and hospital administrative functions.

(Our best-laid plans were interrupted by lack of funds for phases 2 and 3. With the construction of a new hospital in an adjoining county getting underway, it was unclear when funding would become available for the last 2 phases.)

Invitation to Vendors

Representatives of the vendors serving Clinical Pathology were briefed about the plans for renovation of the core section of Clinical Pathology and requested to evaluate the current state of Clinical Pathology and develop proposals to meet the goals stated above. The medical director of Clinical Pathology contacted the major vendors at the 2015 annual meeting of the American Association for Clinical Chemistry (AACC) and solicited their participation. Four vendors with the capability of addressing multiple sections of a clinical laboratory were invited. All 4 vendors expressed interest in the proposal for renovation of Clinical Pathology.

Initial Meeting with Vendors

The medical and administrative directors, along with managers and supervisors, met with the representatives of the vendors and the following issues were discussed:

1. Goals of Clinical Pathology for the outcomes of the renovation: each vendor was provided with a printed copy of the goals.
2. The vendors were invited to analyze the workload, time flow of workload, flow of specimens, storage and retrieval of specimens, processing of specimens for send-outs, opportunities for in-sourcing tests, consolidation of workstations, integration of other Clinical Pathology sections, and anticipated changes in technology, including informatics. This turned out to be an iterative process, especially for the 2 finalists, who presented proposals with increasing detail.
3. The need for the ability of Clinical Pathology to track, retrieve, and analyze the data without seeking involvement of the main information technology vendor for the medical center, was emphasized. To reiterate, the vendors were charged with providing software to address not only the operations of Clinical Pathology but also to facilitate retrieval and meaningful clinical analyses of the data for performance improvement and scientific publications.
    a. Turnaround time: by making changes to the workflow, the core section had already achieved a turnaround time of less than 60 minutes for nearly 90% of automated tests. The vendors were charged with reducing the turnaround time for all routine tests to less than 45 minutes from the time of receipt of specimen in the laboratory. The vendors were advised of the prior experiences of the members of Clinical Pathology and the anticipated problems were outlined along with suggestions by Clinical Pathology, for example, to allow release of part of a panel of test results or some of the tests requested on a given sample.
4. Automation line: a wish list for automation line included
    a. a hopper to receive all properly bar-coded samples and feed the samples to the automation line,
    b. automated recording of specimen receipt and time stamping for various processes,
    c. in-line centrifugation with capacity to alter *g*-force and centrifugation time for specific tests and samples,
    d. a decapper, an aliquoter, labeling of aliquots, and output station for send-out samples,
    e. multiple lanes for samples to bypass analyzers not involved with analysis of a given sample,
    f. output stations for samples flagged by analyzers for manual processing in hematology and chemistry,
    g. recapping and stockyard for 7-day inventory of samples and easy retrieval of samples for add-on tests,
    h. automated purging of effete samples,
    i. an option to extend the automation line to other sections, with integration of microbiology, HLA-immunogenetics, and blood banking,
    j. the ability to install analyzers on both sides of the line,

k. and front end loading; in case of automation line down time, it was expected that all analyzers would have the option of front-end loading without causing undue delay in turnaround time.

5. Third-party analyzers:
   a. Although related to the automation line issues described above, this item was addressed separately due to its importance to both the department and even more so to the vendors. A key requirement was that the automation line accommodate analyzers from third parties.
   b. It was emphasized that the chosen vendor would be the primary supplier of instruments and services and the department would use the vendor for about 70% of its needs. The 70% figure refers to the number of instruments that the vendor markets and the laboratory needs to procure an instrument with similar functions. The Department of Pathology and AU Health reserved the option of choosing third-party instruments if such analyzers have clearly superior features, performance, menu, and efficiency.
   c. The item under this heading was not part of the initial discussions but evolved after the choice of vendor. It was decided, in consultation with the vendor, that any third-party analyzers would be selected in consultation with the vendor, with the laboratory Clinical Laboratory Improvement Amendments director having the final say. The vendor would be responsible for procuring the analyzers or services and include the costs in the charges to the medical center.
6. Point-of-care analyzers:
   a. It was agreed that judicious use of POC analyzers may be cost-effective for AU Health even though it may be more expensive for the laboratory. The vendors were requested to include use of POC analyzers in their plans.
   b. It was specified that POC analyzers must be ready for interface with the medical center electronic medical record.
7. Phased integration: the vendors were advised to develop a timeline for phased integration of microbiology, HLA-immunogenetics and blood bank in their plans.

Evaluation of Proposals

The process of interaction with vendors and evaluation of proposals was conducted jointly by the department and the medical center and lasted about 23 months.

The proposals took the form of initial presentations by the vendors addressing the current state of operations, workload and workflow, and suggested choice of equipment to meet the workload. The next set of proposals included drawings with proposed layout for the automation line and placement of analyzers. Some of the vendors included a project manager in their presentations to address the issue of transition from current state to renovated state and timelines for implementation.

The vendors were queried by the technical staff about operating characteristics of the analyzers, including on-board reagent and quality control storage, final step of water purification, on-board storage of samples for add-on tests, on-the-fly change of reagents, stability of calibrations, daily and weekly maintenance requirements, timeliness of service calls, remote monitoring of the performance of analyzers, and ability for remote trouble shooting. An issue of special concern was the frequency of recalls by the Food and Drug Administration, number of vendor notifications about malfunctions, and ease of replacement of parts like lamps needing periodic replacement. The manpower needed to operate during off-hour operations and the ability to monitor multiple analyzers from a single command center were emphasized. Footprint of the analyzers was a consideration to promote the efficient use of the available space.

The supervisors and technologists were free to voice their experiences with the various vendors and their concerns about the reliability of instruments by various vendors was an important criterion in the evaluation.

Scalable Analyzers

Clinical Pathology has satellite laboratories in the Georgia Cancer Center, Family Medicine Clinic, and pediatrics outpatient area. Availability of smaller analyzers using the same methods and same reference ranges as the main laboratory analyzers was emphasized.

Site Visits

Once the choice of vendors had been narrowed to 2 candidates, visits to 2 sites, 1 each chosen by the vendors, were executed. The site visits were geared to learn firsthand about the performance characteristics of the main analyzers from each vendor. The visits were populated by supervisors and senior medical technologists.

The two finalists were given the opportunity to revise their proposals before the final decision.

The evaluation criteria included (1) the depth and breadth of equipment and services included in the proposals, (2) flexibility to accommodate third-party equipment seamlessly in areas where the chosen vendor may not have products or if the product of a different vendor was judged to be appreciably better in the judgment of the department, (3) the practicality of the transition plan for laboratory renovation and inclusion of any construction that may be needed for optimal operations, and (4) long-term commitment and support of the corporate leadership. A formal scoring mechanism was not used; rather, we relied on consensus among the evaluating parties. The evaluators included bench technical personnel, supervisors, managers, and administrative and medical directors of the laboratory.

Partnership Award Details

Based on the extensive process and thorough evaluation, the department selected Beckman Coulter Diagnostics and other diagnostic companies of Danaher, parent company for Beckman Coulter, as the strategic partner. The terms and conditions were negotiated by the medical center departments of finance, legal affairs, facilities management, and the Medical Executive Committee, with strong support from the president of Augusta University.

Final approval was provided by the Board of Directors of AU Health. The partnership agreement was signed by the presidents of Beckman Coulter and Augusta University at a ceremony during an annual meeting of AACC in Philadelphia, PA. The transition to a new core laboratory was implemented in February 2019. Key features of the agreement are presented in **TABLE 3**.

Governance

The joint working groups–based governance is a unique feature of the alliance. The 5 working groups focused on innovation, technology, service,

performance, and finance are each co-chaired by 1 representative each from AU Health and Danaher companies (**FIGURE 1**).

All working groups report to the Joint Oversight Committee. The governance model ensures that the performance requirements of each functional area achieve or exceed the requirements of the agreement. It serves as the escalation point for all critical business and performance issues, provides monthly performance reports on key performance indicators and milestones, ensures that all actions agreed to by the Joint Oversight Committee are executed, and identifies areas for collaboration and continuous improvement.

Implementation

Fortuitously, while the renovation of Clinical Pathology was being considered, it was noted that the current space did not have the infrastructure to complete the project. The medical center decided to relocate and centralize the laboratories in a new space. This opportunity was seized and led to the development of a comprehensive alliance with a vendor. The relocation was expected to facilitate colocation of all laboratory medicine/clinical pathology operations in 1 open space. The relocation was expected to allow 24-hour coverage for all services, including microbiology and the transplantation laboratory. Cross-training and cross-coverage among the various sections of Clinical Pathology were expected to add to the efficiency of the operations. Cross-coverage among the various sections of the core laboratory was only implemented because this was feasible due to the core laboratory being 1 large open space. The improvement in efficiency was realized as demonstrated by reduction in turnaround time, adding about 100 new tests, and no interruption of any service even during the COVID-19 emergency despite sickness and allowing people to work from home, as needed.

The comprehensive plan for the new core laboratory layout was developed by the laboratory staff with training and under guidance from the Performance Partnership experts from Beckman Coulter Diagnostics.[8]

TABLE 3. Key features of the agreement

15-year master services alliance.
Equipment management according to the TMP (technology management plan), eliminating the need for transactional contracting. The TMP outlines which pieces of equipment are to be installed per contract year (**FIGURE 1**).
Single payment—AU Health issues a monthly payment that provides predictable spending and budgeting with an annual true-up.
Performance Partnership resources to guide implementation of the continuous improvement in AU Health pathology and laboratory medicine operations based on the principles and tools of Danaher Business Systems. The progress of the initiative is measured using dynamic and static key performance indicators (KPI), which capture productivity improvements and cost savings.
Alliance governance based on working groups with equal representation from both AU Health and Danaher companies (**FIGURE 1**).

Specimen Transport

As the new laboratory was to be in a different building than the main hospital, the medical center agreed to extend and update the pneumatic tube specimen transportation system linking the various sites in the medical center to the laboratory. It was fully appreciated that reducing the turnaround in the laboratory by 15 minutes would be meaningless if the specimen transport time increased by a larger amount. The required extension of the pneumatic tube specimen transport was executed before testing at the new location was activated. A clarification may be needed for the actions taken regarding pneumatic tube system. Initially the core laboratory was expected to be renovated in existing space and equipped with a pneumatic tube. The move to an adjoining building came later in the planning process, hence, the stipulation was made with

FIGURE 1. Committee structure for oversight and planning. The Joint Oversight Committee (JOC) is tasked with ensuring the goals and objectives of the agreement are implemented according to the agreement and the guiding principles and the evolving strategic directions of both parties. The JOC also recruits members for the committees reporting to it. The Finance and Operations Working Group (FWG) is responsible for the management of the unitary payment covered under this agreement. they ensure that any changes to the unitary payment based on changes to the technology management plan (TMP), key performance indicators (KPI), or services are communicated to the JOC. This group is responsible for monitoring and managing the annual forecasted consumables and for the "annual true-up" of the unitary payment. The Innovation and Alliance Demonstration Group (AIDG) is responsible for the continuous AU Medical Center/Beckman collaboration in the areas of product and service commercialization and public relations. This group coordinates the launch of clinical innovation pilots and other master service agreement–related events to promote AU Medical Center as a center of excellence and to demonstrate the outcomes of the alliance structure. The Technology and Testing Working Group (TWG) is charged to ensure that software and equipment installation and replacement is scheduled appropriately and all the necessary resources are made available. The TMP is reviewed as part of the annual planning process. Acceleration or deceleration of equipment replacement in the TMP is discussed and voted on by TWG. The Services Working Group (SWG) is responsible for tracking and reporting the performance metrics (uptime and preventative maintenance) to the JOC quarterly. This group also tracks the usage of service, labor, and materials reserve. The Performance Improvement Working Group (PIWG) is the forum for identifying strategic, performance, and process opportunities and is the channel for AU Medical Center executives and administrators to request consulting support for specific strategic, operational, and change management initiatives. This group monitors all KPIs as described in the agreement.

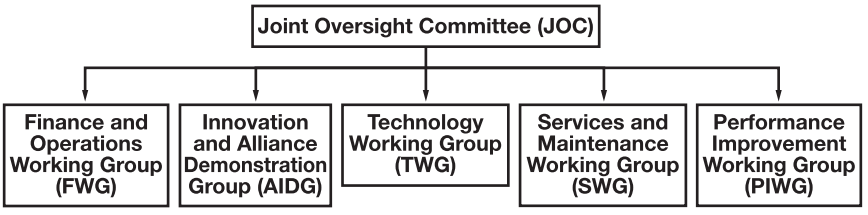

the medical center that the core laboratory would be relocated only after the pneumatic tube extension being fitted to the new space.

Additional Change

While we were executing the above alliance/collaboration, an additional opportunity presented itself that fit into our plans for a paradigm shift. In collaboration with Rutgers University, we offered residency training to 2 candidates for DCLS. (The first DCLS graduate in the US trained with us and was 1 of the 2 DCLS staff members.) The 2 DCLS managers were instrumental in our response to COVID-19, expanding the in-house test menu, and dramatically reducing the reference laboratory costs through judicious stewardship and promotion of appropriate utilization.

Expected Outcomes

The medical center expected to realize a savings of about $2 million per year over the course of the contract compared with current costs.

The turnaround time on more than 90% of routine tests would be less than 45 minutes.

The new laboratory would be better able to support the needs of the new hospital to be built in the adjoining county.

Consolidation of the Clinical Pathology laboratories in 1 location was expected to free up space to allow consolidation of anatomic pathology, histology, cytology, and electron microscopy laboratories in 1 contiguous space to be vacated by the microbiology and HLA-immunogenetics laboratories.

Relocation of the blood bank in the final phase would provide space for the medical center to expand other services as needed, such as operating rooms or emergency medicine services.

Colocation of all Clinical Pathology sections was expected to facilitate cross-coverage and provide 24-hour coverage for microbiology and HLA-immunogenetics.

The choice of the vendor and the resources of the parent company were expected to allow upgrades to anatomic pathology, including implementation of digital pathology and an advanced specimen tracking system.

Training of pathology residents was expected to be enhanced due to colocation of the various sections of Clinical Pathology/Laboratory Medicine. There was an expectation of improvement in the scholarly output of the Laboratory Medicine Division.

Results and Discussion

The process designed for the department has been fully implemented for the core laboratory only. Fiscal exigencies, life, and COVID-19 have stalled the 2 remaining phases for the Clinical Pathology Division renovation. Some items have been implemented in anatomic pathology, but digital transformation remains in process. The new hospital construction in the adjoining county is also in process. The outcomes for the core laboratory are given below.

The core laboratory is operating with 21% lower staffing, that is, 32.5 fewer full-time equivalent (FTE) personnel, for a cost savings of $2,762,500/year ($85,000/FTE for 32.5 FTE). Despite personnel savings, the laboratory still implemented the following improvements in service and scholarly activities:

1. Elimination of stat tests through judicious use of POC analyzers and reducing the turnaround time for tests that could be ordered stat to less than 45 minutes. The average turnaround times for comprehensive metabolic profile and complete blood cell count improved from 42 to 39 minutes and 38 to 28 minutes, respectively.[9]
2. The core laboratory is performing 9.1% more tests per year with 21% fewer staff.
3. About 100 new tests have been implemented in-house, thereby reducing the reference laboratory costs from $4.64 million per year to $3.98 million per year (a 14.25% reduction) despite a more than 9% increase in test volume. The stated cost savings accounted for the expenses of doing tests in-house. A list of the tests brought in-house is given in **TABLE 4**. This reduction in costs was in considerable measure due to the efforts of DCLS staff members, prospective review of test requests, and promotion of appropriate utilization.
4. The ranking of the medical center in laboratory utilization improved from the 94th percentile to the 76th percentile. This measure was provided by Vizient using data derived from academic medical centers using this company for analytics and advisory services. The lower percentile ranking reflects better or more appropriate laboratory utilization. This was achieved through vigorous efforts by the laboratory at improving appropriateness of utilization, a usual cause of discord between bedside providers and the clinical laboratory.
5. An important fringe benefit was improvement in the training of pathology residents in laboratory stewardship.
6. The number of publications in which pathology residents participated increased from 7 in 4 years (2016-2019) to 10 in 3 years (2020-2022), an improvement of 107%. The total publications from the core laboratory improved from 13 in the first 4 years to 22 in the latter 3 years, an improvement of 125%.
7. Extramural support increased from $30,000 in the first 4 years to $251,000 in the latter 3 years.
8. For the sake of simplicity of accounting, we did not estimate the cost avoidance due to improvement in appropriateness of laboratory utilization for inpatients and the additional revenue generated from an increase in testing volume of ambulatory patients. Thus, our estimate of cost savings is, if anything, conservative. No additional personnel were added to accommodate the additional workload from either insourcing of reference laboratory tests or from increase in ambulatory testing, a testament to the improved efficiency of the new way of operations.

Additional Positives

The following challenges and opportunities provided a great test for the enhanced abilities of the laboratory and synergistic response of the alliance.

Improvements in laboratory workflow and increase in efficiency were instrumental in the vigorous response to COVID-19 exigency for patient care. Despite staff shortage, the DCLS staff members spearheaded the effort to provide COVID-19 testing to the State of Georgia and later developed a strong working relationship with the Augusta National Golf Club and supported the annual tournaments. It has been a matter of pride for the institution that the governor of Georgia selected Augusta University over other prestigious institutions in the state to support the state response to COVID-19.

TABLE 4. Tests brought in-house to the core laboratory

1,25-(OH)2 Vitamin D	Insulin	*Rhizopus* spp IgE
Aldosterone	Jo-1 Ab	RNP Ab
Almond IgE	Maple IgE	ROM Plus fetal membrane rupture test
Alternaria spp IgE	MDW (monocyte distribution width)	Sch II/III drug compliance panel
Anti-CCP	Measles IgG	Scl-70 Ab
Aspergillus fumigatus IgE	Milk IgE	Sesame seed IgE
Aspergillus niger IgE	Mitochondrial Ab	*Setomelanomma* (*Helmithosporium*) spp IgE
Bahia IgE	Mouse epithelium/serum/urine IgE	Shrimp IgE
Beech IgE	Mucor spp IgE	Smith Ab
Beta-2 glycoprotein IgG	Mumps IgG	Sorrel IgE
Beta-2 glycoprotein IgM	Myeloperoxidase Ab	Soybean IgE
Birch IgE	Nettle IgE	SSA Ab
Blatella germanica (German cockroach) IgE	Oak IgE	SSB Ab
Box elder IgE	Pancreatic elastase	Timothy IgE
Buprenorphine	Peanut IgE	Tomato IgE
Burmuda IgE	Pecan IgE	Tramadol
Calprotectin	Pecan nut IgE	*Trichophyton* spp IgE
Candida spp IgE	*Penicillium* spp IgE	tTG IgA
Cardiolipin IgA	Pine IgE	tTG IgG
Cardiolipin IgG	Plasma low Hgb	Tuna IgE
Cardiolipin IgM	Proteinase 3	U3RNP Ab
Cashew nut IgE	Quantiferon Gold Plus, TB test	Walnut nut IgE
Cat dander IgE	Ragweed, common IgE	Wheat IgE
Cedar IgE	Ragweed, giant IgE	Willow IgE
Centromere Ab	Renin	

An additional positive outcome of the alliance has been the leading role by the Laboratory Medicine Division in implementing a biomedical advanced research and development authority–supported program for the prediction of sepsis. Implementing a new test for monocyte distribution width and artificial intelligence driven analysis of data are expected to improve timely identification of patients at risk for sepsis.

Implementation of chromogen assay in the core laboratory for factor Xa allowed us to rigorously test 3 different POC instruments using the activated clotting time test for intraoperative monitoring of heparin dosing and choosing the optimal instrument. The results of this investigation led to a publication that was deemed to be the coagulation paper of the year by the cardiothoracic anesthesiologists.[10]

In addition to contribution to peer-reviewed publications originating from the department, the departmental residents have been the recipients of the Cooper Travel Award from the Southeastern chapter of AACC for the last 4 award opportunities. Performance of the residents on in-service examination improved significantly due to improved learning environment.[11–13]

Although microbiology and the blood bank have not undergone renovations, these sections have benefited from analysis of workflow by experts from Danaher. In particular, the urine culture process was revised through the on-site guidance of Danaher experts to streamline the workflow and reduce turnaround time. The blood bank benefitted from installation of Griffols equipment for automation of blood grouping and compatibility testing.

An unquantifiable benefit has been the marked improvement in the work environment for laboratory personnel and a remarkable positive change in their morale. These enhancements contributed to the improvement in efficiency as documented by a 9.1% increase in test volume, adding about 100 new tests, and improvement in client satisfaction scores while operating with 21% fewer personnel. There was no formal measurement of morale in the before and after circumstances. The improved morale is mostly a subjective impression based on virtually nonexistent unscheduled absenteeism, laboratory staff covering for each other and essential services without being told to do so by supervisors, lack of complaints about schedules or workload, absence of employee in-fighting, the cheerfulness observed by the medical director in daily interactions with the staff, and voluntary participation in quality improvement and investigative activities of the laboratory. Improved morale and improved work environment are interrelated, and both contributed to increased output. The collegiality, cooperation among the staff, including cross-coverage, and engaged attitude and dedication of the staff have been commented on by outside parties, for example, vendor representatives and members of accreditation inspection teams.

Critique of Cost Savings

Prior to this agreement, the medical center purchased the capital equipment and had separate contracts for service and supplies. Under this arrangement, the laboratory had to compete with other departments for capital budget and it often resulted in delays in the acquisition of new

TABLE 5. Spreadsheet (simplified) for equipment planning and tracking[a]

Previous asset description	New asset description	Vendor	Serial No.	PO received	Location	Department location	Discipline	Life	First replacement year	First replacement year (modified)	Second replacement year	Gross HW price	HW vendor quote target
Chemistry dimension analyzer	AU480	Beckman Coulter Dx	2021084229	57271725	AN2610	Cancer center	Chemistry	FA 7	2019	2021	2028	$76,500.00	$57,375.00
DxH 1601 Beckman DxH 800	DxH900 1	Beckman Coulter Dx	BE 49558	57891333	AD3301	Core lab	Heme	FA 7	2017	2017	2022	$110,000.00	$82,500.00
DxH 1601 Beckman DxH 800	DxH900 2	Beckman Coulter Dx	BE 49560	57891333	AD3301	Core lab	Heme	FA 7	2017	2017	2022	$110,000.00	$82,500.00
COULTER LH 500 x 2- FAME and CCL	DxH600-Peds	Beckman Coulter Dx	AZ46040	992531	BP	Peds	Heme	FA 7	2017	2017	2024	$143,078.67	$107,309.00
DxH 1601 Slide maker/slide stainer	DxH900 SMS	Beckman Coulter Dx	81966052	57891333	AD3301	Core lab	Heme	FA 5	2017	2017	2022	$77,945.33	$58,459.00
Labcell integrated automation	Power Express	Beckman Coulter Dx	CEN1018FOO566	HI-992531	AD3301	Core lab	Automation	FA 7	2018	2019	2026	$2,866,389.33	$2,149,792.00
Remisol Command Central & WAN	Remisol Advanced	Beckman Coulter Dx	53314873 to 54008047	HI-992531	AD3301	Core lab	IT	FA 7	2018	2019	2026	$308,946.67	$231,710.00
Slide stainer HEMATEK 2000	Hematek 3000 System	Siemens	4488C201099		AD3301	Core lab	Heme	FA 7	2022	2024	2031	$10,000.00	$7,000.00
Stainer RSG 61 SLIDE CMC	Hematek 3000 System	Siemens	483139	1911915	AD3301	Core lab	Heme	FA 5	2019	2019	2024	$9,914.67	$7,436.00
Stainer SLIDE HEMA-TEK 2000	STAINER SLIDE HEMA-TEK 2000	Siemens	HEMATEK	2152192	AD3301	Core lab	Heme	FA 7	2022	2022	2029	$10,000.00	$7,000.00
ADVIA 1800 chemistry system	AU5822	Beckman Coulter Dx	18063995	56099424	AD3301	Core lab	Chemistry	FA 7	2018	2019	2026	$554,750.00	$416,062.50
ADVIA 1800 chemistry system	AU5822	Beckman Coulter Dx	201806399	56099793	AD3301	Core lab	Chemistry	FA 7	2018	2019	2026	$554,750.00	$416,062.50
ADVIA CENTAUR XP IMMUN. SYST.	DxI800 - keep replacement schedule	Beckman Coulter Dx	606669	56099428	AD3301	Core lab	IA	FA 7	2018	2019	2026	$175,616.00	$131,712.00
ADVIA CENTAUR XP IMMUN. SYST.	DxI800 - keep replacement schedule	Beckman Coulter Dx	605693		AD3301	Core lab	IA	FA 7	2017	2017	2024	$175,616.00	$131,712.00
Auto urine chemistry analyzer	IQ 2000 Workcell Urine Analyzer	Beckman Coulter Dx	C16061/12002017	56948406	AD3301	Core lab	Heme	FA 7	2020	2020	2027	$85,397.76	$64,048.32
AUW TRACK/ WORKSTATION	IQ 2000 Workcell -Urine Analyzer *TMP 1-13 & 1-14	Beckman Coulter Dx	C16062/12002016	56952324	AD3301	Core lab	Heme	FA 7	2021	2020	2027	$85,397.76	$64,048.32

[a]*The equipment names and changes in names with either new models or due to change in vendor are listed in the first two columns. Vendor, serial number, the date of purchase order (PO), location, department, section/discipline, etc, are self-explanatory. Life reflects the expected life span of equipment and is considered for replacement date. The performance of equipment is monitored replacement date modified accordingly. The expected cost of replacement is noted for budgetary planning.*

equipment and prolonged delays in improvements. In the new system, the vendor is responsible for acquisition and installation of equipment and providing service and reagents for testing. There is a long-term plan for replacement of equipment at the end of useful life, as described in **FIGURE 1** and **TABLE 5**. This issue is reviewed quarterly among the 5 working groups and the Joint Oversight Committee and changes made to address any new issues. The vendor bills the medical center a fixed unitary payment each month with an annual adjustment or true-up. Thus, it was impractical for us to compare total costs under the old and new systems. The conservative estimate of cost savings exceeded the target.

For the sake of argument, we posit that even if there had been no cost savings with the new system, the improvements in the performance of the laboratory alone would have made the new system worthwhile, as the old system was untenable due to a national shortage of laboratory scientists.

Laboratory Size

It is worthy of note that we may have benefited from an appropriately sized laboratory for such an endeavor. A similar transformation at a smaller or larger laboratory may require different approaches. With a staffing of about 200 people, it is not impractical for the leadership to know all the employees personally and establish rapport with them. Off-campus lunches with new employees include extant employees as well and an effort is made to invite members of different sections for such socialization. Personal involvement of this type may be impractical at a larger laboratory.

Unrealized Potential

In keeping with Linus' Law (There is no heavier burden than a great potential), several potential enhancements have gone unrealized. The most important failure has been to implement phases 2 and 3 of the proposed renovation. Had this renovation occurred on the planned schedule, the laboratory would have provided 24-hour microbiology coverage rather than leaving about 4 hours uncovered at night. Timely processing of blood cultures turning positive during the unstaffed period could have reduced hospital length of stay and promoted more appropriate utilization of antibiotics for sepsis patients. Similarly, having cross-coverage for the blood bank would have allowed us to operate the blood bank with lower staffing at night while having the capability of responding to emergencies such as massive transfusion protocol activation.

For an academic medical center, lack of dedicated research and development resources is a major hinderance to the scholarly activities of the faculty. Although the focus of the alliance was improving patient care and efficiency of the laboratory, an opportunity to transform the departmental support for scholarly activities has not been realized to any meaningful extent. An extension of this failure has been the inability of Laboratory Medicine to secure National Institutes of Health funding for its investigative activities.

The Clinical Pathology Division had anticipated greater ability to leverage the faculty and graduate trainees in advancing thematic investigation. Although there has been an impressive improvement in scholarly activities, the full potential has not been realized, in part due to lack of resources as indicated above and partly due to the inability of leadership to change the culture.

Despite remarkable progress in some areas, such as toxicology testing, enhanced ability to support allergy immunology services, and introducing advanced flow cytometry, slow progress in expanding the technological advancements of the alliance partner, such as next generation hematology, has been a lost opportunity. The alliance has provided an unprecedented opportunity for introducing new investigative methods to clinical care; however, the progress has unfortunately been at a snail's pace.

Conclusions

The lamented inability to realize all the potential notwithstanding, the alliance has been a paradigm-shifting force for the operations of Laboratory Medicine at this medical center. A 9.1% increase in output with 21% fewer staff is worthy of note. Adding 99 new tests has reduced costs for send-outs and shortened the turnaround time. Elimination of stat tests through improved turnaround time for all tests has improved client satisfaction and workflow. Even more important has been the improvement in employee satisfaction and morale in the laboratory.

The total cost savings of $3,424,136/year against an expected target of $2 million per year is remarkable. The cited cost savings are a conservative estimate, as we did not include the decrease in cost for inpatients due to improvements in diagnostic stewardship or additional revenue from increase in testing for ambulatory patients. The increases in scholarly activity and extramural funding, although modest, are nonetheless remarkable for the limited resources at the disposal of the Clinical Pathology Division. Improvement in graduate medical education has been an important added benefit of this endeavor.

This collaboration is continuing and although we have not implemented phases 2 and 3, other sections of Clinical Pathology have benefited from the alliance and expertise provided by Danaher. For example, a Danaher team worked on-site and advised the microbiology laboratory in streamlining urine cultures that resulted in using more appropriate specimens and shortening the turnaround time. Partnership with Danaher also facilitated getting newer equipment and supplies pertinent to the high demand for COVID-19 testing.

This model of long-term alliance and shifting from purchase of equipment to vendor providing the equipment has obviated the need for capital equipment funds and having to compete with other hospital services such as radiology and cardiology for a capital equipment budget. The vendor has updated instruments without the need for entering into negotiations for each procurement. The Technology Working Group has been particularly successful in proactively addressing the needs for equipment and other services.

We are hopeful that phases 2 and 3 will be implemented. (The recently announced merger with WellStar Health System and the promise of investment by the partner is expected to revive the renovation.)

This model of a long-term alliance is eminently transferable to other institutions and other vendors.

Acknowledgments

The authors are grateful to the managers, supervisors, and technical staff of AU Health for their inspired contributions. The dedicated and professional support of Beckman-Coulter/Danaher is gratefully acknowledged.

Performance Partnership is a service mark of Beckman Coulter. DBS is a registered service mark of Danaher Corporation.

Conflict of Interest Disclosure

Dr Singh serves as a consultant to Beckman Coulter and is a member of the Advisory Board of HealthTap.

REFERENCES

1. Center for Medicare and Medicaid Services. https://www.congress.gov/bill/114th-congress/senate-bill/2425/text
2. White L. PAMA Impact on Laboratory Margins. Healthcare Financial Management Association, July 2017. https://go.gale.com/ps/i.do?p=AONE&u=googlescholar&id=GALE%7CA506318604&v=2.1&it=r&sid=AONE&asid=8dd86e3e
3. Michel R, ed. Why small labs, hospitals are at risk from PAMA cuts. *The Dark Report*. November 28, 2016.
4. Grover A, Slavin PL, Wilson P. The economics of academic medical centers. *N Engl J Med.* 2014;370(25):2360-2362.
5. Paxton A. Outreach: forge ahead or accept purchase bid? CAP Today Online, July 2017. http://www.captodayonline.com/outreach-forge-ahead-accept-purchase-bid/
6. Gallup Business Journal, September 2013. http://news.gallup.com/businessjournal/164327/hospitals-suppliers-become-partner-choice.aspx
7. MLO Inline, June 2017. https://www.mlo-online.com/laboratory-network-serves-healthcare-needs-millions-northwest-indiana
8. MLO Online, October 2017. https://www.mlo-online.com/ebook/1gmmj/0A1gmn1/MLO201710/html/index.html?page=58&origin=reader
9. Singh G, Savage NM, Gunsolus B, Foss KA. Requiem for the STAT test: automation and point of care testing. *Lab Med.* 2020;51(2):e27-e31.
10. Thompson T, Larsen R, Savage N, Agarwal S, Chazelle J, Singh G. Intra-operative monitoring of heparin: intraoperative monitoring of heparin: comparison of activated coagulation time and whole-blood heparin measurements by different point-of-care devices with heparin concentration by laboratory-performed plasma anti-Xa assay. *Lab Med.* 2019;50(4):348-356.
11. Singh G, Bollag RJ, Savage NM. Engaging pathology residents in clinical chemistry: the essential ingredient is a committed teacher. *J Appl Lab Med.* 2021;6(2):522-531. doi:10.1093/jalm/jfaa140
12. Singh G, Savage NM, Bollag RJ, Booker D. Pathology job search and interview: perspectives of the United States experience. *Arch Pathol Lab Med*. doi:10.5858/arpa 2022—0247 EP
13. Singh G, Plapp FV, Wiencek J. Roadmap for Training and Education in Clinical Chemistry, and Laboratory Medicine. 21st Century Pathology. 2023;3(1):140-151.

SCIENCE

Red cell distribution width-to-albumin ratio is a predictor of survival in hepatitis B virus–associated decompensated cirrhosis

WeiLin Mao, MD,[1] ManChun Yuan, MD,[1] Xia He, MD,[2] Qiu Zhang, MD[2]

[1]Department of Clinical Laboratory, the First Affiliated Hospital, College of Medicine, Zhejiang University, Hangzhou, China, [2]Department of Clinical Laboratory, Shengzhou People's Hospital, Shengzhou Branch of the First Affiliated Hospital of Zhejiang University, Shengzhou, China. Corresponding author: Qiu Zhang; syzhonghua100@yeah.net

Key words: RAR; predictor; hepatitis B virus; decompensated cirrhosis; systemic inflammation; mortality

Abbreviations: RAR, red cell distribution width-to-albumin ratio; HBV, hepatitis B virus; DC, decompensated cirrhosis; RDW, red cell distribution width; BUN, blood urea nitrogen; INR, international normalized ratio; MELDS, Model For End-Stage Liver Disease score; ROC, receiver operating characteristic; AUC, area under the curve

Laboratory Medicine 2024;55:127-131; https://doi.org/10.1093/labmed/lmad048

ABSTRACT

Objective: The aim of this study was to ascertain whether red cell distribution width-to-albumin ratio (RAR) is associated with survival in hepatitis B virus (HBV)–associated decompensated cirrhosis (DC) patients.

Methods: A cohort of 167 patients with confirmed HBV-DC was enrolled in our study. Demographic characteristics and laboratory data were obtained. The main endpoint was mortality at 30 days. The receiver operating characteristic curve and multivariable regression analysis were used to assess the power of RAR for predicting prognosis.

Results: Mortality at 30 days was 11.4% (19/167). The RAR levels were higher in the nonsurvivors than the survivors, and elevated RAR levels were clearly associated with poor prognosis. Moreover, the predictive powers of RAR and Model for End-Stage Liver Disease score were not obviously different.

Conclusion: Our data indicate that RAR is a novel potential prognostic biomarker of mortality in HBV-DC.

Hepatitis B virus (HBV) infection is the most common cause of cirrhosis in Asian-Pacific countries.[1] Liver cirrhosis is a dynamic condition that changes from a compensated to a decompensated stage at a rate of 5% to 7% per year. The clinical outcome of decompensated cirrhosis (DC) is poor, with a 5-year survival of only 15%.[2–4] Liver transplantation can markedly improve the survival of patients with HBV-associated DC (HBV-DC), but its clinical application is not extensive because of a shortage of liver sources.[5,6] Therefore, finding novel effective and accurate biomarkers that can predict patient prognosis is of paramount importance to help clinicians to identify severe disease at an earlier stage, provide an optimal therapeutic strategy, and consequently reduce mortality in these patients.

Red cell distribution width (RDW) is widely applied as a parameter in the differential diagnosis of anemia. Currently, numerous studies have demonstrated its value as a diagnostic and prognostic indicator in various clinical conditions,[7–10] including liver diseases.[11] Serum albumin is synthesized in the liver, always shows a decrease with a decline in liver synthetic function, and represents one of the important indicators in the assessment of liver function. Therefore, we hypothesized that a combined assessment of RDW and albumin may provide more meaningful prognostic information for patients with liver diseases. In recent years, high RDW-to-albumin ratio (RAR) has emerged as a simple negative predictor for outcomes in patients with aortic aneurysm,[12] stroke,[13] burn surgery,[14] diabetic ketoacidosis,[15] and heart failure.[16] To the best of our knowledge, no studies to date have investigated the relationship between RAR and the outcomes of HBV-DC. Here, our research aimed to ascertain whether RAR is a reliable predictor for the prognosis of these patients.

Methods

Study Population

We retrospectively analyzed the data of HBV-DC patients who were treated in the Department of Hepatology at our hospital from March 2020 to September 2022. Decompensated cirrhosis was characterized by the development of clinical symptoms including ascites, gastrointestinal bleeding, encephalopathy, or hepatorenal syndrome.[3] All participants had persistent hepatitis B surface antigen for >6 months. We excluded patients who met the following criteria: (1) coinfection with other

viruses, (2) complication with other liver diseases, (3) hepatocellular carcinoma, (4) hematological diseases, and (5) age >75 or <18 years. The main study outcome was 30-day mortality. The research was carried out according to the Helsinki Declaration and approved by the Institutional Ethical Committee.

Data Extraction

Data for baseline clinical, demographic, and laboratory parameters were extracted from the electronic medical records, including total protein, albumin, age, gender, alanine transaminase, aspartate transaminase, blood urea nitrogen (BUN), total bilirubin, creatinine, international normalized ratio (INR), hemoglobin, platelets, and RDW in the first 24 hours. The RAR was calculated as RDW/albumin. Liver disease severity was assessed using the Model for End-Stage Liver Disease score (MELDS). The MELDS was calculated from the laboratory data using the following formula: MELDs = 3.8 × ln (total bilirubin) + 11.2 × ln (INR) + 9.6 × ln (creatinine) + 6.4.[17]

Statistical Analysis

Statistical analysis was conducted using SPSS 20 software and MedCalc 19.0.6 software. The significance level was $P < .05$. The variables were reported as median (range) or number. Comparisons between the survivors and nonsurvivors were analyzed using the χ^2 test and Mann–Whitney test. Correlations between RAR and MELDS were examined using Spearman's correlation. Prediction of poor 30-day survival was evaluated by logistic regression analysis. The predictive powers of RAR and MELDS were evaluated by receiver operating characteristic (ROC) curve to calculate the area under the curve (AUC). Survival analyses for 30-day mortality were performed by the Kaplan-Meier method.

Results

Population Characteristics

FIGURE 1 shows the detailed patient recruitment process. Based on the inclusion and exclusion criteria, 167 patients were included in the final selection. These patients comprised 132 males (79%) and 35 females (21%), with a median age of 54.0 years (range: 46.3 to 62.8 years). Many patients had more than 1 complication of DC, with the most frequent being ascites (75%), followed by variceal rebleeding (45%) and encephalopathy (11%). Median RAR was 5.38 (range, 4.58 to 6.63). A positive correlation was seen between RAR and MELDS ($r = 0.427$, $P = .001$).

FIGURE 1. Flow chart of enrolled participants. HBV-DC, hepatitis B virus–associated decompensated cirrhosis; HCV, hepatitis C virus.

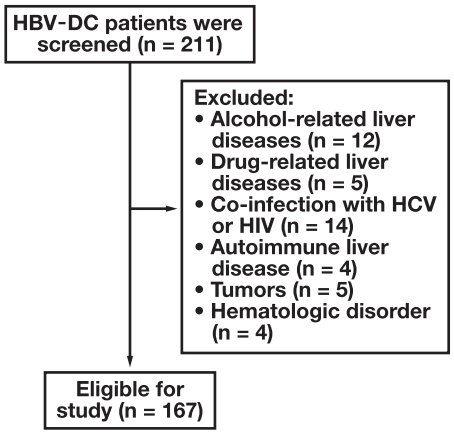

At the 30-day follow-up, 19 patients had died (11.4%). Patients were classified as survivors and nonsurvivors. Baseline clinical laboratory and demographic variable comparisons between survivors and nonsurvivors are given in **TABLE 1**. The nonsurvivors had higher RAR than the survivors (median: 7.02 [6.15-7.83] vs 5.30 [4.50-6.36], $P < .01$). In addition, RDW, creatinine, total bilirubin, INR, BUN, albumin, and MELDS also showed marked difference between the 2 groups ($P < .01$ for all).

Predictors for Mortality

We identified the potential risk factors for mortality in HBV-DC patients using univariate and multivariate analyses. Univariate analysis revealed that albumin, MELDS, RDW, and RAR were correlated with mortality. After adjustment for variables, we found that RAR and MELDS remained independent predictors for mortality (**TABLE 2**). In the ROC analysis, sensitivity was 63.2% and specificity was 87.2% when the MELDS cutoff value was 17.6. Meanwhile, sensitivity was 79.0% and specificity was 68.9% when the RAR cutoff value was 6.12 (**FIGURE 2**). The predictive powers of RAR and MELD score had similar discriminatory power to predict mortality, which is reflected by the similar AUROC (0.773 in RAR vs 0.830 in MELDs; $Z = 1.182$, $P = .237$). Furthermore, patients with RAR ≤6.12 had higher 30-day survival than patients with RAR >6.12 ($P < .001$; **FIGURE 3**).

Discussion

Due to the high mortality in HBV-DC patients, early and accurate prognostic indicators are of considerable importance to clinicians for the management of HBV-DC. Traditional scores for assessment of disease severity, such as the MELDS, are calculated using serum total bilirubin, creatinine, and INR, and are frequently used in such situations but may lack satisfactory accuracy for the prediction of short-term mortality.[18] This may arise because the MELDS does not incorporate some important factors (portal hypertension, ascites, nutritional status, inflammation) that can affect its prognostic performance.[19] The present work sought to determine whether RAR can be used as a useful marker of mortality in HBV-DC. Our data showed that the mortality group had higher RAR than the survival group and that RAR was significantly positively correlated with MELDS, suggesting that increased RAR may be closely linked with the prognosis of HBV-DC. A multivariate analysis further identified MELDS and RAR as independent predictive factors for worse survival, and the predictive power of MELDS was similar to that of RAR. Because the RAR assessment requires only 2 simple variables, it is more convenient than the MELDS for clinical applications. It is noteworthy that prior studies identified associations between some easy-to-perform noninvasive biomarkers and poor outcomes of end-stage liver disease, including INR-to-albumin ratio,[20] monocyte-to-high-density lipoprotein cholesterol ratio,[21] and hemoglobin-to-RDW ratio.[22] Our study suggests that RAR may similarly serve as a risk factor for HBV-DC.

Several factors were considered to explain the relationship between elevated RAR and worse outcome in HBV-DC. On the one hand, our data showed that RDW was obviously higher in the mortality group than in the survival group. Inflammatory response is considered to be a predictor for adverse outcomes in severe liver diseases.[23,24] Numerous studies have identified RDW as an indicator of chronic inflammation and it has

TABLE 1. Patient characteristics at baseline[a]

	All patients (n = 167)	Nonsurviving patients (n = 19)	Surviving patients (n = 148)	*P* value
Sex (female/male)	35/132	6/13	29/119	.363
Age (y)	54.0 (46.3-62.8)	60.0 (50.3-66.8)	53.0 (46.0-62.0)	.102
Total protein (g/dL)	6.15 (5.64-6.70)	5.64 (5.09-6.58)	6.16 (5.76-6.72)	.087
Albumin (g/dL)	3.11 (2.66-3.47)	2.86 (2.45-3.01)	3.15 (2.74-3.23)	.002
Alanine aminotransferase (U/L)	30.0 (17.0-50.3)	41.0 (25.3-59.3)	29.5 (17.0-49.5)	.145
Aspartate aminotransferase (U/L)	46.0 (28.0-74.0)	57.0 (39.5-133.5)	44.0 (28.0-72.3)	.062
Serum creatinine (μmol/L)	73.0 (60.3-85.8)	100.0 (67.8-124.0)	72.0 (59.5-83.5)	.002
Total bilirubin (μmol/L)	37.0 (18.0-96.0)	90.0 (55.0-239.0)	34.0 (17.0-83.5)	<.001
INR	1.33 (1.18-1.59)	1.63 (1.38-1.84)	1.31 (1.16-1.57)	.003
MELDS	11.4 (6.7-16.5)	18.4 (14.4-22.9)	10.6 (6.2-14.9)	<.001
Hemoglobin (g/L)	104.0 (86.0-120.8)	93.0 (77.8-110.3)	105.5 (86.0-121.0)	.111
Platelets ($\times 10^9$/L)	66.0 (43.0-114.8)	72.0 (54.3-171.3)	66.0 (42.5-113.0)	.416
BUN (mmol/L)	5.70 (4.25-7.55)	8.50 (7.10-14.70)	5.35 (4.10-7.20)	<.001
RDW (%)	16.0 (14.9-18.2)	19.2 (16.1-21.1)	15.9 (14.8-17.9)	.004
RAR	5.38 (4.58-6.63)	7.02 (6.15-7.83)	5.30 (4.50-6.36)	.001

[a]*Data are expressed as number or median (range).*
BUN, blood urea nitrogen; INR, international normalized ratio; MELDS, Model for End-Stage Liver Disease score; RAR, red cell distribution width-to-albumin ratio; RDW, red cell distribution width.

TABLE 2. Factors associated with mortality in HBV-DC patients identified by logistic regression analysis

	Univariate			Multivariate		
	Odds ratio	95% CI	*P*	Odds ratio	95% CI	*P* value
MELDS	1.230	1.121-1.351	<.001	1.215	1.098-1.346	<.001
BUN	1.004	0.988-1.021	.607			
Age	1.039	0.992-1.088	.102			
Albumin	0.876	0.798-0.961	.005			
RDW	1.282	1.106-1.485	.001			
RAR	1.825	1.343-2.481	<.001	1.604	1.144-2.249	.006

BUN, blood urea nitrogen; HBV-DC, hepatitis B virus–associated decompensated cirrhosis; MELDS, Model for End-Stage Liver Disease score; RAR, red cell distribution width-to-albumin ratio; RDW, red cell distribution width.

FIGURE 2. Receiver operating characteristic analyses to determine the prognostic value of Model for End-Stage Liver Disease score (MELDS) (AUC = 0.830) and red cell distribution width-to-albumin ratio (RAR) (AUC = 0.773) for hepatitis B virus–associated decompensated cirrhosis patients. AUC, area under the curve.

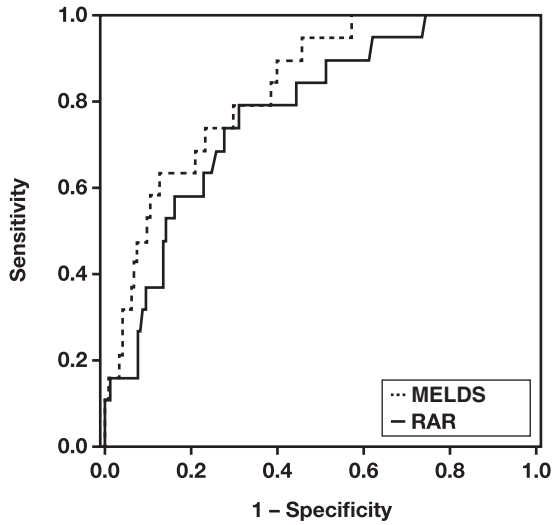

been related to the development and progression of various diseases. In terms of liver disease, abnormal RDW has been demonstrated to be associated with different disease states in HBV-infected patients. For instance, Lou et al[25] found that elevated RDW was linked with worse survival in HBV-infected patients, whereas Chen and colleagues[26] showed that RDW can act as an inexpensive and simple predictive indicator for hepatic fibrosis in chronic HBV infection. A recent study showed that RDW is an effective marker for evaluation of severity and outcomes of patients with HBV-associated diseases.[27] Multiple factors lead to increased RDW in liver disease. First, inflammation is a major contributor to elevated RDW, not only by impairing iron metabolism but also by altering erythropoietin function or shortening erythrocyte survival.[28] Second, liver cirrhosis renders patients susceptible to anemia, which can lead to unfavorable outcomes. Recently, Cai et al[29] identified hemoglobin level as a risk factor for clinical adverse outcomes in advanced liver disease. Our data found that hemoglobin was slightly lower in the mortality group than in the survival group, suggesting that the increased RDW may partly arise through an effect of anemia, as newer and larger reticulocytes may enter into the blood circulation. On the other hand, serum albumin levels were obviously lower in nonsurvivors than survivors. Albumin is considered an indicator for malnutrition inflammatory syndrome, and hypoalbuminemia is commonly observed in cirrhotic patients and associated with worse survival.[30,31] In our study,

FIGURE 3. Kaplan-Meier plots of survival probability according to red cell distribution width-to-albumin ratio (RAR) value ($P < .001$).

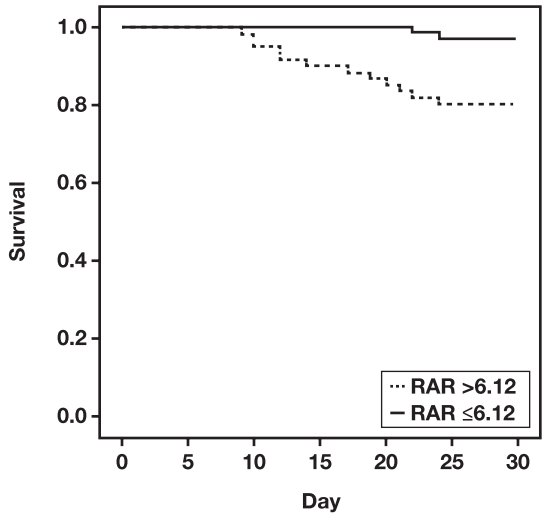

RDW and albumin were associated with mortality in the univariate analysis but not in the multivariate analysis. This may have occurred because RAR is a compound marker; it might provide more objective and comprehensive information about the development and progression of the disease and thus is more precise than each individual indicator alone. Furthermore, our data also indicated that HBV-DC patients with a high RAR had a higher rate of mortality, suggesting that abnormal RAR may reflect the inflammation, organ dysfunction, and nutritional status and may be sufficient to indicate the pathophysiological process of liver diseases, thereby making it a useful prognostic indicator for HBV-DC.

Conclusion

In summary, RAR is closely related to disease severity in HBV-DC and may serve as an inexpensive and readily available indicator to identify high-risk HBV-DC patients for mortality. However, the present research is a single center study and our findings warrant external validation.

Funding

This work was supported by grants from the Project of Department of Education of Zhejiang Province (Y201941475).

Conflict of Interest Disclosure

The authors have nothing to disclose.

REFERENCES

1. Xiao J, Wang F, Wong NK, et al. Global liver disease burdens and research trends: analysis from a Chinese perspective. *J Hepatol.* 2019;71:212–221. doi:10.1016/j.jhep.2019.03.004
2. Tsochatzis EA, Bosch J, Burroughs AK. Liver cirrhosis. *Lancet.* 2014;383:1749–1761. doi:10.1016/S0140-6736(14)60121-5
3. EASL Clinical Practice Guidelines for the management of patients with decompensated cirrhosis. *J Hepatol*. 2018;69:406–460.
4. D'Amico G. The clinical course of cirrhosis. Population based studies and the need of personalized medicine. *J Hepatol.* 2014;60:241–242.
5. Putignano A, Gustot T. New concepts in acute-on-chronic liver failure: implications for liver transplantation. *Liver Transpl.* 2017;23:234–243. doi:10.1002/lt.24654
6. Finkenstedt A, Nachbaur K, Zoller H, et al. Acute-on-chronic liver failure: excellent outcomes after liver transplantation but high mortality on the wait list. *Liver Transpl.* 2013;19:879–886. doi:10.1002/lt.23678
7. Salvagno GL, Sanchis-Gomar F, Picanza A, et al. Red blood cell distribution width: a simple parameter with multiple clinical applications. *Crit Rev Clin Lab Sci.* 2015;52:86–105. doi:10.3109/10408363.2014.992064
8. Chen L, Lu XY, Zhu CQ. Prognostic value of albumin red cell distribution width score in patients with severe community-acquired pneumonia. *Ann Palliat Med.* 2020;9:759–765. doi:10.21037/apm.2020.04.22
9. Xanthopoulos A, Giamouzis G, Melidonis A, et al. Red blood cell distribution width as a prognostic marker in patients with heart failure and diabetes mellitus. *Cardiovasc Diabetol.* 2017;16:81.
10. Kim CH, Park JT, Kim EJ, et al. An increase in red blood cell distribution width from baseline predicts mortality in patients with severe sepsis or septic shock. *Crit Care.* 2013;17:R282 (PMID: 24321201).
11. Mao W, Wu J. Haematologic indices in hepatitis B virus-related liver disease. *Clin Chim Acta.* 2020;500:135–142. doi:10.1016/j.cca.2019.10.007
12. Long J, Xie X, Xu D, et al. Association between red blood cell distribution width-to-albumin ratio and prognosis of patients with aortic aneurysms. *Int J Gen Med.* 2021;14:6287–6294. doi:10.2147/IJGM.S328035
13. Zhao N, Hu W, Wu Z, et al. The red blood cell distribution width-albumin ratio: a promising predictor of mortality in stroke patients. *Int J Gen Med.* 2021;14:3737–3747. doi:10.2147/IJGM.S322441
14. Seo YJ, Yu J, Park JY, et al. Red cell distribution width/albumin ratio and 90-day mortality after burn surgery. *Burns Trauma.* 2022;10:tkab050. doi:10.1093/burnst/tkab050
15. Zhou D, Wang J, Li X. The red blood cell distribution width-albumin ratio was a potential prognostic biomarker for diabetic ketoacidosis. *Int J Gen Med.* 2021;14:5375–5380. doi:10.2147/IJGM.S327733
16. Ni Q, Wang X, Wang J, et al. The red blood cell distribution width-albumin ratio: a promising predictor of mortality in heart failure patients—a cohort study. *Clin Chim Acta.* 2022;527:38–46. doi:10.1016/j.cca.2021.12.027
17. Freeman RB Jr, Wiesner RH, Harper A, et al; UNOS/OPTN Liver Disease Severity Score, UNOS/OPTN Liver and Intestine, and UNOS/OPTN Pediatric Transplantation Committees. The new liver allocation system: moving toward evidence-based transplantation policy. *Liver Transpl.* 2002;8:851–858. doi:10.1053/jlts.2002.35927
18. Targoński R, Sadowski J, Starek-Stelmaszczyk M, et al. Prognostic significance of red cell distribution width and its relation to increased pulmonary pressure and inflammation in acute heart failure. *Cardiol J.* 2020;27:394–403. doi:10.5603/CJ.a2018.0103
19. Stewart CA, Malinchoc M, Kim WR, et al. Hepatic encephalopathy as a predictor of survival in patients with end-stage liver disease. *Liver Transpl.* 2007;13:1366–1371. doi:10.1002/lt.21129
20. Cai M, Han Z, He X, et al. Usefulness of international normalized ratio to albumin ratio for evaluation of mortality in hepatitis B virus-associated decompensated cirrhosis. *Biomed Res Int.* 2021;2021:6664574. doi:10.1155/2021/6664574
21. Wu Q, Mao W. New prognostic factor for hepatitis B virus-related decompensated cirrhosis: ratio of monocytes to HDL-cholesterol. *J Clin Lab Anal.* 2021;35:e24007. doi:10.1002/jcla.24007
22. Yu Z, Zhang T, Shen J. Low hemoglobin-to-red cell distribution width ratio is associated with mortality in patients with HBV-related decompensated cirrhosis. *Biomed Res Int.* 2022;2022:5754790. doi:10.1155/2022/5754790
23. Behroozian R, Bayazidchi M, Rasooli J. Systemic inflammatory response syndrome and MELD score in hospital outcome of patients with liver cirrhosis. *Middle East J Dig Dis.* 2012;4:168–172.
24. Fernández J, Acevedo J, Wiest R, et al., European Foundation for the Study of Chronic Liver Failure. Bacterial and fungal infections

in acute-on-chronic liver failure: prevalence, characteristics and impact on prognosis. *Gut.* 2018;67:1870–1880. doi:10.1136/gutjnl-2017-314240

25. Lou Y, Wang M, Mao W. Clinical usefulness of measuring red blood cell distribution width in patients with hepatitis B. *PLoS One.* 2012;7:e37644.
26. Chen B, Ye B, Zhang J, et al. RDW to platelet ratio: a novel noninvasive index for predicting hepatic fibrosis and cirrhosis in chronic hepatitis B. *PLoS One.* 2013;8:e68780.
27. Wang J, Huang R, Yan X, et al. Red blood cell distribution width: a promising index for evaluating the severity and long-term prognosis of hepatitis B virus-related diseases. *Dig Liver Dis.* 2020;52:440–446. doi:10.1016/j.dld.2019.12.144
28. Markoulaki D, Kostikas K, Papatheodorou G, et al. Hemoglobin, erythropoietin and systemic inflammation in exacerbations of chronic obstructive pulmonary disease. *Eur J Intern Med.* 2011;22:103–107. doi:10.1016/j.ejim.2010.07.010
29. Cai M, Yang N, Lin S, et al. Anemia predicts poor outcomes in patients with HBV-related decompensated cirrhosis. *Clin Lab.* 2021;67.
30. Di Pascoli M, Fasolato S, Piano S, et al. Long-term administration of human albumin improves survival in patients with cirrhosis and refractory ascites. *Liver Int.* 2019;39:98–105. doi:10.1111/liv.13968
31. Bernardi M, Ricci CS, Zaccherini G. Role of human albumin in the management of complications of liver cirrhosis. *J Clin Exp Hepatol.* 2014;4:302–311. doi:10.1016/j.jceh.2014.08.007

SCIENCE

Red cell distribution width-to-albumin ratio is a predictor of survival in hepatitis B virus–associated decompensated cirrhosis

WeiLin Mao, MD,[1] ManChun Yuan, MD,[1] Xia He, MD,[2] Qiu Zhang, MD[2]

[1]Department of Clinical Laboratory, the First Affiliated Hospital, College of Medicine, Zhejiang University, Hangzhou, China, [2]Department of Clinical Laboratory, Shengzhou People's Hospital, Shengzhou Branch of the First Affiliated Hospital of Zhejiang University, Shengzhou, China. Corresponding author: Qiu Zhang; syzhonghua100@yeah.net

Key words: RAR; predictor; hepatitis B virus; decompensated cirrhosis; systemic inflammation; mortality

Abbreviations: RAR, red cell distribution width-to-albumin ratio; HBV, hepatitis B virus; DC, decompensated cirrhosis; RDW, red cell distribution width; BUN, blood urea nitrogen; INR, international normalized ratio; MELDS, Model For End-Stage Liver Disease score; ROC, receiver operating characteristic; AUC, area under the curve

Laboratory Medicine 2024;55:127-131; https://doi.org/10.1093/labmed/lmad048

ABSTRACT

Objective: The aim of this study was to ascertain whether red cell distribution width-to-albumin ratio (RAR) is associated with survival in hepatitis B virus (HBV)–associated decompensated cirrhosis (DC) patients.

Methods: A cohort of 167 patients with confirmed HBV-DC was enrolled in our study. Demographic characteristics and laboratory data were obtained. The main endpoint was mortality at 30 days. The receiver operating characteristic curve and multivariable regression analysis were used to assess the power of RAR for predicting prognosis.

Results: Mortality at 30 days was 11.4% (19/167). The RAR levels were higher in the nonsurvivors than the survivors, and elevated RAR levels were clearly associated with poor prognosis. Moreover, the predictive powers of RAR and Model for End-Stage Liver Disease score were not obviously different.

Conclusion: Our data indicate that RAR is a novel potential prognostic biomarker of mortality in HBV-DC.

Hepatitis B virus (HBV) infection is the most common cause of cirrhosis in Asian-Pacific countries.[1] Liver cirrhosis is a dynamic condition that changes from a compensated to a decompensated stage at a rate of 5% to 7% per year. The clinical outcome of decompensated cirrhosis (DC) is poor, with a 5-year survival of only 15%.[2–4] Liver transplantation can markedly improve the survival of patients with HBV-associated DC (HBV-DC), but its clinical application is not extensive because of a shortage of liver sources.[5,6] Therefore, finding novel effective and accurate biomarkers that can predict patient prognosis is of paramount importance to help clinicians to identify severe disease at an earlier stage, provide an optimal therapeutic strategy, and consequently reduce mortality in these patients.

Red cell distribution width (RDW) is widely applied as a parameter in the differential diagnosis of anemia. Currently, numerous studies have demonstrated its value as a diagnostic and prognostic indicator in various clinical conditions,[7–10] including liver diseases.[11] Serum albumin is synthesized in the liver, always shows a decrease with a decline in liver synthetic function, and represents one of the important indicators in the assessment of liver function. Therefore, we hypothesized that a combined assessment of RDW and albumin may provide more meaningful prognostic information for patients with liver diseases. In recent years, high RDW-to-albumin ratio (RAR) has emerged as a simple negative predictor for outcomes in patients with aortic aneurysm,[12] stroke,[13] burn surgery,[14] diabetic ketoacidosis,[15] and heart failure.[16] To the best of our knowledge, no studies to date have investigated the relationship between RAR and the outcomes of HBV-DC. Here, our research aimed to ascertain whether RAR is a reliable predictor for the prognosis of these patients.

Methods

Study Population

We retrospectively analyzed the data of HBV-DC patients who were treated in the Department of Hepatology at our hospital from March 2020 to September 2022. Decompensated cirrhosis was characterized by the development of clinical symptoms including ascites, gastrointestinal bleeding, encephalopathy, or hepatorenal syndrome.[3] All participants had persistent hepatitis B surface antigen for >6 months. We excluded patients who met the following criteria: (1) coinfection with other

viruses, (2) complication with other liver diseases, (3) hepatocellular carcinoma, (4) hematological diseases, and (5) age >75 or <18 years. The main study outcome was 30-day mortality. The research was carried out according to the Helsinki Declaration and approved by the Institutional Ethical Committee.

Data Extraction

Data for baseline clinical, demographic, and laboratory parameters were extracted from the electronic medical records, including total protein, albumin, age, gender, alanine transaminase, aspartate transaminase, blood urea nitrogen (BUN), total bilirubin, creatinine, international normalized ratio (INR), hemoglobin, platelets, and RDW in the first 24 hours. The RAR was calculated as RDW/albumin. Liver disease severity was assessed using the Model for End-Stage Liver Disease score (MELDS). The MELDS was calculated from the laboratory data using the following formula: MELDs = 3.8 × ln (total bilirubin) + 11.2 × ln (INR) + 9.6 × ln (creatinine) + 6.4.[17]

Statistical Analysis

Statistical analysis was conducted using SPSS 20 software and MedCalc 19.0.6 software. The significance level was $P < .05$. The variables were reported as median (range) or number. Comparisons between the survivors and nonsurvivors were analyzed using the χ^2 test and Mann–Whitney test. Correlations between RAR and MELDS were examined using Spearman's correlation. Prediction of poor 30-day survival was evaluated by logistic regression analysis. The predictive powers of RAR and MELDS were evaluated by receiver operating characteristic (ROC) curve to calculate the area under the curve (AUC). Survival analyses for 30-day mortality were performed by the Kaplan-Meier method.

Results

Population Characteristics

FIGURE 1 shows the detailed patient recruitment process. Based on the inclusion and exclusion criteria, 167 patients were included in the final selection. These patients comprised 132 males (79%) and 35 females (21%), with a median age of 54.0 years (range: 46.3 to 62.8 years). Many patients had more than 1 complication of DC, with the most frequent being ascites (75%), followed by variceal rebleeding (45%) and encephalopathy (11%). Median RAR was 5.38 (range, 4.58 to 6.63). A positive correlation was seen between RAR and MELDS ($r = 0.427$, $P = .001$).

FIGURE 1. Flow chart of enrolled participants. HBV-DC, hepatitis B virus–associated decompensated cirrhosis; HCV, hepatitis C virus.

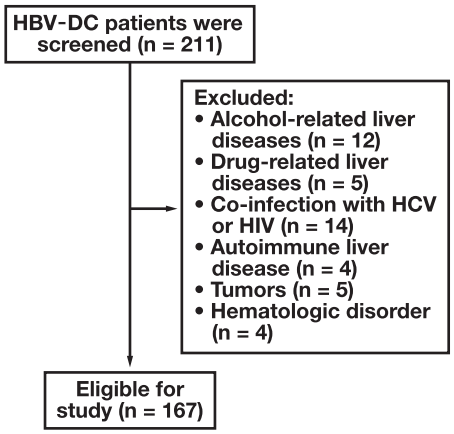

At the 30-day follow-up, 19 patients had died (11.4%). Patients were classified as survivors and nonsurvivors. Baseline clinical laboratory and demographic variable comparisons between survivors and nonsurvivors are given in **TABLE 1**. The nonsurvivors had higher RAR than the survivors (median: 7.02 [6.15-7.83] vs 5.30 [4.50-6.36], $P < .01$). In addition, RDW, creatinine, total bilirubin, INR, BUN, albumin, and MELDS also showed marked difference between the 2 groups ($P < .01$ for all).

Predictors for Mortality

We identified the potential risk factors for mortality in HBV-DC patients using univariate and multivariate analyses. Univariate analysis revealed that albumin, MELDS, RDW, and RAR were correlated with mortality. After adjustment for variables, we found that RAR and MELDS remained independent predictors for mortality (**TABLE 2**). In the ROC analysis, sensitivity was 63.2% and specificity was 87.2% when the MELDS cutoff value was 17.6. Meanwhile, sensitivity was 79.0% and specificity was 68.9% when the RAR cutoff value was 6.12 (**FIGURE 2**). The predictive powers of RAR and MELD score had similar discriminatory power to predict mortality, which is reflected by the similar AUROC (0.773 in RAR vs 0.830 in MELDs; $Z = 1.182$, $P = .237$). Furthermore, patients with RAR ≤6.12 had higher 30-day survival than patients with RAR >6.12 ($P < .001$; **FIGURE 3**).

Discussion

Due to the high mortality in HBV-DC patients, early and accurate prognostic indicators are of considerable importance to clinicians for the management of HBV-DC. Traditional scores for assessment of disease severity, such as the MELDS, are calculated using serum total bilirubin, creatinine, and INR, and are frequently used in such situations but may lack satisfactory accuracy for the prediction of short-term mortality.[18] This may arise because the MELDS does not incorporate some important factors (portal hypertension, ascites, nutritional status, inflammation) that can affect its prognostic performance.[19] The present work sought to determine whether RAR can be used as a useful marker of mortality in HBV-DC. Our data showed that the mortality group had higher RAR than the survival group and that RAR was significantly positively correlated with MELDS, suggesting that increased RAR may be closely linked with the prognosis of HBV-DC. A multivariate analysis further identified MELDS and RAR as independent predictive factors for worse survival, and the predictive power of MELDS was similar to that of RAR. Because the RAR assessment requires only 2 simple variables, it is more convenient than the MELDS for clinical applications. It is noteworthy that prior studies identified associations between some easy-to-perform noninvasive biomarkers and poor outcomes of end-stage liver disease, including INR-to-albumin ratio,[20] monocyte-to-high-density lipoprotein cholesterol ratio,[21] and hemoglobin-to-RDW ratio.[22] Our study suggests that RAR may similarly serve as a risk factor for HBV-DC.

Several factors were considered to explain the relationship between elevated RAR and worse outcome in HBV-DC. On the one hand, our data showed that RDW was obviously higher in the mortality group than in the survival group. Inflammatory response is considered to be a predictor for adverse outcomes in severe liver diseases.[23,24] Numerous studies have identified RDW as an indicator of chronic inflammation and it has

TABLE 1. Patient characteristics at baseline[a]

	All patients (n = 167)	Nonsurviving patients (n = 19)	Surviving patients (n = 148)	*P* value
Sex (female/male)	35/132	6/13	29/119	.363
Age (y)	54.0 (46.3-62.8)	60.0 (50.3-66.8)	53.0 (46.0-62.0)	.102
Total protein (g/dL)	6.15 (5.64-6.70)	5.64 (5.09-6.58)	6.16 (5.76-6.72)	.087
Albumin (g/dL)	3.11 (2.66-3.47)	2.86 (2.45-3.01)	3.15 (2.74-3.23)	.002
Alanine aminotransferase (U/L)	30.0 (17.0-50.3)	41.0 (25.3-59.3)	29.5 (17.0-49.5)	.145
Aspartate aminotransferase (U/L)	46.0 (28.0-74.0)	57.0 (39.5-133.5)	44.0 (28.0-72.3)	.062
Serum creatinine (μmol/L)	73.0 (60.3-85.8)	100.0 (67.8-124.0)	72.0 (59.5-83.5)	.002
Total bilirubin (μmol/L)	37.0 (18.0-96.0)	90.0 (55.0-239.0)	34.0 (17.0-83.5)	<.001
INR	1.33 (1.18-1.59)	1.63 (1.38-1.84)	1.31 (1.16-1.57)	.003
MELDS	11.4 (6.7-16.5)	18.4 (14.4-22.9)	10.6 (6.2-14.9)	<.001
Hemoglobin (g/L)	104.0 (86.0-120.8)	93.0 (77.8-110.3)	105.5 (86.0-121.0)	.111
Platelets ($\times 10^9$/L)	66.0 (43.0-114.8)	72.0 (54.3-171.3)	66.0 (42.5-113.0)	.416
BUN (mmol/L)	5.70 (4.25-7.55)	8.50 (7.10-14.70)	5.35 (4.10-7.20)	<.001
RDW (%)	16.0 (14.9-18.2)	19.2 (16.1-21.1)	15.9 (14.8-17.9)	.004
RAR	5.38 (4.58-6.63)	7.02 (6.15-7.83)	5.30 (4.50-6.36)	.001

[a]*Data are expressed as number or median (range).*
BUN, blood urea nitrogen; INR, international normalized ratio; MELDS, Model for End-Stage Liver Disease score; RAR, red cell distribution width-to-albumin ratio; RDW, red cell distribution width.

TABLE 2. Factors associated with mortality in HBV-DC patients identified by logistic regression analysis

	Univariate			Multivariate		
	Odds ratio	95% CI	*P*	Odds ratio	95% CI	*P* value
MELDS	1.230	1.121-1.351	<.001	1.215	1.098-1.346	<.001
BUN	1.004	0.988-1.021	.607			
Age	1.039	0.992-1.088	.102			
Albumin	0.876	0.798-0.961	.005			
RDW	1.282	1.106-1.485	.001			
RAR	1.825	1.343-2.481	<.001	1.604	1.144-2.249	.006

BUN, blood urea nitrogen; HBV-DC, hepatitis B virus–associated decompensated cirrhosis; MELDS, Model for End-Stage Liver Disease score; RAR, red cell distribution width-to-albumin ratio; RDW, red cell distribution width.

FIGURE 2. Receiver operating characteristic analyses to determine the prognostic value of Model for End-Stage Liver Disease score (MELDS) (AUC = 0.830) and red cell distribution width-to-albumin ratio (RAR) (AUC = 0.773) for hepatitis B virus–associated decompensated cirrhosis patients. AUC, area under the curve.

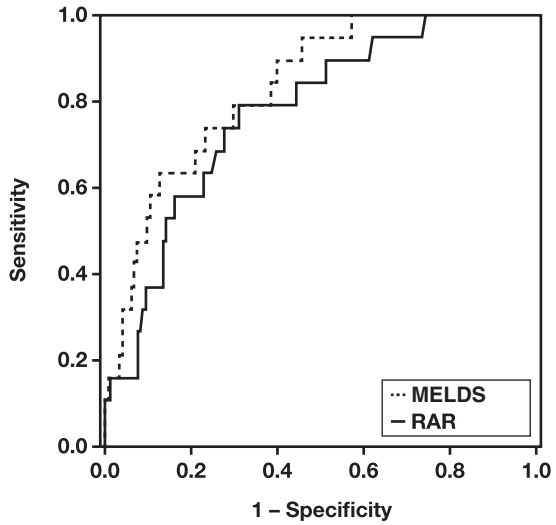

been related to the development and progression of various diseases. In terms of liver disease, abnormal RDW has been demonstrated to be associated with different disease states in HBV-infected patients. For instance, Lou et al[25] found that elevated RDW was linked with worse survival in HBV-infected patients, whereas Chen and colleagues[26] showed that RDW can act as an inexpensive and simple predictive indicator for hepatic fibrosis in chronic HBV infection. A recent study showed that RDW is an effective marker for evaluation of severity and outcomes of patients with HBV-associated diseases.[27] Multiple factors lead to increased RDW in liver disease. First, inflammation is a major contributor to elevated RDW, not only by impairing iron metabolism but also by altering erythropoietin function or shortening erythrocyte survival.[28] Second, liver cirrhosis renders patients susceptible to anemia, which can lead to unfavorable outcomes. Recently, Cai et al[29] identified hemoglobin level as a risk factor for clinical adverse outcomes in advanced liver disease. Our data found that hemoglobin was slightly lower in the mortality group than in the survival group, suggesting that the increased RDW may partly arise through an effect of anemia, as newer and larger reticulocytes may enter into the blood circulation. On the other hand, serum albumin levels were obviously lower in nonsurvivors than survivors. Albumin is considered an indicator for malnutrition inflammatory syndrome, and hypoalbuminemia is commonly observed in cirrhotic patients and associated with worse survival.[30,31] In our study,

FIGURE 3. Kaplan-Meier plots of survival probability according to red cell distribution width-to-albumin ratio (RAR) value ($P < .001$).

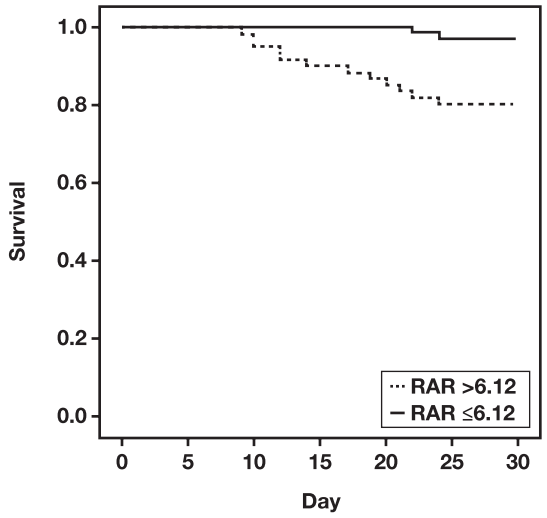

RDW and albumin were associated with mortality in the univariate analysis but not in the multivariate analysis. This may have occurred because RAR is a compound marker; it might provide more objective and comprehensive information about the development and progression of the disease and thus is more precise than each individual indicator alone. Furthermore, our data also indicated that HBV-DC patients with a high RAR had a higher rate of mortality, suggesting that abnormal RAR may reflect the inflammation, organ dysfunction, and nutritional status and may be sufficient to indicate the pathophysiological process of liver diseases, thereby making it a useful prognostic indicator for HBV-DC.

Conclusion

In summary, RAR is closely related to disease severity in HBV-DC and may serve as an inexpensive and readily available indicator to identify high-risk HBV-DC patients for mortality. However, the present research is a single center study and our findings warrant external validation.

Funding

This work was supported by grants from the Project of Department of Education of Zhejiang Province (Y201941475).

Conflict of Interest Disclosure

The authors have nothing to disclose.

REFERENCES

1. Xiao J, Wang F, Wong NK, et al. Global liver disease burdens and research trends: analysis from a Chinese perspective. *J Hepatol.* 2019;71:212–221. doi:10.1016/j.jhep.2019.03.004
2. Tsochatzis EA, Bosch J, Burroughs AK. Liver cirrhosis. *Lancet.* 2014;383:1749–1761. doi:10.1016/S0140-6736(14)60121-5
3. EASL Clinical Practice Guidelines for the management of patients with decompensated cirrhosis. *J Hepatol*. 2018;69:406–460.
4. D'Amico G. The clinical course of cirrhosis. Population based studies and the need of personalized medicine. *J Hepatol.* 2014;60:241–242.
5. Putignano A, Gustot T. New concepts in acute-on-chronic liver failure: implications for liver transplantation. *Liver Transpl.* 2017;23:234–243. doi:10.1002/lt.24654
6. Finkenstedt A, Nachbaur K, Zoller H, et al. Acute-on-chronic liver failure: excellent outcomes after liver transplantation but high mortality on the wait list. *Liver Transpl.* 2013;19:879–886. doi:10.1002/lt.23678
7. Salvagno GL, Sanchis-Gomar F, Picanza A, et al. Red blood cell distribution width: a simple parameter with multiple clinical applications. *Crit Rev Clin Lab Sci.* 2015;52:86–105. doi:10.3109/10408363.2014.992064
8. Chen L, Lu XY, Zhu CQ. Prognostic value of albumin red cell distribution width score in patients with severe community-acquired pneumonia. *Ann Palliat Med.* 2020;9:759–765. doi:10.21037/apm.2020.04.22
9. Xanthopoulos A, Giamouzis G, Melidonis A, et al. Red blood cell distribution width as a prognostic marker in patients with heart failure and diabetes mellitus. *Cardiovasc Diabetol.* 2017;16:81.
10. Kim CH, Park JT, Kim EJ, et al. An increase in red blood cell distribution width from baseline predicts mortality in patients with severe sepsis or septic shock. *Crit Care.* 2013;17:R282 (PMID: 24321201).
11. Mao W, Wu J. Haematologic indices in hepatitis B virus-related liver disease. *Clin Chim Acta.* 2020;500:135–142. doi:10.1016/j.cca.2019.10.007
12. Long J, Xie X, Xu D, et al. Association between red blood cell distribution width-to-albumin ratio and prognosis of patients with aortic aneurysms. *Int J Gen Med.* 2021;14:6287–6294. doi:10.2147/IJGM.S328035
13. Zhao N, Hu W, Wu Z, et al. The red blood cell distribution width-albumin ratio: a promising predictor of mortality in stroke patients. *Int J Gen Med.* 2021;14:3737–3747. doi:10.2147/IJGM.S322441
14. Seo YJ, Yu J, Park JY, et al. Red cell distribution width/albumin ratio and 90-day mortality after burn surgery. *Burns Trauma.* 2022;10:tkab050. doi:10.1093/burnst/tkab050
15. Zhou D, Wang J, Li X. The red blood cell distribution width-albumin ratio was a potential prognostic biomarker for diabetic ketoacidosis. *Int J Gen Med.* 2021;14:5375–5380. doi:10.2147/IJGM.S327733
16. Ni Q, Wang X, Wang J, et al. The red blood cell distribution width-albumin ratio: a promising predictor of mortality in heart failure patients—a cohort study. *Clin Chim Acta.* 2022;527:38–46. doi:10.1016/j.cca.2021.12.027
17. Freeman RB Jr, Wiesner RH, Harper A, et al; UNOS/OPTN Liver Disease Severity Score, UNOS/OPTN Liver and Intestine, and UNOS/OPTN Pediatric Transplantation Committees. The new liver allocation system: moving toward evidence-based transplantation policy. *Liver Transpl.* 2002;8:851–858. doi:10.1053/jlts.2002.35927
18. Targoński R, Sadowski J, Starek-Stelmaszczyk M, et al. Prognostic significance of red cell distribution width and its relation to increased pulmonary pressure and inflammation in acute heart failure. *Cardiol J.* 2020;27:394–403. doi:10.5603/CJ.a2018.0103
19. Stewart CA, Malinchoc M, Kim WR, et al. Hepatic encephalopathy as a predictor of survival in patients with end-stage liver disease. *Liver Transpl.* 2007;13:1366–1371. doi:10.1002/lt.21129
20. Cai M, Han Z, He X, et al. Usefulness of international normalized ratio to albumin ratio for evaluation of mortality in hepatitis B virus-associated decompensated cirrhosis. *Biomed Res Int.* 2021;2021:6664574. doi:10.1155/2021/6664574
21. Wu Q, Mao W. New prognostic factor for hepatitis B virus-related decompensated cirrhosis: ratio of monocytes to HDL-cholesterol. *J Clin Lab Anal.* 2021;35:e24007. doi:10.1002/jcla.24007
22. Yu Z, Zhang T, Shen J. Low hemoglobin-to-red cell distribution width ratio is associated with mortality in patients with HBV-related decompensated cirrhosis. *Biomed Res Int.* 2022;2022:5754790. doi:10.1155/2022/5754790
23. Behroozian R, Bayazidchi M, Rasooli J. Systemic inflammatory response syndrome and MELD score in hospital outcome of patients with liver cirrhosis. *Middle East J Dig Dis.* 2012;4:168–172.
24. Fernández J, Acevedo J, Wiest R, et al., European Foundation for the Study of Chronic Liver Failure. Bacterial and fungal infections

in acute-on-chronic liver failure: prevalence, characteristics and impact on prognosis. *Gut.* 2018;67:1870–1880. doi:10.1136/gutjnl-2017-314240

25. Lou Y, Wang M, Mao W. Clinical usefulness of measuring red blood cell distribution width in patients with hepatitis B. *PLoS One.* 2012;7:e37644.
26. Chen B, Ye B, Zhang J, et al. RDW to platelet ratio: a novel noninvasive index for predicting hepatic fibrosis and cirrhosis in chronic hepatitis B. *PLoS One.* 2013;8:e68780.
27. Wang J, Huang R, Yan X, et al. Red blood cell distribution width: a promising index for evaluating the severity and long-term prognosis of hepatitis B virus-related diseases. *Dig Liver Dis.* 2020;52:440–446. doi:10.1016/j.dld.2019.12.144
28. Markoulaki D, Kostikas K, Papatheodorou G, et al. Hemoglobin, erythropoietin and systemic inflammation in exacerbations of chronic obstructive pulmonary disease. *Eur J Intern Med.* 2011;22:103–107. doi:10.1016/j.ejim.2010.07.010
29. Cai M, Yang N, Lin S, et al. Anemia predicts poor outcomes in patients with HBV-related decompensated cirrhosis. *Clin Lab.* 2021;67.
30. Di Pascoli M, Fasolato S, Piano S, et al. Long-term administration of human albumin improves survival in patients with cirrhosis and refractory ascites. *Liver Int.* 2019;39:98–105. doi:10.1111/liv.13968
31. Bernardi M, Ricci CS, Zaccherini G. Role of human albumin in the management of complications of liver cirrhosis. *J Clin Exp Hepatol.* 2014;4:302–311. doi:10.1016/j.jceh.2014.08.007

Comparison of Sampson and extended Martin/Hopkins methods of low-density lipoprotein cholesterol calculations with direct measurement in pediatric patients with hypertriglyceridemia

S.M. Touhidul Islam, PhD[1], Alagar R. Muthukumar, PhD[1], Patricia Mary Jones, PhD[1,2], Ibrahim Hashim, PhD[1], Jing Cao, PhD[1,2]

[1]University of Texas Southwestern Medical Center, Dallas, TX, US, [2]Children's Health Dallas, TX, US. Corresponding author: Jing Cao; jing.cao2@utsouthwestern.edu

Key words: low-density lipoprotein cholesterol; cardiovascular diseases; LDL-C direct measurement; LDL-C calculation; hypertriglyceridemia; pediatric patients

Abbreviations: LDL-C, low-density lipoprotein cholesterol; TG, triglycerides; CVD, cardiovascular diseases; TC, total cholesterol; HDL-C, high-density lipoprotein cholesterol; VLDL-C, very low-density lipoprotein cholesterol; AACC-LVDD, American Association for Clinical Chemistry-Lipoprotein and Vascular Disease Division.

Laboratory Medicine 2024;55:140-144; https://doi.org/10.1093/labmed/lmad047

ABSTRACT

Objective: The Friedewald equation is the commonly used method of low-density lipoprotein cholesterol (LDL-C) calculation, requiring reflex to direct LDL-C measurement when triglycerides (TG) ≥ 400 mg/dL. Recently formulated Sampson and extended Martin/Hopkins methods have been validated with TG up to 800 mg/dL and thus have the potential to replace direct LDL-C measurement. Given the growing prevalence of childhood dyslipidemia, the objective of this study was to compare Sampson and extended Martin/Hopkins methods of LDL-C calculation with the direct measurement in a pediatric cohort with 400 ≤ TG ≤ 799 mg/dL.

Methods: This study retrieved standard lipid panels and corresponding direct LDL-C measurements of 131 patients with 400 ≤ TG ≤ 799 mg/dL from a pediatric population. Following the application of Sampson and extended Martin/Hopkins calculations, calculated values were compared with direct LDL-C measurements using ordinary least squares linear regression analysis and bias plotting.

Results: Both Sampson and extended Martin/Hopkins LDL-C calculations exhibited a strong correlation with the direct measurements (Pearson r = 0.89) in patients with 400 ≤ TG ≤ 800 mg/dL. Average percentages of bias of 45% and 21% were found between the direct LDL-C measurements and Sampson or extended Martin/Hopkins calculations, respectively.

Conclusion: Both Sampson and extended Martin/Hopkins calculations are applicable as clinical alternatives of direct LDL-C measurement in pediatric patients given 400 ≤ TG ≤ 799 mg/dL.

Low-density lipoprotein cholesterol (LDL-C) is the dominant lipid component of LDL, one of the 5 major classes of circulating lipoprotein particles. Due to the well-established connection between LDL-C and the pathogenesis of atherosclerosis, accurate measurement of LDL-C concentration is essential in directing the prevention and management strategies for treatment of cardiovascular diseases (CVD).[1] Currently, there are 2 available methods of LDL-C measurement in a clinical laboratory setting: calculation and direct measurement methods.[2] Traditionally, LDL-C is calculated from standard lipid panel (total cholesterol [TC], high-density lipoprotein cholesterol [HDL-C], and triglycerides [TG]) using the Friedewald equation (LDL-C = [TC] – [HDL-C] – [TG/5]).[3] The principal source of errors in LDL-C calculation, TG/5, serves as an estimate of very low-density lipoprotein cholesterol (VLDL-C) where the ratio of TG to VLDL-C (= 5) remains fixed. In 2013, Martin et al[4] at Johns Hopkins University formulated an equation that replaces the fixed TG denominator of 5 used in the Friedewald equation with an empirical denominator that varies depending on a TG and non–HDL-C strata (180 cells). The Martin/Hopkins calculation of LDL-C was validated against vertical density gradient ultracentrifugation. According to a recent survey conducted by the American Association for Clinical Chemistry-Lipoprotein and Vascular Disease Division (AACC-LVDD), it is a common practice to report a calculated value of LDL-C concentration instead of direct measurement to avoid the extra cost and turnaround time of adding direct LDL-C to the lipid panel.[5] However, none of the Friedewald and Martin LDL-C calculations is valid when TG ≥ 400 mg/dL.[6] Therefore, the custom is to reflex to direct measurement when TG ≥ 400 mg/dL. Recently, 2 new methods of LDL-C calculation have been formulated with promising accuracy

when TG ≥ 400 mg/dL. In 2020, Sampson et al[6] formulated an equation (LDL-C = (TC/0.948) – (HDL-C/0.971) – ([TG/8.56] + [TG*non–HDL-C/2140] – [TG squared/16,100]) – 9.44), which was developed using multiple least-squares regression for VLDL-C estimation with a TG term divided by a fixed factor. It was proposed to extend LDL-C calculation to triglyceride levels of 800 mg/dL and validated against the reference LDL-C beta-quantitation method. More recently, an extended Martin/Hopkins equation was validated for LDL-C up to 800 mg/dL using a delimited empirical table. These empirical 2-dimensional tables consist of 240, 560, or 1040 cells, where each cell represent a certain median ratio of TG to VLDL-C based on the varying values of TG and non–HDL-C strata.[6] Therefore, extended Martin/Hopkins equation uses an adaptable ratio of TG to VLDL-C instead of a fixed term as used in the Friedewald or Sampson equations. The AACC-LVDD survey revealed that only a few reference laboratories in the United States have adopted alternative LDL-C calculations, whereas the majority of hospital-based laboratories continue to use the Friedewald calculation and reflex to direct LDL-C measurement in cases when TG ≥ 400 mg/dL.[5]

Cholesterol and lipid testing is recommended in children that may identify early onset of genetic lipid disorders and obesity-related dyslipidemias. Early identification of dyslipidemia is important for initiating early treatment to reduce the risk of developing CVD. In 2011, the National Heart, Lung, and Blood Institute published guidelines recommending universal cholesterol (including LDL-C) screening in children.[7] Although validated against the reference method and Friedewald calculation in adult patients,[6,8] no studies have evaluated the performance of Sampson and extended Martin/Hopkins calculations in relation to the direct LDL-C measurement in pediatric patients with hypertriglyceridemia. Therefore, in this study, we performed a comparative assessment of LDL-C measurement between Sampson or extended Martin/Hopkins calculations and direct tests in pediatric patients with 400 ≤ TG ≤ 799 mg/dL.

Materials and Methods

Study Design

In this study, a group of standard lipid panels and corresponding direct LDL-C results (tested on Atellica, Siemens Healthineers) were randomly retrieved from a pediatric patient population of Children's Health Dallas over a 2-year period with 400 ≤ TG ≤ 799 mg/dL or TG < 400 mg/dL. Sampson and extended Martin/Hopkins calculations were performed and compared with direct LDL-C measurements. Ordinary least squares linear regression was performed to test how different estimations of LDL-C are correlated when TG concentrations are delimited within 400 and 799 mg/dL. Bias of direct measurements were plotted against Sampson or extended Martin/Hopkins estimations to test how close direct measurements were to calculations. A total of 131 pediatric patients' data were used in this study.

Statistics

Significance of difference between the groups was determined by 1-way analysis of variance (ANOVA) followed by Tukey's post hoc test. Statistical mean of different methods, mean difference with direct measurements, Pearson *r* value, slope, y-intercept, and x-intercept were determined. Statistical significance was chosen at a *P* value less than .05. Statistical analyses were performed using GraphPad PRISM version 8.

Results

Sampson and Extended Martin/Hopkins Calculations Demonstrated Closer Values of LDL-C Measurements to Direct Method

When TG < 400 mg/dL, Friedewald, Sampson, and Martin calculations showed similar cumulative and average values of LDL-C to the direct method. When 400 ≤ TG ≤ 799 mg/dL, Sampson and extended Martin/Hopkins calculations showed closer values of cumulative and average LDL-C measurements to the direct method. Friedewald calculation showed significantly decreased values of cumulative and average LDL-C measurements compared with Sampson and extended Martin/Hopkins LDL-C calculations. Of note, extended Martin/Hopkins calculation exhibited higher values of cumulative and average LDL-C measurements than the Sampson calculation. Therefore, extended Martin/Hopkins calculation exhibited closer values of cumulative and average LDL-C measurements to the direct method compared with the Sampson calculation (**FIGURE 1** and **TABLE 1**).

Sampson and Extended Martin/Hopkins Calculations Strongly Correlated With Direct Measurement

Correlation regression analyses were performed to compare the lines of best-fit among different measurement methods. When TG < 400 mg/dL, Friedewald, Sampson, and Martin calculations showed similar correlation with direct measurement (*r* = 0.96, 0.96, and 0.93, respectively; slope: 0.84) (**FIGURE 2A** and **TABLE 1**). When 400 ≤ TG ≤ 799 mg/dL, both Sampson and extended Martin/Hopkins LDL-C calculations exhibited a significant correlation of equal level with the direct measurement (*r* = 0.89 [0.84 to 0.92 at 95% CI]; *P* < .0001). Extended Martin/Hopkins calculation displayed a better best-fit to direct measurement as compared with that of Sampson calculation (slope: 0.9439 and 0.9093; y-intercept: 3.1 and 17.8; x-intercept: 3.3 and 19.6, respectively, for extended Martin/Hopkins and Sampson methods). It is noteworthy that Friedewald calculation showed a very different correlation with the direct method (slope: 1.116; y-intercept: -61.29; x-intercept: 54.93) (**FIGURE 2A** and **TABLE 1**).

Sampson and Extended Martin/Hopkins Calculations Displayed Reduced Percentages of Bias With Direct Measurement

When TG < 400 mg/dL, mean values of Friedewald, Sampson, and Martin LDL-C calculations were similar (98.97, 101.8, and 102.9 mg/dL, respectively). Percentages of bias displayed by Friedewald, Sampson, and Martin LDL-C calculations with the direct method were also very similar (28.54%, 23.91%, and 22.33%, respectively) (**TABLE 1**). When 400 ≤ TG ≤ 799 mg/dL, Sampson and extended Martin/Hopkins LDL-C calculations were closer to direct measurement (128.3, 81.84, 98.8, and 118 mg/dL for direct, Friedewald, Sampson, and Martin LDL-C calculations, respectively). Sampson and extended Martin/Hopkins calculations showed percentages of bias of 45% and 21%, respectively, with direct measurement (**FIGURE 2C** and **2D**, **TABLE 1**). Because different Food and Drug Administration–cleared direct LDL-C methods previously reported a bias between 13% and 46% when compared with the beta-quantification reference method, currently observed biases of Sampson and extended Martin/Hopkins calculations with the direct measurement are presumable.[9] Percentage of bias displayed by extended Martin/Hopkins calculation was

FIGURE 1. Graphical representation of cumulative (A and C) and average (B and D) low-density lipoprotein cholesterol (LDL-C) measurements by direct, Friedewald, Sampson, and extended Martin/Hopkins methods when triglycerides (TG) < 400 mg/dL (A and B) and when 400 ≤ TG ≤ 800 mg/dL (C and D) using column bar or box violin. a, b, and c indicate significant differences from direct, Friedewald, and Sampson methods, respectively, when $P \leq .05$. ns, not significant.

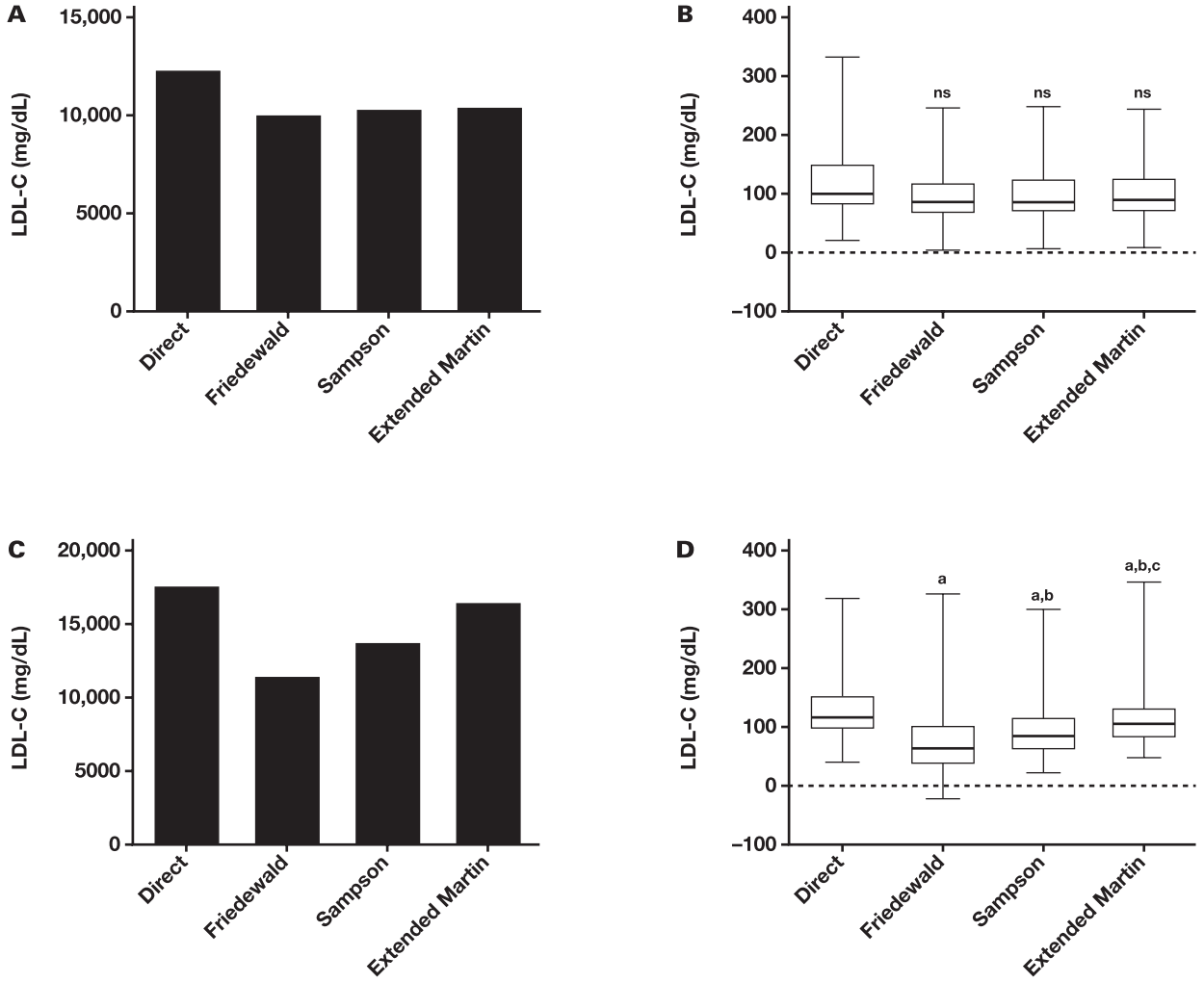

TABLE 1. Results of one-way ANOVA and linear regression analyses

TG level (mg/dL)	One-way ANOVA	Mean (mg/dL)	Mean difference (mg/dL)	Percent bias (%)	Pearson *r*	Regression slope	x-Intercept	y-Intercept
TG < 400	Direct vs Friedewald	121.1 vs 98.97	22.42	28.54	0.9583	0.8407	3.667	–3.083
	Direct vs Sampson	121.1 vs 101.8	19.62	23.91	0.9609	0.8384	0.003	–0.003
	Direct vs extended Martin	121.1 vs 102.9	18.48	22.33	0.9277	0.8375	–1.497	1.254
400 ≤ TG ≤ 799	Direct vs Friedewald	128.3 vs 81.84	46.44 $P < .0001$	196.52	0.8870 $P < .0001$	1.116	54.93	–61.29
	Direct vs Sampson	128.3 vs 98.79	29.48 $P < .0001$	45	0.8898 $P < .0001$	0.9093	19.62	–17.84
	Direct vs extended Martin	128.3 vs 118.0	10.29 $P < .0001$	21	0.8872 $P < .0001$	0.9439	3.28	–3.10

ANOVA, analysis of variance.

significantly less than the percentage of bias displayed by Sampson calculation ($P < .0001$). This demonstrates a better closeness of agreement between extended Martin/Hopkins calculation and direct measurement as compared with that between Sampson calculation and direct measurement. Of note, Friedewald calculation exhibited a percentage of bias of 196.52% with the direct method, which clearly shows the inapplicability of Friedewald LDL-C calculation when TG level is more than 400 mg/dL (**TABLE 1**).

FIGURE 2. Ordinary least squares regression analysis of Friedewald, Sampson, and extended Martin/Hopkins calculations with direct low-density lipoprotein cholesterol (LDL-C) measurement when 400 ≤ TG ≤ 800 mg/dL (A). Absolute bias plot of direct LDL-C measurements against Friedewald, Sampson, and extended Martin/Hopkins calculations when 400 ≤ TG ≤ 800 mg/dL (B-D). TG, triglycerides.

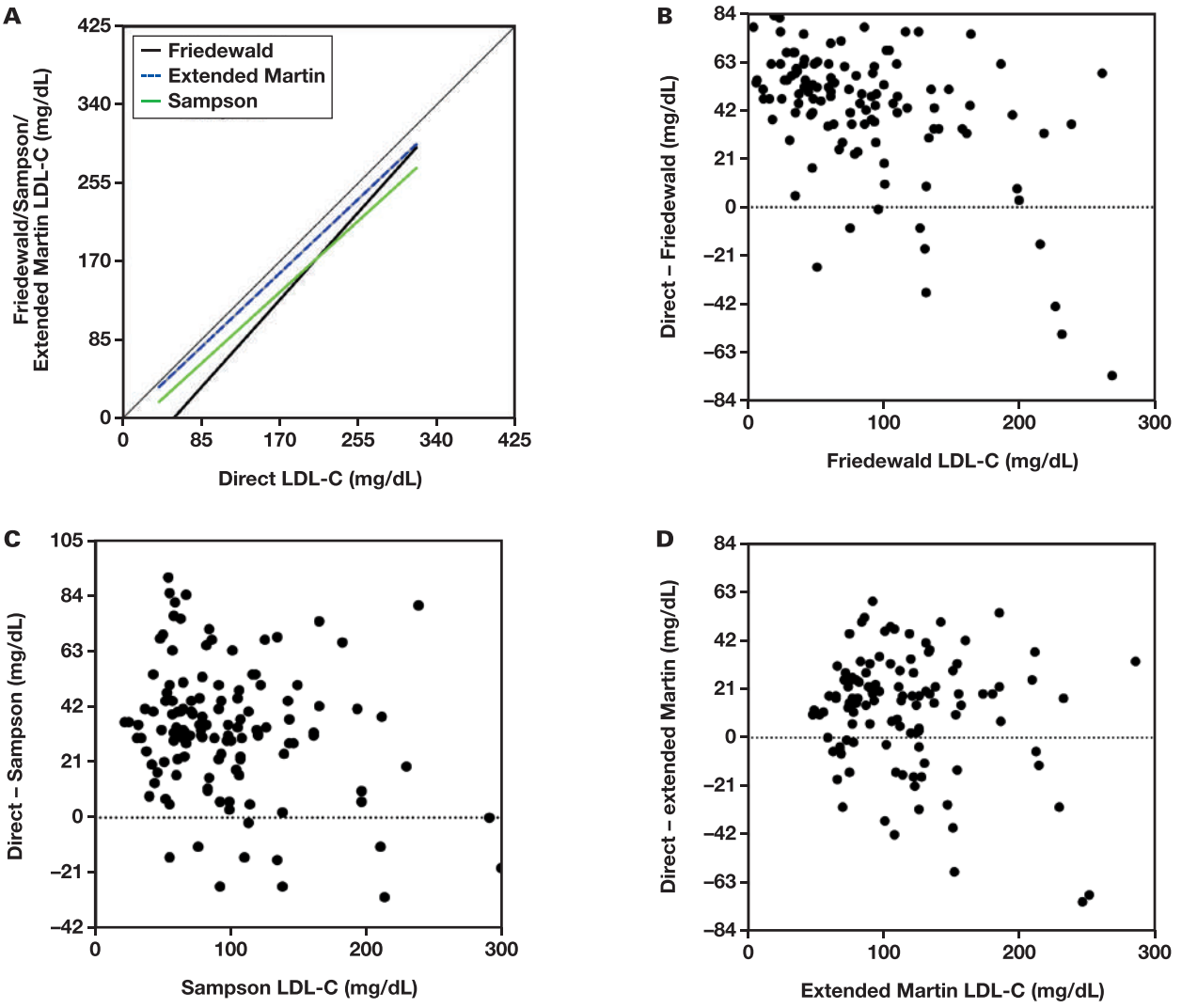

Discussion

Both genetic and acquired factors and a combination of the 2 contribute to hypertriglyceridemia. With the growing prevalence of obesity and metabolic syndrome, hypertriglyceridemia is increasingly identified in pediatric patients.[10,11] In addition to hypertriglyceridemia, elevated level of LDL-C is also an essential indicator for prevention, treatment, and monitoring of cardiovascular diseases. Although TG level is a component of basic lipid panel, measurement of LDL-C is heavily dependent on calculation or direct methods. Considering cost and turnaround time, calculation of LDL-C is preferred over direct measurement. Friedewald remains the mainstay of LDL-C calculation methods while the validity of calculation rests on the assumptions that the subject must be fasting and TG level must be <400 mg/dL.[3] Fasting condition and TG < 400 mg/dL eliminates the possibility of a higher ratio of TG to cholesterol. When TG ≥ 400 mg/dL, LDL-C calculation is underestimated. Therefore, reflex to direct LDL-C measurement is a common practice in clinical laboratories at TG ≥ 400 mg/dL. Sampson calculation of LDL-C is similar to Friedewald calculation in terms of subtracting VLDL-C and HDL-C from the total concentration of cholesterol. Additionally, the Sampson equation includes an intercept and allows the coefficients to vary for each term, which made this equation a better fit with the beta-quantification reference method than the Friedewald equation.[6] Extended Martin/Hopkins calculation is a modified version of Martin/Hopkins calculation. Extended Martin/Hopkins calculation was validated against vertical density gradient ultracentrifugation for LDL-C up to 800 mg/dL using an empirically defined table of 240 cells of median ratios of TG to VLDL-C based on the varying number of TG and non–HDL-C strata.[8] Our study demonstrated a significant correlation of Sampson and extended Martin/Hopkins calculations as compared to direct measurement given 400 ≤ TG ≤ 800 mg/dL,

whereas the extended Martin/Hopkins method exhibited a better best-fit than the Sampson method. Therefore, we suggest both Sampson and extended Martin/Hopkins calculations as alternatives to direct measurement of LDL-C when 400 ≤ TG ≤ 800 mg/dL with a preference for the extended Martin/Hopkins method. Fasting mainly affects TG and therefore is not mandatory for lipid panel screening tests or cholesterol-related congenital dyslipidemia assessment. With more practice of nonfasting lipid testing, more patients' results fall into the range of 400 ≤ TG ≤ 799 mg/dL that our comparison is applicable to. In addition to hypertriglyceridemia, low concentration of LDL-C is also a restricting factor of using the Friedewald calculation. In patients with low concentrations of LDL-C, the Friedewald calculation tends to underestimate LDL-C. In one-fifth of the cases of LDL-C concentrations that are less than 70 mg/dL, the Friedewald calculation underestimates LDL-C concentrations when compared with the measurements obtained using ultracentrifugation or beta-quantification. This discordance is most prevalent when low concentration of LDL-C is concomitant with elevated level of TG (≥200 mg/dL).[12,13] In the future, it would be important to compare Sampson and extended Martin/Hopkins calculations with direct measurements in the presence of both hypertriglyceridemia and low concentration of LDL-C. Regarding reimbursement, it is important to mention that direct LDL-C may not get reimbursed as a direct order. In the United States, per Centers for Medicaid and Medicare Services, the lipid panel must use a calculated LDL-C, and a direct LDL-C cannot be substituted as needed but requires an approved reflex test, which may not be reimbursed by insurance carriers. Given the importance of identifying dyslipidemias early in life, this pilot study lays the foundation for a future comprehensive study to confirm whether the Sampson and extended Martin/Hopkins calculations are in line with direct measurements of LDL-C in children with dyslipidemia.

Conclusion

Given the limitation of the Friedewald equation, Sampson and extended Martin/Hopkins methods have the potential to replace direct measurement of LDL-C when TG ≥ 400 mg/dL. Against the backdrop of a growing prevalence of pediatric dyslipidemia, no study has reported the applicability of these 2 methods in pediatric patients compared with direct measurement of LDL-C. This study demonstrates that both Sampson and extended Martin/Hopkins calculations are applicable as clinical alternatives of direct LDL-C measurement in pediatric patients with a superior accuracy given 400 ≤ TG ≤ 799 mg/dL.

Conflict of Interest Disclosure

The authors have nothing to disclose.

REFERENCES

1. Grundy SM, Stone NJ, Bailey AL, et al. 2018 AHA/ACC/AACVPR/AAPA/ABC/ACPM/ADA/AGS/APhA/ASPC/NLA/PCNA guideline on the management of blood cholesterol. *J Am Coll Cardiol.* 2019;73:e285–e350. doi:10.1016/j.jacc.2018.11.003
2. Nauck M, Warnick GR, Rifai N. Methods for measurement of LDL-cholesterol: a critical assessment of direct measurement by homogeneous assays versus calculation. *Clin Chem.* 2002;48:236–254.
3. Friedewald WT, Levy RI, Fredrickson DS. Estimation of the concentration of low-density lipoprotein cholesterol in plasma, without use of the preparative ultracentrifuge. *Clin Chem.* 1972;18:499–502.
4. Martin SS, Blaha MJ, Elshazly MB, et al. Comparison of a novel method vs the Friedewald equation for estimating low-density lipoprotein cholesterol levels from the standard lipid profile. *JAMA.* 2013;310:2061–2068. doi:10.1001/jama.2013.280532
5. AACC-LVDD. https://ais.swmed.edu/redcap/surveys/?s=M7TC7DFXHYTAE7HC.
6. Sampson M, Ling C, Sun Q, et al. A new equation for calculation of low-density lipoprotein cholesterol in patients with normolipidemia and/or hypertriglyceridemia. *JAMA Cardiol* 2020;5:540–548. doi:10.1001/jamacardio.2020.0013
7. Expert Panel on Integrated Guidelines for Cardiovascular, Heart, Lung, and Blood Institute. Expert panel on integrated guidelines for cardiovascular health and risk reduction in children and adolescents: summary report. *Pediatrics.* 2011;128:S213–S256.
8. Sajja A, Park J, Sathiyakumar V, et al. Comparison of methods to estimate low-density lipoprotein cholesterol in patients with high triglyceride levels. *JAMA Netw Open* 2021;4:e2128817. doi:10.1001/jamanetworkopen.2021.28817
9. Miller WG, Waymack PP, Anderson FP, et al. Performance of four homogeneous direct methods for LDL-cholesterol. *Clin Chem.* 2002;48:489–498.
10. Shah AS, Wilson DP. *Genetic Disorders Causing Hypertriglyceridemia in Children and Adolescents*. MDText.com; 2000.
11. Al-Hamad D, Raman V. Metabolic syndrome in children and adolescents. *Transl Pediatr.* 2017;6:397–407. doi:10.21037/tp.2017.10.02
12. Whelton SP, Meeusen JW, Donato LJ, et al. Evaluating the atherogenic burden of individuals with a Friedewald-estimated low-density lipoprotein cholesterol <70 mg/dL compared with a novel low-density lipoprotein estimation method. *J Clin Lipidol.* 2017;11:1065–1072. doi:10.1016/j.jacl.2017.05.005
13. Meeusen JW, Snozek CL, Baumann NA, et al. Reliability of calculated low-density lipoprotein cholesterol. *Am J Cardiol.* 2015;116:538–540. doi:10.1016/j.amjcard.2015.05.013

A novel pyrosequencing strategy for *RHD* zygosity for predicting risk of hemolytic disease of the fetus and newborn

Piao Lv, MM,[1,] Jixin Li, MM,[1,*] Yuan Yao,[1] Xinxin Fan, BM,[1] Chixiang Liu, MM,[1] Hui Li, MM,[2] Huayou Zhou, MD[1]*

[1]Department of Blood Transfusion, Nanfang Hospital, Southern Medical University, Guangzhou, China, [2]Department of Hematology, Guangdong Provincial Hospital of Traditional Chinese Medicine (The Second Affiliated Hospital of Guangzhou University of Traditional Chinese Medicine), Guangzhou, China. Corresponding author: Huayou Zhou; E-mail: zohoyo@126.com. *First authors.

Key words: Rh blood grouping system; HDFN; *RHD* zygosity; DNA pyrosequencing; mismatch PCR-SSP; Sanger sequencing

Abbreviations: PSQ, pyrosequencing technology; HDFN, hemolytic disease of the fetus and newborn; PCR-SSP, polymerase chain reaction with sequence-specific primers; qPCR, quantitative polymerase chain reaction; SBT, sequence-based genotyping typing; SNV, single nucleotide variant

Laboratory Medicine 2024;55:145-152; https://doi.org/10.1093/labmed/lmad051

ABSTRACT

Objective: The aim of this study was the development of an accurate and quantitative pyrosequence (PSQ) method for paternal *RHD* zygosity detection to help risk management of hemolytic disease of the fetus and newborn (HDFN).

Methods: Blood samples from 96 individuals were genotyped for *RHD* zygosity using pyrosequencing assay. To validate the accuracy of pyrosequencing results, all the samples were then detected by the mismatch polymerase chain reaction with sequence-specific primers (PCR-SSP) method and Sanger DNA sequencing. Serological tests were performed to assess RhD phenotypes.

Results: Serological results revealed that 36 cases were RhD-positive and 60 cases were RhD-negative. The concordance rate between pyrosequencing assay and mismatch PCR-SSP assay was 94.8% (91/96). There were 5 discordant results between pyrosequencing and the mismatch PCR-SSP assay. Sanger sequencing confirmed that the pyrosequencing assay correctly assigned zygosity for the 5 samples.

Conclusion: This DNA pyrosequencing method accurately detect *RHD* zygosity and will help risk management of pregnancies that are at risk of HDFN.

Hemolytic disease of the fetus and newborn (HDFN) develops during pregnancy when maternal red blood cell antibodies pass through the placenta to induce red cell destruction in the newborn. An HDFN leads to alloimmune hemolysis, fetal or neonatal edema, peritoneal effusion, heart failure, and even death in severe cases.[1–5] Hemolytic disease of the fetus and newborn is caused by maternal alloimmunization against red blood cell antigens during the pregnancy.[1,6] It is mainly related to the incompatibility of antigens and antibodies of blood group systems including RhD, RhE, Rhc, Kell, and ABO, etc.[2,7,8] Although prophylactic Rh immunoglobulin is an efficient method to prevent the disease, anti-D during pregnancy has been and remains the major cause of severe HDFN.[9–11] Thus, it is of clinical importance to develop an appropriate method to detect the fetal *RHD* genotype for diagnosis[12] and prevention[2,13] of immune RhD antibody–mediated HDFN.

To date, although noninvasive maternal plasma *RHD* genotyping of RhD-negative (RhD–) women has been a practical method to determine eligibility of Rh immune globulin for the prevention of alloimmunization leading to HDFN,[14] paternal *RHD* genotyping is also clinically important, as it is used to predict the risk of the fetus being RhD-positive (RhD+) when maternal anti-D is present.[10,15–17] If the father is heterozygous, it is possible that the fetus will be RhD– and further prenatal testing will be required to determine fetal status. If the father is *RHD*+ homozygous, it can be predicted that all fetuses will be RhD+. In this case, further consideration should be taken to manage the risk of HDFN, especially in the setting of HDFN history.[16]

Previously, phenotype frequency assessment, based on the serologic testing of RhCcEe antigens, which is relatively inaccurate,[2] has been commonly used for detection of *RHD* zygosity.[18,19] More currently molecular techniques used to detect *RHD* genotype include quantitative polymerase chain reaction (qPCR),[20] microsatellite,[21] single-sperm analysis,[22] DNA sequence-based genotyping typing,[23] and other techniques.[24,25] However, these molecular techniques are considered laborious or technically demanding. Therefore, a more accurate and easy-to-use quantitative technique is needed.

We developed a quantitative DNA pyrosequencing technique to specifically detect *RHD* zygosity. This method is based on the polymorphic sites of the upstream, downstream, and hybrid Rhesus boxes "identity region." We also used the mismatch polymerase chain reaction with sequence-specific primers (PCR-SSP) assay and Sanger DNA sequencing to verify the results of this DNA pyrosequencing method. This technique is expected to be a quick and accurate method to predict HDFN.

Materials and Methods

Study Subjects

In this study, 96 unrelated blood samples provided by healthy donors from Guangzhou Blood Center (Guangzhou, China), Qinhuangdao Blood Center (Qinhuangdao, China) and Jinzhou Red Cross Blood Center (Jinzhou, China) were previously collected and tested for *RHD* zygosity types using different methodologies. Genomic DNA was extracted from peripheral blood using DNA isolation kits (Qiagen) following the manufacturer's instructions, and concentrations of extracted DNA samples were adjusted to 50 to 200 ng/μL. This study was approved by the Ethics Committee of Guangdong Provincial Hospital of Traditional Chinese Medicine.

Assessment of Phenotypes

The RhD phenotypes of all 96 healthy blood donors were assessed using a test tube method with monoclonal anti-D (Immuncor) or using a microcolumn gel method (BoXun) according to the manufacturers' protocols. All negative RhD phenotypes were confirmed with improved anti-human globulin testing. Samples that tested RhD-negative in the improved anti-human globulin testing were further subjected to an absorption and elution test with trichloromethane to determine whether they were DEL phenotype.[26]

Pyrosequencing PCR

To design primers to assess *RHD* zygosity genotypes, *RH* gene sequences were retrieved according to Wagner and Flegel's research.[9,11] The *RH* gene contains the upstream and downstream Rhesus boxes with 98.6% shared homology. Within the upstream and downstream Rhesus boxes, there is a segment of 1463 bp called the identity region. RhD-negative individuals are caused by an *RHD* gene deletion occurring in a 903-bp breakpoint region, which is a part of the identity region through unequal crossing over and formed a hybrid Rhesus box. The pyrosequencing PCR primers were designed according to a previous study reported by Chiu et al.[20] Both upstream and hybrid Rhesus boxes contain a cytosine (C) at the polymorphic site of the 5' end of the identity region, whereas the downstream Rhesus box has a thymine (T) instead; thus, we designed our PCR primers to cover this polymorphic site and determined the zygosity of the *RHD* gene according to the proportion of nucleotides of the polymorphic site (**FIGURE 1A**). For the *RHD+/RHD+* homozygous genotype, both upstream and downstream Rhesus boxes will be either C or T and the theoretical proportion will be C/T = 50%:50%. For *RHD+/RHD–* heterozygous genotype, both upstream and downstream Rhesus boxes could be detected on 1 chromatid, whereas on the other chromatid, a hybrid Rhesus box will occur. This indicates a C/T polymorphism but the theoretical proportion will be C:T = 66.70%: 33.30%. For the *RHD–/RHD* homozygous genotype, only 1 hybrid Rhesus box could be found on both chromatids, leading to 100% of C to be detected, and the theoretical proportion will be C/T = 100%:0%.

All primers (**TABLE 1**) used in this study were designed using the pyrosequencing technology (PSQ) assay design software (Biotage) and were synthesized by Sangon Biotech. The reverse primer was biotinylated at the 5' end and purified using high-performance liquid

FIGURE 1. Illustration of the *RH* genetic structure (A) and orientation and sequences of the mismatch PCR-SSP primers (B). A, There are 2 Rhesus boxes (arrows) at both upstream and downstream of the *RHD* gene within a segment of 1463-bp identity region (double arrows). The RhD-negative individual is caused by an *RHD* gene deletion occurred in a 903-bp breakpoint region (arrowheads), which is a part of the identity region through unequal crossing over and formed a hybrid Rhesus box (arrows). Both upstream and hybrid Rhesus boxes contain a cytosine (C) at the 5' end of the identity region, but the downstream Rhesus box consists of a thymine (T) at this polymorphic site.

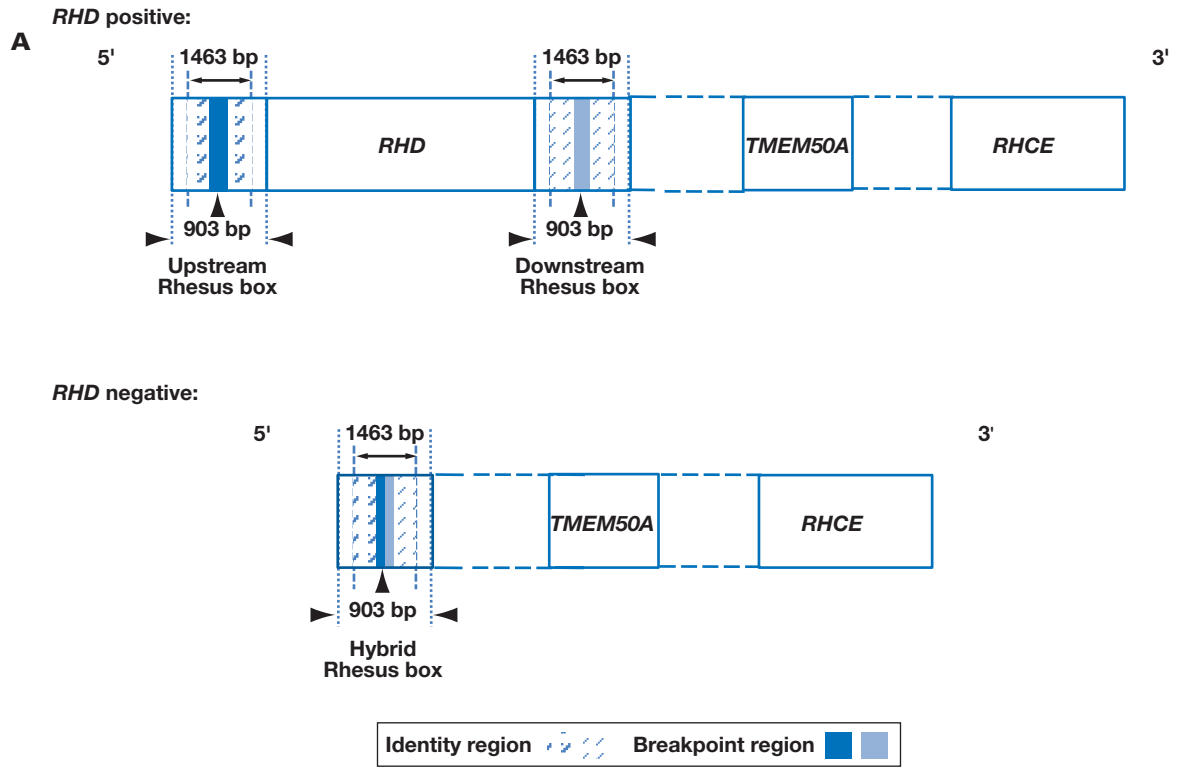

chromatography. The PCR amplification for these blood samples was performed in a total of 50 μL volume containing 25 μL Premix *Taq* (Takara), 1 μL of 10 μM each primer, 22 μL H_2O, and 1 μL genomic DNA at a concentration between 50 and 200 ng/μL on a GeneAmp PCR System 9700 thermocycler (Applied Biosystems). The PCR parameters consisted of an initial denaturation step at 95°C for 5 min and then 40 cycles of 95°C for 15 s, 60°C for 30 s and 72°C for 15 s, followed by a final elongation step at 72°C for 5 min. The PCR products were separated by 2.5% agarose gel electrophoresis.

DNA Pyrosequencing

To pyrosequence these genomic DNA samples, a pyrosequencing reaction mixture was mixed containing 20 μL PCR product, 2 μL Sepharose high-performance beads (GE Healthcare), 40 μL PyroMark Binding Buffer (Qiagen), and 18 μL ddH_2O. The DNA samples were captured by labeling with biotin at the 5' end nucleotides for Sepharose bead separation during washing steps using the PyroMark Q24 Vacuum Prep Workstation (Qiagen). We put the DNA templates into a 24-well plate containing 25 μL reagents of the sequencing primer (0.3 μM) and PyroMark annealing buffer (Qiagen) in each well and incubated the plates at 80°C for 2 min and cooled them at room temperature to allow DNA optimal annealing for the sequencing primers binding to biotinylated template strands. Pyrosequencing was then performed on the PyroMark Q24 System (Qiagen) with PyroMark Gold Q96 reagents, and PyroMark Q24 software was used for analysis, following manufacture's recommendations. Dispensation order was 5'-GTCTCTGA-3', designed to quantify the proportion of polymorphic sites under an AQ mode.

Mismatch PCR-SSP Assay

The mismatch PCR-SSP assay was performed according to the method of Zhou et al[27] (**FIGURE 1B**). At the 5' end of the identity region, the downstream Rhesus box differs by 1 bp in sequence from the upstream and hybrid Rhesus boxes. At the 3' end of the identity region, there is a 1-bp insertion in the upstream Rhesus box compared with the downstream and hybrid Rhesus boxes. For the upstream and hybrid Rhesus boxes, 2 mismatch sites were introduced at the second and third base from the 3' end of the forward primer, whereas for the downstream Rhesus box, 1 mismatch site was introduced at the third base from the 3' end of the forward primer. Additionally, 2 mismatch sites were introduced at the second and third base from the 3' end of the reverse primer for the downstream and hybrid Rhesus boxes, and 1 mismatch site was introduced at the third base from the 3' end of the reverse primer for the upstream Rhesus box. Primer information was present in **TABLE 1**. The

FIGURE 1. (cont) B, The sequences of upstream (U), downstream (D) and hybrid (H) Rhesus boxes at the 5' and 3' end of the identity region are shown in detail. UF and UR amplify the identity region of the upstream Rhesus box. DF and DR amplify the identity region of the downstream Rhesus box. HF and HR amplify the identity region of the hybrid Rhesus box. Allele specificity is conferred by the mismatch sites (underlined) at the 3' end of each primer.

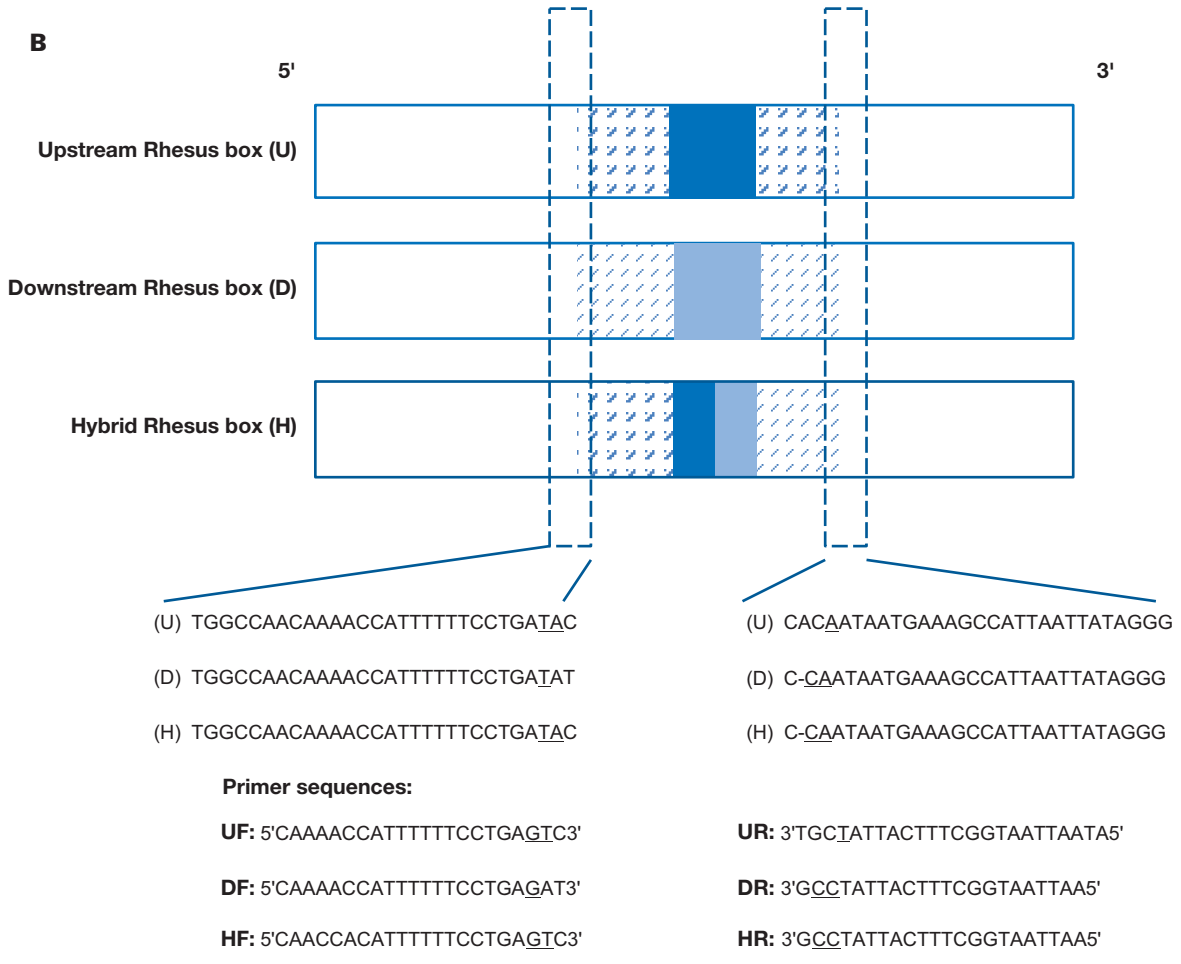

TABLE 1. PCR primers for pyrosequence, mismatch PCR-SSP, and Sanger sequence

Primer	Sequence (5'-3')	Assay	Product size (bp)
RhBox-F	GTCATGGTTGGGAGTGGC	Pyrosequencing	125
RhBox-R	Biotin-ACCCCTCCCATCACAGGT	Pyrosequencing	
Seq	AAACCATTTTTTCCTGATA	Pyrosequencing	
UF	CAAAACCATTTTTTCCTGAGTC	Mismatch PCR-SSP	1509
UR	ATAATTAATGGCTTTCATTATCGT	Mismatch PCR-SSP	
DF	CAAAACCATTTTTTCCTGAGAT	Mismatch PCR-SSP	1510
DR	AATTAATGGCTTTCATTATCCG	Mismatch PCR-SSP	
HF	CAACCACATTTTTTCCTGAGTC	Mismatch PCR-SSP	1510
HR	AATTAATGGCTTTCATTATCCG	Mismatch PCR-SSP	
HGH-5580-S	TGCCTTCCCAACCATTCCCTTA	internal control	434
HGH-5967-A	CCACTCACGGATTTCTGTTGTGTTTC	internal control	
F	GTCATGGTTGGGAGTGGC	Sanger sequencing	125
R	ACCCCTCCCATCACAGGT	Sanger sequencing	

PCR-SSP, polymerase chain reaction with sequence-specific primers.

mismatch PCR-SSP amplification mixture was set at 12.5 μL containing 1 μL genomic DNA (50-200 ng/μL), 1× PCR buffer (50 mM KCl, 10 mM Tris-HCl at pH 8.0), 2.5 mM $MgCl_2$, 200 μM dNTPs, and 0.5 U *Taq* polymerase (Takara). The final concentration of PCR primers was 0.2 μM, and the internal control primers were 0.02 μM. The PCR amplification was set for an initial denaturation at 95°C for 5 min and followed by 35 cycles of 95°C for 1 min, 52°C for 1 min, and 72°C for 1 min, and a final step at 72°C for 10 min. The PCR products were then analyzed by electrophoresis in 2% agarose gel. The gel results were visually inspected and recorded.

Sanger DNA Sequencing

All DNA fragments amplified in pyrosequncing experiments were sequenced using Sanger sequencing to verify accuracy. Primers used for Sanger sequencing are shown in **TABLE 1**. The Sanger DNA sequence assay was performed by Sangon Biotech.

Statistical Analysis

The amount of C and T for different *RHD* zygosity types is expressed as mean ± SD and compared with analysis of variance (ANOVA), followed by Student *t*-test for the comparison of any 2 *RHD* zygosity types. A 2-sided $P < .05$ was considered statistically significant. All statistical analyses were performed with IBM SPSS statistics software (version 21.0).

Results

Serological Phenotype

The RhD phenotyping of 96 donors revealed that 36 cases were of RhD+ phenotypes and 60 cases were of normal RhD- phenotypes.

DNA Pyrosequencing for *RHD* Zygosity Detection

The *RHD* zygosity types of the 96 samples detected by pyrosequencing were: 32 *RHD+/RHD+* homozygotes, 36 *RHD+/RHD–* heterozygotes, and 28 *RHD–/RHD–* homozygotes. Among the 36 samples with RhD+ phenotypes, 32 were *RHD+/RHD+* homozygotes and 4 were *RHD+/RHD–* heterozygotes. Of the 60 samples with RhD– phenotypes, 28 were *RHD–/RHD–* homozygotes and 32 were *RHD+/RHD–* heterozygotes.

According to the peak fluorescence signal released by the chemical reaction of the pyrosequencing assay, specifically, C/T polymorphisms and percentage of different bases were clearly detected at the polymorphic sites (**FIGURE 2**). The C content (%) of *RHD+/RHD+* homozygotes, *RHD+/RHD–* heterozygotes, and *RHD–/RHD–* homozygotes at the tested loci was 50.84 ± 2.08, 66.78 ± 1.82, and 97.86 ± 1.21, respectively. The ANOVA showed significant differences in C content among the 3 genotypes ($P < .001$); the *t*-test for 2-way comparison showed significant differences between different zygosity types ($P < .001$).The T content (%) of *RHD+/RHD+* homozygote, *RHD+/RHD–* heterozygote, and *RHD–/RHD–* homozygote at the loci to be measured was 49.22 ± 2.12, 33.22 ± 1.82, and 2.14 ± 1.21, respectively. The ANOVA showed significant differences in T content among the 3 genotypes ($P < .001$); the *t*-test for 2-way comparison also showed significant differences between different zygosity types ($P < .001$) (**FIGURE 3**).

The above results show that the distribution of C and T contents in different zygotes of the *RHD* gene detected by pyrosequencing was statistically different. The differences of C and T contents at single nucleotide variant (SNV) loci were consistent with the expectation, so the 3 different kinds of *RHD* gene zygosity could be distinguished.

Comparison of *RHD* Gene Zygosity Data Detected by DNA Pyrosequence With The Mismatch PCR-SSP Assay

RHD zygosity of 96 samples detected by mismatch PCR-SSP were: 32 *RHD+/RHD+* homozygotes, 39 *RHD+/RHD–* heterozygotes, and 25 *RHD–/RHD–* homozygotes. Electrophoresis results of the mismatch PCR-SSP assay are shown in **FIGURE 4**.

The concordance rate of the DNA pyrosequence and the mismatch PCR-SSP assay was 94.8% (91/96, 95% CI: 88.4%–97.8%), indicating a high concordant detection of these 2 methods, as shown in **TABLE 2**. Four cases of *RHD–/RHD–* homozygous samples detected by pyrosequencing were identified as *RHD+/RHD–* heterozygotes by the mismatch PCR-SSP method, whereas 1 case of an *RHD+/RHD–* heterozygous sample detected by pyrosequencing was identified as an *RHD–/RHD–* homozygote by the mismatch PCR-SSP method.

Comparison of *RHD* Genotype Data Detected by DNA Pyrosequence with Sanger DNA Sequencing

Sanger DNA sequencing data revealed 28 (29.17%) cases of *RHD–/RHD–* homozygotes, and there were 68 (70.83%) total cases of *RHD+/RHD+* homozygotes and *RHD+/RHD–* heterozygotes (**FIGURE 2**).

Sanger sequencing accurately identified 28 cases of *RHD–/RHD–* homozygotes, the same results as detected by pyrosequencing assay. For samples detected as *RHD+/RHD+* homozygotes and *RHD+/RHD–* heterozygotes by pyrosequencing, the nucleotide sequences obtained by Sanger sequencing were identical. The above results could prove the accuracy of pyrosequencing data.

Furthermore, we performed a Basic Local Alignment Search Tool (BLAST) search and the results showed that all of the Sanger DNA

FIGURE 2. **Comparison of the representative pyrosequencing (left) and Sanger (right) sequencing data on different *RHD* zygosity types. The left panels show the pyrograms of *RHD+/RHD+* (top), *RHD+/RHD–* (middle), and *RHD–/RHD–* (bottom). Different *RHD* zygosity types are reflected by the proportion of cytosine and thymine in the highlight areas. The x-axis shows the dispensation order of nucleotides, the y-axis shows the relative light units of light signal. The right panels show the Sanger sequencing graphs of the *RHD* zygosity. The *RHD–/RHD–* homozygosity (bottom) can be distinguished clearly, as there is no polymorphism detected at the polymorphic site (arrow), whereas the *RHD+/RHD+* homozygous patterns (top) and the *RHD+/RHD–* heterozygous patterns (middle) can be confused, as the peak height of cytosine and thymine will change in some cases and make these graphs difficult to distinguish at the polymorphic site in Sanger sequencing.**

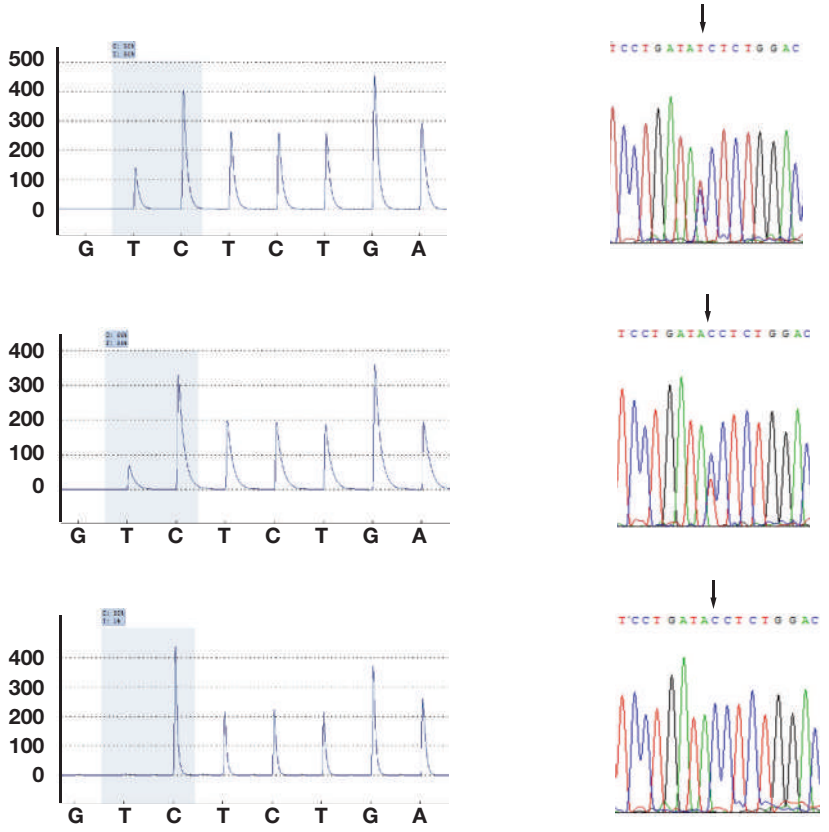

FIGURE 3. **Results of percentage of different bases detected by pyrosequencing at the polymorphic sites. Asterisks represent extreme value within each *RHD* zygosity type. A, The comparison of the amount of cytosine. B, The comparison of the amount of thymine.**

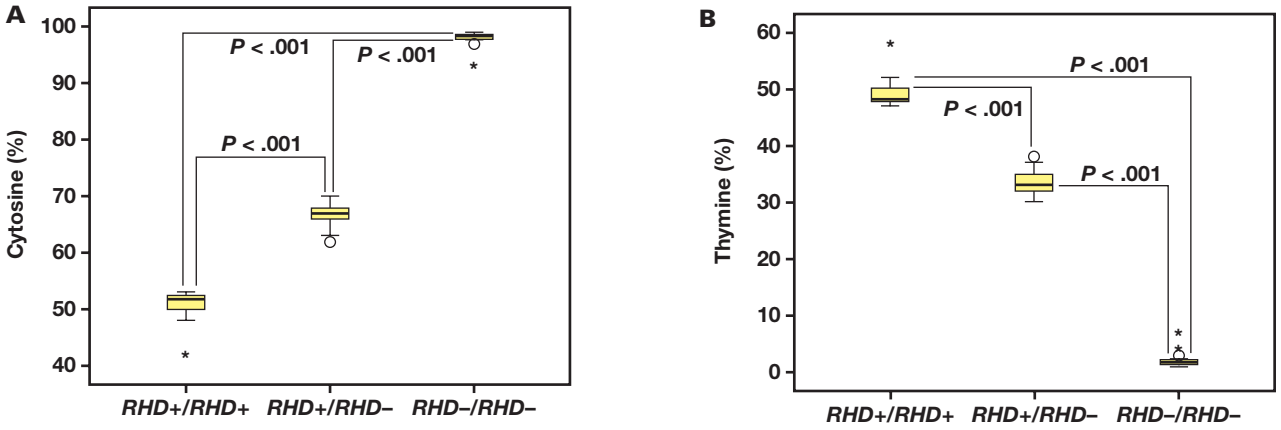

sequencing data contained the same target genes with the accession number AJ252311 for the upstream Rhesus box, AJ252312 for the downstream Rhesus box, and AJ252313 for the hybrid Rhesus box.

Discussion

Rh blood group system incompatibility can cause severe, long-lasting, and lethal alloimmune hemolysis. The Rh system is highly polymorphic,

FIGURE 4. **Determination of *RHD* gene zygosity using the mismatch polymerase chain reaction with sequence-specific primers technique with 2% agarose gel electrophoresis. The lanes 1, 4, and 7 show data on the upstream Rhesus boxes; lanes 2, 5, and 8 report data on the downstream Rhesus boxes; and lanes 3, 6, and 9 represent data on the hybrid Rhesus boxes. Note: Specific bands are 1509 bp (upstream Rhesus box) and 1510 bp (downstream and hybrid Rhesus boxes), respectively. The internal control is 434 bp. For the *RHD+/RHD+* homozygous genotype, both upstream and downstream Rhesus boxes were amplified except the hybrid one. For the *RHD+/RHD–* homozygous genotype, all 3 kinds of Rhesus boxes could be detected, but only hybrid box can be detected in *RHD–/RHD–* homozygous samples. M, molecular weight marker.**

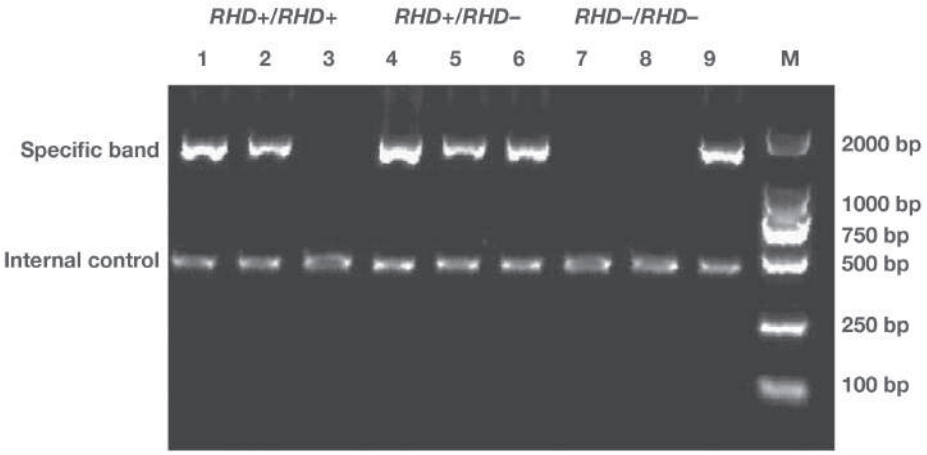

TABLE 2. **Zygosity testing results determine by pyrosequencing method and mismatch PCR-SSP assay**

PCR-SSP	Pyrosequencing			Total
	RHD+/RHD+	*RHD+/RHD–*	*RHD–/RHD–*	
RHD+/RHD+	32	0	0	32
RHD+/RHD–	0	35	4	39
RHD–/RHD–	0	1	24	25
Total	32	36	28	96

PCR-SSP, polymerase chain reaction with sequence-specific primers

and complete serological typing includes a systematic determination of Rh antigens of the D, C, c, E, and e series. Among the above antigens of the Rh blood group system, RhD antigen and antibody incompatibility is the most important cause of alloimmune hemolysis. Accurate detection of *RHD* zygosity (genotype) is a prerequisite for the diagnosis and prevention of RhD antibody-associated HDFN.[11] In this study, an accurate pyrosequencing method was developed and validated for the detection of *RHD* zygosity, which will help management of pregnancies that are at a risk of HDFN.

The serological results revealed that, among the 96 donors, 36 cases were of RhD+ phenotypes and 60 cases of RhD– phenotypes. Because many Chinese individuals with a serologic RhD– phenotype may carry a DEL phenotype,[28] further absorption and elution tests were conducted to confirm these 60 cases of RhD-negative donors had a true RhD– phenotype.

There were significant differences in the proportion of nucleotides at the Rhesus box polymorphic site of the *RHD* gene detected by the developed pyrosequencing method, indicating that pyrosequencing can accurately distinguish the 3 haplotypes of the *RHD* gene. A high concordance in detecting the *RHD* zygosity was observed when compared with the mismatch PCR-SSP assay, with the concordance rate of the DNA pyrosequence and the mismatch PCR-SSP assay as high as 94.8% (91/96). There were 5 samples with inconsistent results. Confirmed by Sanger sequencing, the DNA pyrosequence could correctly detect *RHD* zygosity. However, the mismatch PCR-SSP assay didn't detect the *RHD* zygosity correctly. These results indicate that the accuracy of pyrosequencing method is greater than that of the mismatch PCR-SSP method.

Validation by Sanger sequencing showed that pyrosequencing can accurately detect *RHD–/RHD–* homozygotes. For samples with pyrosequencing results of *RHD+/RHD+* homozygotes and *RHD+/RHD–* heterozygotes, Sanger sequencing showed consistent sequence features with pyrosequencing. Thus, the results of Sanger sequencing could directly or indirectly prove that pyrosequencing is accurate for detecting *RHD* zygosity.

In this study, all the PCR primers designed for these 3 assays to detect the *RHD* zygosity were based on the *RHD* polymorphic sites of Rhesus box identity region. According to a previous study,[20] the polymorphic sites are localized at both the 5' end and 3' end of the Rhesus box identity region. At the 5' end, it is normally a cytosine at both upstream and hybrid Rhesus boxes, whereas the downstream Rhesus box can be a thymine. At the 3' end of the identity region, the upstream Rhesus box differs, with an insertion of adenine from the downstream and hybrid Rhesus boxes at this position. The DNA pyrosequencing technique could quantitatively detected this C/T polymorphism by taking advantage of the 5'-end polymorphic site to determine *RHD* zygosity. However, the mismatch PCR-SSP assay must assess both 5'- and 3'-end polymorphic sites with sequence-specific primers. Another disadvantage of the mismatch PCR-SSP assay is that it can be affected by many factors. Taki et al[29] reported that either the number or the position of mismatched nucleotides introduced in sequence-specific primers may cause false-positive signals. Pantelidis et al[30] reported that rare polymorphisms in the general population may also lead to failed amplification. Lara-Armi and Visentainer[31] reported that the amplification condition can lead to inefficient or no amplification of specific alleles. In the mismatch PCR-SSP strategy of our study, both the forward primers designed for

upstream hybrid Rhesus boxes and the reverse primers designed for downstream hybrid Rhesus boxes use 2 adjacent mismatch sites. These mismatch sites increase the difficulty of amplification, which may lead to incorrect amplification results. In contrast, DNA pyrosequencing is a stable and automation-friendly technique, which can avoid the disadvantages of the mismatch PCR-SSP assay.

DNA pyrosequencing is a real-time sequencing-by-synthesis technique and it has always been recommended for resequencing of diseased genes, difficult secondary DNA structure sequencing, and genotyping.[32,33] In previous studies, the pyrosequencing technique has been commonly used to detect the SNVs of genomic DNA samples through different quantities of polymorphic nucleotides.[32–35] It is also used to distinguish mutant-type alleles from wild-type alleles by diversified constituent ratios and to detect gene copy numbers according to multiples of a reference gene.[34–37] Pyrosequencing has great advantages with less complexity and shorter turnaround time (the average analysis time, including blood component separation and DNA extraction, was less than 2 h), involves fewer steps, and has a superior limit of detection (~5% vs ~20% for Sanger).[38–42] Moreover, the PyroMark Q24 platform (Qiagen) used for the detection of *RHD* zygosity in this study can test 24 or 96 samples at a time flexibly, which can make it suitable for the detection of clinical specimens in daily work.

However, the DNA pyrosequencing method does have some restrictions. For example, it can only detect known gene polymorphisms (mutations). The *RHD* genotyping methods are complicated by the presence of variant *RHD* alleles that frequently occur in non-White populations.[18,43–45] We did not validate the pyrosequencing method established in multiple populations; whether detection performance will be affected by the presence of variant *RHD* alleles is still to be studied. The presence of variant *RHD* alleles will also affect confirmatory results of Sanger sequencing. Fortunately, the most prevalent RhD– in individuals is caused by whole *RHD* gene deletion, whereas variant *D* genes of RhD– phenotypes are rare in White persons. In Chinese people, less than 0.4% are serological RhD–,[46] and of those, almost 70% individuals have a normal *RHD* gene.[47] Consequently, the frequency of detectable RhD– *D* variants with grossly intact or partial *RHD* gene in Chinese persons is considered to be very low. Because the frequency and occurrence of RhD– *D* variants is limited in the epidemiological point of view, the DNA pyrosequencing technique is still useful and applicable to detect normal *RHD* zygosity in practice.

In conclusion, this study established an accurate and quantitative pyrosequencing method to detect *RHD* zygosity. This proposed robust, convenient, and efficient pyrosequencing method has very important clinical significance for genetic counseling and risk management of HDFN related to anti-RhD in pregnancy.

Acknowledgments

The authors thank Dr B.R. Liu of the Department of Cardiology, Second Affiliated Hospital of Guangzhou Medical University (Guangzhou, China), for expert technical assistance in the DNA pyrosequencing assay.

Funding

This work was supported by a grant from National Natural Science Foundation of China (grant number 30971580).

Conflict of Interest Disclosure

The authors have nothing to disclose.

REFERENCES

1. Fasano RM. Hemolytic disease of the fetus and newborn in the molecular era. *Semin Fetal Neonatal Med*. 2016;21(1):28-34. doi:10.1016/j.siny.2015.10.006
2. Delaney M, Matthews DC. Hemolytic disease of the fetus and newborn: managing the mother, fetus, and newborn. *Hematology Am Soc Hematol Educ Program.* 2015;2015(1):146-151. doi:10.1182/asheducation-2015.1.146
3. Song W, Zhou S, Shao L, Wang N, Pan L, Yu W. Non-invasive fetal ABO genotyping in maternal plasma using real-time PCR. *Clin Chem Lab Med.* 2015;53(12):1943-1950. doi:10.1515/cclm-2015-0011
4. Jackson ME, Baker JM. Hemolytic disease of the fetus and newborn: historical and current state. *Clin Lab Med.* 2021;41(1):133-151. doi:10.1016/j.cll.2020.10.009
5. Hyland CA, O'Brien H, Flower RL, et al. Non-invasive prenatal testing for management of haemolytic disease of the fetus and newborn induced by maternal alloimmunisation. *Transfus Apher Sci.* 2020;59(5):102947. doi:10.1016/j.transci.2020.102947
6. Castleman JS, Moise KJ Jr, Kilby MD. Medical therapy to attenuate fetal anaemia in severe maternal red cell alloimmunisation. *Br J Haematol.* 2021;192(3):425-432. doi:10.1111/bjh.17041
7. Verduin EP, Brand A, van de Watering LM, et al. Factors associated with persistence of red blood cell antibodies in woman after pregnancies complicated by fetal alloimmune haemolytic disease treated with intrauterine transfusions. *Br J Haematol.* 2015;168(3):443-451. doi:10.1111/bjh.13130
8. Dziegiel MH, Krog GR, Hansen AT, et al. Laboratory monitoring of mother, fetus, and newborn in hemolytic disease of fetus and newborn. *Transfus Med Hemotherapy*. 2021;48(5):306-315. doi:10.1159/000518782
9. Wagner FF, Flegel WA. RHD gene deletion occurred in the Rhesus box. *Blood.* 2000;95(12):3662-3668.
10. Pirelli KJ, Pietz BC, Johnson ST, Pinder HL, Bellissimo DB. Molecular determination of RHD zygosity: predicting risk of hemolytic disease of the fetus and newborn related to anti-D. *Prenat Diagn.* 2010;30(12-13):1207-1212. doi:10.1002/pd.2652
11. Flegel WA. Molecular genetics and clinical applications for RH. *Transfus Apher Sci.* 2011;44(1):81-91. doi:10.1016/j.transci.2010.12.013
12. Illanes S, Soothill P. Noninvasive approach for the management of hemolytic disease of the fetus. *Expert Rev Hematol.* 2009;2(5):577-582. doi:10.1586/ehm.09.45
13. Bowman JM. Controversies in Rh prophylaxis. Who needs Rh immune globulin and when should it be given? *Am J Obstet Gynecol.* 1985;151(3):289-294. doi:10.1016/0002-9378(85)90288-1
14. Ahmadi MH, Pourfathollah AA, Rabiee M, et al. Noninvasive prenatal diagnosis of fetal RHD status using cell-free fetal DNA in maternal plasma. *J Reprod Infertil*. 2022;23(2):128-134. doi:10.18502/jri.v23i2.8998
15. Clausen FB, Rieneck K, Krog GR, Bundgaard BS, Dziegiel MH. Noninvasive antenatal screening for fetal RHD in RhD negative women to guide targeted anti-D prophylaxis. *Methods Mol Biol.* 2019;1885:347-359. doi:10.1007/978-1-4939-8889-1_23
16. Moise KJ Jr. Management of rhesus alloimmunization in pregnancy. *Obstet Gynecol.* 2008;112(1):164-176. doi:10.1097/AOG.0b013e31817d453c
17. Flegel WA. The genetics of the Rhesus blood group system. *Blood Transfus.* 2007;5(2):50-57. doi:10.2450/2007.0011-07
18. Matheson KA, Denomme GA. Novel 3' Rhesus box sequences confound RHD zygosity assignment. *Transfusion.* 2002;42(5):645-650. doi:10.1046/j.1537-2995.2002.00078.x

19. Kacem N, Chakroun T, Moussa H, et al. RHD zygosity assignments based on most probable genotype and hybrid Rhesus box detection in Tunisia. *Transfus Med*. 2012;22(5):362-366. doi:10.1111/j.1365-3148.2012.01172.x
20. Chiu RW, Murphy MF, Fidler C, Zee BC, Wainscoat JS, Lo YM. Determination of RhD zygosity: comparison of a double amplification refractory mutation system approach and a multiplex real-time quantitative PCR approach. *Clin Chem.* 2001;47(4):667-672.
21. Fichou Y, Chen JM, Le Maréchal C, et al. Weak D caused by a founder deletion in the RHD gene. *Transfusion.* 2012;52(11):2348-2355. doi:10.1111/j.1537-2995.2012.03606.x
22. Reubinoff BE, Avner R, Rojansky N, et al. RhD genotype determination by single sperm cell analysis. *Am J Obstet Gynecol.* 1996;174(4):1300-1305. doi:10.1016/s0002-9378(96)70675-0
23. Wu YY, Csako G. Rapid and/or high-throughput genotyping for human red blood cell, platelet and leukocyte antigens, and forensic applications. *Clin Chim Acta*. 2006;363(1-2):165-176. doi:10.1016/j.cccn.2005.07.010
24. Krog GR, Clausen FB, Dziegiel MH. Quantitation of RHD by real-time polymerase chain reaction for determination of RHD zygosity and RHD mosaicism/chimerism: an evaluation of four quantitative methods. *Transfusion.* 2007;47(4):715-722. doi:10.1111/j.1537-2995.2007.01175.x
25. Zhang J, Zeng Y, Wang Y, et al. RHD genotypes in a Chinese cohort of pregnant women. *Front Genet.* 2021;12:752485. doi:10.3389/fgene.2021.752485
26. Simtong P, Phothi R, Puapairoj C, et al. RHD 1227 A and hybrid Rhesus box analysis in Thai RhD+ and RhD- blood donors: prevalence, RHD zygosity, and molecular screening. *Transfus Apher Sci*. 2022;61(6):103496. doi:10.1016/j.transci.2022.103496
27. Zhou HY, Lan JC, Wang XZ, et al. Determination of human RHD gene rhesus box and its significance. *Zhongguo Shi Yan Xue Ye Xue Za Zhi*. 2005;13(1):130-134.
28. Ji Y, Luo Y, Wen J, et al. Patients with Asian-type DEL can safely be transfused using RhD-positive blood. *Blood.* 2023;141(17):2141-2150. doi:10.1182/blood.2022018152
29. Taki T, Kibayashi K. A simple ABO genotyping by PCR using sequence-specific primers with mismatched nucleotides. *Legal Med*. 2014;16(3):168-172. doi:10.1016/j.legalmed.2014.02.007
30. Pantelidis P, Lympany PA, Foley PJ, Fanning GC, Welsh KI, du Bois RM. Polymorphic analysis of the high-affinity tumor necrosis factor receptor 2. *Tissue Antigens.* 1999;54(6):585-591. doi:10.1034/j.1399-0039.1999.540608.x
31. Lara-Armi FF, Visentainer JEL. Optimization of HLA-B*27 ALLELE genotyping by PCR-SSP. *Clinics (Sao Paulo).* 2020;75:e1840. doi:10.6061/clinics/2020/e1840
32. Ronaghi M. Pyrosequencing sheds light on DNA sequencing. *Genome Res.* 2001;11(1):3-11. doi:10.1101/gr.11.1.3
33. Benzi F, Vanni I, Cassina G, et al. Detection of ganciclovir resistance mutations by pyrosequencing in HCMV-infected pediatric patients. *J Clin Virol.* 2012;54(1):48-55. doi:10.1016/j.jcv.2012.01.006
34. Soderback E, Zackrisson AL, Lindblom B, Alderborn A. Determination of CYP2D6 gene copy number by pyrosequencing. *Clin Chem.* 2005;51(3):522-531. doi:10.1373/clinchem.2004.043182
35. Stigt JA, tHart NA, Knol AJ, et al. Pyrosequencing analysis of EGFR and KRAS mutations in EUS and EBUS-derived cytologic samples of adenocarcinomas of the lung. *J Thorac Oncol*. 2013;8(8):1012-1018. doi:10.1097/JTO.0b013e31829ce93e
36. Liu Z, Obenauf AC, Speicher MR, Kopan R. Rapid identification of homologous recombinants and determination of gene copy number with reference/query pyrosequencing (RQPS). *Genome Res.* 2009;19(11):2081-2089. doi:10.1101/gr.093856.109
37. Park SJ, Sun JY, Hong K, et al. Application of BRAF, NRAS, KRAS mutations as markers for the detection of papillary thyroid cancer from FNAB specimens by pyrosequencing analysis. *Clin Chem Lab Med.* 2013;51(8):1673-1680. doi:10.1515/cclm-2012-0375
38. Harrington CT, Lin EI, Olson MT, Eshleman JR. Fundamentals of pyrosequencing. *Arch Pathol Lab Med*. 2013;137(9):1296-1303. doi:10.5858/arpa.2012-0463-RA
39. Laurini JA, Aoun P, Iqbal J, Chan W, Greiner TC. Investigation of the BRAF V600E mutation by pyrosequencing in lymphoproliferative disorders. *Am J Clin Pathol.* 2012;138(6):877-883. doi:10.1309/AJCP5TWORA0TMXGL
40. Fakhrai-Rad H, Pourmand N, Ronaghi MP. An accurate detection platform for single nucleotide polymorphisms. *Hum Mutat.* 2002;19(5):479-485. doi:10.1002/humu.10078
41. Akca H, Demiray A, Yaren A, et al. Utility of serum DNA and pyrosequencing for the detection of EGFR mutations in non-small cell lung cancer. *Cancer Genet*. 2013;206(3):73-80. doi:10.1016/j.cancergen.2013.01.005
42. Arita H, Narita Y, Matsushita Y, et al. Development of a robust and sensitive pyrosequencing assay for the detection of IDH1/2 mutations in gliomas. *Brain Tumor Pathol.* 2015;32(1):22-30. doi:10.1007/s10014-014-0186-0
43. Avent ND, Reid ME. The Rh blood group system: a review. *Blood.* 2000;95(2):375-387.
44. Grootkerk-Tax MG, Maaskant-van Wijk PA, van Drunen J, van der Schoot CE. The highly variable RH locus in nonwhite persons hampers RHD zygosity determination but yields more insight into RH-related evolutionary events. *Transfusion.* 2005;45(3):327-337. doi:10.1111/j.1537-2995.2005.04199.x
45. Wagner FF, Moulds JM, Flegel WA. Genetic mechanisms of Rhesus box variation. *Transfusion.* 2005;45(3):338-344. doi:10.1111/j.1537-2995.2005.04339.x
46. Ye L, Yue D, Wo D, et al. Molecular bases of unexpressed RHD alleles in Chinese D- persons. *Transfusion.* 2009;49(8):1655-1660. doi:10.1111/j.1537-2995.2009.02181.x
47. Shao CP, Maas JH, Su YQ, Köhler M, Legler TJ. Molecular background of Rh D-positive, D-negative, D(el) and weak D phenotypes in Chinese. *Vox Sang.* 2002;83(2):156-161. doi:10.1046/j.1423-0410.2002.00192.x

Neutrophilic Myeloid-Derived Suppressor Cells and Severity in SARS-CoV-2 Infection

Mona A. Omar, MSc,[1] Rabab El Hawary, MD,[1] Alia Eldash, MD,[1] Khaled M. Sadek, MD,[2] Neveen A. Soliman, MD,[3] Mariam Onsy F. Hanna, MD,[1,] Shereen M. Shawky, MD[1]

Departments of [1]Clinical Pathology, [2]Internal Medicine and Nephrology, and [3]Pediatrics, Cairo University, Cairo, Egypt. Corresponding author: Mariam Onsy F. Hanna; mariamhanna@cu.edu.eg

Keywords: aging, COVID-19, MDSC, mortality, SARS-CoV-2, severity

Abbreviations: MDSCs, myeloid-derived suppressor cells; PMN-MDSC, polymorphonuclear MDSC; M-MDSC, monocytic MDSC; E-MDSC, early MDSC; PBMCs, peripheral blood mononuclear cells; TLC, total leukocytic count

Laboratory Medicine 2024;55:153-161; https://doi.org/10.1093/labmed/lmad050

ABSTRACT

Background: While we strive to live with SARS-CoV-2, defining the immune response that leads to recovery rather than severe disease remains highly important. COVID-19 has been associated with inflammation and a profoundly suppressed immune response.

Objective: To study myeloid-derived suppressor cells (MDSCs), which are potent immunosuppressive cells, in SARS-CoV-2 infection.

Results: Patients with severe and critical COVID-19 showed higher frequencies of neutrophilic (PMN)–MDSCs than patients with moderate illness and control individuals (P = .005). Severe disease in individuals older and younger than 60 years was associated with distinct PMN-MDSC frequencies, being predominantly higher in patients of 60 years of age and younger (P = .004). However, both age groups showed comparable inflammatory markers. In our analysis for the prediction of poor outcome during hospitalization, MDSCs were not associated with increased risk of death. Still, patients older than 60 years of age (odds ratio [OR] = 5.625; P = .02) with preexisting medical conditions (OR = 2.818; P = .003) showed more severe disease and worse outcome. Among the immunological parameters, increased C-reactive protein (OR = 1.015; P = .04) and lymphopenia (OR = 5.958; P = .04) strongly identified patients with poor prognosis.

Conclusion: PMN-MDSCs are associated with disease severity in COVID-19; however, MDSC levels do not predict increased risk of death during hospitalization.

COVID-19 is a battle between SARS-CoV-2 and immune response. COVID-19 can have different clinical presentations, ranging from no symptoms to severe pneumonia and multiorgan failure. This gamut of manifestations implies a diverse host immune response to SARS-CoV-2. Defining the nature of the immune response that leads to recovery rather than severe disease is essential for treating individual patients. However, the pathogenesis of the divergent disease courses and outcomes remains to be fully understood.

A pathologically heightened inflammatory response in patients infected with SARS-CoV-2 is evidenced by elevated blood levels of cytokines and chemokines, such as IL-1β, IL-6, IL-8, TNF-α, IL-18, and IL-12/IL-23.[1] High levels of inflammatory cytokines were considered independent predictors of disease outcome.[2] It has become evident that profound immunosuppression and persistent inflammation contribute to the pathophysiology of SARS-CoV-2 infection.[3] For example, patients with critical illness who needed mechanical ventilation showed a decrease in expression of type I/III interferons (IFNs) and IFN-stimulated genes, suggestive of an innate immune failure to control viral replication.[4]

Marked HLA class II downregulation in monocytes has also been detected in severe infection, indicating an impairment of antigen presentation to T cells.[5] An integral T-cell–mediated immune response is crucial for clearance of viral infection; however, in individuals infected with SARS-CoV-2, profound lymphopenia with substantially reduced numbers of $CD4^+$ and $CD8^+$ T cells was observed in patients who clinically deteriorate during infection.[6] Lung-infiltrating $CD8^+$ T cells from patients with severe disease have demonstrated transcriptional characteristics of T-cell exhaustion. Conversely, patients recovering from COVID-19 showed clonal expansion of effector and memory $CD8^+$ T cells, consistent with an effective adaptive immune response.[7]

The results of some studies have shown that patients with COVID-19 display immunosuppression mediated by myeloid cell populations and accumulation of myeloid-derived suppressor cells (MDSCs).[8,9] MDSCs are heterogeneous myeloid cells, composed of phenotypes, predominantly neutrophilic (polymorphonuclear MDSC [PMN-MDSC]), monocytic MDSC [M-MDSC], and early MDSC [E-MDSC] phenotypes).[10] A feature common to all MDSCs is their remarkable ability to suppress T-cell responses. By suppressing T-cell responses, MDSCs can promote virus survival, driving a highly proinflammatory state. Efforts are continuing to elucidate the contribution of MDSCs as pathogenic and prognostic factors, and possibly as therapeutic targets in COVID-19.[11] In our study, we investigated MDSCs in the pathogenesis of COVID-19 and explored

the relationship between MDSCs and their different phenotypes with COVID-19 disease severity and prognosis.

Methods

Patients

We enrolled 45 patients with confirmed COVID-19 admitted to Cairo University Internal Medicine Isolation Hospital from December 2020 through February 2021. SARS-CoV-2 infection was confirmed by RT-PCR testing. Pregnant patients, patients younger than 18 years, and patients with cancer or autoimmune disease were excluded. We collected clinical data, laboratory parameters, and outcome data through medical records. In total, 27 healthy individuals were enrolled as control individuals. The study protocol was approved by the Research Ethical Committee of Kasr AlAiny Faculty of Medicine, Cairo University. Written informed consent was obtained.

COVID-19 disease severity in patients was determined clinically, based on respiratory symptoms and the need for supplemental oxygen therapy.[12] Moderate illness was defined as evidence of lower respiratory tract disease during clinical assessment or imaging, and oxygen saturation (SpO_2) ≥94% when breathing room air. Patients were considered to have severe illness if they had SpO_2 <94% when breathing room air, respiratory rate of >30 breaths/minute, or lung infiltrates of >50%. Critical illness was defined as having evidence of respiratory failure, septic shock, and/or multiple organ dysfunction. The study included 25 patients with moderate illness and 20 patients with severe or critical illness. According to the institutional protocol at that time, all patients with moderate disease were treated with broad-spectrum antibiotics and remdesivir at the time of study inclusion. Patients with severe/critical illness received antibiotics, remdesivir, dexamethasone, and tocilizumab.

Peripheral-Blood Mononuclear Cell (PBMC) Isolation and Flow Cytometric Analysis

PBMCs were isolated from EDTA-anticoagulated peripheral blood by density gradient centrifugation (Biocoll Separating Solution, Bio&SELL). A multicolor panel of monoclonal antibodies was used for the study of MDSCs via flow cytometry. The panel comprised HLA-DR PE (Clone Immu-357), CD11b PE-Cy7 (Clone Bear1), CD33 PE-Cy5 (Clone D3HL60.251), CD14 ECD (Clone RMO52), and CD15 FITC (Clone 80H5) (all from Beckman Coulter). Monoclonal antibodies were added to 1×10^5 PBMCs suspended in phosphate-buffered saline (PBS) and incubated for 30 minutes at 4°C in the dark, then washed with PBS. The stained cells were acquired using a Beckman Coulter flow cytometer equipped with CXP Software version 2.2.

For defining and estimating circulating MDSCs in patients with COVID-19 and controls, PBMCs were gated on $CD15^+/CD14^-$ cells and cells expressing $CD11b^+$, $CD33^+$, and $HLA\text{-}DR^{-/low}$ were determined to be PMN-MDSCs. $HLA\text{-}DR^{-/low}$ cells expressing CD33 and CD11b were identified as M-MDSCs if expressing $CD14^+/CD15^-$ or E-MDSCs if expressing $CD14^-/CD15^-$.[10,13] MDSC populations were calculated and expressed as percentage of PBMCs.

Statistical Analysis

Using the Statistical Package for the Social Sciences (SPSS), version 20 (IBM) and GraphPad Prism, version 8.0 (GraphPad Software), quantitative variables were compared using nonparametric Kruskal-Wallis and Mann-Whitney testing. For comparing categorical data, χ^2 testing was performed. Correlations between quantitative variables were determined using the Spearman correlation coefficient. Univariate logistic regression was performed to detect independent predictors of poor outcome and death without adjustment for multiple comparisons. $P < .05$ was considered statistically significant.

Results

Clinical and Laboratory Parameters of Patients with COVID-19

The characteristics of patients hospitalized with confirmed SARS-CoV-2 infection are presented in **TABLE 1**. Patients with COVID-19 were stratified according to disease severity. In total, 20 patients were severely or critically ill and required admission to the ICU. This group was compared with 25 patients with moderate illness and 27 healthy individuals. The age of patients ranged between 25 and 88 years, with a median of 59 years. Patients with severe or critical disease were older than patients with moderate disease ($P = .001$). Most patients with severe and critical illness (95%) had underlying medical comorbidities, with a median of 2 preexisting comorbidities, the most common being hypertension (60%), diabetes (45%), and cardiovascular disease (30%). Asthma was the most common chronic pulmonary disease (15%), and hepatitis C virus infection was the cause of hepatic disease in 15% of patients. In total, 14 of 45 patients (31%) died during hospitalization from COVID-19 complications, comprising 70% of patients with severe and critical illness.

C-reactive protein (CRP) levels were higher in patients with severe/critical COVID-19 than in patients with moderate COVID-19 ($P = .006$). Levels of CRP did not correlate with increasing levels of IL-6 in patients with COVID-19 ($r = 0.106$; $P = .63$). High ferritin concentrations were not statistically different between patients with moderate or severe/critical COVID-19 ($P = .61$) (**TABLE 1**). Although not statistically significant, D-dimer levels were 3-fold higher in patients with severe/critical COVID-19 than patients with moderate COVID-19 (median, 2.42 mg/L vs 0.82 mg/L; $P = .16$). D-dimer levels were elevated in 60% of patients in the severe/critical group; this elevation was associated with mild thrombocytopenia in 20% of patients. Higher D-dimer levels and lower platelet counts were detected in patients with severe/critical disease who were older than 60 years, compared with the patients who were younger than 60 years (D-dimer: 3.33 [1.42–6.65] mg/L vs 0.40 [0.36–1.70] mg/L, $P = .045$; and platelets: 145 [69–168] $\times 10^3$/μL vs 193 [187–304] $\times 10^3$/μL, $P = .048$, respectively).

Collectively, our results indicate that age, preexisting comorbidities, increased CRP, and peripheral blood lymphopenia are linked to severity of disease in patients with COVID-19 (**TABLES 1** and **2**). Lymphopenia, defined as a lymphocyte count of <1000/μL, was found in 80% of patients with severe and critical COVID-19 and 28% of those with moderate COVID-19 ($P = .003$) (**TABLE 2**). This finding was associated with an increased neutrophil to lymphocyte ratio in patients with severe/critical disease, compared with patients with moderate disease ($P = .02$). Patients with severe and critical disease also showed lower hemoglobin levels, compared with patients having moderate disease ($P = .01$).

TABLE 1. Clinical and Laboratory Characteristics of Patients with COVID-19

Variable	Moderate COVID-19 (n = 25)	Severe/Critical COVID-19 (n = 20)	*P* Value[a]
Age, y, median (IQR)	51 (46-60)	67 (56-75)	**.001**
Male sex, No. (%)	17 (68)	10 (50)	.22
Comorbidities, No. (%)	8 (32)	19 (95)	**<.001**
No. of comorbidities, median (IQR)	0 (0-1)	2 (1-3)	**<.001**
D-dimer, mg/L FEU, median (IQR)	0.82 (0.44-1.68)	2.42 (0.4-4.32)	.16
CRP, mg/L, median (IQR)	31.5 (8.9-57.6)	82.2 (38.3-144.5)	**.006**
IL-6, pg/mL, median (IQR)	52 (12-239)	43 (24-84)	.67
Procalcitonin, ng/mL, median (IQR)	—	0.9 (0.11-2.4)	—
Ferritin, ng/mL, median (IQR)	812 (592-1247)	604 (253-1258)	.61
ALT, U/L, median (IQR)	30 (13.5-45)	18 (13-28)	.39
LDH, U/L, median (IQR)	310 (226-410)	444 (288-530)	.12
Creatinine, mg/dL, median (IQR)	1.05 (0.81-1.48)	1.1 (0.84-1.38)	.94
Invasive ventilation, No. (%)	—	20 (100)	—
Death, No. (%)	0	14 (70)	—

ALT, alanine aminotransferase; CRP, C-reactive protein; FEU, fibrinogen equivalent units; IQR, interquartile range; LDH, lactate dehydrogenase.
[a]*Bold type indicates statistical significance (*P *< .05).*

TABLE 2. Hematological Parameters in Patients with COVID-19

Variable	Moderate COVID-19 (n = 25)	Severe/Critical COVID-19 (n = 20)	*P* Value[a]
TLC, $\times 10^3$/μL, median (IQR)	8.5 (6.1-12.5)	8.9 (7.0-11.6)	.85
Lymphopenia, No. (%)	7 (28)	16 (80)	**.003**
Lymphocytes, %, median (IQR)	10.4 (5.0-19.0)	6.3 (3.5-10.0)	**.04**
Absolute lymphocyte count,/μL, median (IQR)	1120 (680-1489)	510 (330-820)	**.001**
Monocytes, %, median (IQR)	6 (3-8)	4.7 (2.5-8.5)	.91
Absolute monocytic count,/μL, median (IQR)	489 (352-692)	385 (218-687)	.63
Neutrophils, %, median (IQR)	83 (71-90)	88 (83-92)	.07
Absolute neutrophil count,/μL, median (IQR)	6729 (4772-10,558)	7953 (6150-10,316)	.80
Neutrophil/lymphocyte ratio, median (IQR)	7.1 (2.4-15.8)	14.3 (8.2-25.7)	**.02**
Lymphocyte/monocyte ratio, median (IQR)	2.1 (1.5-3.8)	1.4 (0.9-2.6)	.06
Hemoglobin, g/dL, median (IQR)	12.4 (11.6-13.3)	11 (9.5-12.1)	**.01**
Platelets, $\times 10^3$/μL, median (IQR)	293 (240-334)	181 (133-222)	**<.001**

IQR, interquartile range; TLC, total leukocytic count.
[a]*Bold type indicates statistical significance (*P *< .05).*

Patients with Severe/Critical COVID-19 Present an Expansion in the Proportion of Circulating PMN-MDSCs

We quantified the relative proportions of MDSC populations as a percentage of PBMCs in patients with COVID-19, compared with healthy controls. Circulating neutrophilic MDSCs (PMN-MDSCs), identified as $CD15^+/CD14^-/CD11b^+/CD33^+$ and HLA-$DR^{-/low}$, were found to be significantly higher in patients with severe and critical illness, compared with patients with moderate illness patients and controls (P = .005; **FIGURE 1A**). The median frequency of PMN-MDSCs in patients with severe/critical illness was 2.02%; meanwhile, the median frequency was 0.48% and 0.51% in patients with moderate illness and controls, respectively.

The relative proportions of monocytic MDSCs (M-MDSCs), defined as HLA-$DR^{-/low}$ and $CD11b^+/CD33^+/CD14^+/CD15^-$, did not differ statistically between patients and controls (P = .22; **FIGURE 1B**). M-MDSCs increased significantly with increasing PMN-MDSCs in patients with severe/critical illness (r = 0.713; P <.001) and in patients with moderate illness (r = 0.565; P = .003), but not in healthy controls (**FIGURE 2A-2C**).

Circulating early MDSCs (E-MDSCs), defined as HLA-$DR^{-/low}$ and $CD11b^+/CD33^+/CD14^-/CD15^-$, were decreased in patients with moderate disease than in controls (median, 0.12% and 0.25%, respectively; P = .004) (**FIGURE 1C**). The early phenotype (E-MDSCs) increased with increasing PMN-MDSCs (r = 0.387; P = .046) and M-MDSCs (r = 0.502; P = .008) in healthy controls; however, this positive correlation was lost in moderate and severe/critical disease (**FIGURE 2D-2I**).

Relationship between MDSC Levels and Clinical Characteristics in Patients with COVID-19

To understand whether increased PMN-MDSC proportion in severe/critical disease was affected by patient clinical characteristics, we analyzed PMN-MDSCs in patients stratified by age and sex. Although sex did not influence PMN-MDSC frequency (P = .36), age

FIGURE 1. **Frequency of circulating myeloid-derived suppressor cell (MDSC) phenotypes in peripheral blood mononuclear cells (PBMCs) of patients with COVID-19. A, A significant increase in the relative proportions of circulating polymorphonuclear (PMN)–MDSCs as a percentage of PBMCs was observed in patients with severe/critical illness, compared with patients with moderate illness and healthy control individuals. B, The relative proportions of monocytic MDSCs (M-MDSCs) did not differ between the 3 groups. C, Decreased proportions of early MDSCs (E-MDSCs) was observed in patients with moderate COVID-19, compared with controls.**

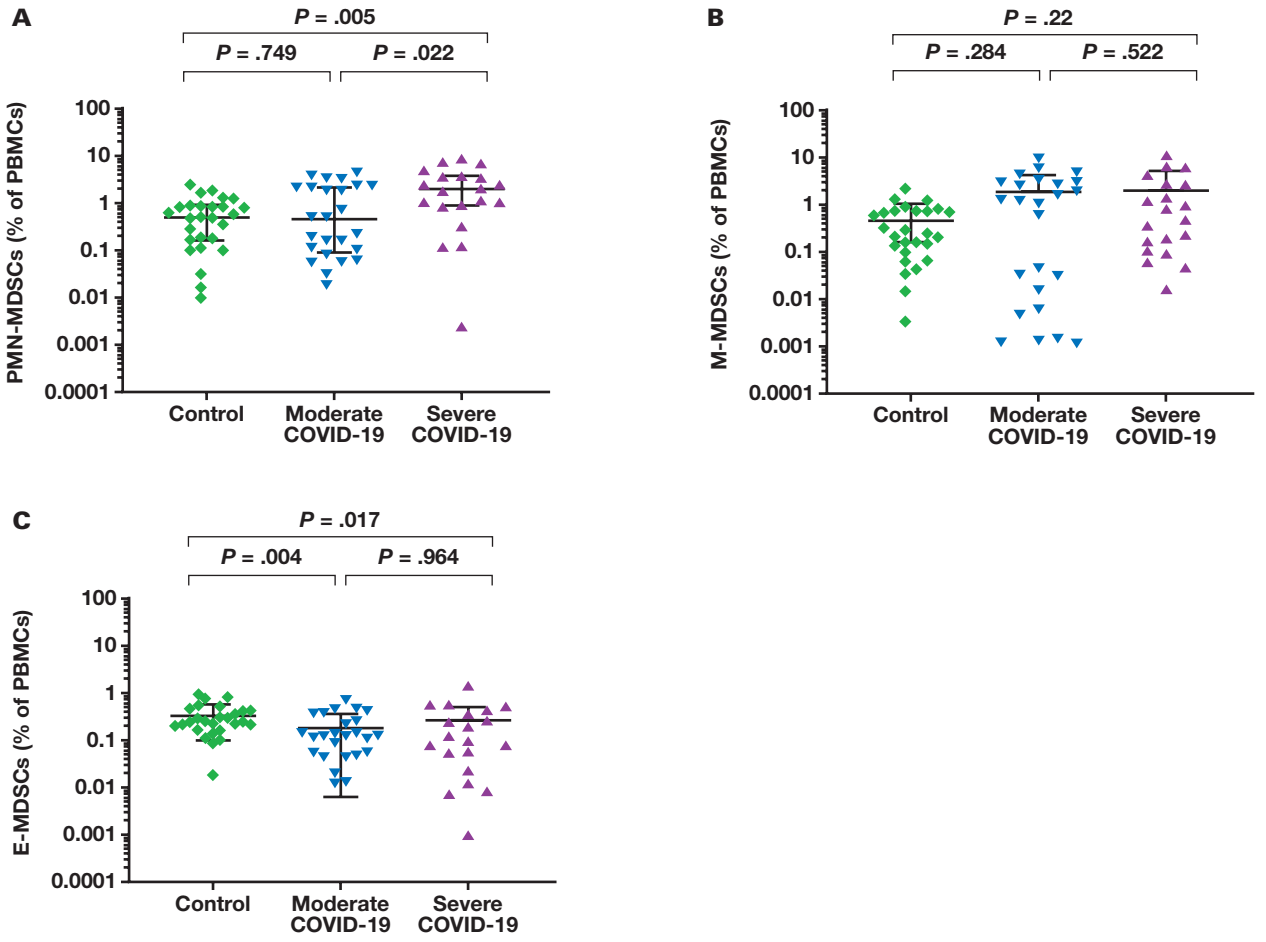

of 60 years and younger was significantly associated with higher PMN-MDSCs, compared with age older than 60 years (median, 6.03% [3.7%–7.5%] vs 1.1% [0.33%–2.1%]; $P = .004$; **FIGURE 3**). This difference in PMN-MDSC proportion between age groups was not associated with a difference in inflammatory markers (CRP, $P = .79$ and IL-6, $P = .54$), lymphocyte count ($P = .12$) or the number of comorbidities ($P = .75$).

We further studied the relationship between MDSC populations and markers of inflammation and injury (IL-6, CRP, D-dimer, ferritin, procalcitonin, lactate dehydrogenase [LDH], and alanine aminotransferase [ALT] levels) and lymphocyte count in all cohort patients with COVID-19. Data from our Spearman correlation matrices are presented in **TABLE 3**. We note that MDSC proportions were not significantly associated with the concentrations of inflammatory markers, such as CRP, IL-6, ferritin, D-dimer levels, and procalcitonin levels. Also, MDSCs did not correlate with decreasing lymphocyte counts. We observed a weak association between the frequency of PMN-MDSCs and increasing LDH ($r = 0.373$; $P = .03$) and ALT ($r = 0.379$; $P = .02$) levels.

Levels of MDSCs Are Not Predictive of Death in Patients with COVID-19

In our cohort, 14 patients died from COVID-19–related complications, comprising 70% of patients with severe and critical illness. Univariate logistic regression analysis was applied to assess the possibility of using the level of circulating MDSCs as a predictive marker of poor outcome in all patients with COVID-19 (**TABLE 4**). The frequency of PMN-MDSCs, M-MDSCs, and E-MDSCs was not predictive of death in COVID-19 ($P = .40$, $P = .27$, and $P = .54$, respectively). Meanwhile, lymphopenia was a significant predictor of poor prognosis in patients with COVID-19 (odds ratio [OR], 5.958 [95% CI, 1.090–32.573]; $P = .04$). CRP was also significantly predictive of death ($P = .04$). The OR for CRP indicated that for each 1-unit increase in CRP, the odds of death increased by 0.015. Considering that the risk of fatal outcome in COVID-19 increases with aging, we further selected age 60 years as the cutoff dividing older vs younger patients, given its use in studies evaluating the relationship of aging with mortality in COVID-19.[14] Age older than 60 years was significantly associated with death (OR, 5.625 [95% CI, 1.349-23.449]; $P = .02$). The risk of death also increased

FIGURE 2. Correlation between the different phenotypes of myeloid-derived suppressor cells (MDSCs) of patients with COVID-19. A, D, G, controls; B, E, H, moderate COVID-19; C, F, I, severe COVID-19. A, No relationship between polymorphonuclear (PMN)–MDSCs and monocytic MDSCs (M-MDSCs) was observed in healthy control individuals ($r = 0.141$; $P = .48$). Still, significant correlation was detected in patients with moderate COVID-19 ($r = 0.565$; $P = .003$) (B) and in patients with severe and critical COVID-19 ($r = 0.713$; $P < .001$) (C). D, PMN-MDSCs correlated positively with early MDSCs (E-MDSCs) in controls ($r = 0.387$; $P = .046$). However, this correlation was not observed in moderate disease ($r = 0.215$; $P = .30$) (E) or severe disease ($r = 0.263$; $P = .26$) (F).

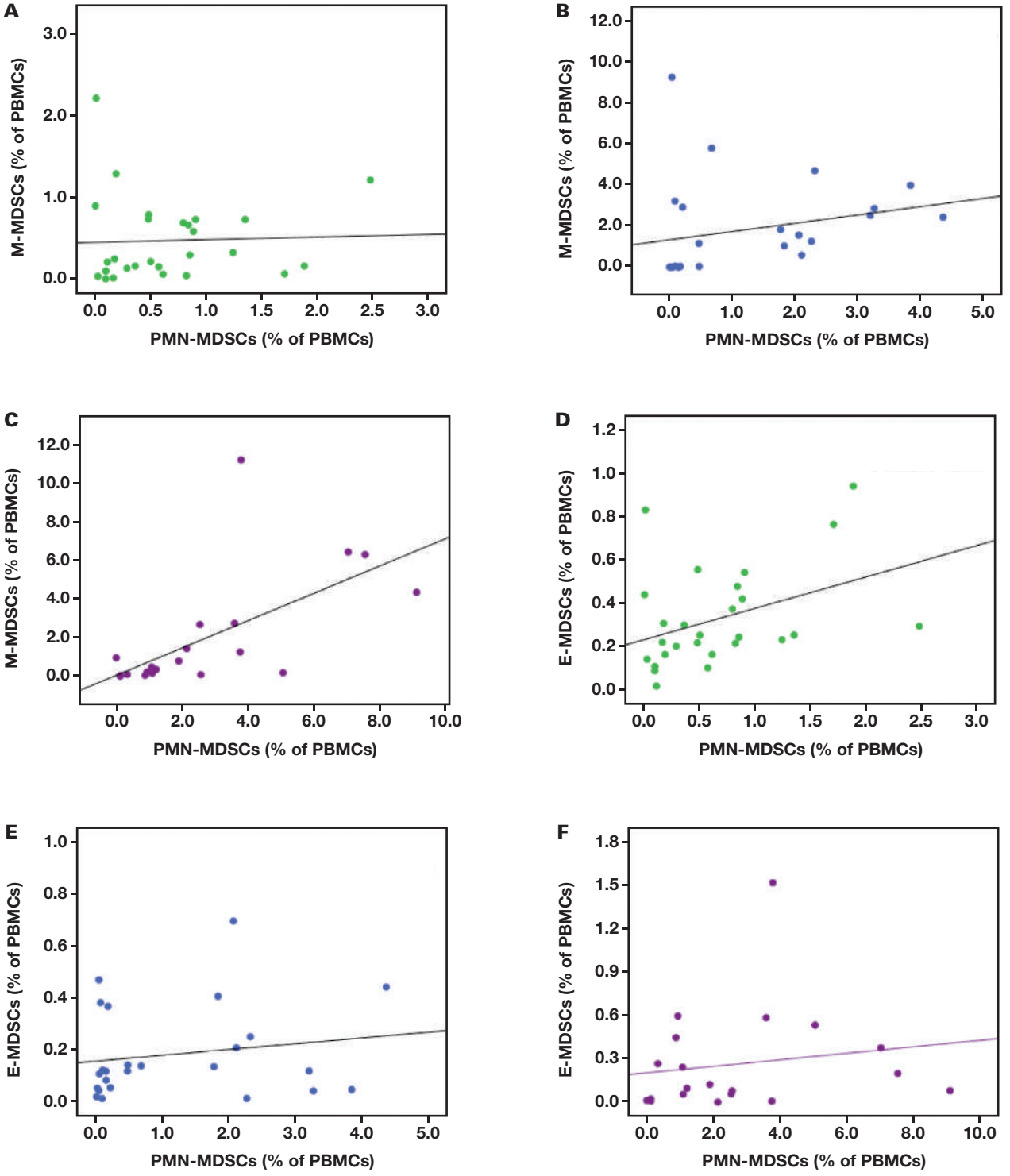

FIGURE 2. (cont) Similarly, M-MDSCs showed a positive correlation with E-MDSCs in controls ($r = 0.502$; $P = .008$) (G) but not in moderate disease ($r = 0.186$; $P = .37$) (H) or severe disease ($r = 0.212$; $P = .37$) (I).

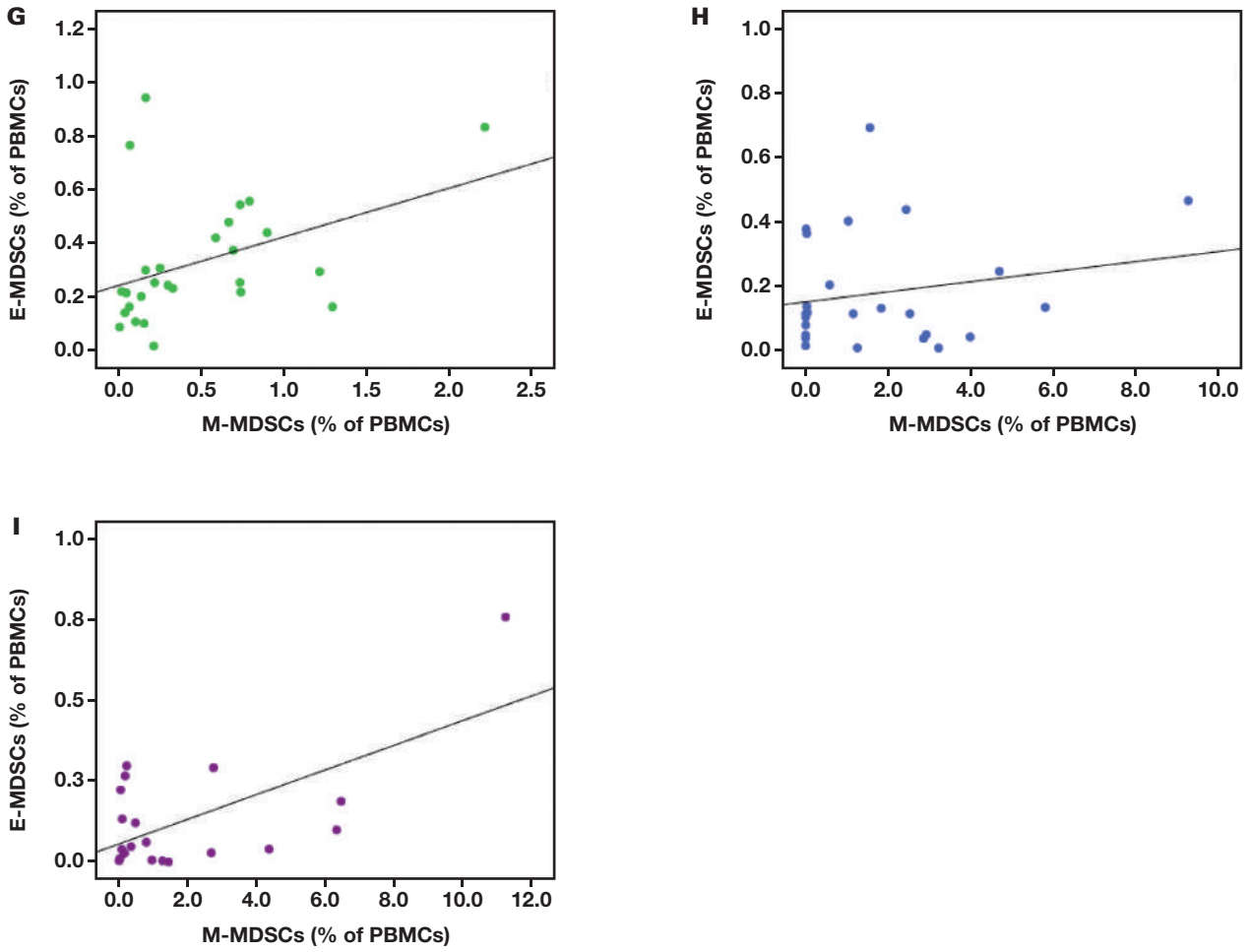

significantly with the number of comorbidities (OR, 2.818 [95% CI, 1.435-5.532]; $P = .003$; **TABLE 4**).

Discussion

MDSCs are present at very low levels during steady state in healthy individuals. We observed high percentages of PMN-MDSCs in patients diagnosed with COVID-19, in association with disease severity; meanwhile, patients with moderate disease showed frequencies of PMN-MDSCs comparable with those in healthy controls. This expansion of PMN-MDSCs may represent a regulatory mechanism, critical for modulation of a highly inflammatory immune response to SARS-CoV-2 to maintain immune tolerance, tissue repair, and homeostasis. Paradoxically, higher PMN-MDSCs can dysregulate antiviral immune responses and exacerbate COVID-19 disease. In this respect, PMN-MDSCs play dual effects: they exert beneficial effects by limiting severe inflammation and excessive organ injury associated with potent antiviral immune response. However, MDSCs inhibit effective immune responses against the virus, favoring severe disease and worse outcomes.

Confirming their potent T-cell–suppressive function in vivo, PMN-MDSCs were shown to inhibit SARS-CoV-2 T-cell response in an antigen-specific manner ex vivo; also, MDSC depletion restored T-cell functions.[8,9] The T-cell–suppressive activity of PMN-MDSCs in severe disease is potently induced by reactive oxygen species, through increased expression of genes of the NADPH oxidase system.[15] PMN-MDSCs from patients with severe disease showed increased expression of genes associated with granulocyte degranulation and inflammation, including metalloproteinases MMP8 and MMP9, alarmins of inflammation S100A8 and A9, myeloperoxidase, and arginase-1.[16]

PMN-MDSCs expressing arginase-1 were found to be infiltrating the lungs of patients who died from COVID-19 complications. Arginase-1 is an enzyme that restricts the availability of L-arginine, an amino acid which is essential for T-cell proliferation.[17] We note that in our study, the expansion of peripheral blood PMN-MDSCs in patients with severe COVID-19 was not isolated because it was associated with decreased lymphocytes, indicating a decrease of adaptive T cells in controlling SARS-CoV-2 infection. PMN-MDSCs, however, did not directly correlate with decreasing lymphocyte numbers, suggesting that there are other pathogenic mechanisms of lymphopenia in SARS-CoV-2 infection. This finding could be due to migration of T lymphocytes from the peripheral blood into infected organs, mainly the lungs, attracted by chemokines released by infected cells at the site of disease.[18] It was also shown that SARS-CoV-2 directly infects and replicates in lymphocytes, leading to apoptosis of T lymphocytes.[19]

PMN-MDSCs and M-MDSCs comprised 0.51% and 0.25%, respectively, of peripheral blood mononuclear cells in healthy individuals. MDSCs were present in low levels in healthy individuals due to the rapid differentiation of those cells into mature granulocytes and monocytes.[20] Patients with severe/critical COVID-19 infection showed a shift towards an immature PMN-MDSC profile, together with a relative increase in

FIGURE 3. **Frequency of myeloid-derived suppressor cells (MDSCs) in patients with severe and critical COVID-19, stratified by age. A, Age of 60 years and younger was significantly associated with higher polymorphonuclear (PMN)–MDSCs than patients older than 60 years (*P* = .004). Monocytic MDSCs (M-MDSCs) (*P* = .08) (B) and early MDSCs (E-MDSCs) (*P* = .93) (C) did not show a statistically significant difference according to age.**

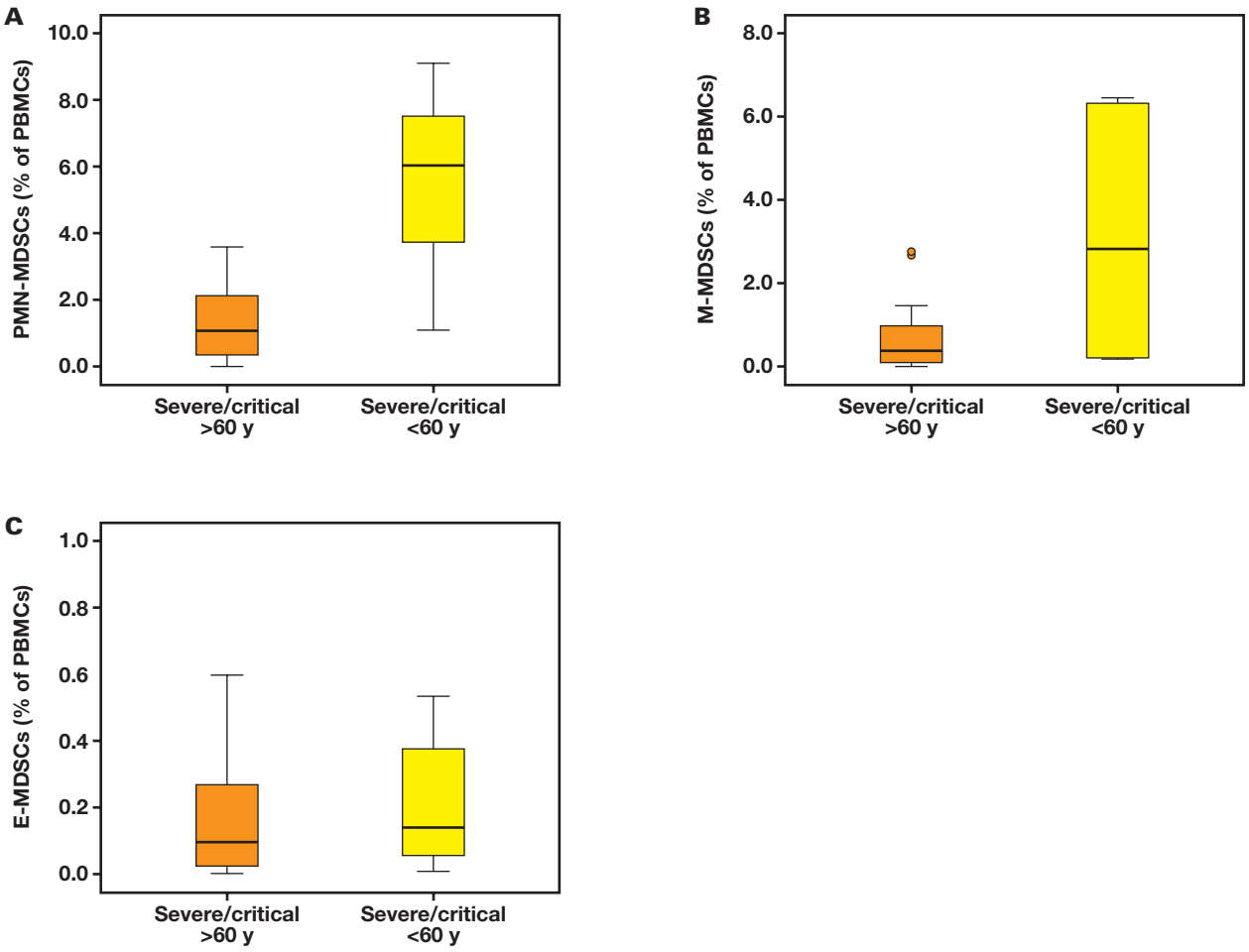

TABLE 3. **Correlation Between MDSCs and Markers of Inflammation and Injury in Patients with COVID-19**[a]

MDSCs	IL-6	CRP	D-dimer	Ferritin	Procalcitonin	LDH	ALT	Lymphocyte Count
PMN-MDSCs, *r* (*P* value)	–0.123 (.57)	0.086 (.63)	–0.053 (.74)	0.046 (.81)	–0.245 (.42)	0.373 (**.03**)	0.379 (**.02**)	–0.173 (.30)
M-MDSCs, *r* (*P* value)	–0.297 (0.16)	0.133 (.45)	–0.057 (0.72)	–0.201 (.30)	–0.050 (.87)	0.255 (.15)	0.207 (.20)	0.078 (.64)
E-MDSCs, *r* (*P* value)	0.073 (.73)	0.008 (.97)	0.030 (.85)	0.024 (.90)	–0.132 (.67)	0.009 (.96)	0.138 (.40)	0.001 (.99)

ALT, alanine aminotransferase; CRP, C-reactive protein; E-MDSCs, early MDSCs; FEU, fibrinogen equivalent units; LDH, lactate dehydrogenase; MDSCs, myeloid-derived suppressor cells; M-MDSCs, monocytic MDSCs; PMN-MDSCs, polymorphonuclear MDSCs.
[a]*Bold type indicates statistical significance (*P < .05)*

mature neutrophils in the peripheral blood. This profile is promoted by emergency myelopoiesis, which is identified as a hallmark of severe COVID-19.[21] Severe inflammation can induce emergency myelopoiesis, particularly granulopoiesis and monopoiesis, with a suppressive function.[22] It seems that massive exposure of myeloid progenitors to SARS-CoV-2 prompts the activation of immunosuppressive programming in myeloid cells, leading to the rapid development of MDSCs.

Also, we detected high levels of CRP, which was shown to promote the expansion of MDSCs.[23] CRP is an acute phase reactant in the IL-6 pathway. There is a critical requirement for IL-6 and STAT3 signaling in expansion of MDSCs in infection.[24] When we plotted levels of this inflammatory cytokine, which we found to be upregulated, against percentages of different MDSCs, we did not observe a significant correlation. Other factors that induce MDSC expansion in COVID-19 remain partly defined but include a variety of factors, such as hypoxia, granulocyte and granulocyte-macrophage colony-stimulating factor, TNF-α, vascular endothelial growth factor, IL-1β, damage-associated molecular patterns, proinflammatory molecules such as alarmins S100A8/9, checkpoint regulators such as PD-1/PD-L1, and pathogen-associated molecular patterns.[21]

Clinically, lymphopenia, increased neutrophil/lymphocyte ratio, and high levels of CRP distinguished severe from moderate disease. Our

TABLE 4. Prediction of Poor Outcome and Death by Different Parameters in Patients with COVID-19

Variable	Univariate OR (95% CI)	*P* Value[a]
Age >60 y	5.625 (1.349-23.449)	**.02**
Male sex	2.800 (0.764-10.264)	.12
No. of comorbidities	2.818 (1.435-5.532)	**.003**
CRP	1.015 (1.001-1.030)	**.04**
IL-6	0.998 (0.991-1.004)	.48
D-dimer	1.097 (0.895-1.344)	.37
Lymphopenia (lymphocyte count <1000/μL)	5.958 (1.090-32.573)	**.04**
PMN-MDSCs	1.132 (0.850-1.506)	.40
M-MDSCs	0.835 (0.606-1.150)	.27
E-MDSCs	0.420 (0.026-6.693)	.54

CRP, C-reactive protein; E-MDSCs, early MDSCs; M-MDSCs, monocytic MDSCs; MDSCs, myeloid-derived suppressor cells; OR, odds ratio; PBMCs, peripheral blood mononuclear cells; PMN-MDSCs, polymorphonuclear MDSCs.
[a]Bold type indicates statistical significance (P < .05).

findings indicate that PMN-MDSC expansion during COVID-19 infection is also a biomarker of disease severity. We found that PMN-MDSCs correlated with increasing ALT and LDH levels, signifying the association with disease severity and effects on multiple organ systems.

Elevated circulating LDH is a marker of pyroptotic cell death, a highly inflammatory form of cell death induced mainly by inflammasome-mediated IL-1β and IL-18 production.[25] The extent of inflammasome activation was shown to correlate with COVID-19 disease severity.[26] This pathway also activates the coagulation cascade; thrombotic events are common in patients with severe disease.[27] In addition to significant pulmonary complications, 60% of patients with severe and critical COVID-19 illness manifested with increased D-dimer levels and unchanged or modestly decreased platelet count. The D-dimer elevation signifies hyperfibrinolysis and increased inflammatory burden induced in SARS-COV-2 infection. Also, PMN-MDSCs can directly activate platelets by decreasing L-arginine, providing a different role of PMN-MDSCs in severe COVID-19 than previously assumed.[28]

It is evident that the outcome of infection with SARS-CoV-2 varies broadly. In our cohort, 14 patients died from COVID-19–related complications, comprising 70% of patients with severe and critical illness. In our analysis to estimate risk factors associated with death, the expansion of PMN-MDSCs was not associated with increased risk of mortality, although it is a distinctive characteristic of severe COVID-19. Contrary to study findings suggesting a prognostic potential of MDSCs for fatal outcomes in COVID-19,[9] a study showed expansion of PMN-MDSCs that was delayed and transient in survivors of severe disease, but such expansion was not observed in those who had died.[29]

Although we did not investigate serial monitoring of MDSCs in assessment of patients with COVID-19, it is possible that during severe COVID-19, the early expansion of PMN-MDSCs may suppress T-lymphocyte response to the virus. In contrast, the expansion of PMN-MDSCs occurring at a later time in infection may promote homeostasis and tolerance. MDSCs in the lungs, the site of infection, can also influence the prognosis. We could not assess MDSCs in the lungs; thus, we focused on circulating MDSCs, on the basis that MDSCs are produced in the bone marrow, first migrating to the peripheral blood and then reaching the lungs. Despite the increasing understanding of COVID-19 immunopathogenesis, the complex multiorgan, comorbidity, and age-dependent nature of the disease and evolving nature of the virus may direct the different COVID-19 disease courses.

The clinical course of our patient cohort is similar to those in earlier reports, in which elderly patients with preexisting medical conditions experienced more-severe disease and higher mortality.[30] Age was a strong independent risk factor for death in COVID-19. The devastating clinical outcome in older age raises the implication of age-related changes of the immune system in determining COVID-19 severity and mortality. An important feature of the aging immune system is inflammaging, a systemic and chronic inflammatory state.[31] Increased inflammation with age is indicative of reduced immune regulatory function. Severe COVID-19 disease in individuals aged older and younger than 60 years was associated with distinct PMN-MDSC frequencies, being predominantly higher in 60 years and younger adults. Meanwhile, both age groups had comparable inflammatory markers, including acute phase reactants, contributing to the clinical outcome. This finding corroborates MDSCs as regulators of the immune response in COVID-19.

These observations suggest that progression to severe disease and death in COVID-19 may proceed by different immunologic mechanisms in younger vs older patients and thus present the possibility of age-based immunomodulating treatments. It remains to be assessed whether PMN-MDSCs could be superior to clinical markers for monitoring treatment response in COVID-19.

Conclusion

In the present study finding, there was a significant association between PMN-MDSC levels and disease severity. Given the role of MDSCs in COVID-19, a consequent question is whether there is a means to therapeutically balance increased inflammation and immunosuppression to improve outcomes in hospitalized patients with COVID-19.

Acknowledgment

This work was funded by Cairo University research fund.

Conflict of Interest Disclosure

The authors have nothing to disclose.

REFERENCES

1. Huang W, Li M, Luo G, et al. The inflammatory factors associated with disease severity to predict COVID-19 progression. *J Immunol*. 2021;206(7):1597-1608. doi:10.4049/jimmunol.2001327
2. Del Valle DM, Kim-Schulze S, Huang H-H, et al. An inflammatory cytokine signature predicts COVID-19 severity and survival. *Nat Med*. 2020;26(10):1636-1643. doi:10.1038/s41591-020-1051-9
3. Loftus TJ, Ungaro R, Dirain M, et al. Overlapping but disparate inflammatory and immunosuppressive responses to SARS-CoV-2 and bacterial sepsis: an immunological time course analysis. *Front Immunol.* 2021;12:5343. doi:10.3389/fimmu.2021.792448
4. Scagnolari C, Pierangeli A, Frasca F, et al. Differential induction of type I and III interferon genes in the upper respiratory tract of patients with coronavirus disease 2019 (COVID-19). *Virus Res*. 2021;295:198283. doi:10.1016/j.virusres.2020.198283
5. Wilk AJ, Rustagi A, Zhao NQ, et al. A single-cell atlas of the peripheral immune response in patients with severe COVID-19. *Nat Med.* 2020;26:1070-1076. doi:10.1038/s41591-020-0944-y
6. Diao B, Wang C, Tan Y, et al. Reduction and functional exhaustion of T cells in patients with coronavirus disease 2019 (COVID-19). *Front Immunol*. 2020;11:827. doi:10.3389/fimmu.2020.00827
7. Wen W, Su W, Tang H, et al. Immune cell profiling of COVID-19 patients in the recovery stage by single-cell sequencing. *Cell Discov*. 2020;6:1-8. doi:10.1038/s41421-020-0168-9
8. Agrati C, Sacchi A, Bordoni V, et al. Expansion of myeloid-derived suppressor cells in patients with severe coronavirus disease (COVID-19). *Cell Death Differ.* 2020;27:3196-3207. doi:10.1038/s41418-020-0572-6
9. Sacchi A, Grassi G, Bordoni V, et al. Early expansion of myeloid-derived suppressor cells inhibits SARS-CoV-2 specific T-cell response and may predict fatal COVID-19 outcome. *Cell Death Dis*. 2020;11:1-9. doi:10.1038/s41419-020-03125-1
10. Bronte V, Brandau S, Chen S-H, et al. Recommendations for myeloid-derived suppressor cell nomenclature and characterization standards. *Nat Commun*. 2016;7:12150. doi:10.1038/ncomms12150
11. Atanackovic D, Avila SV, Lutfi F, et al. Deep dissection of the antiviral immune profile of patients with COVID-19. *Commun Biol*. 2021;4:1389. doi:10.1038/s42003-021-02852-1
12. COVID-19 Treatment Guidelines Panel. Coronavirus Disease 2019 (COVID-19) Treatment Guidelines. National Institutes of Health. Accessed May 9, 2023. https://www.covid19treatmentguidelines.nih.gov/
13. Cassetta L, Bruderek K, Skrzeczynska-Moncznik J, et al. Differential expansion of circulating human MDSC subsets in patients with cancer, infection and inflammation. *J Immunother Cancer*. 2020;8(2):e001223. doi:10.1136/jitc-2020-001223
14. Meslé MMI, Brown J, Mook P, et al. Estimated number of deaths directly averted in people 60 years and older as a result of COVID-19 vaccination in the WHO European Region, December 2020 to November 2021. *Eurosurveillance*. 2021;26(47):2101021. doi:10.2807/1560-7917.ES.2021.26.47.2101021
15. Mukund K, Nayak P, Ashokkumar C, et al. Immune response in severe and non-severe coronavirus disease 2019 (COVID-19) infection: a mechanistic landscape. *Front Immunol*. 2021;122:3928. doi:10.3389/fimmu.2021.738073
16. Dean MJ, Ochoa JB, Sanchez-Pino MD, et al. Severe COVID-19 is characterized by an impaired type I interferon response and elevated levels of arginase producing granulocytic myeloid derived suppressor cells. *Front Immunol*. 2021;12:2726. doi:10.3389/fimmu.2021.695972
17. Rodríguez PC, Ochoa AC. Arginine regulation by myeloid derived suppressor cells and tolerance in cancer: mechanisms and therapeutic perspectives. *Immunol Rev* 2008;222(1):180-191. doi:10.1111/j.1600-065X.2008.00608.x
18. Zhang S, Asquith B, Szydlo R, Tregoning JS, Pollock KM. Peripheral T cell lymphopenia in COVID-19: potential mechanisms and impact. *Immunother Adv.* 202;1(1):ltab015. doi:10.1093/immadv/ltab015
19. Pontelli MC, Castro ÍA, Martins RB, et al. SARS-CoV-2 productively infects primary human immune system cells *in vitro* and in COVID-19 patients. *J Mol Cell Biol.* 2022;14(4):mjac021. doi:10.1093/jmcb/mjac021
20. Gabrilovich DI, Nagaraj S. Myeloid-derived suppressor cells as regulators of the immune system. *Nat Rev Immunol.* 2009;9(3):162-174. doi:10.1038/nri2506
21. Rowlands M, Segal F, Hartl D. Myeloid-derived suppressor cells as a potential biomarker and therapeutic target in COVID-19. *Front Immunol*. 2021;12:2435. doi:10.3389/fimmu.2021.697405
22. Reyes M, Filbin MR, Bhattacharyya RP, et al. Plasma from patients with bacterial sepsis or severe COVID-19 induces suppressive myeloid cell production from hematopoietic progenitors in vitro. *Sci Transl Med*. 2021;13(598):eabe9599. doi:10.1126/scitranslmed.abe9599
23. Jimenez RV, Kuznetsova V, Connelly AN, Hel Z, Szalai AJ. C-reactive protein promotes the expansion of myeloid derived cells with suppressor functions. *Front Immunol*. 2019;10:2183. doi:10.3389/fimmu.2019.02183
24. Medina E, Hartl D. Myeloid-derived suppressor cells in infection: a general overview. *J Innate Immun*. 2018;10(5-6):407-413. doi:10.1159/000489830
25. Rayamajhi M, Zhang Y, Miao EA. Detection of pyroptosis by measuring released lactate dehydrogenase activity. In: *The Inflammasome*. Humana Press; 2013:85-90.
26. Rodrigues TS, de Sá KSG, Ishimoto AY, et al. Inflammasomes are activated in response to SARS-CoV-2 infection and are associated with COVID-19 severity in patients. *J Exp Med.* 2021;218(3):e20201701. doi:10.1084/jem.20201707
27. Middeldorp S, Coppens M, van Haaps TF, et al. Incidence of venous thromboembolism in hospitalized patients with COVID-19. *J Thromb Haemost.* 2020;18(8):1995-2002. doi:10.1111/jth.14888
28. Sacchi A, Grassi G, Notari S, et al. Expansion of myeloid derived suppressor cells contributes to platelet activation by L-arginine deprivation during SARS-CoV-2 infection. *Cells.* 2021;10(8):2111. doi:10.3390/cells10082111
29. Takano T, Matsumura T, Adachi Y, et al. Myeloid cell dynamics correlating with clinical outcomes of severe COVID-19 in Japan. *Int Immunol.* 2021;33(4):241-247. doi:10.1093/intimm/dxab005
30. Weiss P, Murdoch DR. Clinical course and mortality risk of severe COVID-19. *Lancet*. 2020;395(10229):1014-1015. doi:10.1016/s0140-6736(20)30633-4
31. Franceschi C, Campisi J. Chronic inflammation (inflammaging) and its potential contribution to age-associated diseases. *J Gerontol A Biol Sci Med Sci*. 2014;69(suppl 1):S4-S9. doi:10.1093/gerona/glu057

Reactogenicity and Peak Anti-RBD-S1 IgG Concentrations in Individuals with No Prior COVID-19 Infection Vaccinated with Different SARS-CoV-2 Vaccines

Lara Milevoj Kopcinovic, PhD,[1] Adriana Unic, PhD,[1] Nora Nikolac Gabaj, PhD,[1,2] Marijana Miler, PhD,[1] Alen Vrtaric, Msc,[1] Marija Bozovic, Msc,[1] Mario Stefanovic, PhD[1,2]

[1]Department of Clinical Chemistry, Sestre Milosrdnice University Hospital Center, Zagreb, Croatia, and [2]Faculty of Pharmacy and Biochemistry, University of Zagreb, Zagreb, Croatia. Corresponding author: Lara Milevoj Kopcinovic; laramilevoj@gmail.com

Key words: reactogenicity, anti-spike antibody, SARS-CoV-2, COVID vaccine, Comirnaty, Spikevax, Vaxzevria

Abbreviations: WHO, World Health Organization; EU, European Union; EQA, external quality assessment; RfB, Reference Institute for Bioanalytics; anti-RBDS1, anti–receptor-binding domain spike subunit 1; CMIA, chemiluminescent microparticle immunoassay

Laboratory Medicine 2024;55:162-168; https://doi.org/10.1093/labmed/lmad044

ABSTRACT

Objective: To investigate the association of immune response with vaccination adverse effects at peak anti–receptor-binding domain spike subunit 1 (anti-RBDS1) IgG after full vaccination with Comirnaty, Spikevax, or Vaxzevria.

Methods: Anti-RBDS1 IgG concentrations after vaccination were determined in healthy adults vaccinated with the Comirnaty, Spikevax, and Vaxzevria vaccines. The association of reactogenicity and peak antibody response after vaccination was tested.

Results: Anti-RBDS1 IgG values were significantly higher in the Comirnaty and Spikevax group, compared with the Vaxzevria group ($P < .001$). Fever and muscle pain were found to be significant independent predictors of peak anti-RBDS1 IgG in the Comirnaty and Spikevax groups ($P = .03$ and $P = .02$, respectively). The multivariate model, adjusted for covariates, showed that no association between reactogenicity and peak antibody concentrations was found in the Comirnaty, Spikevax, and Vaxzevria groups.

Conclusions: No association between reactogenicity and peak anti-RBDS1 IgG after vaccination with the Comirnaty, Spikevax, and Vaxzevria vaccine was found.

Global efforts to develop immunity at the population level, after the World Health Organization (WHO) declared COVID-19 a pandemic in March 2020, resulted in an unprecedentedly rapid development of safe and effective COVID-19 vaccines. Vaccines against SARS-CoV-2 have proved to be a valuable tool in the prevention and mitigation of SARS-CoV-2 infection.[1–4]

The new generation of mRNA vaccines encoding the SARS-CoV-2 spike (S) protein with lipid nanoparticle delivery systems, and the DNA vaccine encapsulated in nonreplicating adenoviral vectors encoding SARS-CoV-2 S protein, induce the production of high levels of S antigen in the host cells. These signals activate S protein–specific memory T and B cells that circulate along with high levels of anti-SARS-CoV-2 antibodies, to provide protection against SARS-CoV-2 infection.[1,5]

The antibody response after viral infection or vaccination in laboratory practice is measured by serological assays. The clinical value of SARS-CoV-2 serological testing is in the identification of viral exposure and previous infection. However, with the advent of mass immunization programs, antibody testing has been used as a valuable tool for establishing and monitoring vaccine immunogenicity, in terms of antibody development, peak concentration, and the decline of these variables over time.[6,7]

Vaccine reactogenicity refers to reactions that occur soon after vaccination; it represents a physical manifestation of the inflammatory response to vaccination.[8] Reactogenicity symptoms develop early after vaccine administration and are generally mild, localized, and without serious medical consequences. Understanding these factors is important for the individual receiving the vaccine, as well as for the health

care professionals recommending and administering the vaccine. This is particularly applicable to new vaccines (ie, COVID-19 vaccines) because compliance to vaccination strategies and higher vaccine acceptance are associated with the type and number of adverse effects experienced after vaccination.[8]

Reactogenicity symptoms associated with SARS-CoV-2 vaccines include varying degrees of adverse effects that might occur in individuals after COVID-19 vaccination. Reportedly, these symptoms comprise mostly mild to moderate local or systemic side effects (eg, pain and redness at the injection site, fever, headache, fatigue, myalgia, chills, nausea, and diarrhea) that disappear 3 to 5 days after inoculation.[4,9] Serious adverse effects with unexpected outcomes are very rare.[10,11]

Global vaccination against SARS-CoV-2 has revealed heterogeneity in reported individual immune responses and adverse effects.[5] In an effort to broaden the understanding of immunogenicity and reactogenicity of different SARS-CoV-2 vaccines in individuals with no previous COVID-19 infection, we aimed to quantify the immune response at peak antibody concentrations after full vaccination with the Comirnaty (BNT162b2; Pfizer-BioNTech), Spikevax (mRNA-1273; Moderna), or Vaxzevria (AZD1222; Oxford-AstraZeneca) vaccine and to document vaccination adverse effects and frequency. Our primary aim was to investigate the possible association of vaccination adverse effects and peak antibody response after vaccination with all 3 of the aforementioned COVID-19 vaccines.

Methods

Study Design

This cross-sectional investigation was part of a large prospective, observational, longitudinal study carried out in a cohort of volunteers, fully vaccinated (prime-boost vaccination) with the Comirnaty, Spikevax, and Vaxzevria COVID-19 vaccines. Participants were recruited from January 2021 through February 2022 in our tertiary care hospital.

The original study cohort included apparently healthy adult volunteers (≥18 years old) who were employed in our hospital or recruited from the general population (**FIGURE 1**). The participants were invited via oral communication or by email invitation. The only inclusion criteria was full vaccination, per vaccination protocol, with 1 of the 3 most frequently administered COVID-19 vaccines in the European Union (EU): Comirnaty, Spikevax, or Vaxzevria. No exclusion criteria were applied for the original cohort.

FIGURE 1. Flowchart of participant enrollment.

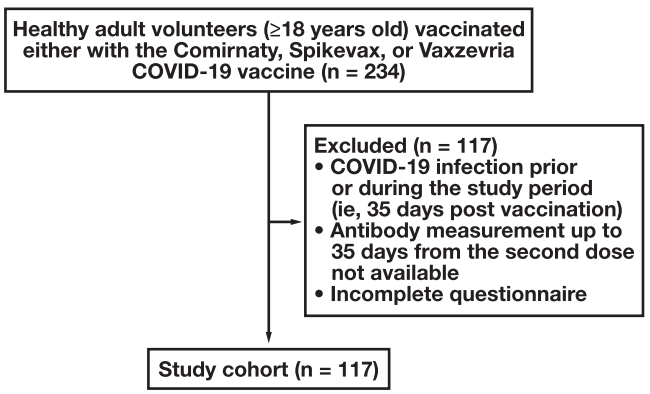

All participants were asked to complete a standardized written questionnaire, including questions on baseline demographics and SARS-CoV-2 epidemiologic history, and COVID-19 vaccination details, including postvaccination adverse effects (reactogenicity). The reported adverse effects were selected from those already reported and were associated with the second vaccine dose. All participants from the original cohort were invited to attend quantitative monitoring of antibody concentrations on a monthly basis after full vaccination for 1 year (or until inoculation with a booster vaccine dose).

The investigation was conducted in accordance with the Code of Ethics of the World Medical Association (Declaration of Helsinki) for experiments involving humans and was approved by the hospital Ethics Committee. All participants agreed to participate by signing written informed consent documentation.

Subjects

A total of 234 participants met the inclusion criteria for the original cohort. For the purpose of this investigation, we initially excluded from final analysis all participants with a history of COVID-19 infection before and up to 35 days after vaccination (as confirmed with a positive result via SARS-CoV-2 reverse transcription polymerase chain reaction testing). To detect the peak antibody concentration after full vaccination, the final analysis included only participants with antibody concentrations measured up to 35 days from the second inoculation dose, which comprised 1 measurement per participant (ie, a single measurement taken no later than 35 days after the second vaccine dose per participant). Further, participants with incomplete questionnaires were also excluded from further analysis, leaving a total of 117 participants in the final study group (70 in the Comirnaty group, 14 in the Spikevax group, and 33 in the Vaxzevria group; **FIGURE 1**).

Quantitative Determination of Anti-RBDS1 IgG Antibodies

A venous blood specimen was taken from each participant in the final study group within the first 35 days after the second vaccine dose. Participants were not required to be fasting. Blood was collected into tubes containing serum clot activator without gel separator (Vacuette 4 mL, Greiner Bio-One International). Tubes were mixed according to manufacturer recommendations and left in an upright position for 10 minutes. Specimens were then centrifuged for 7 minutes on the 2800*g* setting. After centrifugation, concentrations of anti–receptor-binding domain spike subunit 1 (anti-RBDS1) IgG antibodies were measured using the chemiluminescent microparticle immunoassay (CMIA) on the ARCHITECT *i*2000SR analyzer (Abbott) with proprietary reagents (SARS-CoV-2 IgG II, Abbott Laboratories). The manufacturer assay cutoff for positivity is set to ≥50 AU/mL. The analytical performance of the SARS-CoV-2 IgG II assay was previously evaluated; these results confirmed high sensitivity and specificity (98% and 100%, respectively, ≥14 days after positive molecular testing).[12,13] Further, our test performance was verified using the external quality assessment (EQA) scheme of the Reference Institute for Bioanalytics (RfB). All of the EQA specimens met the criteria of the organizers and were correctly classified.

Finally, based on our professional experience and available data from the literature, we defined a peak antibody response as the concentration of anti-RBDS1 IgG antibodies >10,000 AU/mL when measured up to 35

days from the second vaccine dose. This value is 200-fold higher than the cutoff for seropositivity defined by the manufacturer.[14,15]

Statistical Analysis

The primary end point of this investigation was the peak concentration of anti-RBDS1 IgG antibodies; the secondary end point was vaccine reactogenicity. Normality distribution was tested using the D'Agostino-Pearson test. Continuous variables were presented as median (interquartile range [IQR]) and as number (percentage) in the case of categorical variables. Age in years was presented as median (range). Differences between multiple groups were measured using the Kruskal-Wallis test paired with the Dunn post hoc test; categorical variables were measured using the χ^2 test. The association of vaccination adverse effects and peak antibody response after vaccination was tested using univariate and multivariate logistic regression analysis. The dataset was developed in a Microsoft Excel spreadsheet, version 2013 (Microsoft). Statistical analysis was performed using MedCalc software (version 20.008; MedCalc Software). The level of statistical significance was set at $P < .05$.

Results

The median age of our cohort was 40 years (range, 22-70 years). Most of the participants enrolled were female (93/117 [79.5%]). The second vaccine dose was administered after a median (IQR) of 27 (22-29) days, 28 (28-42) days, and 56 (55-83) days from the first dose for Comirnaty, Spikevax, and Vaxzevria, respectively. The demographic characteristics of the study group are presented in **TABLE 1**. No statistically significant differences were found comparing sex, age, body mass index (BMI), and autoimmune disease among the Comirnaty, Spikevax, and Vaxzevria groups.

TABLE 2 presents peak anti-RBDS1 IgG antibody concentrations and the time elapsed from the second vaccination dose. Anti-RBDS1 IgG antibody concentrations were significantly higher in the Comirnaty and Spikevax group, compared with those found in the Vaxzevria group. Further, the percentage of participants with antibody concentrations >10,000 AU/mL was the highest in the Spikevax group of vaccine recipients. In the Vaxzevria group, none of the participants showed antibody concentrations >10,000 AU/mL (the median concentration measured in this group was 1223 AU/mL). Finally, other than heterogeneous anti-RBDS1 IgG concentrations found in comparing each vaccine group, we observed a heterogeneous response within each group, as demonstrated by the wide IQR of antibody concentrations.

The self-reported vaccine adverse effects associated with the second dose are presented in **TABLE 3**. Of the 117 participants, 104 (88.9%) reported at least 1 adverse effect after full vaccination. The 13 participants reporting no adverse effects after vaccination were only from the Comirnaty group of vaccine recipients. Statistically significant differences in reported frequencies of adverse effects were observed for redness/swelling at the injection site, fever, headache, and muscle pain. When comparing reported adverse effects according to individual vaccine subgroup, redness/swelling at the injection site and headache were the most common in recipients of the Spikevax vaccine; fever and muscle pain were mostly reported after vaccination with Vaxzevria. No statistically significant differences in the reported frequency of pain at the injection site, fatigue, and nausea/vomiting after second vaccination with Comirnaty, Spikevax, and Vaxzevria were observed. Serious local or systemic adverse effects were rare: 2 participants reported loss of consciousness and facial weakness after second-dose vaccination (with the Comirnaty vaccine and the Vaxzevria vaccine, respectively). No allergic/anaphylactic reactions were reported after full vaccination with either of those vaccines.

The association of adverse effects after second vaccination with the Comirnaty and Spikevax vaccines and peak antibody concentrations

TABLE 1. Demographic Characteristics of Study Participants

Characteristic	All Vaccines (n = 117)	Comirnaty (Pfizer-BioNTech) (n = 70)	Spikevax (Moderna) (n = 14)	Vaxzevria (AstraZeneca) (n = 33)	*P* Value[a]
Age, y, median (range)	40 (22-70)	42 (22-65)	46 (31-65)	26 (24-70)	.10
Sex, female, No. (%)	93 (79.5)	58 (82.9)	13 (92.9)	22 (66.7)	.07
BMI, kg/m^2, median (IQR)	25 (22-27)	25 (22-27)	26 (24-27)	23 (21-26)	.09
Autoimmune disease, No. (%)	9 (7.7)	8 (11.4)	0	1 (3.0)	.17

BMI, body mass index; IQR, interquartile range.
[a]*P < .05 is considered statistically significant.*

TABLE 2. Peak Antibody Concentrations per Vaccine Administered[a]

Variable	All Vaccines (n = 117)	Comirnaty (Pfizer-BioNTech) (n = 70) (1)	Spikevax (Moderna) (n = 14) (2)	Vaxzevria (AstraZeneca) (n = 33) (3)	*P* Value[b]	Post Hoc
Time from the second dose, d, mean (IQR)	19 (11-35)	21 (11-35)	21 (14-35)	15 (12-35)	<.001	(1)(2)/(3)
Peak antibody concentration, (AU/mL), mean (IQR)	10,969 (2669-21,406)	16,489 (9568-27,652)	18,737 (10,869-34,246)	1223 (875-1876)	<.001	(1)(2)/(3)
Participants with antibody concentrations >10,000 AU/mL, No. (%)	63 (53.9)	50 (71.4)	13 (92.9)	0	<.001	—
Participants with antibody concentrations >1000 AU/mL, No. (%)[c]	—	—	—	21 (63.6)	—	—

IQR, interquartile range.
[a]*Differences between multiple groups were tested using the Kruskal-Wallis test paired with the Dunn post hoc test. Proportions were tested using χ^2 testing.*
[b]*P < .05 is considered statistically significant.*
[c]*Calculated only for the Vaxzevria group.*

TABLE 3. Self-Reported Adverse Effects After the Administration of the Second Vaccine Dose[a]

Reported Adverse Effect	All Vaccines (n = 117)	Comirnaty (Pfizer-BioNTech) (n = 70)	Spikevax (Moderna) (n = 14)	Vaxzevria (AstraZeneca) (n = 33)	*P* Value[b]
Pain at the injection site	89 (76.1)	53 (75.7)	13 (92.9)	23 (69.7)	.23
Redness/swelling at the injection site	26 (22.2)	13 (18.6)	7 (50.0)	6 (18.1)	.03
Fatigue	57 (48.7)	32 (45.7)	5 (35.7)	20 (60.6)	.22
Fever	52 (44.4)	11 (15.7)	11 (78.6)	30 (90.9)	<.001
Headache	30 (25.6)	15 (21.4)	7 (50.0)	8 (24.2)	.002
Nausea/vomiting	10 (8.6)	4 (5.7)	1 (7.1)	5 (15.2)	.27
Muscle pain	49 (41.9)	18 (25.7)	6 (42.9)	25 (75.8)	<.001
Loss of consciousness	1 (1.0)	1 (1.4)	0	0	.71
Facial weakness	1 (1.0)	0	0	1 (3.0)	.28
Allergic reaction/anaphylaxis	0	0	0	0	>.99

[a]*Data are given as No. (%).*
[b]*P < .05 is considered statistically significant.*

TABLE 4. Prediction of Peak Antibody Concentrations >10,000 AU/mL Using Vaccination Adverse Effects for Comirnaty and Spikevax[a]

Adverse Effect	Univariate Logistic Regression Results		Multivariate Logistic Regression Results[b]	
	OR (95% CI)	*P* Value[c]	OR (95% CI)	*P* Value[c]
Pain at the injection site	0.53 (0.14-2.06)	.34	—	—
Redness/swelling at the injection site	1.45 (0.42-4.94)	.55	—	—
Fatigue	1.39 (0.50-3.81)	.52	—	—
Fever	4.42 (0.94-20.83)	.03	3.63 (0.62-21.20)	.15
Headache	2.59 (0.68-9.85)	.13	—	—
Nausea/vomiting	0	.08	—	—
Muscle pain	5.10 (1.09-23.93)	.02	2.81 (0.51-15.46)	.23
Loss of consciousness	0	.09	—	—

[a]*Comirnity is manufactured by Pfizer-BioNTech; Spikevax is manufactured by Moderna.*
[b]*Adjusted for age, sex, body mass index, presence of autoimmune disease, and time from second dose.*
[c]*P <. 05 is considered statistically significant.*

are presented in **TABLE 4**. All of the participants were included (those who did and did not experience adverse effects), comprising a group of 84 participants eligible for this analysis. The association of adverse effects and peak antibody concentrations in the Vaxzevria group (n = 33) was analyzed separately because of the obtained lower antibody concentrations in comparison with the Comirnaty and Spikevax vaccine groups (**TABLE 5**).

In the Comirnaty and Spikevax groups, the results of univariate logistic regression analysis showed that fever and muscle pain were significantly associated with peak antibody concentrations as long as 1 month after vaccination. These values in both groups have been shown to be significant independent predictors of peak antibodies >10,000 AU/mL during the observed time period (OR [95% CI] for fever, 4.42 [0.94-20.83], *P* = .03; for muscle pain, 5.10 [1.09-23.93], *P* = .02). When fever and muscle pain were combined into a multivariate model adjusted for covariates (ie, age and sex, BMI, presence of autoimmune disease, and time from second dose), none of the independent predictors remained statistically significant (*P* = .15 and *P* = .23 for fever and muscle pain, respectively). Since the univariate logistic regression analysis for the Vaxzevria vaccine showed no association with peak antibody concentrations >1000 AU/mL in the observed time period, the multivariate analysis was not performed (**TABLE 5**).

Discussion

The anti-RBDS1 IgG peak antibody concentrations in our study were higher in individuals vaccinated with mRNA vaccines (Comirnaty and Spikevax). Despite the difficulties we experienced in directly comparing immunological results obtained from studies with different designs and methodologies used (ie, serological assays used for quantification of antibody response), we state that our results confirm previous findings on more-robust antibody responses to S antigens found in recipients of mRNA vaccines.[16–19]

Đaković Rode et al[20] performed a prospective longitudinal study (January 2021–September 2021) in a Croatian cohort of health care workers with similar demographic characteristics to those of our cohort (82% female participants, with a mean [range] age of 42 [19-67] years), and measured the dynamics of anti-RBDS1 IgG antibodies up to 6 months after full vaccination with the Comirnaty vaccine, using the same methods utilized in our study. One month after full vaccination, in a cohort without a history of COVID-19, the researchers measured median (IQR) anti-RBDS1 IgG concentrations of 9927 (5461-17,414) AU/mL. These results are lower than our results (in the Comirnaty group), which once more outlines the variability of early humoral response (found even in vaccine recipients inoculated with the same vaccine).

TABLE 5. Prediction of Peak Antibody Concentrations >1,000 AU/mL Using Vaccination Adverse Effects for Vaxzevria[a]

Adverse Effect	Univariate Logistic Regression Results	
	OR (95% CI)	*P* Value[b]
Pain at the injection site	0.67 (0.14-3.27)	.61
Redness/swelling at the injection site	0.21 (0.03-1.39)	.09
Fatigue	1.16 (0.27-4.93)	.84
Fever	4.00 (0.32-46.60)	.26
Headache	0.25 (0.05-1.20)	.07
Nausea/vomiting	2.59 (0.25-26.31)	.39
Muscle pain	1.07 (0.21-5.54)	.94
Facial weakness	0	.15

[a]*Vaxzevria is manufactured by AstraZeneca.*
[b]*P < .05 is considered statistically significant.*

Various determinants influencing the immune response after vaccination are still poorly understood.[16,21]

Immunogenicity data (apart from those obtained in clinical trials) or comparative investigations of multiple vaccines, including the Vaxzevria vaccine, are scarce.[15,22] We found that anti-RBDS1 IgG peak antibody concentrations in the Vaxzevria group of vaccine recipients were substantially lower, compared with those values in recipients of Comirnaty and Spikevax, which is in line with previous results.[23]

The research group van Gils et al[24] presented a head-to-head comparison of binding (and neutralizing) activity after vaccination with BNT162b2 (ie, Comirnaty), mRNA-1273 (ie, Spikevax), AZD1222 (ie, Vaxzevria), or Ad26.COV2.S (ie, Janssen). Similar to our results, these researchers reported that mRNA vaccines were superior to the adenovirus vector-based vaccines at inducing binding (and neutralizing) antibodies at the time of their expected peak of immunity.

Several factors could explain the marked differences found in peak anti-RBDS1 IgG concentrations. First, Vaxzevria encodes for wild-type S glycoprotein; Comirnaty and Spikevax, however, encode a proline-modified S protein stabilized in its prefusion configuration, which improves immunogenicity.[23,25] Further, apart from the differences found in the vaccine immunogen, other differences pertaining to adjuvants found in the vaccine formulation and differences in dosing intervals might also play a role in triggering a different humoral response after vaccination.[1] This information should be taken into account when designing vaccination strategies.

After administration of COVID-19 vaccines, similarly to all other vaccines, unwanted reactions are expected to occur.[8] Our investigation revealed that 89% of the participants reported at least 1 adverse effect after full vaccination. The most frequent local adverse effect after full vaccination, irrespective of the COVID-19 vaccine administered, was pain at the injection site; fatigue and fever were the most frequent systemic adverse effects reported. In general, our results are comparable to frequencies reported in clinical trials of COVID-19 vaccines.[26–28] After analyzing adverse effect profiles corresponding to individual vaccines, the most frequent adverse effects reported after vaccination with Comirnaty were pain at the injection site, fatigue, and muscle pain; with Spikevax, pain at the injection site, fever, and headache; and with Vaxzevria, fever, muscle pain, and pain at the injection site (adverse effects listed by frequency).

Further, the individual vaccine reactogenicity profiles found in our investigation were somewhat similar to previously obtained results; however, we found that participants in the Spikevax and Vaxzevria groups reported fever more frequently than in previous reports.[29–31] Conversely, the Comirnaty group reported fever less frequently than previously described.[31–33]

Vaccination is associated with a common belief, namely, that adverse effects after vaccination are desirable because they indicate that the vaccine is working—ie, it is inducing immune response to generate protection from a specific disease. In this context, limited data are available to support the association of reactogenicity of COVID-19 vaccines with their immunogenicity.[34,35]

We investigated the association of adverse effects reported after vaccination with the Comirnaty, Spikevax, and Vaxzevria vaccines, and their corresponding peak anti-RBDS1 IgG antibody response. We found that fever and muscle pain were independent predictors of peak antibody responses >10,000 AU/mL up to 1 month after vaccination with the Comirnaty and Spikevax vaccines. After adjusting the multivariate model for covariates (age, sex, BMI, presence of autoimmune disease, and time from second dose), no adverse effects were found to be predictive for high peak antibody concentrations.

Similarly to our study, Coggins et al[34] investigated the association of adverse effects caused by vaccination with Comirnaty and the magnitude of vaccine-induced antibody concentrations in a cohort of health care workers. Their results showed no correlation between vaccine-related adverse effects and the magnitude of vaccine-induced antibody concentrations, which is in agreement with our findings. Further, our results showed no association of reported adverse effects and peak antibody response >1000 AU/mL up to 1 month after vaccination with Vaxzevria. To our knowledge, this lack of association has not yet been reported in the literature.

Our investigation has certain limitations. We did not assess neutralizing antibody activity or cellular immunity, both of which reflect protective immunity after vaccination. Instead, we used a quantitative anti-RBDS1 IgG assay to assess the immunogenicity of the vaccines we investigated. Although these quantitative measurements could be regarded as surrogate indicators of neutralizing activity, the cutoff antibody concentration required for protection after vaccination is still unknown. This factor prevented us from making any inferences on protection after vaccination.

Another limitation of our investigation is that the majority of our cohort consisted of female participants aged 22-70 years (although the age distribution between vaccine groups was homogeneous). Because previous investigations emphasized the role of sex and age in antibody response after infection and vaccination, this factor could have impacted our results. Indeed, women and girls have been shown to display higher antibody response, whereas older individuals (>60 years) display decreased antibody titers and reactogenicity due to immunosenescense.[15,21,22]

Although we adjusted for sex and age, the wider transferability of our results is limited. Further, the limited number of participants and the difference in size of the groups inoculated with the vaccines investigated should be addressed. The difference in number of participants per group reflected the real-world scenario (ie, the vaccine recipients were inoculated with the vaccine available at the time of vaccination). The limited numbers of vaccine recipients included in the Spikevax and Vaxzevria groups limits the reliability and generalization of our results, which should be confirmed in sufficiently powered future investigations. The adverse effects after vaccination were self-reported and thus subjective (ie, susceptible to a range of factors, including perception of pain

and mood). Finally, the influence of new SARS-CoV-2 variants that emerged during the period of our investigation, with possible impact on vaccine-induced immunity, has not been investigated.

In conclusion, our results contribute to the knowledge concerning reactogenicity and immunogenicity of COVID-19 vaccines. Previous studies mainly focused on 1 or 2 vaccines; herein, we present results from a real-world, direct comparison of data from recipients of 3 COVID-19 vaccines. Immunogenicity, measured by the peak concentration of anti-RBDS1 IgG antibodies, was found to be superior for mRNA COVID-19 vaccines, in comparison with Vaxzevria. Whether the observed difference in peak antibody concentrations translates into different duration of immune responses after vaccination remains to be elucidated.

Further, our results confirmed that frequency of reported adverse effects from Comirnaty, Spikevax, and Vaxzevria were comparable to those described in clinical trials; also, reactogenicity profiles were similar to those reported from real-world investigations. These data strengthen the confidence in the moderate reactogenicity of COVID-19 vaccines and support public health vaccination policies.

Although fever and muscle pain were independently associated with peak antibody concentrations 1 month after vaccination with the Comirnaty and Spikevax vaccines, when adjusted for covariates, the model showed no association between vaccination adverse effects and peak anti-RBDS1 IgG antibody response after vaccination with the Comirnaty, Spikevax, and Vaxzevria vaccines. Thus, irrespective of the vaccine adverse effects experienced, all 3 COVID-19 vaccines should provide a robust immune response.

Data Availability

Data are available from the authors on reasonable request.

Conflict of Interest Disclosure

The authors have nothing to disclose.

REFERENCES

1. Mistry P, Barmania F, Mellet J, et al. SARS-CoV-2 variants, vaccines, and host immunity. *Front Immunol.* 2022;12:809244.
2. Poland GA, Ovsyannikova IG, Kennedy RB. SARS-CoV-2 immunity: review and applications to phase 3 vaccine candidates. *Lancet.* 2020;396(10262):1595-1606. doi:10.1016/S0140-6736(20)32137-1
3. World Health Organization (WHO). WHO Coronavirus (COVID-19) Dashboard. Accessed April 22, 2023. https://covid19.who.int/
4. Rotshild V, Hirsh-Raccah B, Miskin I, Muszkat M, Matok I. Comparing the clinical efficacy of COVID-19 vaccines: a systematic review and network meta-analysis. *Sci Rep.* 2021;11(1):22777. doi:10.1038/s41598-021-02321-z
5. Teijaro JR, Farber DL. COVID-19 vaccines: modes of immune activation and future challenges. *Nat Rev Immunol.* 2021;21:195-197. doi:10.1038/s41577-021-00526-x
6. Bohn MK, Ping Loh T, Wang C-B, et al. IFCC interim guidelines on serological testing of antibodies against SARS-CoV-2. *Clin Chem Lab Med.* 2020;58(12):2001-2008.
7. Centers for Disease Control and Prevention (CDC). *Interim Guidelines for COVID-19 Antibody Testing.* Accessed on April 22, 2023. https://www.cdc.gov/coronavirus/2019-ncov/lab/resources/antibody-tests-guidelines.html
8. Hervé C, Laupèze B, Del Giudice G, Didierlaurent AM, Tavares Da Silva F. The how's and what's of vaccine reactogenicity. *NPJ Vaccines.* 2019;4:39. doi:10.1038/s41541-019-0132-6
9. World Health Organization (WHO). Coronavirus Disease (COVID-19): Vaccines safety. Accessed April 22, 2023. https://www.who.int/news-room/questions-and-answers/item/coronavirus-disease-(covid-19)-vaccines-safety
10. European Medicine Agency (EMA). COVID-19 Vaccines Safety Update February 2022. Accessed April 22, 2023. https://www.ema.europa.eu/en/documents/covid-19-vaccine-safety-update/covid-19-vaccines-safety-update-17-february-2022_en.pdf
11. Beatty AL, Peyser ND, Butcher XE, et al. Analysis of COVID-19 vaccine type and adverse effects following vaccination. *JAMA Netw Open*. 2021;4(12):e2140364. doi:10.1001/jamanetworkopen.2021.40364
12. English E, Cook LE, Piec I, et al. Performance of the Abbott SARS-CoV-2 IgG II quantitative antibody assay including the new variants of concern, VOC 202012/V1 (United Kingdom) and VOC 202012/V2 (South Africa), and first steps towards global harmonization of COVID-19 antibody methods. *J Clin Microbiol.* 2021;59(9):e0028821. doi:10.1128/JCM.00288-21
13. Narasimhan M, Mahimainathan L, Araj E, et al. Clinical evaluation of the Abbott Alinity SARS-CoV-2 spike-specific quantitative IgG and IgM assays among infected, recovered, and vaccinated groups. *J Clin Microbiol.* 2021;59(7):e0038821. doi:10.1128/JCM.00388-21
14. Ikezaki H, Nomura H, Shimono N. Dynamics of anti-spike IgG antibody level after the second BNT162b2 COVID-19 vaccination in health care workers. *J Infect Chemother.* 2022;28(6):802-805. doi:10.1016/j.jiac.2022.02.024
15. Eyre DW, Lumley SF, Wei J, et al. Quantitative SARS-CoV-2 anti-spike responses to Pfizer-BioNTech and Oxford-AstraZeneca vaccines by previous infection status. *Clin Microbiol Infect.* 2021;27(10):1516.e7-1516.e14. doi:10.1016/j.cmi.2021.05.041
16. Moncunill G, Aguilar R, Ribes M, et al. Determinants of early antibody responses to COVID-19 mRNA vaccines in a cohort of exposed and naïve healthcare workers. *EBioMedicine*. 2022;75:103805. doi:10.1016/j.ebiom.2021.103805
17. Steensels D, Pierlet N, Penders J, Mesotten D, Heylen L. Comparison of SARS-CoV-2 antibody response following vaccination with BNT162b2 and mRNA-1273. *JAMA.* 2021;326(15):1533-1535. doi:10.1001/jama.2021.15125
18. Collier AY, Yu J, McMahan K, et al. Differential kinetics of immune responses elicited by Covid-19 vaccines. *N Engl J Med.* 2021;385(21):2010-2012. doi:10.1056/NEJMc2115596
19. Goel RR, Painter MM, Apostolidis SA, et al; UPenn COVID Processing Unit. mRNA vaccines induce durable immune memory to SARS-CoV-2 and variants of concern. *Science.* 2021;374(6572):abm0829. doi:10.1126/science.abm0829
20. Đaković Rode O, Bodulić K, Zember S, et al. Decline of anti-SARS-CoV-2 IgG antibody levels 6 months after complete bnt162b2 vaccination in healthcare workers to levels observed following the first vaccine dose. *Vaccines*. 2022;10(2):153. doi:10.3390/vaccines10020153
21. Zimmermann P, Curtis N. Factors that influence the immune response to vaccination. *Clin Microbiol Rev.* 2019;32(2):e00084-e00018. doi:10.1128/CMR.00084-18
22. Ramasamy MN, Minassian AM, Ewer KJ, et al. Safety and immunogenicity of ChAdOx1 nCoV-19 vaccine administered in a prime-boost regimen in young and old adults (COV002): a single-blind, randomised, controlled, phase 2/3 trial. *Lancet.* 2020;396(10267):1979-1993.
23. Kang YM, Minn D, Lim J, et al. Comparison of antibody response elicited by ChAdOx1 and BNT162b2 COVID-19 vaccine. *J Korean Med Sci.* 2021;36(46):e311. doi:10.3346/jkms.2021.36.e311
24. van Gils MJ, Lavell AHA, van der Straten K, et al; Amsterdam UMC COVID-19 S3/HCW study group. Antibody responses against SARS-CoV-2 variants induced by four different SARS-CoV-2 vaccines in health care workers in the Netherlands: a prospective

cohort study. *PLoS Med.* 2022;19(5):e1003991. doi:10.1371/journal.pmed.1003991

25. Sanders RW, Moore JP. Virus vaccines: proteins prefer prolines. *Cell Host Microbe.* 2021;29(3):327-333. doi:10.1016/j.chom.2021.02.002
26. Polack FP, Thomas SJ, Kitchin N, et al, C4591001 Clinical Trial Group. Safety and efficacy of the BNT162b2 mRNA Covid-19 vaccine. *N Engl J Med.* 2020;383(27):2603-2615. doi:10.1056/NEJMoa2034577
27. Baden LR, El Sahly HM, Essink B, et al, COVE Study Group. Efficacy and safety of the mRNA-1273 SARS-CoV-2 vaccine. *N Engl J Med.* 2021;384(5):403-416. doi:10.1056/NEJMoa2035389
28. Voysey M, Clemens SAC, Madhi SA, et al; Oxford COVID Vaccine Trial Group. Safety and efficacy of the ChAdOx1 nCoV-19 vaccine (AZD1222) against SARS-CoV-2: an interim analysis of four randomised controlled trials in Brazil, South Africa, and the UK. *Lancet.* 2021;397(10269):99-111. doi:10.1016/S0140-6736(20)32661-1
29. Sauserienė J, Liseckienė I, Neverauskė V, et al. Adverse events and immunogenicity of mRNA-based COVID-19 vaccine among healthcare workers: a single-centre experience. *Medicina*. 2022;58(3):441. doi:10.3390/medicina58030441
30. Chapin-Bardales J, Gee J, Myers T. Reactogenicity following receipt of mRNA-based COVID-19 vaccines. *JAMA.* 2021;325(21):2201-2202. doi:10.1001/jama.2021.5374
31. Park C, Sakong J, Jo S, Kim M, Baek K. Adverse effects on work and daily life interference among healthcare workers after the first and second ChAdOx1 and BNT162b2 COVID-19 vaccine doses. *Vaccines (Basel)*. 2021;9(8):926. doi:10.3390/vaccines9080926
32. Modenese A, Paduano S, Bargellini A, et al. Neutralizing anti-SARS-CoV-2 antibody titer and reported adverse effects, in a sample of Italian Nursing Home personnel after two doses of the BNT162b2 vaccine administered four weeks apart. *Vaccines (Basel)*. 2021;9(6):652. doi:10.3390/vaccines9060652
33. Rivera-Izquierdo M, Soler-Iborte E, de Rojas JP, et al. Factors associated with adverse reactions to BNT162b2 COVID-19 vaccine in a cohort of 3969 hospital workers. *Vaccines*. 2021;10(1):15. doi:10.3390/vaccines10010015
34. Coggins SA, Laing ED, Olsen CH, et al. Adverse effects and antibody titers in response to the BNT162b2 mRNA COVID-19 vaccine in a prospective study of healthcare workers [preprint]. *Open Forum Infect Dis*. 2021;9:ofab575.
35. Debes AK, Xiao S, Colantuoni E, et al. Association of vaccine type and prior SARS-CoV-2 infection with symptoms and antibody measurements following vaccination among health care workers. *JAMA Intern Med*. 2021;181(12):1660-1662. doi:10.1001/jamainternmed.2021.4580

Relationship between the systemic immune-inflammatory index and the severity of acute bronchiolitis in children

Ömer Furkan Kızılsoy, MD[1], Muhammet Furkan Korkmaz, MD[1], Gülsüm Elif Şenkan, MD[1], Şefika Elmas Bozdemir, MD[2], Merve Korkmaz, MD[3]

[1]Departments of Pediatrics and [2]Pediatric Infectious Diseases, University of Health Sciences, Bursa Faculty of Medicine, City Training and Research Hospital, Bursa, Turkey, [3]Department of Pediatric Pulmonology, Uludag Faculty of Medicine, Bursa, Turkey. Corresponding author: Muhammet Furkan Korkmaz; korkmazmfurkan@gmail.com

Key words: acute bronchiolitis; child; severity; systemic immune-inflammatory index

Abbreviations: AB, acute bronchiolitis; SII, systemic immune-inflammatory index; CRP, C-reactive protein; NLR, neutrophil-to-lymphocyte ratio; PLR, platelet-to-lymphocyte ratio; RDW, red cell distribution width; MTS, modified Tal score; SpO_2, O_2 saturation; ICU, intensive care unit; ROC, receiver operating curve; AUC, area under the curve

Laboratory Medicine 2024;55:169-173; https://doi.org/10.1093/labmed/lmad055

ABSTRACT

Objective: Acute bronchiolitis (AB) is one of the most common respiratory diseases in early childhood and is still an important health problem worldwide. The systemic immune-inflammatory index (SII) is thought to have potential to be a new-generation inflammatory biomarker. We sought to investigate the value of SII for severity assessment in children with AB.

Methods: A total of 74 AB patients were included in a prospective observational study. Patients were classified into 3 AB groups according to this classification: mild (1-5 points), moderate (6-10 points), and severe (11-12 points). Complete blood count, C-reactive protein, and procalcitonin tests were carried out. Modified Tal score was evaluated to determine severity. The performance of parameters to predict the severity of AB was assessed using the receiver operating characteristic (ROC).

Results: Whereas neutrophil count (P = .037), neutrophil-to-lymphocyte ratio (P = .030), and SII (P = .030) values increased significantly with disease severity, red cell distribution width (P = .048) values were higher in the moderate AB group. The SII was found to have the highest area under the curve in the comparison of the mild-moderate groups combination and the high group on ROC analysis (P = .009).

Conclusion: The SII values of pediatric patients hospitalized with the diagnosis of AB were significantly higher in the high-severity group. The SII may offer additional severity stratification in children with AB.

Acute bronchiolitis (AB) is an acute lower respiratory tract disease characterized by tachypnea, intercostal retraction, and wheezing. Acute bronchiolitis is predominantly seen in children under 2 years and is mostly caused by viral agents.[1] As a matter of fact, 50% of AB cases are caused by the respiratory syncytial virus alone.[2,3] Bronchiolitis is characterized by diffuse inflammation and edema of the airways, increased mucus secretion, necrosis of epithelial cells, and ciliary dysfunction. The binding of the virus to the epithelial cells of the lower respiratory tract causes epithelial necrosis and ciliary dysfunction. As the destruction of cells triggers the inflammatory response through the proliferation of polymorphonuclear cells and lymphocytes, mucus secretion increases, and edema develops in the lower airways.[2,4,5]

The number of neutrophils in the blood increases during the inflammatory processes, whereas lymphocyte count decreases due to increased apoptosis. Although the platelets are involved in homeostasis and coagulation, the proliferation of megakaryocytic series and platelet count also increases during chronic inflammatory processes.[6]

There are many publications in the literature on the role of various biomarkers in inflammatory conditions observed during childhood. One of these biomarkers, C-reactive protein (CRP), is a frequently used marker to indicate acute and chronic inflammation. Neutrophil-to-lymphocyte ratio (NLR) and platelet-to-lymphocyte ratio (PLR) are cost-effective parameters studied in the context of many systemic inflammatory conditions. There are also many studies on the relationship of red cell distribution width (RDW) with chronic inflammation. The systemic immune-inflammatory index (SII), a new-generation inflammatory biomarker, has been created by including all these parameters under a single parameter. Accordingly, SII is calculated by dividing the product of the neutrophil count and the platelet count by the

lymphocyte count.[7-9] Compared with PLR and NLR, which have been associated with many disease activities in recent studies, SII stands out as a much more promising marker in showing inflammation and immune response. High SII values were reportedly associated with the severity of disease and poor prognosis in the context of many diseases and malignancies.[10-13] However, most of the studies on the efficacy of SII have been conducted with adult patient populations, and only a few have addressed pediatric patient populations. A thorough review of the literature revealed only 1 study that addressed the relationship between SII values and malignancy in a pediatric patient population.[14] Apart from this study, other studies available in the literature on the efficacy of SII in pediatric patients featured children with obesity, myocarditis, and appendicitis.[15-17]

It is very difficult to determine the severity of AB based on the results of laboratory tests or pulmonary function tests only. Therefore, various scoring systems have been developed to assess the severity of AB, including Tal,[18] modified Tal,[19] Lowell,[20] Wang,[21] and Liu[22] scoring systems. The use of many different scoring systems causes difficulties in the comparative interpretation of clinical results. Moreover, the complexity of some clinical scoring systems makes it difficult to apply and repeat the respective measurements and include them in routine clinical evaluations. Hence, a single valid scoring system that can be used worldwide is needed. For this purpose, McCallum et al[23] reviewed the scoring systems designed to determine the severity of AB in children and suggested that modified Tal score (MTS) as the most convenient and straightforward system for clinical use.

This study was carried out to investigate the relationship between SII values and disease severity in pediatric patients with AB.

Material and Methods

Research Setting and Study Population

The population of this single-center prospective study consisted of pediatric patients aged 1 to 24 months who were hospitalized with the diagnosis of AB in Bursa Faculty of Medicine, City Training and Research Hospital Pediatric Emergency Service, a tertiary hospital in Turkey, between January and June 2022. Ethical approval was obtained from the university ethics committee (2019-KAEK-140 2022/01-18). Written informed consent was obtained from the parents of the participants involved.

The children included in the study were diagnosed with AB based on the definition that AB is an acute infection of the lower airway characterized by increased respiratory effort (tachypnea [more than 50 respirations per minute] or use of accessory respiratory muscles) and expiratory wheezing or crackles. Patients with immunodeficiency and other infectious or chronic disease predisposing to severe bronchiolitis (asthma, recurrent [more than 2] wheezing episodes, cystic fibrosis, bronchopulmonary dysplasia, congenital heart disease, etc) were excluded from the study.

The patients were clinically evaluated after they were admitted to the emergency department and followed up during their hospital stay until they were discharged. Blood samples were taken from each patient after admission to the emergency room.

The MTS[19] was used to assess the clinical severity of AB. The MTS consists of 4 specific components: respiratory rate, accessory muscle use, wheezing or crackles, and room air arterial O_2 saturation (SpO_2) measurement, which replaces "cyanosis" in the original Tal[18] score. Each component is scored between 0 and 3 points; hence, the total score from MTS will be between 0 and 12 points. Respiratory rate was counted over 60 seconds. Accessory muscle use was defined as non, mild, moderate, or severe and scored 0, 1, 2, or 3. The degree of wheezing or crackles was defined as expiration only, during inspiration and expiration, or heard without stethoscope, and scored between 0 to 3. According to the level of oxygen saturation in room air, the patient was scored 0, 1, 2, or 3 for O_2 saturation ≥95%, 92% to 94%, 90% to 91%, and ≤89%. If SpO_2 was ≤89%, oxygen was immediately provided to the patient and 3 points given for the SpO_2 component. The higher the MTS score, the more severe the bronchiolitis. The patients included in this study were divided into 3 groups based on their MTS scores. Patients with ≤5 points, 6 to 10 points, and ≥11 points were placed in the mild, moderate, and severe AB groups, respectively.

Data Collection

Patients' age, gender, and birth week information, as well as their preadmission complaints and the duration of these complaints, were recorded. In addition, patients' signs and symptoms related to AB, vital signs, type of radiological findings, and other physical examination findings were recorded at admission. Furthermore, oxygen support, mechanical ventilation, intensive care unit (ICU) needs,and treatment outcomes were recorded.

Laboratory Measurements

Blood samples were obtained from all AB patients at admission. Complete blood count, CRP, and procalcitonin tests were performed using the blood samples at the biochemistry laboratory of the hospital where this study was conducted. The NLR was calculated by dividing the absolute neutrophil count by the absolute lymphocyte count. The PLR was calculated by multiplying the platelet count by the absolute lymphocyte count. Finally, SII was calculated based on the following formula: SII = platelet count × neutrophil count/lymphocyte count.[7]

Statistical Analysis

The descriptive statistics obtained from the collected data were expressed as numbers (n) and percentage (%) values in the case of categorical variables and as mean ± SD or median and minimum-maximum values, whichever were appropriate, in the case of continuous variables. Pearson's χ^2 test or Fisher's exact test were used to compare qualitative variables. Multiple group comparisons were made using the Kruskal-Wallis test. Tamhane post hoc analysis was applied when necessary.

The prognostic power of biomarkers in predicting AB severity was evaluated using the receiver operating curve (ROC) analysis. To this end, 95% CI of the area under the curve (AUC) values were calculated. Sensitivity, specificity, and positive and negative predictive values of biomarkers were calculated for each cut-off value. Statistical analyses were performed using the SPSS 22.0 (Statistical Product and Service Solutions for Windows, Version 22.0, IBM) software package. A $P \leq .05$ was deemed to indicate statistical significance.

Results

Characteristics of the Study Group

The median age of the 74 pediatric patients hospitalized with the diagnosis of AB was 8 (minimum: 1, maximum: 24) months. There

were 49 males and 25 females in the study group. The male-female ratio was 1.96. Whereas 79.7% of the patients presented to the hospital with a complaint of cough, 36.4% presented with shortness of breath, and 31.0% presented with respiratory distress. The most common clinical finding was rales or rhonchi, which was detected in 71.6% of the patients, whereas the most common radiological finding in posteroanterior chest radiographs was peribronchial infiltrates, which was detected in 41.8% of the patients. Detailed baseline clinical and radiological characteristics and treatment data of the patients are shown in **TABLE 1**.

Severity of Acute Bronchiolitis

The MTS was used to determine the severity of AB. Median MTS was 2 (minimum: 0, maximum: 12) points. Accordingly, 57 (77.0%), 10 (13.5%), and 7 (9.5%) patients were classified into the mild, moderate, and severe AB groups, respectively.

There were no significant differences between the groups in terms of age or sex (P = .12 and P = .17, respectively). On the other hand, the groups significantly differed in neutrophil count, NLR, RDW, and SII values. The distribution of the median values of laboratory measurements by the MTS groups is shown in **TABLE 2**.

The ROC analysis revealed that SII had the highest AUC in differentiating the severe AB group from the mild and moderate AB groups compared with other biomarkers (**FIGURE 1**). The optimal cut-off value of SII was 408.01 (sensitivity: 85.7%, specificity: 40.3%) (**TABLE 3**).

TABLE 1. Patient characteristics[a]

Characteristic	Acute bronchiolitis patients (n = 74)
Demographics	
Male sex	49 (66.2)
Age (mo), median (min-max)	8 (1-24)
Duration of pre-admission complaint (d), median (min-max)	3 (0-28)
Gestational age (wk), median (min-max)	39 (27-42)
Clinical sign	
Temperature ≥38.5°C	19 (25.6)
Cough	59 (79.7)
Runny nose	15 (20.2)
Sputum	7 (9.4)
Dyspnea	27 (36.4)
Respiratory distress	23 (31.0)
Clinical findings	
Rales/rhonchi	53 (71.6)
Tachypnea	17 (22.9)
O_2 saturation (room air) <95%	21 (28.3)
Retractions	15 (20.2)
Radiographic findings	
Peribronchial infiltration	31 (41.8)
Interstitial infiltration	12 (16.2)
Consolidation	1 (1.3)
Treatments	
Antibiotics	37 (50.0)
Oxygen therapy	22 (29.7)
Corticosteroids	29 (39.1)
Inhaled corticosteroids	43 (58.1)
Inhaled bronchodilators	58 (78.3)

[a]*Data are given as No. (%) except where indicated.*

Clinical Outcomes

The median length of hospital stay was 4 (minimum: 2, maximum: 34) days. The median duration of providing oxygen support was 3 (minimum: 1, maximum: 15) days. Nine (12.2%) patients were required to be transferred to the ICU. Of these patients, 4 (44.4%) required high-flow oxygen therapy and 2 (22.2%) needed nasal continuous positive airway pressure therapy. No complications were observed in any of the patients. Median length of stay in the ICU was 5 (minimum: 3, maximum: 15) days.

Discussion

The findings of this prospective single-center study indicated that the SII values of pediatric patients hospitalized with the diagnosis of AB were significantly higher in the severe AB group. Recently, SII has been associated with poor clinical outcomes, especially in adults with malignancies.[12] The correlation of SII values with poor clinical outcomes in adults with coronary artery diseases, Behçet's disease, and obesity with concomitant chronic inflammation has also been investigated in different studies.[24-26] In the last 5 years, a number of studies have been carried out on the relationships between SII values in adult patients, but few have been carried out in pediatric patients. To the best of our knowledge, there is only 1 study that addressed the relationship between SII values in pediatric cancer patients. That study was conducted by Ertan et al[14] with 97 children with malignancy and 97 healthy children. There was no significant difference between cancer patients and healthy children in SII values. However, further analysis of malignancy patients revealed that the SII values of children with solid tumors were significantly higher than children with tumors originating from the central nervous system. In a study conducted with 35 healthy children, 20 children with overweight, 47 children with obesity, and 92 children with morbid obesity, it was reported that SII values increased gradually from 381 to 538.[15] In another study conducted with 106 pediatric patients diagnosed with myocarditis, Yaradılmış et al[16] reported a significant increase in SII values from 351 to 1927 in fulminant myocarditis patients compared with nonfulminant patients and significantly higher SII values in patients with myocarditis due to multisystem inflammatory syndrome in children than in patients with myocarditis caused by active COVID infection or other viral agents. Kart et al[17] reported a significant increase in SII values in children diagnosed with acute appendicitis than in healthy control subjects (2597 vs 353).

Using SII enables assessing the 3 hemostatic system markers involved in the inflammation process together. High platelet and neutrophil counts may imply inflammation, whereas low lymphocyte counts may imply an uncontrolled inflammatory pathway. The groups stratified according to the severity of AB significantly differed in neutrophil count, NLR, RDW, and SII values. Accordingly, although neutrophil count, NLR, and SII values increased significantly with disease severity, RDW values

TABLE 2. Levels of biomarkers according to severity groups[a]

Biomarkers	Study group (n = 74)	Mild group (n = 57)	Moderate group (n = 10)	Severe group (n = 7)	*P* value[b]	*P* value[c]	*P* value[d]	*P* value[e]
WBC count (x10^9)	12.03 (4.60-32.59)	11.52 (5.90-32.59)	12.48 (4.66-24.08)	15.91 (4.60-30.26)	.245			
Neutrophil count (x10^9)	4.40 (0.19-26.96)	3.72 (0.19-26.96)	6.52 (0.89-13.35)	8.80 (2.30-19.50)	**.037**	.740	**.011**	.138
Lymphocyte count (x10^9)	4.91 (0.55-24.20)	5.08 (1.60-15.85)	4.79 (0.66-11.14)	2.71 (0.55-24.20)	.168			
NLR	0.83 (0.04-16.48)	0.69 (0.04-8.00)	0.83 (0.28-16.48)	3.24 (0.68-11.69)	**.030**	.157	**.008**	.450
PLR	87.21 (6.69-536.36)	84.66 (13.56-290.67)	77.53 (31.15-257.58)	166.53 (6.69-536.36)	.204			
Platelet count (x10^3/mm^3)	380.00 (48.00-816.00)	379.50 (144.00-842.00)	361.50 (48.00-514.00)	346.50 (162.00-408.00)	.195			
MPV (fL)	9.30 (8.30-12.30)	9.45 (8.30-11.30)	9.55 (8.50-12.30)	9.20 (9.10-11.00)	.808			
RDW (%)	13.80 (12.20-21.30)	13.10 (12.20-18.80)	15.70 (12.30-21.30)	14.20 (12.80-19.60)	**.048**	**.023**	.986	.093
CRP (mg/L)	4.30 (0.10-95.60)	3.75 (0.10-95.60)	3.90 (0.60-27.70)	15.40 (0.60-34.50)	.289			
Procalcitonin (μg/L)	0.10 (0.03-12.64)	0.10 (0.03-1.72)	0.12 (0.06-5.00)	0.10 (0.05-12.64)	.622			
SII	336.16 (20.47-5594.27)	295.03 (20.47-4304.00)	312.69 (88.11-2802.42)	1175.64 (136.83-5594.27)	**.030**	.766	**<.001**	**.002**

CRP, C-reactive protein; MPV, mean platelet volume; NLR, neutrophil lymphocyte ratio; PLR, platelet lymphocyte ratio; RDW, red cell distribution width; SII, systemic immune-inflammatory index; WBC, white blood cell.
[a]Data are expressed as median and minimum-maximum values. Bold values indicate statistical significance (P < .05).
[b]Kruskal-Wallis test.
[c]Significance between Mild and Moderate group.
[d]Significance between Mild and Severe group.
[e]Significance between Moderate and Severe group.

FIGURE 1. Receiver operating characteristic curves for neutrophil count, neutrophil-to-lymphocyte ratio (NLR), red cell distribution width (RDW), and systemic immune-inflammatory index (SII) to differentiate high-severity pediatric acute bronchiolitis from mild and moderate severity, classified by modified Tall score.

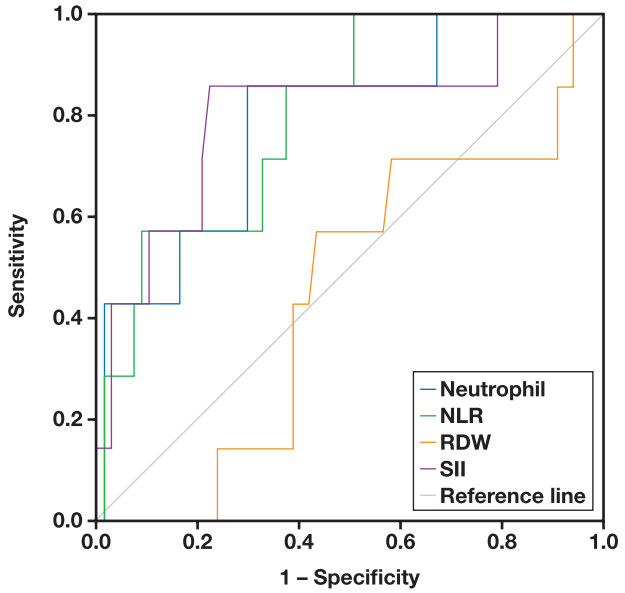

were higher in the moderate AB group. The results of the ROC analysis, which was designed to show the relationship of biomarkers with disease severity, indicated that SII had the highest AUC in predicting patients with high disease severity.

In a meta-analysis, Yang et al[12] suggested 560 as the optimal cut-off value for SII in predicting overall survival in 22 adult malignancy patient populations. Yaradılmış et al[16] suggested 1378 (sensitivity: 68.8%, specificity: 94.4%) as the optimal cut-off value for SII in predicting fulminant myocarditis in pediatric patients. Kart et al[17] suggested 651.47 (sensitivity: 95%, specificity: 98%) as the optimal cut-off value for SII in predicting acute appendicitis in pediatric patients as a result of ROC analysis. In comparison, in this study, the optimal SII cut-off value for differentiating patients with severe AB from those with mild and moderate AB was determined to be 408.01 (sensitivity: 85.7%, specificity: 40.3%).

Study Limitations

The single-center design of this study constituted its primary limitation. Second, given the strict exclusion criteria, the sample size was relatively small. Third, biomarker levels were measured only at admission. Serial measurements of biomarker levels might have given a better correlation with the clinical course of the disease. Fourth, a conclusion about the usefulness of biomarkers in predicting the etiology of AB could not be drawn because the etiology could not be identified in a significant proportion of the study population. Finally, the fact that only inpatients were included in this study might have resulted in more exacerbated results than expected if outpatients had been included in the study sample.

Conclusion

The findings of this study indicate that the SII values of pediatric patients hospitalized with the diagnosis of AB were significantly higher in the severe AB group than in the moderate and mild AB groups. The fact that SII can be assessed immediately within the scope of routine hemogram tests may enable clinicians to predict adverse outcomes earlier in severe AB cases. To the best of our knowledge, this is the first study to assess the efficacy of SII in predicting AB severity in pediatric patients. Nevertheless, further large-scale studies, which should also include outpatients, are needed to corroborate the findings of this study.

TABLE 3. Receiver operator curve evaluating parameters in predicting severe acute bronchiolitis patients

Parameters	Cut-off value	Sensitivity (%)	Specificity (%)	AUC (95 % CI)	*P* value
Neutrophil count ($x10^9$)	5.72	85.7	29.9	0.789 (0.614-0.964)	**.012**
NLR	1.06	85.7	40.3	0.800 (0.649-0.950)	**.009**
RDW (%)	16.10	69.2	55.5	0.408 (0.227-0.638)	.678
SII	408.01	85.7	40.3	0.830 (0.607-0.999)	**.009**

AUC, area under the curve; NLR, neutrophil lymphocyte ratio; RDW, red cell distribution width; SII, systemic immune-inflammatory index.
[a]*Bold values indicate statistical significance (P < .05).*

Data Availability

The data generated and analyzed in this study are included in this article and will be made available upon reasonable request to the corresponding author.

Conflict of Interest Disclosure

The authors have nothing to disclose.

REFERENCES

1. Kou M, Hwang V, Ramkellawan NB. From practice guideline to clinical practice. *Emerg Med Clin North Am.* 2018;36:275-286.
2. Florin TA, Plint AC, Zorc JJ. Viral bronchiolitis. *Lancet.* 2017;389:211-224. doi:10.1016/S0140-6736(16)30951-5
3. Coates BM, Camarda LE, Goodman DM. Wheezing, bronchitis and bronchiolitis. In: Behrman RE, ed. *Nelson Textbook of Pediatrics*. 20th ed. Philadelphia: Elsevier; 2015:2044-2048.
4. Ali S, Plint AC, Klassen TP. Bronchiolitis. In: Wilmott RW, Kendig EL, Boat TF, et al, eds. *Kendig and Chernick's Disorders of the Respiratory Tract in Children*. 8th ed. Philadelphia: Elsevier Saunders; 2012:443-452.
5. Aherne W, Bird T, Court SD, et al. Pathological changes in virus infections of the lower respiratory tract in children. *J Clin Pathol.* 1970;23:7-18. doi:10.1136/jcp.23.1.7
6. Maurizi G, Della Guardia L, Maurizi A, et al. Adipocytes properties and crosstalk with immune system in obesity-related inflammation. *J Cell Physiol.* 2018;233:88-97. doi:10.1002/jcp.25855
7. Ustundag Y, Huysal K, Gecgel SK, et al. Relationship between C-reactive protein, systemic immune inflammation index, and routine hemogram related inflammatory markers in low grade inflammation. *Int J Med Biochem.* 2018;1:24-28.
8. Hu B, Yang XR, Xu Y, et al. Systemic immune inflammation index predicts prognosis of patients after curative resection for hepatocellular carcinoma. *Clin Cancer Res.* 2014;20:6212-6222. doi:10.1158/1078-0432.ccr-14-0442
9. Sun Y, Li W, Li AJ, et al. Increased systemic immune inflammation index independently predicts poor survival for hormone receptor negative, HER2-positive breast cancer patients. *Cancer Manag Res.* 2019;11:3153-3162. doi:10.2147/CMAR.S190335
10. Akpinar MY, Ozin YO, Kaplan M, et al. Platelet-to lymphocyte ratio and neutrophil-to-lymphocyte ratio predict mucosal disease severity in ulcerative colitis. *J Med Biochem.* 2018;37:155-162. doi:10.1515/jomb-2017-0050
11. Endo K, Satoh T, Yoshino Y, et al. Neutrophil-to-lymphocyte and platelet-to-lymphocyte ratios as noninvasive predictors of the therapeutic outcomes of systemic corticosteroid therapy in ulcerative colitis. *Inflamm Intest Dis.* 2021;6:218-224. doi:10.1159/000520523
12. Yang R, Chang Q, Meng X, et al. Prognostic value of systemic immune-inflammation index in cancer: a meta-analysis. *J Cancer.* 2018;9:3295-3302. doi:10.7150/jca.25691
13. Zhong JH, Huang DH, Chen ZY. Prognostic role of systemic immune-inflammation index in solid tumors: a systematic review and meta-analysis. *Onco Target.* 2017;8:75381-75388.
14. Ertan K, Kara B, Disci SI, et al. The importance of systemic inflammatory response index, systemic immune-inflammation index, and hemoglobin-albumin-lymphocytes-platelets (HALP) score in children with cancer. *Iran J Pediatr.* 2021;31:e118121.
15. Donma MM, Donma O. Evaluation of systemic immune-inflammation index in obese children. *Int J Med Sci Public Health.* 2018;12:362-365.
16. Yaradilmiş RM, Güneylioğlu MM, Öztürk B, et al. A novel marker for predicting fulminant myocarditis: systemic immune–inflammation index. *Pediatr Cardiol.* 2023;44:647-655.
17. Kart Y, Uğur C. Evaluation of systemic immune-inflammation index as novel marker in the diagnosis of acute appendicitis in children. *J Contemp Med.* 2022;12:593-597.
18. Tal A, Bavilski C, Yohai D, et al. Dexamethasone and salbutamol in the treatment of acute wheezing in infants. *Pediatrics.* 1983;71:13-18.
19. Golan Tripto I, Goldbart A. Modified Tal score: validated score for prediction of bronchiolitis severity. *Pediatr Pulmonol.* 2018;53:796-801.
20. Lowell DI, Lister G, Von Koss H, et al. Wheezing in infants: the response to epinephrine. *Pediatrics.* 1987;79:939-945.
21. Wang EE, Milner RA, Navas L, et al. Observer agreement for respiratory signs and oximetry in infants hospitalized with lower respiratory infections. *Am Rev Respir Dis.* 1992;145:106-109. doi:10.1164/ajrccm/145.1.106
22. Liu LL, Gallaher MM, Davis RL, et al. Use of a respiratory clinical score among different providers. *Pediatr Pulmonol.* 2004;37:243-248. doi:10.1002/ppul.10425
23. McCallum GB, Morris PS, Wilson CC. Severity scoring systems: are they internally valid, reliable and predictive of oxygen use in children with acute bronchiolitis? *Pediat Pulmonol.* 2013;8:797-803.
24. Yang YL, Wu CH, Hsu PF, et al. Systemic immune-inflammation index (SII) predicted clinical outcome in patients with coronary artery disease. *Eur J Clin Invest.* 2020;50:e13230. doi:10.1111/eci.13230
25. Tanacan E, Dincer D, Erdogan FG, et al. A cut-off value for the systemic immune-inflammation index in determining activity of Behcet disease. *Clin Exp Dermatol.* 2021;46:286-291. doi:10.1111/ced.14432
26. Wang J, Zhou D, Dai Z, et al. Association between systemic immune-inflammation index and diabetic depression. *Clin Interv Aging.* 2021;16:97-105.

Nitrate Reductase Assay for Rapid Determination of Methicillin-Resistant *Staphylococcus aureus* Clinical Isolates

Kubra Yildirim, PhD,[1,2] Cemilenur Atas, BSc,[3] Esra Tanyel Akcit, MSc,[1,3] Majda Licina, BSc,[3] Ozlem Koyuncu Ozyurt, MD,[4] Mehmet Akif Gun, MD, PhD,[5] Ece Simsek, PhD,[1-3] Ahmet Yilmaz Coban, PhD[1-3]

[1]Akdeniz University Tuberculosis Research Center, Antalya, Türkiye, [2]Department of Nutrition and Dietetics, Faculty of Health Sciences, Akdeniz University, Antalya, Türkiye, [3]Department of Medical Biotechnology, Institute of Health Sciences, Akdeniz University, Antalya, Türkiye, [4]Department of Medical Microbiology, Akdeniz University, Antalya, Türkiye, [5]19 Mayis State Hospital, Samsun, Türkiye. Corresponding author: Cemilenur Atas; atascemile07@gmail.com

Key words: *Staphylococcus aureus*, methicillin-resistance, nitrate reductase assay, colorimetric method, infectious disease, rapid detection

Abbreviations: MRSA, methicillin-resistant *Staphylococcus aureus*; MSSA, methicillin-susceptible *Staphylococcus aureus*; PBPs, penicillin-binding proteins; PB2a, penicillin-binding protein 2a; SCCmec, staphylococcal cassette chromosome; BMD, broth microdilution; MIC, minimum inhibitory concentration; REMA, resazurin microtiter assay; NRA, nitrate reductase assay; MTT, dimethyl thiazole diphenyl tetrazolium bromide; CAMBH, cation-adjusted Mueller-Hinton broth

Laboratory Medicine 2024;55:174-178; https://doi.org/10.1093/labmed/lmad056

ABSTRACT

Objective: To evaluate the performance of nitrate reductase assay (NRA), a rapid, colorimetric method for the determination of methicillin resistance in *Staphylococcus aureus* isolates obtained from the culture collection of the Akdeniz University Hospital Central Laboratory, Antalya, Türkiye.

Materials and Methods: Identification for all 290 *S aureus* isolates at the species level was performed via matrix-assisted laser desorption/ionization-time of flight. Isolates were tested with NRA for methicillin resistance. The cefoxitin broth microdilution (BMD) method recommended by the Clinical and Laboratory Standards Institute was used as the reference method in the study. *S aureus* ATCC 29213 and *S aureus* ATCC 43300 strains were used for quality control.

Results: According to Food and Drug Administration criteria, the category agreement between NRA and BMD was found to be 100%. The essential agreement between both methods was determined to be 96.20%. There is no minor, major, or extremely major discrepancy between both methods.

Conclusion: The results show that NRA is a rapid, practical, and reliable colorimetric method for detecting MRSA.

Staphylococcus aureus is a commensal microorganism found in the skin, oral cavity, gastrointestinal tract, upper respiratory tract, and lower urogenital tract in humans.[1] It is an opportunistic pathogen that can cause infection because of its ability to adapt to different hosts and environmental conditions. This pathogen, which can be community- and hospital-acquired, is concerning for clinicians because it can develop methicillin resistance. Moreover, methicillin-resistant *S aureus* (MRSA) is more difficult to treat than methicillin-susceptible *S aureus* (MSSA) strains.[2–4]

In the early 1940s, the antibiotic penicillin worked therapeutically for staphylococcal infections. With the emergence of penicillin-resistant *S aureus* strains in the hospital and community, new drug candidates were investigated.[5] In 1959, a semisynthetic beta-lactam antibiotic called methicillin replaced penicillin. However, after a short time, staphylococci developed methicillin resistance. Later, when it was reported that these strains were also resistant to cefoxitin, oxacillin, and other beta-lactam antibiotics, the strains with this resistance profile were named MRSA.[1,6,7]

The most important property of MRSA is that it exhibits a heterogeneous pattern with different levels of resistance under routine growing conditions. This heterogeneous profile is present in most clinical isolates.[8] Heterogeneous strains consist of 2 bacterial populations: one is relatively susceptible and the other is highly resistant. Therefore, only a few of them (one in 10^4-10^6) express the phenotype.[9] Heterogeneous resistance to methicillin in *S aureus* isolates arises due to variations in the expression of the *mecA* gene or alteration of constitutive penicillin-binding protein (PBPs).[10] However, factors such as incubation temperature and salt concentration, as well as other genes, affect the expression of *mecA*, resulting in heterogeneous resistance.[11] Heterogeneous expression of methicillin resistance may complicate the precise determination of the resistance phenotype. Therefore, detection of *mecA* by molecular methods such as polymerase chain reaction (PCR) remains the criterion standard.[12]

Methicillin resistance in staphylococci is caused by a penicillin-binding protein 2a (PBP2a), encoded by *mecA* (*mecA* is part of the staphylococcal cassette chromosome [SCCmec] and is a mobile genetic element), which is responsible for methicillin resistance.[8,13] Today, MRSA can be detected by amplification- and probe-based methods that detect specific gene regions.

PBP2a antibody agglutination tests are another testing method used in MRSA detection. MRSA treatment worldwide has improved significantly due to molecular diagnosis. Because molecular methods provide faster results, the treatment can start more quickly.[12,14,15] However, these methods are not always easily accessible because their implementation is expensive and requires the use of technical equipment. Therefore, they cannot be used in every laboratory.

Another preferred option for determining methicillin resistance is culture-based conventional methods. The broth microdilution (BMD) method is the reference method for the determination of the minimum inhibitory concentration (MIC) of cefoxitin and oxacillin. Still, cefoxitin disk diffusion and oxacillin salt agar screening tests can also be used to determine methicillin resistance. All 3 methods are recommended by the Clinical and Laboratory Standards Institute (CLSI).

An incubation period of 16-24 hours is required for the results of these culture-based susceptibility methods.[16] However, when culture-based methods are combined with some colorimetric methods, susceptibility results are obtained more quickly. Resazurin microtiter assay (REMA), nitrate reductase assay (NRA),[17] dimethyl thiazole diphenyl tetrazolium bromide (MTT),[18] Quicolor ES Agar (QC agar; Salubris),[19] and StaResMet (AYCMED Medical and Medical Devices Industry and Trade)[20] are colorimetric test methods used for rapid detection of methicillin resistance in *S aureus*.

Using these colorimetric methods, methicillin resistance can be detected in approximately 4-7 hours. Among these methods, NRA is a biochemical test generally used to distinguish *Mycobacterium tuberculosis* from other mycobacteria. According to the working principle of the test, when live bacteria are present, their nitrate reductase enzyme converts nitrate to nitrite. Then, Griess reagent is added to the medium, and if bacteria are present, a purple-violet color is formed.[21,22] The NRA method is also used to detect methicillin resistance in *mecA*-positive and -negative *S aureus* isolates.[17] In this study we evaluatde the performance of NRA, a rapid colorimetric method for the detection of methicillin resistance in *S aureus* isolates.

Materials and Methods

Bacterial Isolates

In our study, 290 *S aureus* specimens were isolated from various clinical specimens (urine, blood, catheter, and pus), for which species-level identification had been performed with the matrix-assisted laser desorption/ionization-time of flight MS Microflex LT, version 5.0 (Bruker Daltonik), and were tested. All isolates were obtained from the culture collection of Akdeniz University Hospital Central Laboratory, Anatalya, Türkiye.

S aureus ATCC 29213 (methicillin-susceptible) and *S aureus* ATCC 43300 (methicillin-resistant) strains were used as control strains. According to CLSI recommendations, the cefoxitin MIC 1-4 µg/mL QC range for *S aureus* ATCC 29213 and the cefoxitin MIC >4 µg/mL QC range for *S aureus* ATCC 43300 were used.[16]

Antimicrobials and Chemicals

Cefoxitin, sulfanilamide, N-(1-naphthyl) ethylenediamine dihydrochloride and potassium nitrate were purchased in commercial powder form. For the cefoxitin antibiotic, stocks were prepared at a final concentration of 4096 µg/mL. The antibiotics were stored in aliquots at −80°C until use. For the Griess reagent used in NRA, 1 unit of concentrated hydrochloric acid, 2 units of 0.2% sulfanilamide, and 2 units of 0.1% N-1-naphthyl-ethylenediamine dihydrochloride were combined.[17] The reagent was prepared fresh on a working day and added to the plates.

Preparation of Media

Commercially available cation-adjusted Mueller-Hinton broth (CAMHB; Becton, Dickinson and Company; calcium: 20-25 mg/L, magnesium: 10.0-12.5 mg/L) was used for the preparation of BMD and NRA test plates. The media were prepared according to manufacturer recommendations. In the preparation of NRA plates, potassium nitrate at a concentration of 1000 µg/mL was added to the medium. Bacteria were grown on blood agar medium; the medium was prepared according to manufacturer recommendations.

Preparation of Bacterial Inoculum

Fresh bacterial cultures grown on blood agar were used for all test methods. Bacterial inoculums were prepared via the direct colony suspension method. Bacterial inoculums were adjusted to McFarland No. 0.5 turbidity. The same bacterial inoculum was used for both methods.

Preparation of BMD and NRA Plates

Cefoxitin concentrations to be tested for BMD were determined according to breakpoints specified by the CLSI.[16] The cefoxitin was diluted with CAMHB. Two-fold serial dilutions were made in 96-well U-bottom microplates with 6 different concentrations in the range of 0.5-16.0 µg/mL. The prepared plates were stored at −80°C until use. Plates were brought to room temperature before use.

For NRA plates, the cefoxitin was diluted in sterile distilled water. It was prepared at the final concentration (0.5-16.0 µg/mL), and 100 µL was distributed on 96-well U-bottom microplates. Then the plates were lyophilized with a Freeze Dryer (Labconco). After lyophilization, cefoxitin plates were stored at 4°C until use. In both methods, a growth control well (positive control) and a sterility control well (negative control) were included.

Susceptibility Tests

BMD

The BMD method recommended by CLSI was used as the reference method to determine the MIC of cefoxitin.[16] Bacterial suspension adjusted to McFarland standard No 0.5 turbidities were diluted 1:100 with CAMHB. We inoculated 100 µL into all wells except the sterility well. Plates were incubated for 16-20 hours at 35 °C ± 2 °C. After incubation, the lowest antibiotic concentration with no visible growth was recorded as the MIC value. According to CLSI criteria, strains with an MIC of cefoxitin ≤4 µg/mL were methicillin-susceptible; strains with a MIC of cefoxitin ≥8 µg/mL were considered methicillin-resistant.

Nitrate Reductase Assay

CAMHB containing 1000 µg/mL potassium nitrate was added as 100 µL to all wells. After the addition of the medium to the lyophilized cefoxitin plates, the concentration of cefoxitin in the wells was in the

range of 0.5-16.0 μg/mL. We inoculated 5 μL of the prepared bacterial suspensions into all the wells except the sterility well. Plates were incubated for 5 hours at 35 °C ± 2 °C. After 5 hours of incubation, 50 μL of Griess reagent was added to all growth control wells. After the instant violet-purple color change in the growth control wells, Griess reagent was added to all wells, and the color change was recorded. The MIC was defined as the lowest drug concentration without color change.

Analysis of Results

Results were analyzed according to US Food and Drug Administration (FDA) criteria.[23] In the analysis, minor, major, and extremely major discrepancies and category and essential agreement were determined comparatively.

Results

S aureus ATCC 29213 (methicillin-susceptible) and *S aureus* ATCC 43300 (methicillin-resistant) strains were used as control strains. MIC values in both methods were determined to be 4 μg/mL for *S aureus* ATCC 29213, and MIC was determined at 8 μg/mL for *S aureus* ATCC 43300.

According to the BMD test method used as the reference method in the study, cefoxitin MICs were determined as >16 μg/mL for 153 isolates, 16 μg/mL for 3 isolates, 4 μg/mL for 128 isolates, 2 μg/mL for 4 isolates, and 1 μg/mL for 2 isolates. According to CLSI criteria, 156 isolates were defined as MRSA and 134 isolates as MSSA (**FIGURE 1**).

According to the NRA method, cefoxitin MICs were determined as >16 μg/mL for 114 isolates, 16 μg/mL for 33 isolates, 8 μg/mL for 9 isolates, 4 μg/mL for 96 isolates, 2 μg/mL for 36 isolates, and 1 μg/mL for 2 isolates. According to CLSI criteria, 156 isolates were defined as MRSA and 134 isolates as MSSA (**FIGURE 1**). In our study, according to FDA criteria, category agreement between the reference method and NRA was found to be 100%, and the essential agreement was 96.20%. There is no minor, major, or extremely major discrepancy between both methods (**TABLE 1**).

Discussion

Rapid and precise identification of MRSA is a prerequisite for the control of nosocomial infections. Rapid detection of methicillin resistance presents the clinician with the chance to start treatment on day of identification. Today, MRSA using amplification-based molecular methods such as BD GeneOhm MRSA, BD GeneOhm StaphSR (Becton, Dickinson and Company), Xpert (Cepheid), and IsoAmp Rapid Detection kit (BioHelix) can be performed directly.[14] For PCR-based assays, sequence changes in the *S aureus* chromosome and the instability of SCCmec elements pose a challenge.

Methicillin resistance is determined very rapidly with these methods. However, their high prices limit their use, especially in low-income laboratories. In total, 16-24 hours are required for the detection of methicillin resistance with conventional culture-based methods. In this case, colorimetric test methods seem appropriate in terms of time and cost.

In the NRA, nitrate is reduced to nitrite by the nitrate reductase enzyme in the bacteria; then, Griess (a specific reagent) reagent is added to the medium. If bacteria are present in the medium, a purple-violet color is formed.[21,22] BMD was used as the reference method in the study and was performed according to CLSI recommendations. NRA is a newly developed method, which is aimed at evaluating the performance of this new method in our study.

NRA was also performed in CAMHB with KNO_3 based on the broth microdilution test. The antibiotic concentrations used were the same as for BMD. However, the number of bacteria used in NRA was more intense, and Griess reagent was added at the end of the test to evaluate the

FIGURE 1. Scatterplot comparing nitrate reductase assay (NRA) and broth microdilution method (BMD; reference method) for cefoxitin minimum inhibitory concentration (MIC) values (A) filtered by isolate type variable (B).

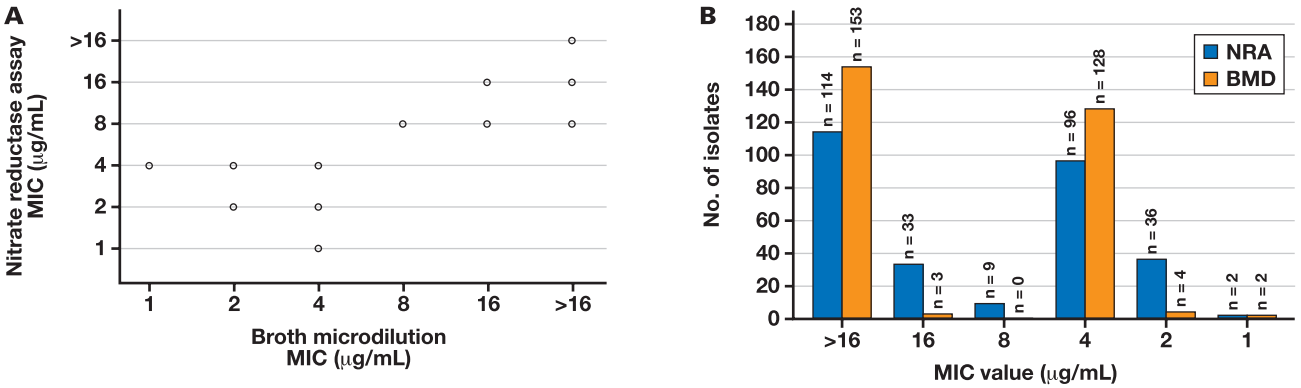

TABLE 1. FDA Criteria for Discrepancies and Agreement Between BMD and NRA for Cefoxitin Susceptibility of *Staphylococcus aureus*

Method	Discrepancies with BMD, No. (%)		Discrepancies with BMD, No. (%)		
	Category	Essential	Minor	Major	Extremely Major
NRA	290/290 (100%)	279/290 (96.2%)	0	0	0

BMD, broth microdilution method; FDA, Food and Drug Administration; NRA, nitrate reductase assay.

test. The NRA was evaluated by color change. The obtained results were compared with the BMD (reference method) results. Category agreement between NRA and reference method was found to be 100%. The essential agreement between both methods was determined to be 96.20%. This value is above the level recommended by the FDA.[23] There is no minor, major, or extremely major discrepancy between the 2 tested methods.

Coban[17] applied NRA and REMA for the cefoxitin MIC of a total of 275 *S aureus* clinical isolates, containing 151 MRSA and 124 MSSA, and compared the test results with those from BMD. The category agreement of both methods with BMD was found to be 100%, and the essential agreement was 99.6%. All 3 test methods were found to be 100% compatible with PCR results for *mecA*. In our study, in addition to applying the findings of the Coban study, we used NRA after the antibiotic cefoxitin was lyophilized in 96-well plates. Lyophilized cefoxitin plates were used in this study because preparing a lyophilized plate confers an advantage in shelf life.

In 2014, Çoban et al[24] investigated the effectiveness of NRA based on breakpoint susceptibility testing for rapid detection of methicillin resistance. A total of 135 *S aureus* isolates were tested at a single concentration (4 mg/L cefoxitin) via the breakpoint testing method. One of the tubes contained 1 mL of medium with fresh cefoxitin, and the other tube was lyophilized. In their study, the specificity, sensitivity, and positive predictive values and negative predictive values of NRA were determined to be 100%. NRA results were found to be 100% compatible with BMD and PCR results. The results of that study also demonstrate the advantages of combining the cefoxitin antibiotic in lyophilized form into colorimetric NRA.

Niveditha and Sistla[25] determined the MIC of oxacillin with BMD and NRA for the detection of methicillin resistance. They found 99.4% category agreement and 89.7% essential agreement between the 2 methods for 155 isolates. The essential agreement in their study is below the level recommended by the FDA.

Niveditha and Sistla[25] reported that 5 *S aureus* isolates did not show positive growth at the fifth hour of incubation and therefore were not included in the evaluation. We faced the same problem. In our study, a total of 19 *S aureus* isolates containing 16 MRSA and 3 MSSA did not show any color change at the fifth hour of incubation. These 19 *S aureus* isolates that did not show positive growth were not included in the evaluation. In routine practice, as considered in the Niveditha and Sistla study, there may be some slow-growing isolates for which this test cannot be applied. The isolates tested in the study were taken from the culture collection of a central laboratory. In the absence of color change in these 19 isolates at the fifth hour, they were identified as coagulase-negative staphylococcus in further tests, to see if they were *S aureus*. For this reason, we excluded those isolates from the study.

In addition, NRA is a biochemical test often used to distinguish *M tuberculosis* from other mycobacteria. Thanks to the ability of *M tuberculosis* to reduce nitrate to nitrite, the presence of nitrite in the medium can be detected with Griess reagent. NRA is used for the detection of *M tuberculosis* and rapid determination of drug susceptibilities.[21,22,26]

Today, there are other colorimetric methods developed for the rapid detection of methicillin resistance. One of them, StaResMet, is a rapid antibiotic susceptibility kit based on the colorimetric test method. Methicillin resistance can be detected in *S aureus* isolates at the sixth hour of incubation with the StaResMet kit. MRSA can be detected on the same day of identification. In a multicenter study by Milletli Sezgin et al,[27] 217 MRSA and 252 MSSA isolates were tested using the StaResMet kit. The susceptibility results of the isolates are 100% compatible with VITEK-2, BD Phoenix, and PCR (for the detection of *mecA*). Cefoxitin MICs of all isolates were determined at the sixth hour of incubation with the StaResMet kit.

More-rapid susceptibility results can be obtained with both colorimetric test methods, compared with conventional culture-based methods. However, although methicillin resistance can be determined instantly after the addition of the reagent at the fifth hour of incubation with NRA, resazurin should be added at the fifth hour of incubation with REMA and incubated for 1 more hour for color change. The advantage of NRA is that the color change is instantaneous, and susceptibility results can be obtained immediately. In our study, NRA was applied on test plates containing lyophilized cefoxitin. In this way, we were able to store the plates at 2°-8°C until the end of the study.

The lower MIC values in the NRA in some isolates are probably due to the shorter incubation period. Category agreement compatibility is observed in these isolates. However, for this reason, the essential agreement was determined to be 96.2%.

For rapid detection of MRSA, NRA application on lyophilized cefoxitin plates yields the most advantageous, easy-to-use, reliable result among the existing colorimetric test methods. In this study, the modification made is the use of lyophilized plates. By preparing a lyophilized plate, an advantage is conferred in shelf life. The NRA is easy to use and time-saving because such rapid colorimetric methods can also determine methicillin resistance on the same day as the identification of *S aureus*. Considering that MRSA is an important nosocomial infection on a global scale, NRA has great potential for clinical use.

Conflict of Interest Disclosure

The authors have nothing to disclose.

REFERENCES

1. Jaradat ZW, Ababneh QO, Sha'aban ST, et al. Methicillin resistant *Staphylococcus aureus* and public fomites: a review. *Pathog Glob Health*. 2020;114(8):426-450. doi:10.1080/20477724.2020.1824112
2. Buonomini AR, Riva E, Di Bonaventura G, Gherardi G. Rapid detection of methicillin-resistant *Staphylococcus aureus* directly from blood for the diagnosis of bloodstream infections: a mini-review. *Diagnostics.* 2020;10(10):830.
3. Lowy FD. Antimicrobial resistance: the example of *Staphylococcus aureus*. *J Clin Invest.* 2003;111(9):1265-1273. doi:10.1172/JCI18535
4. Cosgrove SE, Sakoulas G, Perencevich EN, et al. Comparison of mortality associated with methicillin-resistant and methicillin-susceptible *Staphylococcus aureus* bacteremia: a meta-analysis. *Clin Infect Dis.* 2003;36(1):53-59. doi:10.1086/345476
5. Rammelkamp CH, Maxon T. Resistance of *Staphylococcus aureus* to the action of penicillin. *Proc Soc Exp Biol Med.* 1942;51(3):386-389. doi:10.3181/00379727-51-13
6. Duckworth G. Controlling methicillin resistant *Staphylococcus aureus*. *BMJ.* 2003;327(7425):1177-1178. doi:10.1136/bmj.327.7425.1177
7. Guignard B, Entenza JM, Moreillon P. Beta-lactams against methicillin-resistant *Staphylococcus aureus*. *Curr Opin Pharmacol.* 2005;5(5):479-489. doi:10.1016/j.coph.2005.06.002
8. Marin M. Resistance of *Staphylococcus* to methicillin [in Spanish]. *Medicina*. 2002;62(3):30-35.
9. Panda RK, Mahapatra A, Mallick B, Chayani N. Evaluation of genotypic and phenotypic methods for detection of methicillin resistant *Staphylococcus aureus* in a tertiary care hospital of

Eastern Odisha. *J Clin Diagn Res*. 2016;10(2):19-21. doi:10.7860/JCDR/2016/17476.7278

10. Bhattacharya S, Bir R, Majumdar T. Evaluation of multidrug resistant *Staphylococcus aureus* and their association with biofilm production in a tertiary care hospital, Tripura, Northeast India. *J Clin Diagn Res*. 2015;9(9):DC01-DC04.
11. Tiwari HK, Sapkota D, Das AK, Sen MR. Assessment of different tests to detect methicillin resistant *Staphylococcus aureus*. *Southeast Asian J Trop Med Public Health.* 2009;40(4):801-806.
12. Jonas D, Speck M, Daschner FD, Grundmann H. Rapid PCR-based identification of methicillin-resistant *Staphylococcus aureus* from screening swabs. *J Clin Microbiol.* 2002;40(5):1821-1823. doi:10.1128/JCM.40.5.1821-1823.2002
13. Tasneem U, Mehmood K, Majid M, Ullah SR, Andleeb S. Methicillin resistant *Staphylococcus aureus*: a brief review of virulence and resistance. *J Pak Med Assoc.* 2022;72(3):509-515. doi:10.47391/JPMA.0504
14. Kurlenda J, Grinholc M. Current diagnostic tools for methicillin-resistant *Staphylococcus aureus* infections. *Mol Diagn Ther.* 2010;14(2):73-80.
15. Tenover FC, Tickler IA. Detection of methicillin-resistant *Staphylococcus aureus* infections using molecular methods. *Antibiotics.* 2022;11(2):239. doi:10.3390/antibiotics11020239
16. Clinical and Laboratory Standards Institute (CLSI). *Performance Standards for Antimicrobial Susceptibility Testing*, 30th ed. CLSI standard M100. CLSI; 2020.
17. Coban AY. Rapid determination of methicillin resistance among *Staphylococcus aureus* clinical isolates by colorimetric methods. *J Clin Microbiol.* 2012;50(7):2191-2193. doi:10.1128/JCM.00471-12
18. Mahmoud BS, ElMasry SA, Fahim NAEMM, Elsattar MAA, Shaker OA. Detection of antibiotic susceptibility by colorimetric minimum inhibitory concentration in staphylococcal isolates. *J Appl Microbiol.* 2019;127(3):693-700. doi:10.1111/jam.14347
19. Kocagöz T, Erciş S, Darka O, et al. Quicolor: a novel system for rapid antibacterial susceptibility testing. *Ann Microbiol.* 2007;57:131-135. doi:10.1007/bf03175062
20. Soysal M, Çoban AY. Evaluation of StaResMet®' for rapid detection of methicillin resistance in clinical isolates of *Staphylococcus aureus* [in Turkish]. 2017;30(2):64-67. doi:10.5152/kd.2017.16
21. Palomino JC, Martin A, Portaels F. Rapid drug resistance detection in *Mycobacterium tuberculosis*: a review of colourimetric methods. *Clin Microbiol Infect.* 2007;13(8):754-762. doi:10.1111/j.1469-0691.2007.01698.x
22. Kumar M, Khan IA, Verma V, et al. Microplate nitrate reductase assay versus Alamar Blue assay for MIC determination of *Mycobacterium tuberculosis*. *Int J Tuberc Lung Dis.* 2005;9(8):939-941.
23. United States Food and Drug Administration (FDA). Guidance for Industry and FDA Class II Special Controls Guidance Document: Antimicrobial Susceptibility Test (AST) Systems. FDA; 2009.
24. Çoban AY, Demirpek U, Çifçi A, et al. Nitrate reductase assay for the rapid detection of *Staphylococcus aureus* methicillin resistance: a breakpoint susceptibility testing method [in Turkish]. *Mikrobiyol Bul.* 2014;48(1):40-47.
25. Niveditha N, Sistla S. Evaluation of colorimetric nitrate reductase assay for rapid detection of methicillin resistance in clinical isolates of *Staphylococcus aureus*. *Indian J Med Res.* 2016;144(1):87-91. doi:10.4103/0971-5916.193294
26. Coban AY, Birinci A, Ekinci B, Durupinar B. Drug susceptibility testing of *Mycobacterium tuberculosis* with nitrate reductase assay. *Int J Antimicrob Agents.* 2004;24(3):304-306. doi:10.1016/j.ijantimicag.2004.02.027
27. Milletli Sezgin F, Vural A, Kiraz A, Çaycı, et al. Same-day detection of methicillin resistance in *Staphylococcus aureus* isolates by StaResMet® Kit. *Jundishapur J Microbiol.* 2017;10:e14937.

Clinical impacts of the rapid diagnostic method on positive blood cultures

Ya-Wen Tsai[1,2], Bin Zhang[3], Hsiu-Yin Chou[1], Hung-Jui Chen[4], Yu-Chi Hsu[5], Yow-Ling Shiue[2,6]

[1]Center for Integrative Medicine, [4]Division of Infectious Diseases, Department of Internal Medicine, and [5]Information Systems Office, Chi Mei Medical Center, Tainan City, Taiwan, [2]Institute of Biomedical Sciences and [6]Institute of Precision Medicine, National Sun Yat-sen University, Kaohsiung, Taiwan, [3]Division of Biostatistics and Epidemiology, Cincinnati Children's Hospital Medical Center, Cincinnati, OH, US. Corresponding author: Yow-Ling Shiue; shirley@imst.nsysu.edu.tw

Key words: bloodstream infections; bacterial identification; clinical outcomes

Abbreviations: STI, short-term incubation; BSI, bloodstream infection; TAT, turnaround time; AST, antimicrobial susceptibility testing; GNB, Gram-negative bacteria; MALDI-TOF MS, matrix-assisted laser desorption ionization time-of-flight mass spectrometry; GP, Gram-positive; EMR, electronic medical records; ICU, intensive care unit; GPC, GP cocci; ASP, antimicrobial stewardship programs; ICD-10, International Classification of Diseases-10

Laboratory Medicine 2024;55:179-184; https://doi.org/10.1093/labmed/lmad057

ABSTRACT

Objective: This study aimed to evaluate the impact of short-term incubation (STI) protocol on clinical outcomes of bloodstream infection (BSI) patients.

Methods: A total of 1363 positive blood culture records from January 2019 to December 2021 were included. The main clinical outcomes included pathogen identification turnaround time (TAT), antimicrobial susceptibility testing (AST) TAT, and length of total hospital stay.

Results: The TAT of pathogen identification and AST significantly decreased after implementing the STI protocol (2.2 vs 1.4 days and 3.4 vs 2.5 days, respectively, with $P < .001$ for both). Moreover, for patients with Gram-negative bacteria (GNB)–infected BSIs, the length of total hospital stay decreased from 31.9 days to 27.1 days, indicating that these patients could be discharged 5 days earlier after implementing the STI protocol ($P < .01$).

Conclusion: The protocol led to a significant reduction in TAT and improved clinical outcomes, particularly for GNB organisms. The findings suggest that the STI protocol can improve patient outcomes and hospital resource utilization in the management of BSIs.

Introduction

Bloodstream infection (BSI) is a potentially life-threatening condition and may develop into sepsis or septic shock with high mortality. The incidence varies from 113 to 204 per 100,000 person-years in North America and Europe, and the estimated case fatality rate is about 12%-30% worldwide.[1–4] Previous studies have shown that delay in administering appropriate and effective antimicrobial agents to sepsis patients led to increased mortality by 0.3%-7.6% for each hour delay.[5–7] Early adequate antimicrobial therapy improves patient prognosis, especially for sepsis or septic shock patients, based on guidelines and direct examination of all available samples.[8] Blood cultures are considered the standard and most common method to identify BSIs in clinical settings. However, prolonged turnaround time (TAT) of blood culture delays the diagnosis and treatment for BSI.

Molecular techniques and matrix-assisted laser desorption ionization time-of-flight mass spectrometry (MALDI-TOF MS) currently play an important role in identifying pathogens in the suspected cases. Although technology innovation and process optimization in clinical microbiology laboratories shorten the overall TAT, it takes at least 3 d in the overnight subculture conventional method with MALDI-TOF MS. Given the high cost and limited target pathogens of multiplex molecular techniques, modified MALDI-TOF MS methods were developed from different studies. It has been shown that aerobic Gram-negative (GN) and Gram-positive (GP) bacteria were identified at genus level after 4 h of subculture incubation on solid medium with an accuracy of 95.2%-98.0% and 48.9%-92.2%, respectively.[9–12]

Our microbiology laboratory previously established a short-term incubation (STI) protocol and achieved 96.1% and 97.4% identification accuracy after 4.5 hour subculture from GP and 3.5 hour subculture from GN bacterial samples, respectively.[13]

As more powerful tools or methods for positive blood culture identification are available, further research on clinical outcome and economic impact is needed to understand the effectiveness of rapid diagnostic testing. Studies have demonstrated that patients with positive blood culture may benefit from molecular rapid diagnostic testing in terms of an earlier approach to optimal therapy, decreased broad-spectrum antibiotic use, and reduced length of stay.[14–16] Therefore, this study aimed to evaluate the clinical outcomes of the STI protocol implementation.

Materials and Methods

Study Design

This retrospective study was a before and after quasi-experiment conducted at the Chi-Mei Medical Center (Tainan, Taiwan), a 1288-bed

hospital that provides comprehensive health care services, with 10,090 outpatients and 3900 admissions monthly. The institutional review board, with a waiver consent (IRB NO.111-03-009), approved the study. This study aimed to evaluate the clinical outcomes of BSI patients (≥20 years old) after implementing the STI protocol. Collected samples (BD BACTEC Plus Aerobic/F culture vials and BACTEC Lytic/10 Anaerobic/F culture vials) were incubated with the BD BACTEC FX blood culture system (Becton Dickinson). Gram staining and subculturing were followed after the culture system flagged the bottle as positive.

Conventional Method

The BAP/EMB bi-plate (BBL Trypticase Soy Agar with 5% sheep blood/Levine EMB Agar, BD) was applied for the incubation at 35°C with CO_2 overnight. The bacterial colonies were subsequently identified by MALDI-TOF MS with the Bruker Biotyper reference database (Bruker Daltonik) followed by the disk diffusion antimicrobial susceptibility testing (AST) system.

Short-Term Incubation Protocol

The STI protocol was to subculture the positive blood culture samples for 3.5 hours for GN and 4.5 hours for GP without any intermediate process, followed by MALDI-TOF MS analysis. Criteria for the preliminary report were achieved at ≥1.7 (genus level), and afterwards the sample was used for an AST test with the BD Phoenix M50 system. The original plate continued to incubate overnight to ensure no slow-growing organisms or polymicrobial samples. This protocol was previously developed and validated and has been used in our microbiology laboratory since July 2020.[13]

Data Collection and Outcome Measures

We reviewed the electronic medical records (EMRs) of adult patients with positive blood cultures from January 2019 to December 2021. The first positive blood culture was used in the study for each patient per admission. Patients were excluded if the positive blood cultures showed polymicrobial infection, fungus infection, or no growth until 72 hours after subculture.

In addition to demographic features (age, sex), this study extracted blood culture reports (TAT, Gram, stain and pathogen reports), diagnostic codes (International Classification of Diseases, ICD-10), previous baseline characteristics, admission time, discharge time, all-cause 30-day mortality, and total hospitalization cost to evaluate the clinical outcomes. Based on the previous study, ICD-10-CM codes determined sepsis. Other codes used were patients with a discharge diagnosis of septic shock (ICD-10-CM: R6521), severe sepsis (ICD-10-CM: R6520), nonsevere sepsis, organism-specific sepsis (ICD-10-CM: A409, A412, A4101, A4102, A411, A403, A414, A4150, A413, A4151, A4152, A4153, A4159, A4189, A021, A227, A267, A327, A400, A401, A408, A4181, A427, A5486, B377), and nonsevere sepsis, unspecified, specified (ICD-10:A419).[17] Outcome measures included pathogen identification TAT, AST-TAT, length of total hospital stay, length of intensive care unit (ICU) stay, ICU admission rate, 30-day all-cause mortality, and 14-day all-cause readmission rate.

Statistical Analysis

All analyses were performed using SAS software, version 9.4 (SAS Institute). The descriptive analysis delineated the characteristics of the variables of interest. Either 2-sample *t*-test or Mann–Whitney *U* test was used to compare continuous variables between 2 groups as appropriate. The χ^2 test or Fisher's exact test was used to compare categorical variables. A *P* value less than .05 was considered statistically significant.

FIGURE 1. Study design and flowchart of the study population.

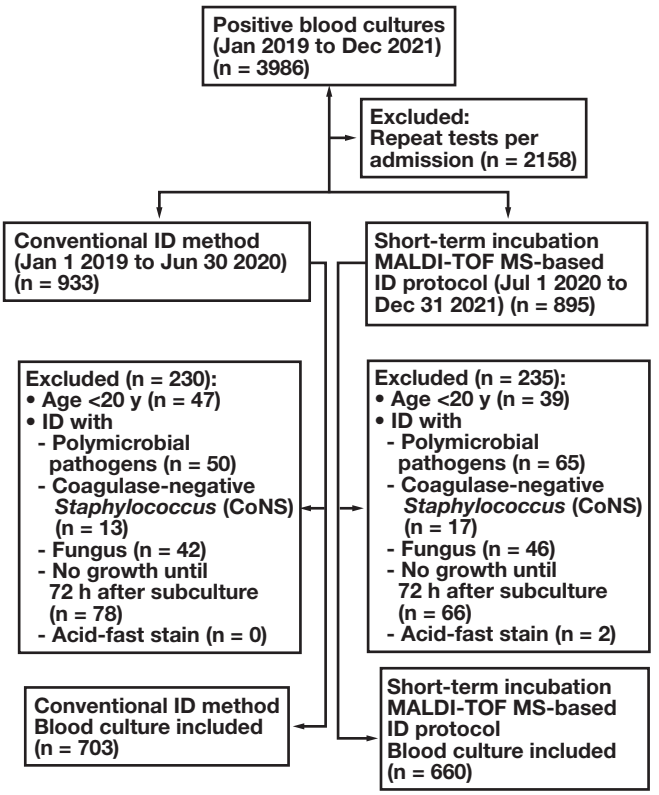

Results

A total of 3986 positive blood cultures from January 2019 to December 2021 were initially extracted from the EMR, and 1363 records were eligible for the study (**FIGURE 1**). Among the 1363 records, 703 were diagnosed using the conventional method and 660 after STI protocol was implemented. **TABLE 1** shows the patient demographics, clinical characteristics, and comorbidities. The mean age was 64.4 ± 14.6 years in the conventional group and 64.9 ± 15.1 years in the STI protocol (*P* = .24). Cancer was the most common underlying disease in both groups, accounting for more than 40% of all conditions. Most of the clinical features were similar between the 2 groups except for a lower percentage of cerebrovascular disease (3.6% vs 6.8%, *P* = .01), and diabetes (10.5% vs 15.2%, *P* = .01) in the conventional group.

The overall TAT of pathogen identification and AST time decreased after implementing the STI protocol, from 2.2 days to 1.4 days (*P* < .001) and 3.4 days to 2.5 days (*P* < .001), respectively. In addition, the STI protocol shortened the average length of total hospital stay by 2.3 days (29.6 days vs 31.9 days, *P* = .06), and other clinical outcomes, including the 30-day all-cause mortality rate, 14-day all-cause readmission rate, and length of ICU stay decreased in the STI group, although no significant difference was detected (**TABLE 2**).

The GN bacilli (GNB) (50.6%) and GP cocci (GPC) (43.0%) represented the major types of identified organisms from all blood

TABLE 1. Patient demographics, clinical characteristics, and comorbidities

	Conventional method (n = 703)	STI protocol (n = 660)	*P*
Demographics			
Age, mean (SD), y	64.4 (14.6)	64.9 (15.1)	.24
Female, n (%)	257 (36.6)	243 (36.8)	.92
ICU admission rate, n (%)	173 (24.6)	174 (26.4)	.46
Comorbidity			
Cerebrovascular disease, n (%)	48 (6.8)	24 (3.6)	.01
Cancer, n (%)	311 (44.2)	276 (41.8)	.37
Diabetes, n (%)	107 (15.2)	69 (10.5)	.01
Liver disease, n (%)	98 (13.9)	85 (12.9)	.57
Mild liver disease, n (%)	93 (13.2)	82 (12.4)	.66
Moderate or severe liver disease, n (%)	14 (2.0)	10 (1.5)	.78
Renal disease, n (%)	95 (13.5)	101 (15.3)	.35
Sepsis, n (%)	101 (14.4)	115 (17.4)	.12
Charlson comorbidity index, median (range)	2 (1-9)	2 (1-14)	.03
Polymicrobial rate, n (%)	50 (5.4)	65 (7.3)	.09

ICU, intensive care unit; STI, short-term incubation.

TABLE 2. Clinical outcomes of all patients with blood infections

	Conventional method (n = 703)	STI protocol (n = 660)	*P*
Pathogen identification TAT, mean (SD), d	2.2 (0.87)	1.4 (0.73)	<.001
Final AST-TAT, mean (SD), d	3.4 (1.37)	2.5 (0.98)	<.001
Length of ICU stay, mean (SD), d	28.9 (22.4)	28.3 (19.3)	.48
Length of total hospitalization stay, mean (SD), d	31.9 (31.6)	29.6 (24.6)	.06
30-day all-cause mortality, n (%)	179 (25.5)	160 (24.2)	.58
14-day all-cause readmission, n (%)	101 (14.4)	89 (13.5)	.67

AST-TAT, antimicrobial susceptibility testing turnaround time; ICU, intensive care unit; STI, short-term incubation.

culture samples in the study. **TABLE 3** shows that TAT of pathogen identification was shorter for the GNB organisms in the STI group (GNB: 1.2 days vs GPC: 1.5 days). Compared with the conventional method, the STI protocol decreased about 42.8% and 37.5% of identification time for GNB and GPC, respectively ($P < .001$). Moreover, the length of total hospital stay decreased from 31.9 days to 27.1 days for patients with GNB-infected BSIs, suggesting that patients could be discharged nearly 5 days earlier after implementing the STI protocol ($P < .01$).

Positive blood cultures with sepsis ICD-10 codes were analyzed to determine the impact of the STI protocol on the sepsis population. The length of ICU stay decreased by 1.2 days (27.0 days vs 28.2 days, $P = .84$), the length of total hospital stay increased by 1.1 days (30.3 vs 28.9 d, $P = .67$), 30-day all-cause mortality rate decreased from 31.7% to 27.0% ($P = .45$), and 14-d all-cause readmission rate decreased from 11.9% to 7.0% ($P = .21$), in the STI group. However, these differences did not reach statistical significance. For patients whose infection did not develop into sepsis, the length of total hospital stay decreased by 3.1 days (29.4 days vs 32.5 days, $P = .007$) (**TABLE 4**).

Discussion

This study retrospectively evaluated the clinical impacts of implementing a STI protocol for positive blood culture samples. Compared with the conventional method, the STI protocol decreased about 36.4% of pathogen identification TAT and 26.4% of AST-TAT. The length of total hospital stay was 2.3 days shorter after implementing the STI protocol despite no statistical difference. In addition, the length of total hospital stay decreased from 31.9 days to 27.1 days in the subgroup of GNB-associated BSIs, suggesting that patients could be discharged nearly 5 days earlier after implementing the STI protocol ($P < .01$).

The rapid diagnosis of BSIs still remains a critical unmet need in the urgent care field. However, according to our previous study, anaerobic bacteria and coagulase-negative *Staphylococcus* did not meet the validation criteria for using the immature subculture samples to provide preliminary identification and AST reports; therefore, these 2 types of organisms have been identified in our laboratory using the conventional method.[13] Furthermore, the Taiwan Antimicrobial Resistance Surveillance Annual Report indicated an increasing trend of antibiotic-resistant GNB in both community and health care-associated infections

TABLE 3. Clinical outcomes of patients infected by different types of bacteria

	Gram-negative bacilli			Gram-positive cocci		
	Conventional method (n =368)	STI protocol (n =322)	*P*	Conventional method (n =308)	STI protocol (n = 278)	*P*
Pathogen identification TAT, mean (SD), d	2.1 (0.7)	1.2 (0.7)	<.001	2.4 (1.0)	1.5 (0.6)	<.001
Final AST-TAT, mean (SD), d	3.6 (1.1)	2.4 (0.9)	<.001	3.5 (1.1)	2.7 (0.8)	<.001
Length of ICU stay, mean (SD), d	30.7 (24.6)	27.8 (19.1)	.21	27.1 (20.0)	27.9 (18.8)	.40
Length of total hospitalization stay, mean (SD), d	31.9 (33.5)	27.1 (21.2)	.01	32.2 (29.7)	33.2 (27.8)	.33
30-day all-cause mortality, n (%)	97 (26.4	68 (21.1)	.11	74 (24.0)	68 (24.5)	.90
14-day all-cause readmission, n (%)	55 (14.9)	13 (13.4)	.55	41 (13.3)	39 (14.0)	.80

AST-TAT, antimicrobial susceptibility testing-turnaround time; ICU, intensive care unit; STI, short-term incubation.

TABLE 4. Clinical outcomes of patients with sepsis

	Sepsis			Nonsepsis		
	Conventional method (n = 101)	STI protocol (n = 115)	*P*	Conventional method (n = 602)	STI protocol (n = 545)	*P*
Length of ICU stay, mean (SD), d	28.2 (27.0)	27.0 (18.5)	.84	29.1 (21.4)	28.6 (19.5)	.84
Length of total hospitalization stay, mean (SD), d	28.9 (26.9)	30.3 (24.5)	.67	32.5 (32.4)	29.4 (24.6)	.07
30-day all-cause mortality, n (%)	32 (31.7)	31 (27.0)	.45	147 (24.4)	129 (23.7)	.77
14-day all-cause readmission, n (%)	12 (11.9)	8 (7.0)	.21	89 (14.8)	81 (14.9)	.97

ICU, intensive care unit; STI, short-term incubation.

after 2016, including *Escherichia coli*, *Klebsiella pneumoniae*, and *Pseudomonas aeruginosa*. In contrast to GNB, methicillin-resistant *Staphylococcus aureus* has decreased stably from 60% to 50% since 2016.[18] The various prevalence of antimicrobial-resistant GNB and GPC may influence the decision making in antimicrobial prescribing for clinicians, who may be more vigilant with regard to potential antibiotic-resistant GNB infections, thus leading to faster modification of antibiotics and a shorter hospitalization time.

Many studies have verified the value of rapid pathogen identification from blood cultures with different diagnostic tools used in suspected BSI cases. Most rapid blood culture identification assays were based on the molecular method. The Accelerate Pheno blood culture detection system, which uses fluorescent in situ hybridization, allows for the identification of pathogens in just 1.5 hours. Dare et al[19] showed that hospital length of stay improved, with discharge being 1.8 days earlier for GNB and GPC-related BSIs. Moreover, Roth et al[20] indicated a hospital discharge 6.6 days earlier after implementing Accelerate Pheno blood culture detection system use for GNB identification. Other molecular assays also led to similar outcomes. Felsenstein and colleagues[15] implemented use of the BC-GP assay (Nanopore) in a pediatric hospital, and the outcome showed a reduction in the length of stay in general pediatric admissions for all GPC organisms and *S aureus*-related BSIs (1.5 days and 5.6 days, respectively).

Our study showed an average of 30 days of hospitalization, but this may be due to the severity of illness in the medical center and because a 14-day hospitalization for each BSI patient is covered by national health insurance in Taiwan. Researchers found that the positive effects on health care delivery would continue to grow when rapid diagnostics shorten the TAT of test results with reduced financial burden.[21] It was reported that the median inpatient cost for an episode of GN-BSI was US$12,939 (interquartile range [IQR], $6205-$38,278) and the median hospital stay was 10 days (IQR, 5.5-23.0 days) for patients with multidrug-resistant GNB,[22] with an average cost of $1293.9/d. This study found the length of total hospital stay to be 4.8 days shorter for patients with GNB infection after implementing the MALDI-TOF MS-based STI protocol. Accordingly, it saved about US$6210.7 for each patient and $2.8 million, with an average 450 BSI patients annually, for the hospital where the study was conducted.

Our findings suggested no difference between the conventional method and the rapid molecular assay, consistent with those in the studies of ICU length of stay, in-hospital mortality, and 30-day all-cause hospital readmission rate.[16,19,23–25] On the other hand, a meta-analysis found a significant reduction in mortality associated with rapid molecular testing combined with direct communications to clinicians.[26]

Studies have shown de-escalation rates in septic patients ranged from 19.6% to 43%.[27,28] It has been estimated that antibiotic de-escalation rates remained at approximately 25% before and after implementing the STI protocol. Gonzalez et al[29] reported that reasons for no de-escalation were lack of microbiological documentation, initial appropriate antibiotic therapy that could not be de-escalated, inadequate initial antibiotics, and clinical worsening despite appropriate antibiotic therapy. Further study will be required to understand the factors that influence de-escalation rates in septic patients and to identify strategies to improve these rates over time.

Previous studies found a relationship between a longer hospital stay and delayed treatment in bacteremia resulting from the lack of an appropriate advocation program, timely pharmacist intervention, and prompt physician action.[30,31] Therefore, it is imperative to report the results to the clinical team, who could change therapies based on the laboratory results. Laboratory professionals have pursued faster TAT in pathogen identification and antimicrobial susceptibility testing by implementing new techniques, adjusting working shifts, and adopting process optimization for years. Nevertheless, cost-effectiveness has not been fully achieved and the positive impact on patients not properly appreciated.

Our facility had been dedicated to promoting antimicrobial stewardship programs (ASP) since 2013. This strategy has led to an average of 8.0 mL blood volume in blood culture bottles, 90% of sample sent for incubation within 2 hours of blood draw, and a less than 2% contamination rate. Furthermore, it helped lay the foundation for successfully implementing the STI protocol by optimizing the laboratory workflow and prioritizing identification practices. For years, our laboratory has been monitoring contamination rate, adhering to the procedure manual based on guidelines, and providing antibiograms to disclose susceptibility patterns within the institution. The values of the ASP have been reported previously. Pliakos et al[32] compared the cost-effectiveness of MALDI-TOF analysis with an ASP vs conventional laboratory methods without an ASP. The analysis found that MALDI-TOF analysis with an ASP was the most cost-effective strategy, preventing 1 death per 14 patients tested and resulting in the highest savings per quality-adjusted life years gained.

Furthermore, a meta-analysis, primarily of observational studies, demonstrated a mortality benefit when blood culture diagnostics were used in conjunction with stewardship programs.[33]

This study was a retrospective study, and it limited the selection of patient demographics and preexisting comorbidities. Also, the study lacked antibiotic use data, such as time from positive Gram stain to first active antibiotic, first de-escalation or escalation of antibiotics, time to optimal therapy, and duration of antimicrobial treatment to measure the primary outcomes. Further studies will be needed to monitor

real-time antibiotic modifications after reporting the result to combat antimicrobial resistance.

Conclusion

The implementation of the STI protocol benefited patients with BSIs by not only improving the pathogen identification and antimicrobial susceptibility testing TAT but also reducing the length of hospital stay.

Conflict of Interest Disclosure

The authors have nothing to disclose.

REFERENCES

1. Dat VQ, Vu HN, Nguyen The H, et al. Bacterial bloodstream infections in a tertiary infectious diseases hospital in Northern Vietnam: aetiology, drug resistance, and treatment outcome. *BMC Infect Dis.* 2017;17(1):493. https://doi.org/10.1186/s12879-017-2582-7
2. Goto M, Al-Hasan MN. Overall burden of bloodstream infection and nosocomial bloodstream infection in North America and Europe. *Clin Microbiol Infect.* 2013;19(6):501-509. https://doi.org/10.1111/1469-0691.12195
3. Hattori H, Maeda M, Nagatomo Y, et al. Epidemiology and risk factors for mortality in bloodstream infections: a single-center retrospective study in Japan. *Am J Infect Control.* 2018;46(12):e75-e79. https://doi.org/10.1016/j.ajic.2018.06.019
4. Jin L, Zhao C, Li H, Wang R, Wang Q, Wang H. Clinical profile, prognostic factors, and outcome prediction in hospitalized patients with bloodstream infection: results from a 10-year prospective multicenter study. *Front Med*. 2021;8:629671. https://doi.org/10.3389/fmed.2021.629671
5. Liu VX, Fielding-Singh V, Greene JD, et al. The timing of early antibiotics and hospital mortality in sepsis. *Am J Respir Crit Care Med.* 2017;196(7):856-863. https://doi.org/10.1164/rccm.201609-1848OC
6. Kumar A, Roberts D, Wood KE, et al. Duration of hypotension before initiation of effective antimicrobial therapy is the critical determinant of survival in human septic shock. *Crit Care Med.* 2006;34(6):1589-1596. https://doi.org/10.1097/01.CCM.0000217961.75225.E9
7. Seymour CW, Gesten F, Prescott HC, et al. Time to treatment and mortality during mandated emergency care for sepsis. *N Engl J Med.* 2017;376(23):2235-2244. https://doi.org/10.1056/NEJMoa1703058
8. Timsit JF, Ruppe E, Barbier F, Tabah A, Bassetti M. Bloodstream infections in critically ill patients: an expert statement. *Intensive Care Med.* 2020;46(2):266-284. https://doi.org/10.1007/s00134-020-05950-6
9. Idelevich EA, Schule I, Grunastel B, Wullenweber J, Peters G, Becker K. Rapid identification of microorganisms from positive blood cultures by MALDI-TOF mass spectrometry subsequent to very short-term incubation on solid medium. *Clin Microbiol Infect.* 2014;20(10):1001-1006. https://doi.org/10.1111/1469-0691.12640
10. Kohlmann R, Hoffmann A, Geis G, Gatermann S. MALDI-TOF mass spectrometry following short incubation on a solid medium is a valuable tool for rapid pathogen identification from positive blood cultures. *Int J Med Microbiol.* 2015;305(4-5):469-479. https://doi.org/10.1016/j.ijmm.2015.04.004
11. Johnsson ATA, Wong AYW, Ozenci V. The impact of delayed analysis of positive blood cultures on the performance of short-term culture followed by MALDI-TOF MS. *J Microbiol Methods.* 2020;177:106027. https://doi.org/10.1016/j.mimet.2020.106027
12. Frobose NJ, Idelevich EA, Schaumburg F. Short incubation of positive blood cultures on solid media for species identification by MALDI-TOF MS: which agar is the fastest? *Microbiol Spectr.* 2021;9(1):e0003821. https://doi.org/10.1128/Spectrum.00038-21
13. Tsai YW, Lin TC, Chou HY, et al. Shortening the time of the identification and antimicrobial susceptibility testing on positive blood cultures with MALDI-TOF MS. *Diagnostics.* 2021;11(8):1514. https://doi.org/10.3390/diagnostics11081514
14. Banerjee R, Teng CB, Cunningham SA, et al. Randomized trial of rapid multiplex polymerase chain reaction-based blood culture identification and susceptibility testing. *Clin Infect Dis.* 2015;61(7):1071-1080. https://doi.org/10.1093/cid/civ447
15. Felsenstein S, Bender JM, Sposto R, Gentry M, Takemoto C, Bard JD. Impact of a rapid blood culture assay for gram-positive identification and detection of resistance markers in a pediatric hospital. *Arch Pathol Lab Med.* 2016;140(3):267-275. https://doi.org/10.5858/arpa.2015-0119-OA
16. MacVane SH, Hurst JM, Boger MS, Gnann JW Jr. Impact of a rapid multiplex polymerase chain reaction blood culture identification technology on outcomes in patients with vancomycin-resistant enterococcal bacteremia. *Infect Dis.* 2016;48(10):732-737. https://doi.org/10.1080/23744235.2016.1185533
17. Buchman TG, Simpson SQ, Sciarretta KL, et al. Sepsis among Medicare beneficiaries: 1. The burdens of sepsis, 2012-2018. *Crit Care Med.* 2020;48(3):276-288. https://doi.org/10.1097/CCM.0000000000004224
18. Taiwan Centers for Disease Control. Antimicrobial Resistance Surveillance Annual Report, Taiwan; 2021.
19. Dare RK, Lusardi K, Pearson C, et al. Clinical impact of accelerate pheno rapid blood culture detection system in bacteremic patients. *Clin Infect Dis.* 2021;73(11):e4616-e4626. https://doi.org/10.1093/cid/ciaa649
20. Roth F, Leedahl ND, Leedahl DD, Guerrero DM. Clinical and financial impact of rapid antimicrobial susceptibility testing in blood cultures. *Antibiotics.* 2022;11(2):122. https://doi.org/10.3390/antibiotics11020122
21. She RC, Bender JM. Advances in rapid molecular blood culture diagnostics: healthcare impact, laboratory implications, and multiplex technologies. *J Appl Lab Med.* 2019;3(4):617-630. https://doi.org/10.1373/jalm.2018.027409
22. Thaden JT, Li Y, Ruffin F, et al. Increased costs associated with bloodstream infections caused by multidrug-resistant gram-negative bacteria are due primarily to patients with hospital-acquired infections. *Antimicrob Agents Chemother.* 2017;61(3):e01709-16. doi: 10.1128/AAC.01709-16
23. Banerjee R, Komarow L, Virk A, et al. Randomized trial evaluating clinical impact of RAPid IDentification and susceptibility testing for gram-negative bacteremia: RAPIDS-GN. *Clin Infect Dis.* 2021;73(1):e39-e46. https://doi.org/10.1093/cid/ciaa528
24. Gritte AS, Morneau KM, Frei CR, Cadena-Zuluaga JA, Walter EA, Hopkins TL. Clinical impact of implementation of rapid diagnostic testing of blood cultures with *Staphylococcus aureus* on patient outcomes. *Diagn Microbiol Infect Dis.* 2021;101(3):115474. https://doi.org/10.1016/j.diagmicrobio.2021.115474
25. Ehren K, Meissner A, Jazmati N, et al. Clinical impact of rapid species identification from positive blood cultures with same-day phenotypic antimicrobial susceptibility testing on the management and outcome of bloodstream infections. *Clin Infect Dis.* 2020;70(7):1285-1293.
26. Buehler SS, Madison B, Snyder SR, et al. Effectiveness of practices to increase timeliness of providing targeted therapy for inpatients with bloodstream infections: a laboratory medicine best practices systematic review and meta-analysis. *Clin Microbiol Rev.* 2016;29(1):59-103. https://doi.org/10.1128/CMR.00053-14
27. Heenen S, Jacobs F, Vincent JL. Antibiotic strategies in severe nosocomial sepsis: why do we not de-escalate more often? *Crit Care Med.* 2012;40(5):1404-1409. https://doi.org/10.1097/CCM.0b013e3182416ecf
28. Moraes RB, Guillen JA, Zabaleta WJ, Borges FK. De-escalation, adequacy of antibiotic therapy and culture positivity in septic patients: an observational study. *Rev Bras Ter Intensiva*. 2016;28(3):315-322. https://doi.org/10.5935/0103-507X.20160044

29. Gonzalez L, Cravoisy A, Barraud D, et al. Factors influencing the implementation of antibiotic de-escalation and impact of this strategy in critically ill patients. *Crit Care.* 2013;17(4):R140. https://doi.org/10.1186/cc12819

30. Carver PL, Lin SW, DePestel DD, Newton DW. Impact of mecA gene testing and intervention by infectious disease clinical pharmacists on time to optimal antimicrobial therapy for *Staphylococcus aureus* bacteremia at a university hospital. *J Clin Microbiol.* 2008;46(7):2381-2383. https://doi.org/10.1128/JCM.00801-08

31. Frye AM, Baker CA, Rustvold DL, et al. Clinical impact of a real-time PCR assay for rapid identification of staphylococcal bacteremia. *J Clin Microbiol.* 2012;50(1):127-133. https://doi.org/10.1128/JCM.06169-11

32. Pliakos EE, Andreatos N, Shehadeh F, Ziakas PD, Mylonakis E. The cost-effectiveness of rapid diagnostic testing for the diagnosis of bloodstream infections with or without antimicrobial stewardship. *Clin Microbiol Rev.* 2018;31(3):e00095-17. doi: 10.1128/CMR.00095-17

33. Timbrook TT, Morton JB, McConeghy KW, Caffrey AR, Mylonakis E, LaPlante KL. The effect of molecular rapid diagnostic testing on clinical outcomes in bloodstream infections: a systematic review and meta-analysis. *Clin Infect Dis.* 2017;64(1):15-23. https://doi.org/10.1093/cid/ciw649

A novel high-resolution melting analysis strategy for detecting cystic fibrosis–causing variants

Gerardo Raúl Díez Rodríguez, BSc[1,], Juan Emilio Figueredo Lago, MSc[1], Anny Armas Cayarga, MSc[1], Yaimé Josefina González González, PhD[1], Iria García de la Rosa, MSc[1], Teresa Collazo Mesa, PhD[2], Ixchel López Reyes, MSc[2], Yulaimy Batista Lozada, BSc[1], Fidel Ramón Rodríguez Calá, MD[3], Juan Bautista García Sánchez, MD[4]*

[1]Immunoassay Center, Playa, Havana, Cuba, [2]National Center of Medical Genetics, Medical University of Havana, Playa, Havana, Cuba, [3]Calixto García University Hospital, Plaza de la Revolución, Havana, Cuba, [4]Juan Manuel Márquez Pediatric Teaching Hospital, Marianao, Havana, Cuba. Corresponding author: Gerardo Raúl Díez Rodríguez; gerardod@cim.sld.cu. *Dr Díez Rodríguez is currently with the Department of Biomarkers, Center of Molecular Immunology, Playa, Havana, Cuba.

Key words: cystic fibrosis; allele-specific polymerase chain reaction; high-resolution melting analysis.

Abbreviations: CF, cystic fibrosis; CFTR, cystic fibrosis transmembrane conductance regulator; AS, allele-specific; HRMA, high-resolution melting analysis; DBS, dried blood spots; CNGM, National Center of Medical Genetics; *wt*, wild type genotype; *mut*, mutant genotype; Ct, cycle threshold; Tm, melting temperature; IRT, immunoreactive trypsin

Laboratory Medicine 2024;55:185-197; https://doi.org/10.1093/labmed/lmad058

ABSTRACT

Cystic fibrosis (CF), an autosomal recessive disease, is caused by variants in both alleles of the *CF transmembrane conductance regulator* (*CFTR*) gene. A new assay based on allele-specific polymerase chain reaction and high-resolution melting analysis was developed for the detection of 18 CF-causing *CFTR* variants previously identified in Cuba and Latin America. The assay is also useful for zygosity determination of mutated alleles and includes internal controls. The reaction mixtures were normalized and evaluated using blood samples collected on filter paper. The evaluation of analytical parameters demonstrated the specificity and sensitivity of the method to detect the included *CFTR* variants. Internal and external validations yielded a 100% agreement between the new assay and the used reference tests. This assay can complement CF newborn screening not only in Cuba but also in Latin America.

Introduction

Cystic fibrosis (CF) is the most common autosomal recessive genetic disease in the White population. It affects over 90,000 individuals heterogeneously distributed worldwide. The c.1521_1523delCTT is the most prevalent CF-causing variant, affecting approximately 82% of the CF population.[1]

Cystic fibrosis causes an accumulation of mucus in exocrine- and exocrine-associated organs. The main symptoms include a persistent cough that produces mucous, recurrent lung infection, intestinal obstruction, malabsorption, nasal polyps, rectal prolapse, pancreatitis, increased blood sugar level, and growth hormone disorders.[2]

Although rare, CF is among the most common genetic disorders that shorten lifespan. Symptoms often appear in infancy, such as intestinal obstruction or meconium ileus in newborns.[3] As it is a progressive and incurable disease, its early diagnosis enables the establishment of appropriate treatment, adequate follow-up, and timely genetic counseling.[4]

The disease is caused by variants in the CF transmembrane conductance regulator (*CFTR*) gene that encodes a 1480 amino acid protein forming an ionic channel in the apical epithelial cell membrane.[5] To date, more than 2000 disease-associated variants in this gene have been reported (www.genet.sickkids.on.ca/cftr).

A diagnosis of CF can be made if the sweat chloride value is ≥60 mmol/L in individuals presenting with a positive newborn screen, clinical features consistent with CF, or a positive family history.[6-8]

The goal of molecular diagnostic testing is to provide genetic characterization of individuals with clinical suspicion of CF in the presence of consistent clinical symptoms, a family history of CF, or a similar condition. The benefits of *CFTR* variant testing include early and definitive diagnosis, personalized treatment, clarification of atypical and indeterminate cases, and counseling on recurrence risk and fertility options.[9,10]

Cystic fibrosis is the second-most frequent autosomal recessive hereditary disease in Cuba[11] with an estimated incidence of 1 in 9862 live births, and it is considered a public health issue.[12]

Whereas in Latin America, the most frequent *CFTR* variants are c.1521_1523delCTT (46.69%), c.1624G>T (5.08%), c.3909C>G (1.65%), c.3846G>A (1.13%), and c.3484C>T (0.96%),[13] Cuba presents some differences in the spectrum of CF-causing variants. According to a study by Armas et al[14] in a cohort of Cuban CF patients, higher frequencies are found for c.1521_1523delCTT (35.9%), c.1000C>T (7.4%), c.1624G>T (7%), c.1519_1521delATC (5.8%), c.3484C>T (2.7%), c.254G>A (1.9%), c.1657C>T (1.6%), and c.2988 + 1G>A (1.2%).

At present, CF carrier screening panels are very expensive and do not contain all the variants identified in Latin America. This article describes the development and performance evaluation of an

affordable assay based on allele-specific (AS) polymerase chain reaction (PCR) and high-resolution melting analysis (HRMA) for the detection of 18 *CFTR* variants frequently found in Cuban and Latin American populations.

Materials and Methods

Samples

A total of 250 whole blood samples (dried blood spots, DBS), obtained by finger or heel (newborns) puncture and collected on Whatman BFC 903 filter paper cards (Whatman International), were provided by the National Center of Medical Genetics (CNGM). Thirty of them came from patients with some respiratory symptoms but whose clinical criteria had ruled out CF. The others were specimens from patients diagnosed with CF. In a part of this latter group, some *CFTR* variants had been already found either by using automated DNA sequencing[15] or with the CNGM panel.[11,16] The CNGM Ethics Committee obtained written informed consent from all patients or their parents.

Two samples donated by the Brazilian Neonatal Screening Program and carrying c.3196C>T and c.3846G>A variants, not previously described in the Cuban CF population, were also included.

Primers

The Oligonucleotide Synthesis Group of the Center for Genetic Engineering and Biotechnology carried out synthesis and purification of all primers. The synthesized primers were diluted in nuclease-free water to 50 μmol/L.

DNA Extraction

Genomic DNA was extracted from DBS according to a modification of the procedure described by Kain and Lanar.[17] Three 3 mm blood discs per sample were perforated with a P51 manual puncher (Immunoassay Center) and placed into a 1.5 mL tube. After addition of 1 mL nuclease-free water, samples were incubated for 30 minutes and centrifuged at 16,500*g* for 2 minutes at room temperature (20°C–25°C). Approximately 970 μL of the supernatant were gently aspirated from the surface without reaching the bottom and then discarded. The paper discs were left inside the tubes. A volume of 170 μL 5% Chelex-100 resin (Sigma-Aldrich) (w/v) was added to the remaining 30 μL, followed by incubation at 56°C for 20 minutes. Specimens were then shaken for 10 seconds and incubated at 100°C for 8 minutes. Samples were shaken again for 10 seconds and centrifuged at 16,500*g* for 2 minutes at room temperature. The supernatant with the extracted DNA was transferred to a fresh 1.5 mL tube. The DNA concentration of each sample was determined using the NanoDrop UV-Vis spectrophotometer (Thermo Fisher Scientific). Specimens were stored at −20°C until use.

Prior to PCR, extracted DNA samples were tempered to room temperature, shaken for 10 seconds, and centrifuged at 16,500*g* for 2 minutes at room temperature.

Characterization of Samples

Specimens from CNGM were evaluated with the commercial CF StripAssay 4–410 panel (ViennaLab Diagnostics) for the identification of 34 variants and 1 polymorphism in *CFTR* by PCR and reverse-hybridization (according to the instructions for use, CF StripAssay 4–410, 2020).

A panel of carrier controls was formed with samples presenting all available variants with homozygous, compound heterozygous, and simple heterozygous genotypes. Specimens from patients without clinical criteria for CF and in which no mutations could be identified were selected as noncarrier controls.

Design and Evaluation of Primers for the Detection of 18 *CFTR* Variants and Zygosity Determination

Three PCR primers were designed for detecting each variant: 2 AS primers (to identify the wild type and mutant genotypes, *wt* and *mut*, respectively) and a common primer, running in the opposite sense to the previous ones. The target mutant points on the gene (nucleotides) were identified by means of the *CFTR* database (www.genet.sickkids.on.ca/cftr). For each AS mutant primer, the nucleotide of the 3'-OH end was modified according to the base change described. In some AS primers, an extra mismatch was introduced adjacent to the terminal 3' nucleotide to achieve greater specificity when amplifying. All primer sequences were analyzed with the Oligo Primer Analysis Software v.5 (DBA Oligo). Primer sequences are available on request to the corresponding author.

The specificity of each primer trio was evaluated by comparing parallel AS real-time PCRs (*wt* and *mut*) using noncarrier controls. Reaction mixtures contained 12.5 μL 2X ABsolute qPCR SYBR Green Mix (Thermo Fisher Scientific), 0.25 μL of each primer prediluted at 50 μmol/L, and nuclease-free water to a total volume of 22 μL. Finally, 3 μL extracted DNA was added. Reactions were run in triplicate in capped 8-well tube strips (4titude, Brooks Automation) by using the SLAN-96P real-time PCR system (Shanghai Honshi Medical Technology). The program was 95°C for 15 minutes and 32 cycles: 95°C for 10 seconds, 59°C for 15 seconds with fluorescence reading at 510 nm, and 72°C for 25 seconds. The ΔCt (cycle threshold) was calculated between the average values of *mut* and *wt* reactions of each region of interest (ΔCt = C*tmut*−C*twt*) to determine the specificity of the AS primers.[18]

Determination of the Average Melting Temperature Value of the AS PCR Products

Simple AS PCRs (mutated) were carried out to amplify each of the 18 target regions in the *CFTR* by evaluating the performance of every pair of primers (mutated AS and common) in the presence of a control carrying the corresponding DNA variation. Three replicates per reaction were made. The reaction mixtures and PCR were performed as described above. The average melting temperature (Tm) value of each of the 18 resulting DNA fragments was determined in a final HRMA step between 65°C and 95°C with a ramp rate of 0.01°C/s and capture of fluorescence at 510 nm. Melt curves were analyzed with commercial SLAN-96P software, version 8.2.2 (Shanghai Honshi Medical Technology). The HRMA pre- and postmelting values were set between 72°C and 73°C and 82°C and 83°C, respectively, for fluorescence normalization. To establish a temperature range for the detection of each amplified product, the average Tm value and its SD were calculated when HRMA was completed.

Preparation and Evaluation of Primer Mixes for AS Multiplex PCR

Four primer mixes (A, B, C, and D) were prepared for mutated AS multiplex PCR and HRMA. According to the Tm ranges obtained for every single DNA fragment and to avoid melt peaks overlapping, primer pairs

(mutated AS and common) were selectively added into mixtures. Each mix was composed of 6 µL of each primer prediluted at 50 µmol/L and nuclease-free water to a total volume of 300 µL.

Each primer mix was evaluated by using 5 control samples carrying the corresponding variants in the *CFTR* (**TABLE 1**) and 20 noncarrier controls. Three replicates per reaction were made. The composition of each reaction mixture was 12.5 µL of 2X ABsolute qPCR SYBR Green Mix and 7.5 µL of primer mix (A-D). Finally, 5 µL extracted DNA was added. The program performed in the SLAN-96P thermal cycler was 95°C for15 minutes; 26 cycles of 95°C at10 seconds, 59°C for 15 seconds with fluorescence reading at 510 nm, and 72°C for 25 seconds, and a final HRMA step of 68°C to 85°C. Melt curves were analyzed with SLAN-96P software, version 8.2.2. All the inflections obtained in the standard melt curve (Raw Melt) for each mixture were identified, and the corresponding Tm values were determined using the derivative melt curve (Melt Peak). From the results, the working concentration of primer pairs in the mixtures was readjusted and the evaluation was repeated with the same control samples until their proper performance was verified.

Inclusion of an Internal Amplification Control in B and C Primer Mixes

An internal amplification control was included in B and C primer mixes. Two *wt* AS primers designed for the detection of changes in the sequence of bases that occupy positions c.1519_1523 of the *CFTR* gene were selected for both amplifying an internal control and determining the zygosity pattern of samples carrying c.1519_1521delATC and c.1521_1523delCTT. The Tm of the resulting 58-bp DNA fragment was predicted by means of the Tm Tool v1.7b (https://dna-utah.org/tm/tool.html) to avoid interference with other Tm values in mixes A through D. The chosen primers were added to B and C mixes at a final concentration of 1 µmol/L. Those mixtures were retested by using 10 carrier controls: 4 with homozygous genotype (2 for c.1519_1521delATC and 2 for c.1521_1523delCTT), 2 with compound heterozygous genotype (c.1519_1521delATC/c.1521_1523delCTT), and 4 with simple heterozygous genotype (2 c.1519_1521delATC and 2 c.1521_1523delCTT). In addition, 20 carrier controls with other genotypes were analyzed. The amplification and detection were performed as described in the "Preparation and Evaluation of Primer Mixes for AS Multiplex PCR" section. Once the HRMA was finished, the internal control average Tm value and its SD were determined.

TABLE 1. Genotype of the samples selected as controls for the evaluation of the primer mixes for multiplex polymerase chain reaction[a]

Primer mixes	Carrier controls
A	c.1000C>T/*c.2988 + 1G>A*; *c.1521_1523delCTT/c.3909C>G*; *c.1521_1523delCTT/c.1624G>T*; c.1657C>T/*c.3909C>G*; *c.1000C>T/ c.1000C>T*
B	c.1521_1523delCTT/*c.3140-26A>G*; c.1521_1523delCTT/*c.2051-2052delAAinsG*; c.1521_1523delCTT/*c.3276C>A*; c.1519_1521delATC/*c.3484C>T*; c.254G>A/*c.3484C>T*
C	c.1519_1521delATC/*c.2657 + 5G>A*; *c.254G>A/c.1585-1G>A*; *c.1397C>G*/wt; **c.1521_1523delCTT/*c.3196C>T***; *c.254G>A/* c.1521_1523delCTT
D	c.1000C>T/*c.1519_1521delATC*; c.3484C>T/*c.3718-2477C>T*; ***c.3846G>A*/c.3909C>G**; c.1521_1523delCTT/*c.1657C>T*; *c.1657C>T/c.3718-2477C>T*

[a]*The samples donated by the Brazilian Neonatal Screening Program are marked in bold. Alleles relevant to each primer mix are indicated in italics.*

Preparation and Evaluation of Primer Mixes for Zygosity Determination

Sixteen primer mixes (*wt*) were prepared to determine by PCR-HRMA the zygosity pattern of an equal number of variants. To include an internal amplification control in these mixtures, a new primer pair (sense and antisense) was designed and synthesized, which also amplifies a 58-bp fragment. The Tm Tool v1.7b allowed us to predict the Tm of the amplified fragment and to know whether it could interfere with the rest of the products.

All *wt* primer mixes were made up of a *wt* AS primer and its common primer plus the internal control primer pair. Each mixture was composed of 0.45 µL of each primer prediluted at 50 µmol/L and nuclease-free water to a total volume of 7.5 µL.

Mixes were evaluated with specific carrier heterozygous controls for 16 variants and with homozygous controls for c.1000C>T and c.1624G>T variants, as these were the only homozygous genotypes available. The PCR-HRMA mixes were prepared with 12.5 µL 2X ABsolute qPCR SYBR Green Mix, 7.5 µL *wt* primer mix, and 5 µL extracted DNA. The PCR-HRMA program described in the "Preparation and Evaluation of Primer Mixes for AS Multiplex PCR" section was used.. Each mixture was analyzed according to the presence of 1 (homozygous) or 2 peaks (heterozygous) in the corresponding curves.

Evaluation of the AS Multiplex PCR Assay for the Detection of 18 *CFTR* Variants

Repeatability

By using 5 control samples (**TABLE 1**) for each mixture (A-D), 8 PCR-HRMA replicas were made for each variant under study. The average Tm value, its SD, and the confidence interval (temperature) for each DNA fragment (variant) were determined by using the MINITAB Release 14 statistical program (Pennsylvania State University).

Agreement Analysis

Two-hundred and thirty samples were analyzed by the AS multiplex PCR assay (including zygosity determination when needed, ie, supposedly simple heterozygous specimens without c.1519_1521delATC or c.1521_1523delCTT variants), including those donated by the Brazilian Neonatal Screening Program. The reference tests were CF StripAssay 4–410 and automated DNA sequencing, the latter for some specific cases. This study allowed us to determine the clinical and analytical specificities of the developed assay and the percentage of agreement with the reference methods.

External Validation

The Molecular Biology Department of the CNGM performed this evaluation. Ninety-four DBS were obtained and collected as described above. In 69 samples from patients diagnosed with CF, some *CFTR* variants had been already found, either by using automated DNA sequencing[15] or with the CNGM panel.[11,16] Twenty-five specimens came from patients with some respiratory symptoms but whose clinical criteria had ruled

out CF. The 2 samples donated by the Brazilian Neonatal Screening Program were included to analyze at least 1 carrier sample for each variant. Both presumed noncarrier and partially genotyped samples were scanned with the CF StripAssay 4–410 panel.

All samples were analyzed in 6 experiments (16 samples per experiment) with the AS multiplex PCR assay (including zygosity determination when needed, ie, supposedly simple heterozygous specimens without c.1519_1521delATC or c.1521_1523delCTT variants), and the results were compared with those reported by the CNGM and with those obtained with the CF StripAssay 4–410 kit. By using 2 samples of a known genotype and with alleles relevant to each primer mix (A, B, C, and D), 4 PCR-HRMA replicas were made in a repeatability test.

Results

Characterization of Samples

Genomic DNA was extracted from DBS collected by the CNGM. The resulting DNA concentration was between 10 and 50 ng/μL (data not shown). The variant c.2657 + 5G>A was detected through the evaluation with the CF StripAssay 4–410 panel, which constitutes the first finding of this variant in Cuban CF patients. None of the 34 variants identified by the commercial assay were found in the 30 samples from patients without CF, so these could be used as noncarrier controls.

A set of control samples carrying 18 *CFTR* variants was formed: 8 common to CNGM and CF StripAssay 4–410 panels (c.254G>A, c.1000C>T, c.1519_1521delATC, c.1521_1523delCTT, c.1624G>T, c.1657C>T, c.2988 + 1G>A, and c.3484C>T); 7 from the CF StripAssay 4–410 panel and described in the Cuban population (c.1585-1G>A, c.2051_2052delAAinsG, c.2657 + 5G>A, c.3140-26A>G, c.3276C>A, c.3718-2477C>T, and c.3909C>G); 1 described in the Cuban population (c.1397C>G), and 2 frequently found in Latin America (c.3196C>T and c.3846G>A).

Evaluation of PCR Primers for the Detection of *CFTR* Variants and Zygosity Determination

The designed primer trios for each *CFTR* variant were evaluated by comparing parallel AS PCRs (*wt* and *mut*) with noncarrier controls. **TABLE 2** provides the average Ct values of the *wt* and *mut* reactions and the corresponding ΔCt for each region of interest. For all cases, a ΔCt>3 was considered an appropriate specificity of the AS primers.

Determination of Average Tm of the Mutated AS PCR Products and Normalization of Primer Mixes for Multiplex PCR

TABLE 3 shows the average Tm and SD values corresponding to each DNA fragment. A temperature interval of 1°C was empirically established for the identification of DNA fragments (variants) from their average Tm ± 0.5°C (**TABLE 3**). Conditioned by the average Tm value of each DNA fragment, 4 primer mixes for mutated AS multiplex PCR (A-D) were prepared. **TABLE 3** shows the distribution of primer pairs in every mixture and thus the *CFTR* variants intended to detect.

All melt peaks (variants) were detected within the predetermined Tm range but with varying differences in height. From this result, a peak height interval (8≤-d(Rn)/dT≤50) was empirically set to limit the effect of the DNA concentration on the interpretation of the final result.

The use of the SLAN-96P software allowed us to differentiate the DNA melt profiles of mixtures by color: A in green, B in red, C in yellow, and D in blue. The example presented in **FIGURE 1A** is the melt curve resulting for a sample carrying c.1521_1523delCTT variant (mixture A), whereas **FIGURE 1B** shows its corresponding derivative melt curve, from which the Tm value of the amplified DNA fragment can be determined.

Samples with 2 detectable variants in the same pool were carefully analyzed. For the c.1000C>T/c.2988 + 1G>A and c.1521_1523delCTT/c.3909C>G genotypes (mixture A), HRMA yielded 2 peaks per case.

TABLE 2. Cycle threshold (Ct) values obtained in the wild-type (*wt*) and mutant (*mut*) genotype reactions during the evaluation of the primer trios using noncarrier controls

Region (variant)	Average Ct *wt*	Average Ct *mut*	ΔCt
c.254G>A	23.49	28.82	5.33
c.1000C>T	22.76	29.35	6.59
c.1397C>G	22.52	No Ct	>7
c.1519_1521delATC	22.13	26.58	4.45
c.1521_1523delCTT	22.53	28.24	5.71
c.1585-1G>A	22.48	26.17	3.69
c.1624G>T	23.07	27.47	4.4
c.1657C>T	22.61	No Ct	>7
c.2051_2052delAAinsG	24.91	No Ct	>7
c.2657 + 5G>A	22.08	29.03	6.95
c.2988 + 1G>A	22.98	No Ct	>7
c.3140-26A>G	21.94	26.07	4.13
c.3196C>T	22.65	29.11	6.46
c.3276C>A	22.11	25.40	3.29
c.3484C>T	21.21	26.18	4.97
c.3718-2477C>T	23.73	29.65	5.92
c.3846G>A	23.13	27.72	4.59
c.3909C>G	24.18	No Ct	>7

TABLE 3. Final composition of the primer mixes for allele-specific multiplex polymerase chain reaction (A-D) for the detection of 18 *CFTR* variants[a]

Mix	Variant	Tm ± SD (°C)	Interval (°C)	Concentration (µmol/L)	Amplicon length (pb)
A	c.3909C>G	74.86 ± 0.04	74.36–75.36	1.7	206
	c.2988 + 1G>A	75.94 ± 0.01	75.44–76.44	1	197
	c.1624G>T	77.10 ± 0.01	76.60–77.60	1	257
	c.1521_1523delCTT	78.11 ± 0.18	77.61–78.61	1.7	157
	c.1000C>T	80.69 ± 0.03	80.19–81.19	1	140
B	c.3140-26A>G	75.73 ± 0.02	75.23–76.23	0.35	165
	c.3276C>A	77.56 ± 0.05	77.06–78.06	0.5	157
	c.2051_2052delAAinsG	79.08 ± 0.06	78.58–79.58	1	170
	c.3484C>T	80.69 ± 0.07	80.19–81.19	0.6	200
C	c.254G>A	74.27 ± 0.06	73.77–74.77	0.4	245
	c.1585-1G>A	75.99 ± 0.17	75.49–76.49	0.8	149
	c.2657 + 5G>A	77.29 ± 0.07	76.79–77.79	0.2	205
	c.1397C>G	78.77 ± 0.15	78.27–79.27	0.65	184
	c.3196C>T	81.05 ± 0.09	80.55–81.55	0.42	145
D	c.1519_1521delATC	75.39 ± 0.05	74.89–75.89	0.4	94
	c.3718-2477C>T	76.83 ± 0.09	76.33–77.33	1.7	152
	c.1657C>T	77.92 ± 0.08	77.42–78.42	1.7	291
	c.3846G>A	80.16 ± 0.09	79.66–80.66	1	178

[a]*An interval of 1°C from the average melting temperature (Tm) values was established for the detection of each amplified fragment. The final concentration of each primer pair and the length of the amplified fragments (amplicons) are shown.*

FIGURE 1. Standard (A) and derivative (B) melt curves obtained by denaturing a DNA fragment obtained from a sample with genotype c.1521_1523delCTT/*wt* (mix A). In the standard melt plot, the inflection around 78°C corresponds to the presence of variant c.1521_1523delCTT; parallel lines to the right and left of the melting point delimit the pre- and postmelting intervals, respectively, for normalization of fluorescence values; and Rn is the normalized reporter intensity. In the derivative melt plot, the peak corresponding to the detected fragment is shown and parallel lines delimit the temperature range where variants can be detected.

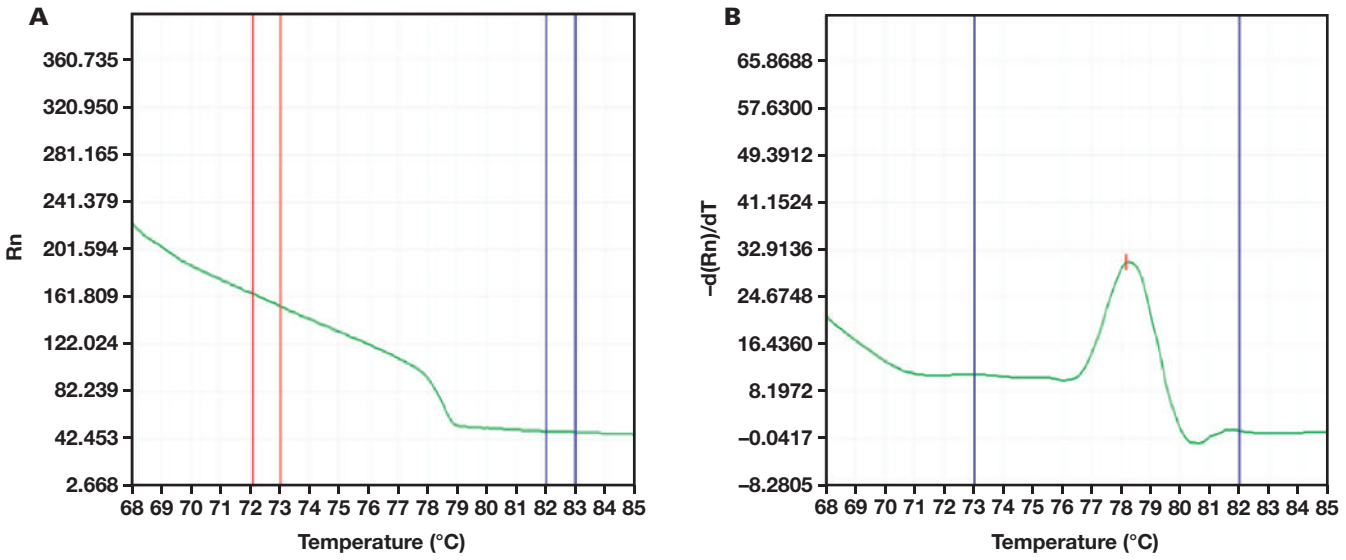

However, the samples with genotypes c.1521_1523delCTT/c.1624G>T (**FIGURE 2**) detectable in A and c.1657c>T/c.3718-2477C>T detectable in D, exhibited 2 consecutive inflections in the standard melt curve but a single peak in the derivative melt curve. This occurs due to the proximity of the inflections in whose narrow temperature range 2 peaks cannot accommodate. Nonspecific amplifications or false-positives were not evidenced.

All variants were detected in the predetermined temperature range. For the noncarrier controls evaluated, no inflections or peaks were observed (data not shown).

FIGURE 2. **Standard (A) and derivative (B) melt curves obtained by denaturing DNA fragments obtained from a sample with genotype c.1521_1523delCTT/c.1624G>T (mix A). In the standard melt plot, 2 consecutive inflections observed between 77°C and 79°C indicate the presence of c.1624G>T and c.1521_1523delCTT variants in that order; parallel lines to the right and left of the melting point delimit the pre- and postmelting intervals, respectively, for normalization of fluorescence values; and Rn is the normalized reporter intensity. In the derivative melt plot, a single peak is observed in the presence of both variants whose detection intervals are contiguous; and parallel lines delimit the temperature range where variants can be detected.**

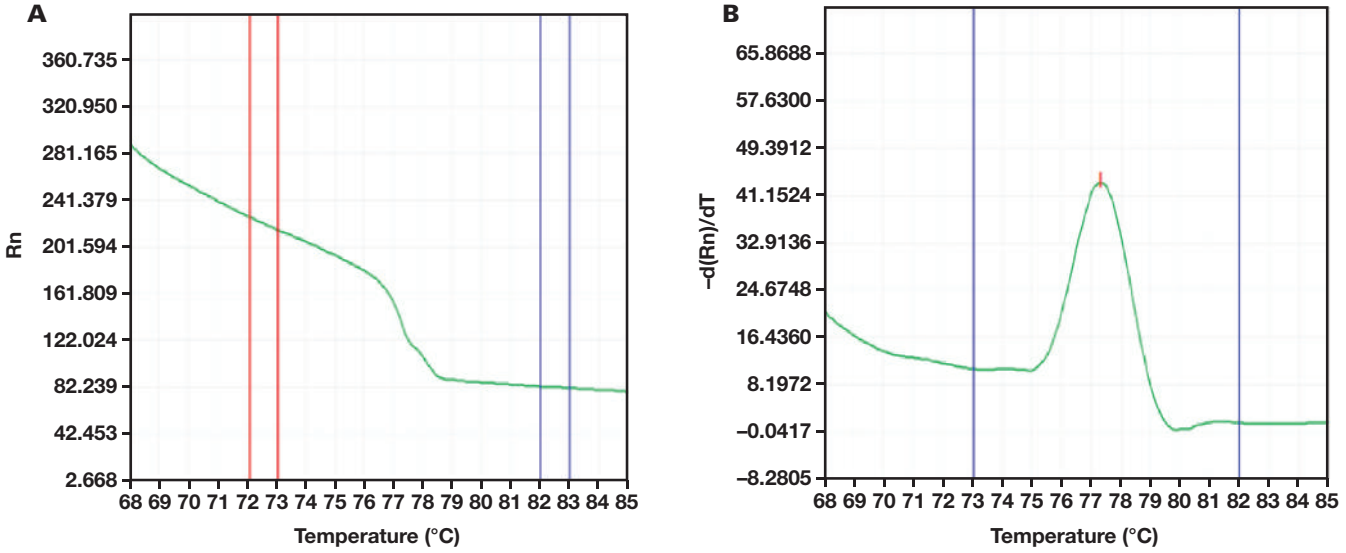

Internal Amplification Control

An internal amplification control was included in mixtures B and C according to the theoretical Tm value obtained in both mixes (72.2°C). For all the c.1519_1521delATC/c.1519_1521delATC, c.1519_1521delATC/c.1521_1523delCTT, and c.1521_1523delCTT/c.1521_1523delCTT samples, the internal control was negative whereas the specimens with different genotypes exhibited a peak before 73°C, which corresponds to the Tm interval defined for the internal control.

FIGURE 3A and **3B** show the results of 2 homozygous samples for c.1521_1523delCTT and 1 c.1519_1521delATC/c.1521_1523delCTT (blue/green), respectively, where the internal control was negative (red and yellow for mixtures B and C, respectively). **FIGURE 3C** shows an example where the genotype of the sample was determined from the presence of the internal control. An average Tm value of 71.45°C was obtained, and its detection interval was set between 70.5°C and 72.4°C. A fluorescence interval (8≤-d(Rn)/dT≤50) or acceptable peak height was arbitrarily established for the interpretation of the final result. Under these conditions, the assay's quality parameters were set according to the genotype of the analyzed sample. A result is valid for genotypes c.1519_1521delATC/c.1519_1521delATC, c.1519_1521delATC/c.1521_1523delCTT, and c.1521_1523delCTT/c.1521_1523delCTT when the internal control in mixes B and C yields -d(Rn)/dT<8. For the rest of the genotypes, the result is valid when the internal control reaches an acceptable peak height; otherwise, it is recommended to repeat the test.

Zygosity Determination

In specimens in which only 1 variant was detected, it was necessary to determine its zygosity pattern. The predetermined Tm range for the identification of DNA fragments was also assumed for the amplicons resulting from the zygosity study. In the evaluation of these mixtures, the internal control was detected before 72°C, which validates the used primer pairs. For all heterozygous samples, a second peak was obtained after 73°C, which demonstrates the presence of 1 *wt* allele for the analyzed variant. For the homozygous samples evaluated, only the internal control peak was obtained. Peaks were higher than those yielded by reactions of mixtures A through D; therefore, no limits for peak height were set in the reactions of the 16 primer mixes for zygosity determination.

FIGURE 4 provides the results of 3 evaluated samples with different genotypes: 2 heterozygous for c.2988 + 1G>A (yellow) and c.1624G>T (blue) variants and 1 homozygous for c.1000C>T (pink). For this last specimen, no *wt* peak between 80.19°C and 81.19°C (Tm range for the aforementioned variant) was observed.

Repeatability Study

The 95% confidence interval for each DNA fragment's average Tm presented in **FIGURE 5** confirms that there is no peak overlap in the mixtures and that the composition of primer mixes for multiplex PCR was correct. The closest peaks correspond to variants c.1521_1523delCTT (77.75°C to 78.08°C) and c.1624G>T (77.01°C to 77.10°C) in mixture A and c.3718-2477C>T (76.80°C to 76.92°C) and c.1657C>T (77.83°C to 77.96°C) in mixture D.

Agreement Analysis

Once the parameters of the assay developed for the detection of 18 *CFTR* variants had been established, 230 samples were analyzed and their results regarding 16 variants were confirmed using the CF StripAssay 4–410 test or by comparing with previous scanning in the case of 2 samples of the known genotype that carried c.1397C>G and c.3196C>T variants. In 88 samples, at least 1 *CFTR* variant was detected, of which 53 had 2 variants (34 compound heterozygous and 19 homozygous) and the remaining 35 had 1 variant. **TABLE 4** presents the 141 mutated alleles identified.

FIGURE 3. Derivative melt curves obtained for 2 homozygous c.1521_1523delCTT samples (green) with negative internal control in mixes B (red) and C (yellow) (A), a sample carrying c.1519_1521delATC (blue) and c.1521_1523delCTT (green) variants with negative internal control in mixes B (red) and C (yellow) (B), and a sample carrying c.1000C>T variant (green), with positive internal control in mixes B (red) and C (yellow) (C). Parallel lines delimit the temperature range where variants can be detected.

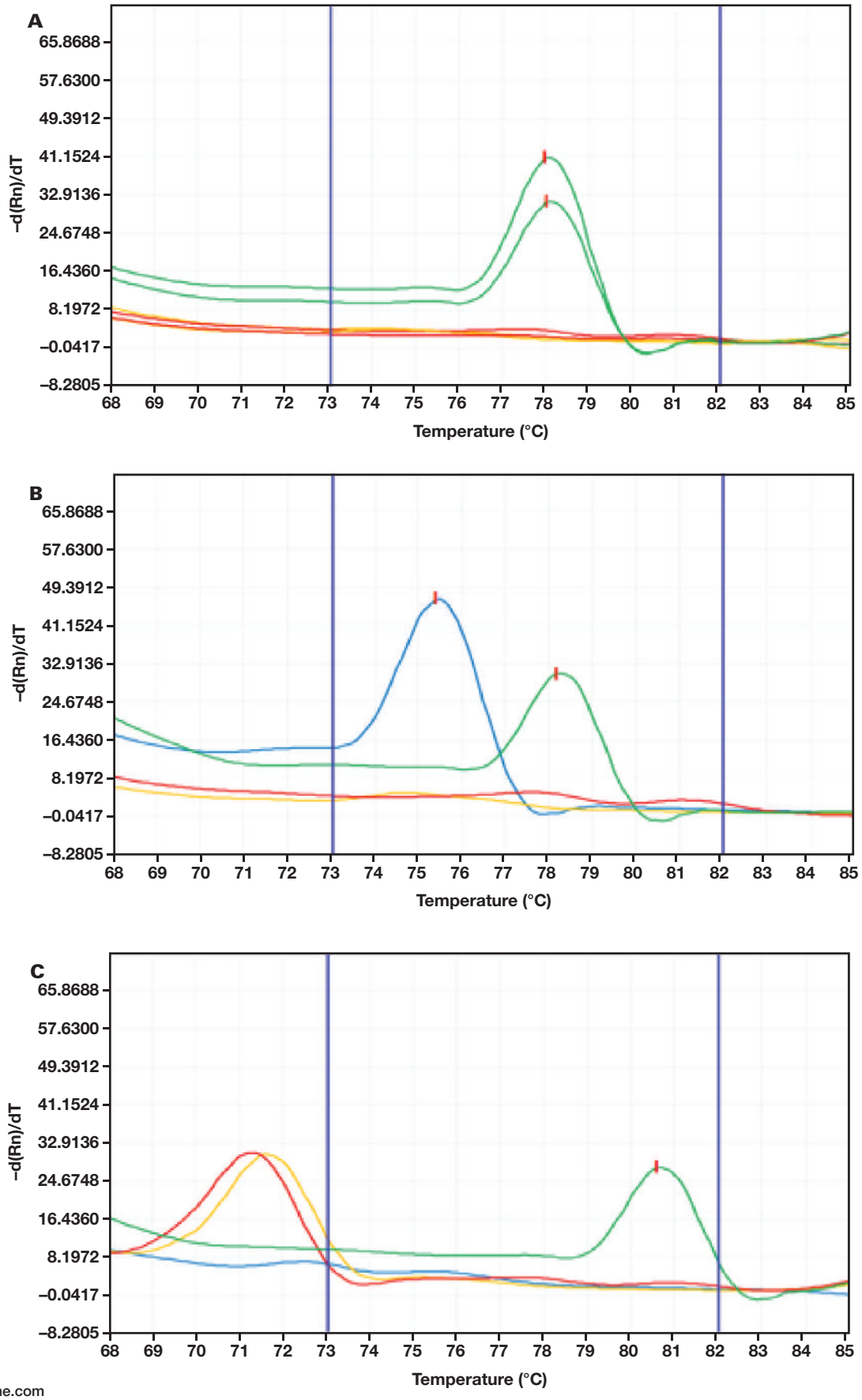

FIGURE 4. **Derivative melt curves of the study of the zygosity pattern. In contrast to samples heterozygous for the variants c.2988 + 1G>A (yellow) and c.1624G>T (blue), the homozygous specimen for c.1000C>T variant (pink) showed no peak after 73°C. Note in each case the peak before 72°C corresponding to the internal control. The color pattern used in these curves was random.**

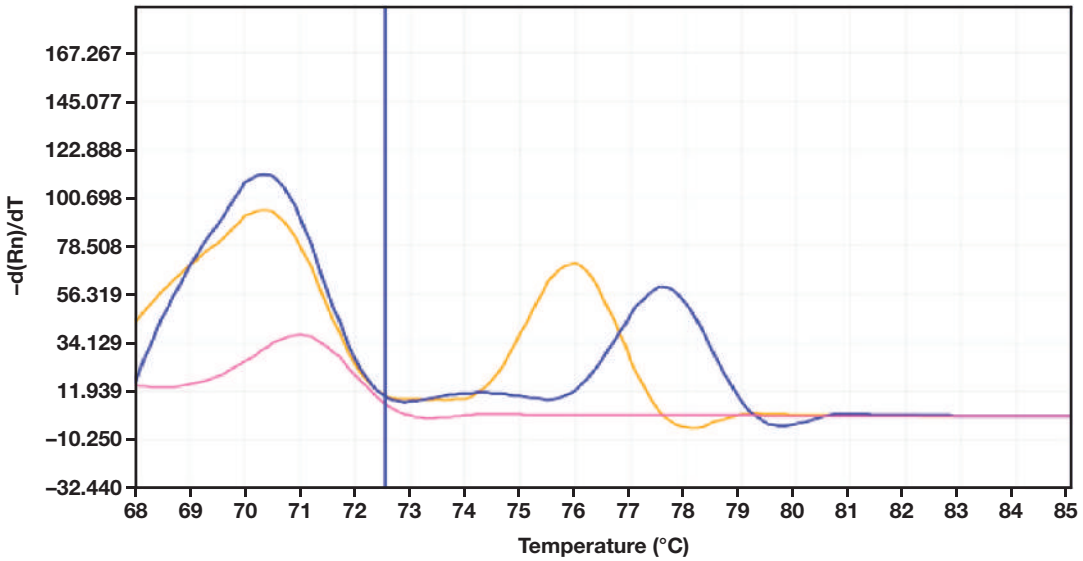

FIGURE 5. **Graph showing the 95% confidence intervals for each DNA fragment's mean melting temperature obtained in the evaluation of allele-specific primer mixtures (A-D) for multiplex polymerase chain reaction. 1: c.3909C>G; 2: c.2988 + 1G>A; 3: c.1624G>T; 4: c.1521_1523delCTT; 5: c.1000C>T; 6: c.3140-26A>G; 7: c.3276C>A; 8: c.2051_2052delAAinsG; 9: c.3484C>T; 10: c.254G>A; 11: c.1585-1G>A; 12: c.2657 + 5G>A; 13: c.1397C>G; 14: c.3196C>T; 15: c.1519_1521delATC; 16: c.3718-2477C>T; 17: c.1657C>T; 18: c.3846G>A.**

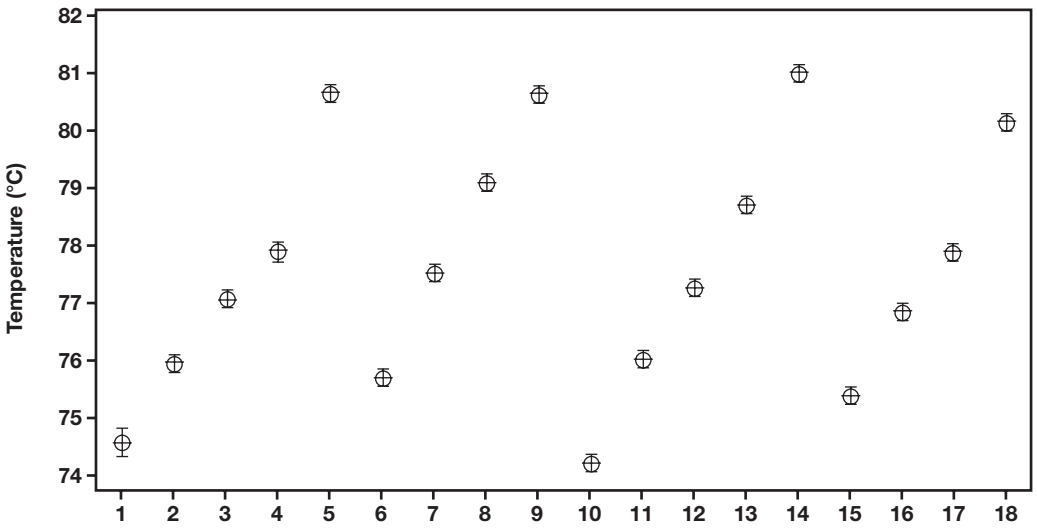

Results agreed 100% with those obtained by the reference tests and demonstrate that the AS multiplex PCR assay can detect these 18 *CFTR* variants with high specificity. Each variant was detected in only a single mixture (A, B, C or D) with no cross-reactions between them for 100% analytical specificity. The 142 samples in which no mutation was detected were shown to be noncarriers, confirming a clinical specificity of 100%. The most-detected variants were c.1521_1523delCTT, c.1000C>T, and c.1624G>T, whereas c.2988 + 1G>A, c.3276C>A, c.2051-2052delAAinsG, c.1397C>G, and c.3846G>A variants were only detected in 1 sample. In this study, the c.3196C>T variant was identified for the first time in a Cuban CF patient, which represents an advance in the diagnosis of this disease in the country. To confirm this finding in that sample, the exon 20 of the *CFTR* gene was sequenced, and the change of cytosine per thymine was detected at position c.3196 of 1 of its alleles (data not shown).

External Validation

The study of 96 DBS with AS multiplex PCR assay followed by zygosity determination yielded 71 samples with at least 1 *CFTR* variant, of which 49 had 2 variants (32 compound heterozygous and 17 homozygous) and the remaining 22 had 1 variant. **TABLE 4** presents the 120 mutated

TABLE 4. Mutated alleles found in the evaluation of samples with the allele-specific multiplex polymerase chain reaction assay followed by zygosity determination[a]

Variants (number of alleles)			
Mix A	**Mix B**	**Mix C**	**Mix D**
c.3909C>G (**2**/*4*)	c.3140-26A>G (**2**/*3*)	c.254G>A (**4**/*2*)	c.1519_1521delATC (**8**/*8*)
c.2988 + 1G>A (**1**/*2*)	c.3276C>A (**1**/*1*)	c.1585-1G>A (**3**/*2*)	c.3718-2477C>T (**2**/*2*)
c.1624G>T (**14**/*12*)	c.2051_2052delAAinsG (**1**/*1*)	c.2657 + 5G>A (**2**/*2*)	c.1657C>T (**6**/*4*)
c.1521_1523delCTT (**67**/*51*)	c.3484C>T (**6**/*7*)	c.1397C>G (**1**/*1*)	c.3846G>A (**1**/*1*)
c.1000C>T (**18**/*15*)		c.3196C>T (**2**/*2*)	

[a]*The variants of each primer mix are sorted according to the intervals of melting temperature values. The numbers of mutated alleles found in the evaluation of 230 samples in the agreement analysis are indicated in bold. The numbers of mutated alleles found in the evaluation of 96 samples in the external validation are indicated in italics.*

alleles identified. The 25 samples in which no mutation was detected were shown to be noncarriers. Results agreed 100% with those obtained by the reference tests and confirmed that the assay has analytical specificity and clinical specificity of 100%.

In the AS multiplex PCR assay, the internal control was positive in all the samples with genotypes other than c.1519_1521delATC/c.1519_1521delATC, c.1519_1521delATC/c.1521_1523delCTT, and c.1521_1523delCTT/c.1521_1523delCTT, so there was no enzyme inhibition in any case. For most of the samples (90/96), the peak height of the internal control in mixes B and C was within the acceptable interval, which indicates that the genomic DNA concentration in the evaluated samples was adequate for amplification. In cases where the peak exceeded this range, the samples were diluted 10-fold for reevaluation.

The repeatability test demonstrated that the assay is reproducible. The Tm values of all peaks were within the temperature interval determined for each variant.

Discussion

Cystic fibrosis is an autosomal recessive disease caused by mutations in both alleles of the *CFTR* gene.[19] The *CFTR* genotype correlates with several key features of CF, including sweat chloride concentration, severity of pancreatic exocrine disease, and variation in severity of lung disease.[20] Complete analysis of the *CFTR* gene is too laborious and expensive. A general rule would be that most common variants that have been observed in the national or regional populations are those that are routinely screened. A typical cut-off would be to screen for all variants having a frequency of 0.5% or higher. In most European countries, when screening for the most frequent variants (>0.5%) in a given population, a variant will be identified in 90% to 95% of the *CFTR* genes derived from CF individuals.[21] In large heterogeneous regions, such as North America, a recommendable standard is that a variant should be present in at least 0.1% of CF patient chromosomes.[21,22]

This work describes the development and validation of an AS PCR and HRMA assay for the detection of 18 disease-causing variants. It aimed at extending the molecular screening of CF in Cuba.

For inclusion of variants in the assay, we first considered the availability of carrier samples to validate the method and demonstrate that these variants can be detected with the highest possible specificity. After guaranteeing this premise, the most frequent variants in Latin America and in Cuban patients were considered: c.1521_1523delCTT, c.1624G>T, c.3909C>G, and c.3484C>T with frequencies ≥1%; and c.1000C>T, c.254G>A, c.1657C>T, c.3718-2477C>T, c.1585-1G>A, c.2988 + 1G>A, c.1519_1521delATC, c.2657 + 5G>A, c.2051_2052delAAinsG, and c.3276C>A with frequencies between 0.1% and 1%, according to data published by Pérez et al.[13] Regarding c.2657 + 5G>A, a variant described for the first time in Cuba in this work, Pérez et al[13] indicated it has an overall frequency of 0.21% in Latin America, according to reports of its presence in Argentina, Brazil, Colombia, and Uruguay.

The c.3846G>A and c.3196C>T variants account for frequencies of 1.13% and 0.14%, respectively, in Latin America,[13] and despite not having been found in any Cuban patient prior to this work, were included due to the donation of carrier samples from Brazilian CF individuals. The c.1397C>G and c.3140-26A>G variants were incorporated in the new assay because they had been previously identified in Cuban CF patients, according to data published by Barbón et al[23] and Armas et al,[14] respectively.

Because the presence of c.1397C>G and c.3196C>T variants could not be confirmed by using the reference CF StripAssay 4–410 test, specimens with homozygous or compound heterozygous genotype (other variants) were considered as noncarrier controls during the evaluation of the AS primers for the detection of both variants. "Complex alleles" are very rare; that is, those with more than 1 CF-causing variant,[24] which justifies the use of CF samples with both alleles affected as noncarrier controls for other variants.

Allele-specific real-time PCR is a simple procedure that does not require additional processing of the product formed, which minimizes the risk of contamination by amplification.[25] It is based on the inability of the Taq polymerase enzyme to add nucleotides to a primer when there is no correct pairing between the last base of the 3'-OH end of the primer and the template DNA strand to which it binds. As these bases cannot match, amplification does not occur or is significantly reduced.[26] Given this principle, 2 primers were designed for each variant: 2 AS (*wt* and *mut*) and a common primer oriented in the opposite direction to the previous ones. The last base of the 3'-OH end of each mutated AS primer was modified according to the nucleotide change described. In some primers, the penultimate base was further changed to increase specificity during amplification. The incorrect pairing between the penultimate base of the 3'-OH end of the primer and the template chain reduces the possibility of binding the last base to the chain itself, unless there is complementarity of Watson–Crick-type bases in this position.[27]

Given the proximity of some variants in the *CFTR* gene, a few primers were intended for more than 1 amplification reaction. This was the case of the *wt* AS primer for the c.1521_1523delCTT variant, which can act as a common primer for the c.1397C>G variant. Similarly, the same common primer was used for the c.1585-1G>A and c.1624G>T variants.

Regarding the simplicity of its use as well as its absorption-emission spectrum, 2X ABsolute qPCR SYBR Green Mix was selected for performing real-time PCR and HRMA. The identification of the amplified DNA fragments was based on the comparison of their melting curves by means of HRMA. This post-PCR technique allows genotyping of a large number of samples with a high level of precision.[28]

After synthesizing the primer trios for each region of interest of the *CFTR* gene, their specificity was determined by comparing *wt* and *mut* AS real time-PCRs and calculating ΔCt between both reactions. This approach constitutes the basis for quantitative PCR and has been applied in genotyping studies[29] and even for the detection of *CFTR* variants.[18,30]

Detection and zygosity determination of every *CFTR* variant were possible once the specificity of the primer trios had been verified. However, using 2 reactions to determine the presence of a single variant would make the testing of a sample a complex and expensive process. To analyze the 18 proposed variants, no less than 36 reactions would be needed, with a higher consumption of reagents and excessive handling by the analysts. In contrast, the AS multiplex PCR strategy would successfully detect several variants in the same reaction.

Given the number of variants to be included in the assay, several primer mixes for mutated AS multiplex PCR combined with HRMA were created for the detection of no more than 7 variants per mixture to prevent nonspecific amplifications due to primer dimer interference. For this, it was necessary to predetermine the average Tm value of each of the 18 amplified fragments containing the corresponding *CFTR* variants. The empirically established temperature interval of 1°C was used to examine the effect of the initial DNA concentration or background fluorescence on the denaturation temperature of the DNA fragment, as recommended by Erali et al[31] for the performance of HRMA. As the obtained Tm values were between 74°C and 81°C, the temperature range of the analysis was reduced to shorten the execution time of the test.

The presence of a single melt peak per reaction demonstrates that primer pairs do not undesirably amplify other regions of the human genome. As the melt peaks of DNA fragments with similar Tm (different base sequences) could overlap in HRMA, the sets of primers (*mut* and common) that amplify those segments were put in different mixes. In addition, other aspects were considered before adding the primer pairs to a given mixture. Taking advantage of the proximity of some variants, some of the designed primers were used to amplify more than 1 target. For example, c.1519_1521delATC and c.1521_1523delCTT are adjacent deletions, and they have in common the loss of a cytosine in the coding position 1521 of the *CFTR* gene. Additionally, the c.1397C>G variant is also found in exon 11 and its common primer is, at the same time, the *wt* AS primer for c.1521_1523delCTT. It was also considered that the c.1585-1G>A variant in the last base of intron 12 of the *CFTR* gene and c.1624G>T and c.1657C>T variants in the contiguous exon 12 are positioned very close in the *CFTR* gene. The c.1585-1G>A and c.1624G>T variants share the same common primer, as mentioned. Finally, it was considered that the c.3140-26A>G variant is located in intron 20 of the *CFTR* gene, followed by exon 20 containing c.3196C>T and c.3276C>A variants (http://www.genet.sickkids.on.ca/cftr).

The proximity of the variants is advantageous in mutation screening methods, even if this means that they cannot be properly identified.[32] In this study, their closeness complicated the design of the primer mixes and made it necessary to detect them separately to avoid the occurrence of unwanted amplification with the accumulation of nonspecific products.

According to the previous analysis, 4 primer mixes (A, B, C, and D) were formed for mutated AS multiplex PCR combined with HRMA. In every mixture each melt peak is associated with a specific *CFTR* variant.

Primer mixes A thorough D were evaluated by using both carrier and noncarrier controls. For the normalization of the mixtures, control samples with homogeneous DNA concentration values were selected, thus regulating the amplification of each variant.

In HRMA, the area under the peak is proportional to the concentration of double-stranded DNA.[33] From the results of each variant, and given that all the control samples had homogeneous DNA concentration values, an acceptable range of peak height was established between 8 and 50 fluorescence units ($8 \leq -d(Rn)/dT \leq 50$). Readjustments were made in the concentrations of the primer pairs for which the peak height was not within this interval. Afterwards, the analysis of each mixture was repeated and the correct detection of each of the variants was verified.

As some samples carried 2 detectable variants in the same mixture, 2 inflections were observed in the melt curve. When these 2 inflections had differences in their Tm values of more than 3°C, 2 peaks were observed in the derivative melt curve (for example, c.1000C>T/c.2988 + 1G>A and c.1521_1523delCTT/c.3909C>G). In contrast, for samples in which 2 consecutive inflections (contiguous variants in the mixture) were obtained in a narrow temperature range, a single peak was obtained in the derivative melt curve, with an intermediate Tm value between the intervals of the variants involved. This could be verified in the samples with genotypes c.1521_1523delCTT/c.1624G>T, c.254G>A/c.1585-1G>A, and c.1657C>T/c.3718-2477C>T. As it is easier to determine the value of Tm through a peak than from an inflection, the use of the derivative melt curve is usually more frequent in HRMA.[34] However, the results of this study suggest identifying the variant (s) in the standard melt curve first (inflections) and, once confirmed, switch to the derivative melt curve to determine their Tm value.

The correct selection of the primer pairs for the mixtures A through D enabled us to generate, in each case, a specific HRMA profile, which was able to distinguish a given DNA fragment (with a *CFTR* variant) from its denaturation temperature. However, as Erali et al[31] demonstrated, an internal amplification control was required to identify false-negative results produced by insufficient extracted DNA, inadequate collection or preservation of the sample, possible enzyme inhibition, or expiration of the reagents.

For the selection of a sequence as internal control of the test, it was considered that it should have a lower Tm value than the rest of the fragments to avoid overlapping with the peaks obtained by the presence of variants. The solution could be a short, low-GC-content DNA sequence.

About 45% of CF patients are homozygous for the c.1521_1523delCTT variant,[35] so the detection of this genotype guarantees the definitive diagnosis of a good part of them. This precedent motivated the search for a common solution for the determination of the c.1521_1523delCTT/c.1521_1523delCTT genotype and the inclusion of an internal amplification control. The *wt* AS primers designed for zygosity determination of c.1519_1521delATC and c.1521_1523delCTT variants were selected for the amplification of the internal control. The use of this pair (sense and antisense) to amplify a 58-bp region and detect the loss of cytosine at position 1521 of the *CFTR* gene at the same time would provide a solution to the problems raised. Thus, the internal amplification control would also allow determining the zygosity pattern of c.1519_1521delATC and c.1521_1523delCTT variants, which

means that when identifying c.1519_1521delATC/c.1519_1521delATC, c.1521_1523delCTT/c.1521_1523delCTT, and c.1519_1521delATC/c.1521_1523delCTT genotypes in mixes A, D, or both, there would not be amplification of internal control in mixes B and C. As the internal control primer pair identifies the *wt* sequences of these variants, it had to be excluded from mixtures A and D, in which the primer pairs for the detection of the *mut* genotypes of c.1521_1523delCTT and c.1519_1521delATC are respectively found, or the unwanted amplification of fragments would constantly occur, regardless of the presence of these variants. These homozygous genotypes are recognized by means of the internal amplification control without requiring additional detection steps, which would instead be necessary to determine the zygosity pattern for the rest of the variants.

The theoretical value of Tm for the internal control was lower than all of the variant-bearing fragments, which also supported its inclusion in mixes B and C. In mixture C, only the addition of the sense primer was required, as the corresponding antisense (*wt* primer for c.1521_1523delCTT) is the common primer for c.1397C>G variant.

The height of the peak can be used as an indicator of the DNA concentration in the evaluated sample.[36] Therefore, establishing a peak height interval for the internal control could check the effect of the DNA concentration of the sample on the final result, as suggested by Erali et al,[31] during the normalization of an HRMA-based assay. A peak height between 8 and 50 fluorescence units ($8 \leq -d(Rn)/dT \leq 50$) was empirically established as an acceptable range for the internal control. For $-d(Rn)/dT < 8$, the internal control was considered negative. On the other hand, for $-d(Rn)/dT > 50$ it was determined that it would be necessary to dilute the sample before reevaluation due to excess genomic DNA. Thus, small peaks resulting from nonspecific amplification that could be misinterpreted as variants in the sample were ruled out.

The inclusion of the internal amplification control allows defining the quality parameters of the assay, giving the analyst the reference to use to accept or reject the results. This control also guarantees that amplification occurs in at least 1 of the mixtures, even if the sample does not carry *CFTR* variants, thus allowing early detection of any failure during assay execution.

Unlike some variants that cause the disease, most are found at such low frequencies that for some researchers it is impractical to seek them in both alleles of the gene. Genetic analysis of the parents of an individual with CF clinical patterns can also confirm the presence of the same variant in both alleles of the *CFTR* gene.[37] Despite these considerations, it was decided to include the zygosity determination for the rest of the variants.

High-resolution melting analysis has been used in many studies for discrimination between heterozygotes and homozygotes through the identification of DNA sequences that differ by only 1 base due to small variations in the resulting curves.[38] However, HRMA using SYBR Green is classified as not very robust due to its low sensitivity for the detection of small changes in the nucleotide sequence. Also, not all equipment designed for HRMA has the required resolution for detecting small changes in a sequence,[39] so the design of the assay in these cases must be thorough.

During this study, it was found that the PCR-HRMA system used (SLAN-96P) does not detect variations at this level of sensitivity because it can yield different Tm values for fragments that have the same base sequence. Even for a repeatedly analyzed sample, different Tm values are obtained. This disadvantage was also considered for the inclusion of internal controls, a possible alternative for HRMA systems with lower resolution according to Herrmann et al.[39] Therefore, it was convenient to determine the zygosity pattern of the variants by identifying amplified DNA fragments from a predetermined Tm interval, a similar strategy to that followed in this study for the detection of *CFTR* variants.

The sequences of the mutated and *wt* fragments corresponding to a given region only differ by 1 or 2 bases; therefore, their Tm values should be almost identical. The same predetermined temperature range (in mixes A through D) was assumed for each amplified DNA fragment in the *wt* AS reactions. It was considered that in *wt* mixtures, the amplification and detection of a specific fragment would correspond to the presence of at least 1 *wt* allele of the variant under analysis. On the contrary, the absence of amplified product in a determined *wt* mixture would be equivalent to the presence of the homozygous genotype for a mutation in the analyzed sample. However, the lack of amplified product due to other causes (enzyme inhibition, procedural failures) could be interpreted in the same way, so it was decided to also include an internal amplification control in all primer mixes for *wt* AS PCR. To amplify an internal control in these mixtures, 2 *wt* AS primers (sense and antisense) different from those used in mixtures B and C were selected. These primers also generate a 58-bp fragment that, due to its length and base composition, has a lower Tm than the rest of the AS fragments. The evaluation of these mixtures was carried out with the use, in each case, of samples with the corresponding variants.

Normalization of *wt* mixtures was performed by using classified samples. Although our work was limited because of the unavailability of samples for most of the homozygous genotypes, this did not hinder the study. As already demonstrated from comparisons relative to Ct, the *wt* AS primers recognize the sequences without genetic changes; therefore, in the presence of the corresponding variant in both alleles of the *CFTR* gene, their possibilities of generating amplified product are minimal,[40] thereby yielding amplicons undetectable by HRMA.

The CF StripAssay 4–410 reference panel identifies *wt* genotypes in the same reactions as mutated ones. Sequences of 1 type or another are detected by inverse hybridization with specific complementary probes, fixed in different parallel bands on a strip. The absence of *wt* product in a given band indicates homozygosity of the corresponding mutated allele. Other available assays for the characterization of the *CFTR* gene such as INNO-LiPA CFTR 19 follow the same strategy.[41]

Two batches of the test were produced after establishing the working conditions of the primer mixes for the detection of 18 *CFTR* variants and for their zygosity determination. The assay was validated by evaluating analytical parameters (clinical and analytical specificity) in accordance with Food and Drug Administration guidance.[42]

As in a study published by Pugliese et al,[43] an interval graph was used for the comparison of the Tm intervals of each mixture. It was found that the closest Tm intervals correspond to variants c.1521_1523delCTT and c.1624G>T in mixture A, and c.3718-2477C>T and c.1657C>T in mixture D. The evaluation of samples with these combinations allowed to verify that those variants can be differentiated, although for these cases a single melt peak is obtained only.

The repeatability study validated the initially established Tm range of 1°C for the detection of variants in mixes A through D, with the exception of the c.1624G>T and c.1521_1523delCTT variants. Although the confidence intervals of these 2 variants did not overlap, the separation

between their average values was only 0.83°C, so it was decided to reduce the Tm interval for them. Thus, to identify the c.1624G>T variant, a Tm value up to 77.5°C is considered, whereas higher values correspond to c.1521_1523delCTT. However, if Tm values are obtained within ±0.1°C from this value (in samples that do not carry both variants), it is recommended to analyze whether the peak height of the internal control is on range and, consequently, to perform a new extraction of DNA from the sample.

In the agreement analysis, 230 samples were analyzed by the developed assay and by the reference methods, CF StripAssay 4–410 and automated DNA sequencing, the latter for some specific cases. More than 150 of these samples had an unknown genotype (blind evaluation). The validation analysis yielded a 100% agreement of the test with the reference methods. Similar results were obtained by Van der Stoep and collaborators[44] when comparing an HRMA-based method for the detection of variants in the *BRCA1* (breast cancer 1) gene with DNA sequencing, both with 100% specificity. The *CFTR* variant c.3196C>T was detected for the first time in the Cuban population, specifically in a patient who had an incomplete CF genotype until then. This finding was confirmed by sequencing exon 20 of the *CFTR* gene in CNGM. Other variants such as c.1585-1G>A and c.2657 + 5G>A, identified during the characterization of samples at the beginning of this work, were also found in other Cuban CF patients. Analytical sensitivity and clinical sensitivity of 100% were obtained, parameters that are decisive in the standardization of tests for the determination of genotypes as described by Norambuena et al[45] during the evaluation of a similar HRMA-based method.

The assay was externally validated by the Molecular Biology Department of the CNGM. The study of 96 DBS confirmed the analytical parameters obtained in the first performance evaluation of the test, providing further evidence of the reliability of the assay's results.

In Cuba, current diagnosis of CF is led by the CF National Commission based in the clinical characteristics of the disease and a positive sweat test (≥60 mmol/L).[16] Since January 2019, a CF newborn screening program based on an immunoreactive trypsin (IRT)/IRT/DNA algorithm was extended throughout the country.[46] The detection of *CFTR* variants is carried out by the CNGM by using denaturing gradient gel electrophoresis and single stranded conformation polymorphism, time-consuming and laborious techniques, so the introduction of this new test would be very advantageous in saving time and reagents. In addition, the use of an expanded mutation panel (CF StripAssay 4–410) for the study of 129 Cuban CF individuals detected 65.9% of mutated alleles,[14] in contrast to the 55.5% sensitivity for 153 Cuban CF patients of the CNGM panel.[16] Therefore, the method presented in this work for the detection of 18 CF-causing *CFTR* variants will be more suitable for the demographic characteristics of our country's population. It will also enable the evaluation of a greater number of cases and the study of healthy carriers to reduce the risk of CF in their offspring.

This assay can complement CF newborn screening not only in Cuba but also in Latin America. As it was validated with DBS, it benefits from the advantages of this sample support, widely used for the collection of samples in newborn screening of inherited metabolic diseases.

A limitation of this study is that only 1 thermal cycler (SLAN 96P) was used to evaluate the samples and perform the assay validation. This will be corrected in the future by carrying out a validation process with equipment from other commercial vendors for providing greater robustness to the molecular assay. Another limitation is that there were insufficient samples for some of the *CFTR* variants evaluated, such as c.2051_2052delAAinsG, c.1397C>G, c.3846G>A, and c.3276C>A, for which only 1 sample was available, because they have a frequency of <1% in Cuba.

Conclusions

In summary, the proposed assay is a novel, effective, rapid, and affordable method for the detection of 18 CF-causing *CFTR* variants based on AS PCR and HRMA. It significantly expands the spectrum of *CFTR* variants to be detected in Cuban patients with suspected CF and is also suitable for Latin America, a large region with a heterogeneous ethnic makeup.

Conflict of Interest Disclosure

The authors have nothing to disclose.

REFERENCES

1. Lopes-Pacheco M. CFTR modulators: the changing face of cystic fibrosis in the era of precision medicine. *Front Pharmacol.* 2019;10(1662). https://dx.doi.org/10.3389/fphar.2019.01662
2. Mirtajani SB, Farnia P, Hassanzad M, Ghanavi J, Farnia P, Velayati AA. Geographical distribution of cystic fibrosis; the past 70 years of data analysis. *Biomed Biotechnol Res J.* 2017;1(2):105-112. https://doi.org/10.4103/bbrj.bbrj_81_17
3. Cutting GR. Cystic fibrosis genetics: from molecular understanding to clinical application. *Nat Rev Genet.* 2015;16(1):45-56. https://doi.org/10.1038/nrg3849
4. Girón R, Salcedo A, Casanova A. Antecedentes históricos y epidemiología. In: Girón R, Salcedo A, eds. *Fibrosis Quística*. Vol. VIII. Madrid: Ergón; 2005:9-20.
5. Kerem BS, Rommens JM, Buchanan JA, et al. Identification of the cystic fibrosis gene: genetic analysis. *Science.* 1989;245(4922):1073-1080. https://doi.org/10.1126/science.2570460
6. Ratjen F, Bell SC, Rowe SM, Goss CH, Quittner AL, Bush A. Cystic fibrosis. *Nat Rev Dis Primers.* 2015;1:15010. https://doi.org/10.1038/nrdp.2015.10
7. DeBoeck K, Vermeulen F, Dupontet L. The diagnosis of cystic fibrosis. *Presse Med.* 2017;46:97-108. https://doi.org/10.1016/j.lpm.2017.04.010
8. Farrell PM, White TB, Ren CL, et al. Diagnosis of cystic fibrosis: consensus guidelines from the Cystic Fibrosis Foundation. *J Pediatr.* 2017;181S:S4-S15.e1. https://doi.org/10.1016/j.jpeds.2016.09.064
9. Brennan ML, Schrijver I. Cystic fibrosis: a review of associated phenotypes, use of molecular diagnostic approaches, genetic characteristics, progress, and dilemmas. *J Mol Diagn.* 2016;18(1):3-14. https://doi.org/10.1016/j.jmoldx.2015.06.010
10. Lucarelli M, Porcaro L, Biffignandi A, et al. A new targeted CFTR mutation panel based on next-generation sequencing technology. *J Mol Diagn.* 2017;19(5):788-800. https://doi.org/10.1016/j.jmoldx.2017.06.002
11. Collazo T, López I, Santos EN, et al. Estudio molecular de fibrosis quística en Cuba. *An Acad Cienc Cuba.* 2015;5(3):13-18.
12. González JA, Abreu G, Rodríguez F. Reseña histórica de la fibrosis quística y su estudio y tratamiento en Cuba. *Rev Cubana Pediatr.* 2014;86(4):535-540.
13. Pérez MM, Luna MC, Pivetta OH, Keyeux G. CFTR gene analysis in Latin American CF patients: heterogeneous origin and distribution of mutations across the continent. *J Cyst Fibros.* 2007;6:194-208. https://doi.org/10.1016/j.jcf.2006.07.004

14. Armas A, Figueredo JE, González YJ, et al. Perfil de las mutaciones del gen CFTR en una cohorte de pacientes cubanos con fibrosis quística. *Genética Médica y Genómica.* 2019;3(3):67-73.
15. Men AE, Wilson P, Siemering K, Forrest S. Sanger DNA sequencing. In: Janitz M, ed. *Next-Generation Genome Sequencing: Towards Personalized Medicine*. Weinheim: Wiley-VCH Verlag; 2008:1-11. https://doi.org/10.1002/9783527625130.ch1
16. Collazo T, Bofill AM, Clark Y, et al. Common mutations in Cuban cystic fibrosis patients. *J Cyst Fibros.* 2009;8(1):47-49. https://doi.org/10.1016/j.jcf.2008.09.004
17. Kain KC, Lanar DE. Determination of genetic variation within *Plasmodium falciparum* by using enzymatically amplified DNA from filter paper disks impregnated with whole blood. *J Clin Microbiol.* 1991;29(6):1171-1174. https://doi.org/10.1128/jcm.29.6.1171-1174.1991
18. Figueredo-Lago JE, Armas-Cayarga A, González-González YJ, et al. Development of a method to detect three frequent mutations in the CFTR gene using allele-specific real time PCR. *Biotec Apl.* 2015;32:4301-4306.
19. De Boeck K, Amaral MD. Progress in therapies for cystic fibrosis. *Lancet Respir Med.* 2016;4(8):662-674. https://doi.org/10.1016/S2213-2600(16)00023-0
20. Collaco JM, Cutting GR. Cystic fibrosis. In: Pyeritz RE, Korf BR, Grody WW, eds. *Emery and Rimoin's Principles and Practice of Medical Genetics and Genomics (Seventh Edition). Cardiovascular, Respiratory, and Gastrointestinal Disorders*. Cambridge: Academic Press; 2020:285-339. https://doi.org/10.1016/B978-0-12-812532-8.00012-4
21. WHO Human Genetics Programme. *The Molecular Genetic Epidemiology of Cystic Fibrosis: Report of a Joint Meeting of WHO/ECFTN/ICF(M)A/ECFS*. Genoa, Italy, 19 June 2002, World Health Organization; 2004. https://apps.who.int/iris/handle/10665/68702
22. Watson MS, Cutting GR, Desnick RJ, et al. Cystic fibrosis population carrier screening: 2004 revision of American College of Medical Genetics mutation panel. *Genet Med.* 2004;6(5):387-391. https://doi.org/10.1097/01.gim.0000139506.11694.7c
23. Barbón Sánchez C, Santos González EN, Collazo Mesa T, López Reyes I, Reyes Navarro L. Cribaje de mutaciones y polimorfismos en el gen CFTR en pacientes cubanos con Fibrosis Quística. Congreso Genética Comunitaria 2017. Accessed January 26, 2022. http://geneticacomunitaria2017.sld.cu/index.php/gencom/2017/paper/view/373
24. Bergougnoux A, Boureau-Wirth A, Rouzier C, et al. A false positive newborn screening result due to a complex allele carrying two frequent CF-causing variants. *J Cyst Fibros.* 2016;15(3):309-312. https://doi.org/10.1016/j.jcf.2016.04.003
25. Navarro E, Serrano-Heras G, Castaño MJ, Solera J. Real-time PCR detection chemistry. *Clin Chim Acta.* 2015;439:231-250. https://doi.org/10.1016/j.cca.2014.10.017
26. Nasis O, Thompson S, Hong T, et al. Improvement in sensitivity of allele-specific PCR facilitates reliable noninvasive prenatal detection of cystic fibrosis. *Clin Chem.* 2004;50(4):694-701. https://doi.org/10.1373/clinchem.2003.025981
27. Kwok S, Kellogg DE, McKinney N, et al. Effects of primer-template mismatches on the polymerase chain reaction: human immunodeficiency virus type 1 model studies. *Nucleic Acids Res.* 1990;18(4):999-1005. https://doi.org/10.1093/nar/18.4.999
28. Montgomery JL, Sanford LN, Wittwer CT. High-resolution DNA melting analysis in clinical research and diagnostics. *Expert Rev Mol Diagn.* 2010;10(2):219-240. https://doi.org/10.1586/erm.09.84
29. Zhang L, Zhao J, Cui G, Wang H, Wang DW. Genotyping on ALDH2: comparison of four different technologies. *PLoS One.* 2015;10(3):e0122745. https://doi.org/10.1371/journal.pone.0122745
30. Soloviov OO, Pampukha VM, Livshits LA. Development of ARMS PCR tests for detection of common CFTR gene mutations. *Biopolym Cell.* 2010;26(5):378-383. https://doi.org/10.7124/bc.00016c
31. Erali M, Voelkerding KV, Wittwer CT. High resolution melting applications for clinical laboratory medicine. *Exp Mol Pathol.* 2008;85(1):50-58. https://doi.org/10.1016/j.yexmp.2008.03.012
32. Kakavas KV, Plageras P, Vlachos TA, Papaioannou A, Noulas AV. PCR–SSCP: a method for the molecular analysis of genetic diseases. *Mol Biotechnol.* 2008;38(2):155-163. https://doi.org/10.1007/s12033-007-9006-7
33. Bruzzone CM, Steer CJ. High-resolution melting analysis of single nucleotide polymorphisms. *Methods Mol Biol.* 2015;1310:5-27. https://doi.org/10.1007/978-1-4939-2690-9_2
34. Ruskova L, Raclavsky V. The potential of high resolution melting analysis (HRMA) to streamline, facilitate and enrich routine diagnostics in medical microbiology. *Biomed Pap Med Fac Univ Palacky Olomouc Czech Repub.* 2011;155(3):239-252. https://doi.org/10.5507/bp.2011.045
35. Wainwright CE, Elborn JS, Ramsey BW, et al., TRAFFIC Study Group. Lumacaftor–ivacaftor in patients with cystic fibrosis homozygous for Phe508del CFTR. *N Engl J Med.* 2015;373(3):220-231. https://doi.org/10.1056/NEJMoa1409547
36. Minucci A, De Paolis E, Concolino P, et al. Competitive PCR-high resolution melting analysis (C-PCR-HRMA) for large genomic rearrangements (LGRs) detection: a new approach to assess quantitative status of BRCA1 gene in a reference laboratory. *Clin Chim Acta.* 2017;470:83-92. https://doi.org/10.1016/j.cca.2017.04.026
37. Dequeker E, Stuhrmann M, Morris MA, et al. Best practice guidelines for molecular genetic diagnosis of cystic fibrosis and CFTR-related disorders-updated European recommendations. *Eur J Hum Genet.* 2009;17:51-65. https://doi.org/10.1038/ejhg.2008.136
38. Audrezet MP, Dabricot A, Le Marechal C, Ferec C. Validation of high-resolution DNA melting analysis for mutation scanning of the cystic fibrosis transmembrane conductance regulator (CFTR) gene. *J Mol Diagn.* 2008;10(5):424-434. https://doi.org/10.2353/jmoldx.2008.080056
39. Herrmann MG, Durtschi JD, Wittwer CT, Voelkerding KV. Expanded instrument comparison of amplicon DNA melting analysis for mutation scanning and genotyping. *Clin Chem.* 2007;53(8):1544-1548. https://doi.org/10.1373/clinchem.2007.088120
40. Lo YM. The amplification refractory mutation system. *Methods Mol Med.* 1998;16:61-69. https://doi.org/10.1385/0-89603-499-2:61
41. Lentini ER, Navarta LM, López Millán A. Diagnóstico genético de la fibrosis quística: una experiencia provincial de 10 años, Mendoza, Argentina. *Rev Asoc Méd Argent.* 2017;130(2):4-8.
42. Food and Drug Administration. CFTR Gene Mutation Detection Systems - Class II Special Controls Guidance for Industry and FDA Staff. Accessed January 31, 2022. https://www.fda.gov/medical-devices/guidance-documents-medical-devices-and-radiation-emitting-products/cftr-gene-mutation-detection-systems-class-ii-special-controls-guidance-industry-and-fda-staff
43. Pugliese L, Casabianca S, Perini F, Andreoni F, Penna A. A high resolution melting method for the molecular identification of the potentially toxic diatom Pseudo-nitzschia spp. in the Mediterranean Sea. *Sci Rep.* 2017;7(1):42-59. https://doi.org/10.1038/s41598-017-04245-z
44. Van der Stoep N, Van Paridon CDM, Janssens T, et al. Diagnostic guidelines for high-resolution melting curve (HRM) analysis: an interlaboratory validation of BRCA1 mutation scanning using the 96-well LightScanner. *Hum Mutat.* 2009;30(6):899-909. https://doi.org/10.1002/humu.21004
45. Norambuena PA, Copeland JA, Krenkova P, Stambergova A, Macek M. Diagnostic method validation: high resolution melting (HRM) of small amplicons genotyping for the most common variants in the MTHFR gene. *Clin Biochem.* 2009;42(12):1308-1316. https://doi.org/10.1016/j.clinbiochem.2009.04.015
46. Castells EM, Sánchez A, Frómeta A, et al. Pilot study for cystic fibrosis neonatal screening: the Cuban experience. *Clin Chem Lab Med.* 2020;58(11):1857-1864. https://doi.org/10.1515/cclm-2020-0037

Blood usage and wastage at an academic teaching hospital before the initial wave of COVID-19 and during and after its quarantine periods

Amber Nguyen, MSCLS, (ASCP)CM, Sarah Burnett-Greenup, MS, MLS(ASCP)CMSBBCM, Diana Riddle, MS, MLS(ASCP)CMSBBCM, Janet Enderle, PhD, MLS(ASCP)CM, Carol Carman, PhD, Rajkumar Rajendran, DCLS, MLS(ASCP)CM

Department of Clinical Laboratory Sciences, University of Texas Medical Branch, Galveston, TX. Corresponding author: rarajend@utmb.edu

Key words: blood banking/transfusion medicine, blood product usage, blood product wastage, quarantine, COVID-19, cost savings

Abbreviations: CRYO, cryoprecipitate; ESPs, elective surgical procedures; NBCUS, National Blood Collection & Utilization Survey; IRB, institutional review board; MTP, massive transfusion protocol

Laboratory Medicine 2024;55:198-203; https://doi.org/10.1093/labmed/lmad059

ABSTRACT

Background: Transfusion services aim to maintain sufficient blood inventory to support patients, even with challenges introduced by COVID-19.

Objectives: To review blood usage and wastage before, during, and after COVID-19 surges, and to evaluate effects on inventory.

Methods: In a retrospective review, we evaluated the association between time periods corresponding to the initial wave of COVID-19 (pre–COVID-19, quarantine, and postquarantine) and blood usage/wastage. Data were stratified by period, and χ^2 testing was used to examine the association between these time periods and blood usage/wastage.

Results: In the period before COVID-19, the transfusion service used more units, and in the period after quarantine, more units went to waste. Across all time periods, the most-used product was RBCs, and the most wasted product was plasma. A statistically significant association existed between usage (χ^2 [6/3209 (0.2%)]) = 24.534; $P \leq .001$; Cramer V = 0.62), wastage (χ^2 [6/775 (0.8%)]) = 21.673; $P = .001$; Cramer V = 0.118), and time period. The postquarantine period displayed the highest wastage costs ($51,032.35), compared with the pre–COVID-19 period ($29,734.45).

Conclusion: Changes in blood inventory use and waste are significantly associated with the onset and continuation of COVID-19.

Blood products have direct therapeutic and life-saving effects.[1] More than 85 million units of blood are transfused annually worldwide, in treatment of conditions including cancer, blood disorders, and blood loss due to major operations or trauma.[2,3] Commonly transfused blood components include packed red blood cells (RBCs), plasma, platelets (PLTs), and cryoprecipitate (CRYO), each with their own separate handling and storage protocols.[4,5] To retain sufficient inventory, ensure proper stewardship, minimize costs, and guarantee traceability, transfusion services must manage and track the utilization and wastage of these products.

Waste is an important consideration for transfusion services. Wastage in the health care system in the United States accrues costs as high as $910 billion per year, with blood products accounting for approximately 1% of total hospital expenditures.[6,7] In addition to the financial burden, wastage jeopardizes blood availability for all patients. Common reasons for wastage include broken bags and seals, expired units, clotted blood, and/or products returned late to storage.[1]

Emergency preparedness relies on hospitals having the necessary tools, supply, and procedures to meet patient needs.[8] Maintaining sufficient blood inventory requires adjustments by transfusion services as the supply changes. Reasons for fluctuations in blood availability include seasonality of supply, natural disasters, emergency situations, and pandemics.[9-11] Modern transfusion services have experienced pandemics in the past but none as influential as COVID-19. One drastic impact of the COVID-19 pandemic has been a severe reduction in the blood supply due to donor center constraints, including staffing, donor availability, and donation site availability.[10,12] These circumstances, as previously observed in other outbreaks, such as SARS in 2003 and Ebola in 2014, cause a unique set of problems for transfusion services working to maintain blood product inventory.[13]

The unique scenarios brought on by COVID-19 require transfusion services to reevaluate inventory management strategies. To begin this

evaluation, transfusion services must review how COVID-19 has affected blood inventory, utilization, and wastage. At our academic medical center, the University of Texas Medical Branch in Galveston, we performed a review of blood product usage and wastage data from 2017 through 2019. The results showed similar blood product usage patterns for those years but increased wastage in 2019, which prompted the need for this pilot study.

The purpose of this study was to quantify and categorize the usage and wastage of blood products at our academic medical center during the pre–COVID-19 period and the time periods during quarantine and after quarantine (referencing the quarantine from the initial wave of SARS-CoV-2). By doing so, we aimed to determine whether there was a significant association between usage or wastage and time period. We also quantified the dollar amount of wastage, to determine differences among time periods and to identify cost-savings opportunities.

Methods

We performed a retrospective review of blood utilization and wastage records from the multiple transfusion service locations of our academic medical center. Data collected included blood-product type, quantity in units, date of use or waste, and reasons for waste (if applicable). Data were stratified into the following time periods: pre–COVID-19, during quarantine, and postquarantine. Pre–COVID-19 was defined as March 17–April 21, 2019; during quarantine was defined as March 17–April 21, 2020; and postquarantine was defined as March 17–April 21, 2021. All of these time periods corresponded to the initial wave of COVID-19 (at the time known only as SARS-CoV-2). The dates of the quarantine period correspond to the pausing of elective surgical procedures (ESPs) due to an executive stay-at-home order by the State of Texas, Galveston County. ESPs were cancelled on March 17, 2020, and resumed on April 22, 2020. Similar periods in the preceding and following year were selected for the pre–COVID-19 and postquarantine time frames, to account for any potential seasonal variation.

A total of 3984 blood units were included in this study. We used χ^2 testing to examine the association between blood-product usage or wastage and the different time periods related to COVID-19 (ie, pre–COVID-19, during quarantine, and postquarantine). Data analysis was conducted using SPSS software, version 28.0.1.1 (IBM). $P < .05$ was considered statistically significant.

We also calculated the dollar amount of wastage for each time period. We retrieved acquisition costs for each blood product from the 2019 National Blood Collection & Utilization Survey (NBCUS).[14] To calculate potential cost-savings opportunities, we multiplied the number of blood products wasted by the cost of each product, for each study period. The institutional review board (IRB) approved this project as a quality assessment/quality improvement project that did not require IRB approval or oversight because this study did not use any patient data and did not pose any harm or threat to any human subjects.

Results

Blood Product Usage

The different blood products included in this study were RBCs, plasma, PLTs, and CRYO. Across all time periods, 3209 blood products were used, with RBCs being the most used product, followed by plasma. During the pre–COVID-19 period, PLTs were the least utilized product. However, during the quarantine and postquarantine periods, CRYO was the least-utilized product. In **TABLE 1**, we show the breakdown of products and the number of products utilized for each period. A Pearson χ^2 test was performed, which revealed a significant association between blood product usage and COVID-19 time periods: χ^2 (6/3209 [0.2%]) = 24.534; $P \leq .001$; Cramer V = 0.62.

Blood Product Wastage

Across all time periods, 775 units were wasted, with the most-wasted product being plasma, followed by PLTs, RBCs, and CRYO. In **TABLE 2**, we show the breakdown of products and number of products wasted for each period. Pearson χ^2 testing was performed, which revealed a significant association between product wastage and COVID-19 time periods: χ^2 (6/775 [0.8%]) = 21.673; $P = .001$; Cramer V = 0.118. Product wastage was defined as expired, having a hole in

TABLE 1. Usage of Blood Products

Blood Product	Pre–COVID-19, No. of Units	During Quarantine, No. of Units	Postquarantine, No. of Units	Total
Red blood cells	944	536	771	2251
Plasma	130	111	171	412
Platelets	92	74	116	282
Cryoprecipitate	115	56	93	264
Total	1281	777	1151	3209

TABLE 2. Wastage of Blood Products

Blood Product	Pre–COVID-19, No. of Units	During Quarantine, No. of Units	Postquarantine, No. of Units	Total
Red blood cells	10	28	21	59
Plasma	172	156	170	498
Platelets	43	75	78	196
Cryoprecipitate	3	7	12	22
Total	228	266	281	775

the bag containing the product, returned warm/not used, clotted, or other reasons of low occurrence such as a recall notification, returned in cooler incorrectly packed/late, entered into the laboratory log and not used, or laboratory accident.

Across all time periods, the most common reason for wastage was product expiration, with 202 units expiring in the pre–COVID-19 period (88.6%), 250 units expiring during quarantine (94.0%), and 262 units expiring in the postquarantine period (93.2%). We listed reasons for blood product wastage for the 3 studied COVID-19 periods in **TABLE 3**. A detailed description of the number of products wasted, with reason for wastage for each period, is shown in **FIGURE 1**.

Cost Analysis

We performed a cost analysis of wastage to demonstrate where possible savings could have occurred. The highest waste in dollars occurred in the postquarantine period ($51,032.35), followed by the quarantine period ($48,966.95). The lowest waste in dollars was found in the pre–COVID-19 period ($29,734.45). An itemization of the cost of each wasted product is listed in **TABLE 4**. The most expensive product wasted was apheresis PLTs, costing $473.65 per unit, followed by pooled CRYO, costing $295 per unit. RBCs cost $194.65 per unit, and plasma was the least expensive product at $38 per unit.[14]

Discussion

Our study results showed a statistically significant association between blood product usage and COVID-19 time periods ($P \leq .001$). The pre–COVID-19 period had the most transfusions (1281 units), followed by the postquarantine period (1151 units), and the quarantine period had the fewest transfusions (777 units). Others have also observed decreased transfusions during the same period.[15-17] Our observed drop in utilization may potentially be attributed to the statewide stay-at-home order enacted in Texas in early to the middle of March 2020 that resulted in cancellation of ESPs. To confirm this hypothesis, our study identified the number of surgical procedures performed in the pre–COVID-19 period (1448 cases), during quarantine (585 cases), and the postquarantine period (1376 cases); its results revealed that the number of procedures was severely affected by the lockdown mandate.

Cancellation of ESPs may be expected to reduce utilization because large surges in RBC transfusion have been attributed to surgical bleeding, and trends in RBC utilization have been associated with surgical volume.[18,19] The results of a study of 72 institutions found that after the Centers for Medicare & Medicaid Services alert to discontinue ESPs, RBC and platelet utilization declined significantly, with the lowest use occurring in April 2020.[20] Even without a mandate, COVID-19 surges may result in fewer ESPs being performed because

TABLE 3. Reasons for Blood Product Wastage[a]

Reason	Pre–COVID-19, No. (%) of Units	During Quarantine, No. (%) of Units	Postquarantine, No. (%) of Units
Expired	202 (88.6)	250 (94)	262 (93.2)
Hole in bag	15 (6.6)	5 (1.9)	6 (2.1)
Returned warm/not used	5 (2.2)	7 (2.6)	7 (2.5)
Clotted	3 (1.3)	0 (0)	4 (1.4)
Other[b]	3 (1.3)	4 (1.5)	2 (0.7)

[a]*Percentages may not total 100 because of rounding.*
[b]*Includes reasons that rarely occurred (ie, recall notification, returned to cooler incorrectly, packed late, entered into medical log and not used, or laboratory accident).*

FIGURE 1. Wastage by blood product and reason. Blood product wastage for pre–COVID-19, during quarantine, and postquarantine periods. Categorized by blood product and wastage reason. CRYO, cryoprecipitate; PLTs, platelets; RBCs, red blood cells.

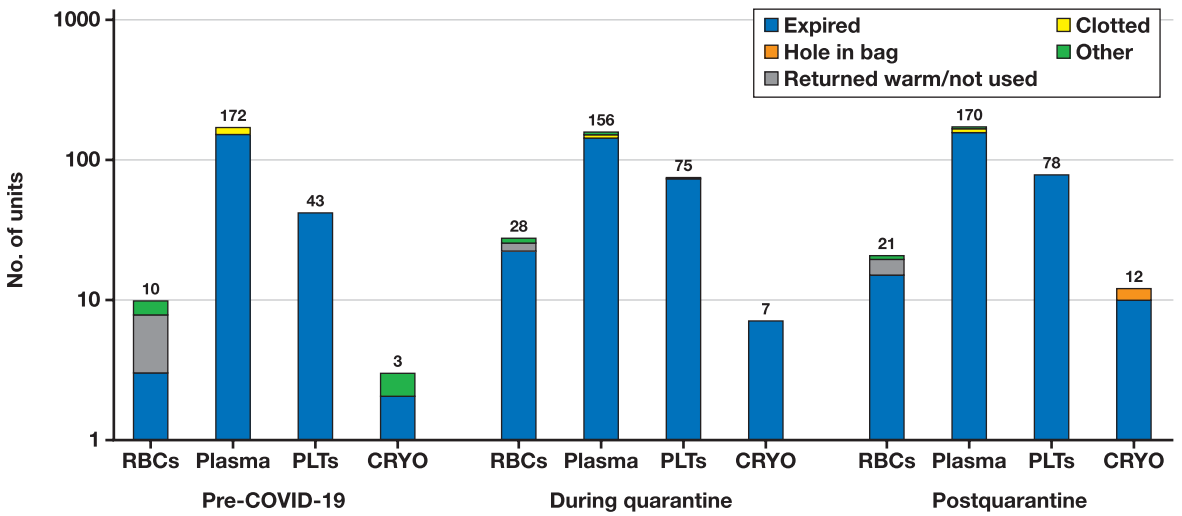

TABLE 4. Cost Analysis of Blood Product Wastage[13]

Blood Product	UTMB Cost Estimate	Pre–COVID-19		During Quarantine		Postquarantine	
		No. of Units	Cost	No. of Units	Cost	No. of Units	Cost
Red blood cells	$194.65	10	$1946.50	28	$5450.20	21	$4087.65
Plasma	$38.00	172	$6536.00	156	$5928.00	170	$6460.00
Pooled cryoprecipitate	$295.00	3	$885.00	7	$2065.00	12	$3540.00
Apheresis platelets	$473.65	43	$20,366.95	75	$35,523.75	78	$36,944.70
Total			$29,734.45		$48,966.95		$51,032.35

UTMB, University of Texas Medical Branch.

procedures may be cancelled due to lack of bed availability, COVID-19 caseloads, and reduced blood availability.[10] Reduced quarantine utilization may also be due to the reduced transfusion needs of most patients with COVID-19, compared with other hospitalized patients.[21] The severity of COVID-19 illness also affects utilization, with mild or moderate cases requiring less blood than severe cases, indicating that the percentage of severe cases may be important in determining inventory needs.[22]

We found that the most-used blood product across all periods was RBCs, followed by plasma, which matches previously reported patterns.[23] CRYO was the least-utilized product, and its utilization was not different when comparing all 3 time periods. However, unlike in other study reports, we found that PLTs were the least-utilized component during the pre–COVID-19 period.[1,19] It is not immediately clear why CRYO and PLT utilization were reversed in this period. Possibly, this was due to high outlying CRYO utilization in a single case or a limited number of cases. This reversal also surprised us in that it occurred in the pre–COVID-19 period, as opposed to the quarantine period. Although the rates of RBC, plasma, and PLT transfusion are lower in patients with COVID-19, compared with other hospitalized patients, the rate of CRYO transfusion is similar.[21]

We found a statistically significant association between product wastage and COVID-19 time periods ($P = .001$), with the highest amount of waste occurring in the postquarantine period and the next-highest in the quarantine period. The least waste was accumulated in the pre–COVID-19 period. We were not surprised that more waste accumulated in the quarantine period, compared with the pre–COVID-19 period. Previous inventory par levels and blood supply orders likely did not anticipate the cancellation of ESPs and associated decrease in demand. Other study reports, including Kracalik et al,[20] also spoke of an increase in RBC and platelet discards after cancellation of ESPs. This finding was unexpected because the number of surgical cases was similar between the pre–COVID-19 and postquarantine periods.

Rajbhandary et al[10] found a greater number of hospitals reporting component waste in May 2020 (54%), compared with March 2020 (25%). However, that number declined to 4.5% by the end of June 2020 and remained low throughout the rest of the year. Other study reports, such as one by Lu et al,[24] also show that waste was trending to baseline after the initial COVID-19 surge. Our study results include the unique finding of persistently higher waste 1 year after the initial COVID-19 surge. Because others have not reported the same trend to date, to our knowledge, this change may or may not be related to the pandemic.

In our study, plasma was the most-wasted product across all time periods. However, other studies have found RBCs or PLTs to be the most-wasted products.[25] Our differing result may be due to the practice of our transfusion service of always maintaining prethawed plasma available in preparation for any massive transfusion protocol (MTP) activation, in accordance with the recommendation of the American College of Surgeons.[26] Once thawed, these plasma units expire within 5 days and must be discarded if not used.[27,28] MTP activations are resource-intensive and often have high rates of waste.[29,30] During the pandemic, some institutions adopted changes to their MTP, such as altered ratios, to address supply-related and wastage concerns.[31]

PLTs were the next-most-wasted product in our study findings, followed by RBCs. PLT waste may have been lower than plasma in part due to the practice of our institution of utilizing pan-genera detection testing to extend PLT expirations from 5 days to 6 or 7 days. Results from a previous single-center study[32] demonstrated a 58% reduction in platelet waste after implementation of this strategy.

Transfusion services have the difficult responsibility of balancing optimal blood inventory while maintaining minimal waste.[33] For all 3 studied time periods, we found that the most common discard reason by far was product being out of date, as also found by other researchers.[34,35] Our most-wasted product, plasma, has an expiration date of 5 days once thawed; this situation may have contributed to our high number of outdated products because thawed plasma was required at all times for any potential MTP activation.[27-29] Although they made up a much smaller percentage of waste, the next-most-common reasons for discard included holes in bags containing components and components not used/returned warm. Units discarded due to holes in the bag were exclusively frozen plasma components. Due to the freezing process used to prepare these products, the bags are susceptible to breakage.[36]

A cost analysis of waste was performed, revealing increasing wastage costs each year. Waste in dollars was highest in the postquarantine period ($51,032.35), followed by the quarantine period ($48,966.95), then the pre–COVID-19 period ($29,734.45). The pattern of waste in our study does not appear to be solely related to pandemic cancellation of ESPs. We suspect that a significant portion of plasma waste in our study was due to use of prethawed plasma for MTP readiness. One potential solution is the use of liquid plasma, which has a longer expiration date of 26 days.

To address broken bags, appropriate and timely communication to suppliers allows blood centers to make changes to manufacturing or shipping practices that may reduce this occurrence.[36] Extending platelet outdates to 6 or 7 days may have an effect on platelet waste during the study period, but appropriate interventions regarding platelet policy should be explored because all platelet wastage we uncovered was due to product expiration.

Other institutions have explored cold storage platelets, which have a longer 14-day outdate, to help address waste and availability issues associated with the short shelf life of room temperature platelets.[37] Although they constitute a small portion of our overall waste, effective interventions, for units returned warm or improperly stored after being issued, include educational measures targeted to clinicians and improved transportation options.[38]

Lastly, as part of emergency preparedness, optimal staffing levels at transfusion services and blood centers is a critical component to understanding the effect on blood utilization and wastage. During any pandemic, the demand on the workforce and the blood supply are almost doubled.[12] In our institution, it was hypothesized that staffing levels in the transfusion services and blood center fluctuated, especially during 2019, and this may have an influence on our blood utilization and wastage.

There were some limitations to our study. It was conducted at a single academic medical center with 4 local hospital campuses and may not be generalizable to other locations or populations. The exact data on staffing levels during the study time period were not available for analysis. Also, our study evaluated waste based on number of products, rather than a normalized ratio of waste to products issued, and only evaluated potential cost savings based on the acquisition price of products.

In conclusion, our study findings revealed how a pandemic may seriously impact blood use and waste in the transfusion service. Our findings showed a significant association between time period and the usage or wastage of blood products, with the pre–COVID-19 period utilizing the most blood products and the postquarantine period yielding the largest amount of waste. Our findings also identified significant potential cost savings in reducing blood product waste. Given our unexpected finding that waste was higher in the 2021 postquarantine period, future studies on the long-term effects of the pandemic on waste are needed.

Acknowledgments

We thank the entire Clinical Laboratory Sciences Department and the Clinical Blood Bank Laboratory at University of Texas Medical Branch in Galveston, TX, for their continued support and dedication.

Conflict of Interest Disclosure

The authors have nothing to disclose.

REFERENCES

1. Kurup R, Anderson A, Boston C, Burns L, George M, Frank M. A study on blood product usage and wastage at the public hospital, Guyana. *BMC Res Notes.* 2016;9(1):307. https://doi.org/10.1186/s13104-016-2112-5
2. Arya RC, Wander G, Gupta P. Blood component therapy: which, when and how much. *J Anaesthesiol Clin Pharmacol*. 2011;27(2):278-284. https://doi.org/10.4103/0970-9185.81849
3. Chegini A, Ebrahimi A, Maghari A. The evaluation of blood requests for transfusion and it's [sic] utilization in four Iranian hospitals. *Int Blood Res Rev.* 2015;4(2):1-6. https://doi.org/10.9734/IBRR/2015/17177
4. Shamshirian A, Mohseni AR, Pourfathollah AA, et al. A review of blood usage and wastage in a tertiary heart center. *Acta Clin Belg.* 2020;75(2):96-103. https://doi.org/10.1080/17843286.2018.1555113
5. Raval JS, Griggs JR, Fleg A. Blood product transfusion in adults: indications, adverse reactions, and modifications. *Am Fam Physician.* 2022;102(1):30-38.
6. Berwick DM, Hackbarth AD. Eliminating waste in US Health Care. *JAMA.* 2012;307(14):1513-1516. https://doi.org/10.1001/jama.2012.362
7. Levin JH, Collins L, Adekunle O, et al. Blood product wastage reduction by utilising low-cost, low-impact multimodal physician-to-physician communication initiatives. *Transfus Med.* 2019;29(6):389-393. https://doi.org/10.1111/tme.12640
8. Yahia AIO. Management of blood supply and demand during the COVID-19 pandemic in King Abdullah Hospital, Bisha, Saudi Arabia. *Transfus Apher Sci.* 2020;59(5):102836. https://doi.org/10.1016/j.transci.2020.102836
9. Hauk L. Approaches to minimize blood product wastage. *AORN J.* 2018;107(5):P7-P10. https://doi.org/10.1002/aorn.12163
10. Rajbhandary S, Shmookler A, Cohn CS, et al. Hospital transfusion service operations during the SARS-CoV-2 pandemic: lessons learned from the AABB hospital survey in preparation for the next infectious disease outbreak. *Transfusion.* 2021;61(11):3129-3138. https://doi.org/10.1111/trf.16643
11. Pagano MB, Cataife G, Fertrin KY, et al. Blood use and transfusion needs at a large health care system in Washington state during the SARS-CoV-2 pandemic. *Transfusion.* 2020;60(12):2859-2866. https://doi.org/10.1111/trf.16051
12. Ngo A, Masel D, Cahill C, Blumberg N, Refaai MA. Blood banking and transfusion medicine challenges during the COVID-19 pandemic. *Clin Lab Med.* 2020;40(4):587-601. https://doi.org/10.1016/j.cll.2020.08.013
13. Walsh GM, Shih AW, Solh Z, et al. Blood-borne pathogens: a Canadian blood services centre for innovation symposium. *Transfus Med Rev.* 2016;30(2):53-68. https://doi.org/10.1016/j.tmrv.2016.02.003
14. Mowla SJ, Sapiano MRP, Jones JM, Berger JJ, Basavaraju SV. Supplemental findings of the 2019 National Blood Collection and Utilization Survey. *Transfusion.* 2021;61(suppl 2):S11-S35. https://doi.org/10.1111/trf.16606
15. Senapati J, Aggarwal M, Louis L, et al. Transfusion practices during the COVID-19 pandemic: an experience from a hematology daycare in India. *Transfus Apher Sci.* 2021;60(2):103025. https://doi.org/10.1016/j.transci.2020.103025
16. Murphy C, Jackson B, Fontaine M. Tools for rapid analysis of blood usage and inventory during the COVID-19 pandemic. *Transfusion.* 2020;60(10):2199-2202. https://doi.org/10.1111/trf.15996
17. Shopsowitz KE, Lim C, Shih AW, et al. Impacts of COVID-19 and elective surgery cancellations on platelet supply and utilization in the Canadian Province of British Columbia. *Vox Sang.* 2022;117(2):251-258. https://doi.org/10.1111/vox.13180
18. Perelman I, Fergusson D, Lampron J, et al. Exploring peaks in hospital blood component utilization: a 10-year retrospective study at a large multisite academic centre. *Transfus Med Rev.* 2021;35(1):37-45. https://doi.org/10.1016/j.tmrv.2020.10.002
19. Jones JM, Sapiano MRP, Mowla S, Bota D, Berger JJ, Basavaraju SV. Has the trend of declining blood transfusions in the United States ended? Findings of the 2019 National Blood Collection and Utilization Survey. *Transfusion.* 2021;61(suppl 2):S1-S10. https://doi.org/10.1111/trf.16449
20. Kracalik I, Mowla S, Katz L, Cumming M, Sapiano MRP, Basavaraju SV. Impact of the early coronavirus disease 2019 pandemic on blood utilization in the United States: a time-series analysis of data reported to the National Healthcare Safety Network Hemovigilance Module. *Transfusion.* 2021;61(suppl 2):S36-S43. https://doi.org/10.1111/trf.16451
21. Barriteau CM, Bochey P, Lindholm PF, Hartman K, Sumugod R, Ramsey G. Blood transfusion utilization in hospitalized COVID-19 patients. *Transfusion.* 2020;60(9):1919-1923. https://doi.org/10.1111/trf.15947

22. DeSimone RA, Costa VA, Kane K, et al. Blood component utilization in COVID-19 patients in New York City: transfusions do not follow the curve. *Transfusion.* 2021;61(3):692-698. https://doi.org/10.1111/trf.16202

23. Jones JM, Sapiano MRP, Savinkina AA, et al. Slowing decline in blood collection and transfusion in the United States - 2017. *Transfusion.* 2020;60(suppl 2):S1-S9. https://doi.org/10.1111/trf.15604

24. Lu W, Yazer M, Li N, et al; Biomedical Excellence for Safer Transfusions Collaborative. Hospital red blood cell and platelet supply and utilization from March to December of the first year of the COVID-19 pandemic: the BEST collaborative study. *Transfusion.* 2022;62(8):1559-1570. https://doi.org/10.1111/trf.17023

25. Figueroa CF, Motsinger CM. Blood product management: operating room emerges most wasteful. *Int J Nurs Healthc Res*. 2020;3:1167. doi: 10.29011/2688-9501.101167

26. American College of Surgeons. COVID-19: Guidance for Triage of Non-Emergent Surgical Procedures; 2020. Accessed June 25, 2023. https://www.facs.org/for-medical-professionals/covid-19/clinical-guidance/triage/

27. Tholpady A, Monson J, Radovancevic R, Klein K, Bracey A. Analysis of prolonged storage on coagulation Factor (F)V, FVII, and FVIII in thawed plasma: is it time to extend the expiration date beyond 5 days? *Transfusion.* 2013;53(3):645-650. https://doi.org/10.1111/j.1537-2995.2012.03786.x

28. Islam A, Rafiq S, Karim S, Laher I, Rashid H. Convalescent plasma therapy in the treatment of COVID-19: practical considerations: correspondence. *Int J Surg.* 2020;79:204-205. https://doi.org/10.1016/j.ijsu.2020.05.079

29. Dunbar NM, Olson NJ, Szczepiorkowski ZM, et al. Blood component transfusion and wastage rates in the setting of massive transfusion in three regional trauma centers. *Transfusion.* 2017;57(1):45-52. https://doi.org/10.1111/trf.13880

30. Paganini M, Abowali H, Bosco G, et al. Quality improvement project of a massive transfusion protocol (MTP) to reduce wastage of blood components. *Int J Environ Res Public Health.* 2021;18(1):274. https://doi.org/10.3390/ijerph18010274

31. Jacobs JW, Booth GS. Blood shortages and changes to massive transfusion protocols: survey of hospital practices during the COVID-19 pandemic. *Transfus Apher Sci.* 2022;61(1):103297. https://doi.org/10.1016/j.transci.2021.103297

32. Booth AL, Bingham K, Guerra D, Bryant BJ, Yates S. Cost-minimization analysis before and after implementation of rapid bacterial testing at an academic medical center. Presented at the 2018 AABB meeting; October 14, 2018; Boston, MA. Accessed July 4, 2023. https://aabb.confex.com/aabb/2018/meetingapp.cgi/Paper/4084

33. Yates N, Stanger S, Wilding R, Cotton S. Approaches to assessing and minimizing blood wastage in the hospital and blood supply chain. *ISBT Sci Ser.* 2017;12(1):91-98. https://doi.org/10.1111/voxs.12330

34. Kelly SL, Reed MJ, Innes CJ, Manson L. A review of blood component usage in a large UK emergency department after implementation of simple measures. *Emerg Med J.* 2013;30(10):842-845. https://doi.org/10.1136/emermed-2012-201747

35. Yazer MH, Abraham S, Beckman N, Folléa G. International Society for Blood Transfusion international survey on blood product wastage in hospitals. *ISBT Sci Ser.* 2016;11(1):24-31. https://doi.org/10.1111/voxs.12236

36. Hyatt W, Yon JR, Haley-Andrews S. Minimizing time to plasma administration and fresh frozen plasma waste: a multimodal approach to improve massive transfusion at a level 1 trauma center. *J Trauma Nurs.* 2019;26(5):234-238. https://doi.org/10.1097/jtn.0000000000000460

37. Warner MA, Kurian EB, Hammel SA, van Buskirk CM, Kor DJ, Stubbs JR. Transition from room temperature to cold-stored platelets for the preservation of blood inventories during the COVID-19 pandemic. *Transfusion.* 2021;61(1):72-77. https://doi.org/10.1111/trf.16148

38. Collins RA, Wisniewski MK, Waters JH, Triulzi DJ, Yazer MH. Effectiveness of multiple initiatives to reduce blood component wastage. *Am J Clin Pathol.* 2015;143(3):329-335. https://doi.org/10.1309/AJCP42WMHSSTPHXI

Molecular and phenotypical findings of a novel de novo *SYNGAP1* gene variant in an 11-year-old Iranian boy with intellectual disability

Atefeh Mir, PhD,[1] Yongjun Song, DVM, MSc,[2] Hane Lee, PhD,[2] Zakiye Nadeali, MSc,[1] Fahimeh Akbarian, MSc,[1] Mohammad Amin Tabatabaiefar, PhD[1,3,4,]

[1]Department of Genetics and Molecular Biology, School of Medicine, [3]Pediatric Inherited Diseases Research Center, Research Institute for Primordial Prevention of Noncommunicable Disease, and [4]GenTArget Corp (GTAC), Deputy of Research and Technology, Isfahan University of Medical Sciences, Isfahan, Iran, [2]Division of Medical Genetics, 3Billion, Seoul, South Korea. Corresponding author: Mohammad Amin Tabatabaiefar; tabatabaiefar@med.mui.ac.ir

Key words: SYNGAP1; de novo; IDD; MRD; Iran; intellectual disability; developmental delay; ataxia

Abbreviations: IDD, intellectual developmental disorder; AD, autosomal dominant; ID, intellectual disability; International Classification of Diseases; MRD, mental retardation; ASD, autism spectrum disorder; SYNGAP1, SYNaptic GTPase activating protein; WES, whole exome sequencing; ACMG, American College of Medical Genetics and Genomics; CADD, Combined Annotation Dependent Depletion; COBALT, Constraint-Based Multiple Alignment Tool; HGMD, Human Gene Mutation Database

Laboratory Medicine 2024;55:204-208; https://doi.org/10.1093/labmed/lmad064

ABSTRACT

Objective: Intellectual developmental disorder (IDD) type 5 is an autosomal dominant (AD) disorder and is characterized by intellectual disability (ID), psychomotor developmental delay, variable autism phenotypes, microcephaly, and seizure. IDD can be caused by mutations in the *SYNGAP1* gene, which encodes a Ras GTPase-activating protein. This study revealed a novel de novo nonsense variant in *SYNGAP1*. The identification of such variants is essential for genetic counseling in patients and their families.

Methods: Exome sequencing implicated the causative variant. Sanger sequencing and cosegregation analyses were used to confirm the variant. Multiple in silico analysis tools were applied to interpret the variant using the American College of Medical Genetics and Genomics and the Association for Molecular Pathology guidelines.

Results: The de novo NM_006772.3(*SYNGAP1*):c.3685C>T variant was identified in an 11-year-old boy with severe intellectual disability, neurodevelopmental delay, speech disorder, ataxia, specific dysmorphic facial features, and aggressive behavior.

Conclusion: The current study findings expand the existing knowledge of variants in *SYNGAP1* that have been previously associated with nonsyndromic intellectual disability and autism, extending the spectrum of phenotypes associated with this gene. The data have implications for genetic diagnosis and counseling in similar phenotypic presentations.

Introduction

Intellectual disability (ID) is defined as the inability to mature cognitively and reach an age-appropriate IQ level with onset before 18 years of age. It affects 2% to 3% of the world's population.[1] The classification working group on ID in the World Health Organization's International Classification of Diseases (ICD) presented the term intellectual developmental disorders (IDD) as a group of developmental conditions characterized by a significant deficiency in cognitive functioning accompanied by limitations in learning, adaptable behavior, and life skills.[2] A person with IDD has both an "intellectual disability" (defined as an IQ of below 70 at age 5 years or older)[3,4] and a "global developmental delay" (term used at an age younger than 5 years, defined as deficits in 2 or more developmental domains, eg, fine/gross motor skills, speech, and interaction).[5] IDD has a diverse etiology and has been categorized as a meta-syndromic condition by the ICD Working Group. However, genetic etiologies are the most common cause of IDD[6] and represent up to 50% of IDDs, ranging from chromosomal abnormalities to single gene defects.[7] To date, more than 1000 types of IDD have been identified with a genetic origin. Autosomal dominant IDD was previously known as AD mental retardation (MRD), which is a group of about 69 disorders (ie, MRD1-69).[8]

In this context, MRD5 (OMIM #612621) is characterized by ID and psychomotor developmental delay, in addition to autism spectrum disorder (ASD), microcephaly, and seizures. It is caused by mutations in *SYNGAP1* at 6p21.3.[9] *SYNGAP1* encodes a 140 kDa brain-specific cytosolic SYNaptic GTPase activating protein (SYNGAP1) localized

to dendritic spines of neocortical pyramidal neurons and negatively regulates Rap, Ras, and the α-amino-3-hydroxy-5-methyl-4-isoxazole propionic acid receptor trafficking to the postsynaptic membrane to regulate synaptic plasticity and neuronal homeostasis.[10] It functions as a component of the *N*-methyl-D-aspartate receptor–mediated signaling complex. The SYNGAP1 protein plays a vital role in the establishment of morphology, function, and plasticity of synapsis excitatory glutamatergic neurons, and therefore haploinsufficiency of *SYNGAP1* increases the number of mushroom-shaped dendritic spines during brain development, leading to disorders of brain development and function.[9] Investigations and discovery of disease-causing *SYNGAP1* variants may further elucidate genotype-phenotype correlations.

In this study, we report a novel de novo pathogenic *SYNGAP1* variant in an 11-year-old boy with severe intellectual disability, neurodevelopmental delay, speech disorder, ataxia, and aggressive behavior. The whole exome sequencing (WES) technique was used to identify the causative mutation and lead to the confirmation of the diagnosis of MRD5 and expand the mutational and clinical knowledge of the *SYNGAP1* gene.

Materials and Methods

Case Presentation and DNA Extraction

The patient's medical history was obtained through genetic counseling, and the pedigree was drawn by using Progeny software. Peripheral blood was collected after obtaining informed written consent from the legal guardian. DNA extraction was performed using the DNSol Miniprep Kit provided by Rojetechnologies, Tehran, Iran. This study was approved by the ethics committee of the Isfahan University of Medical Science, Isfahan, Iran (Ethics code: IR.MUI.MED.REC.1400.042).

Exome Capture, Whole Exome Sequencing, and Variant Prioritization

Exome capturing was performed using xGen Exome Research Panel v2 (Integrated DNA Technologies). WES was performed using NovaSeq 6000 (Illumina), and sequence alignment was done to the Genome Reference Consortium Human Build 37 and revised Cambridge Reference Sequence of the mitochondrial genome. Variant interpretation was performed using EVIDENCE software[11] to prioritize variants and interpreted based on the guideline recommended by the American College of Medical Genetics and Genomics (ACMG) and the Association for Molecular Pathology.[12] Only clinically significant variants relevant to the patient's primary clinical symptoms at the time of variant interpretation were considered. Exome capture, WES, and variant prioritization were performed by 3Billion, Seoul, Korea.

Sanger Sequencing and Cosegregation Analysis

The candidate variant was confirmed using Sanger sequencing, and cosegregation analysis was performed on the family. Specific primers for the variant were designed using the Primer3 online tool (Primer3web, version 4.1.0) and validated by online tools such as Primer-BLAST,[13] MFEprimer3.1,[14] and SNPCheck (gene tools, SNPCheck V3). The used primer sequences are listed in **TABLE 1**.

In Silico Analysis

We used the Genome Aggregation Database (gnomAD v2.1.1), Iranome (http://www.iranome.com/), and GTAC domestic databases for population allele frequency analysis. The potential pathogenicity of the variants was assessed using the following prediction tools: FATHMM-MKL (Functional Analysis through Hidden Markov Models [FATHMM] [v2.3], http://fathmm.biocompute.org.uk), BayesDel (addAF and noAF) (https://fengbj-laboratory.org/BayesDel/BayesDel.html), EIGEN (http://www.columbia.edu/~ii2135/eigen.html), LRT (http://genetics.wustl.edu/jflab/lrt_query.html), and MutationTaster (https://www.mutationtaster.org/). The Combined Annotation Dependent Depletion (CADD) scores (https://cadd.gs.washington.edu/snv) were obtained. The CADD-SV scores on the Phred scale range from 0 (potentially benign) to 48 (potentially pathogenic), indicating the position of the novel variant within the gnomAD-SV score distribution.[15] The National Center for Biotechnology Information Constraint-Based Multiple Alignment Tool (COBALT) server was used to analysis of conservation (https://www.ncbi.nlm.nih.gov/tools/cobalt/cobalt.cgi?CMD=Web).

Results

Subject

The proband was an 11-year-old boy with severe ID with a history of delayed milestones. He was not ambulatory until 5 years of age and experienced 1 seizure at 4 years of age. He had ataxia while walking (ataxic gait). He showed aggressive behavior and speech problems. He did not show skeletal abnormalities, but subtle dysmorphic facial features included prominent eyebrows, short philtrum, broad mouth with diastemata of the upper teeth, cupid bow upper lip, hypertelorism, full nasal tip, and small pointed chin. His parents are first cousins once removed (**FIGURE 1A**). There was no family history of ID, but a female cousin died for an unknown reason at birth and a mother's cousin had a movement disability (**FIGURE 1A**; the IV:9 member in the pedigree).

Sequencing Findings

Exome sequencing revealed a de novo deleterious variant (**TABLE 2**), NM_006772.3:c.3685C>T (p.Gln1229Ter), in the *SYNGAP1* gene related to AD IDD type 5. Sanger sequencing confirmed the variant in the patient, and cosegregation analysis confirmed the variant is in de novo condition and represents no observation of the variant in nonaffected members of the family. Thus, the patient carried a de novo heterozygous NM_006772.3 (*SYNGAP1*):c.3685C>T (p.Gln1229Ter) variant confirmed by Sanger sequencing.

In Silico Findings

The variant was not found in the gnomAD, Iranome, or other public or domestic databases. Multiple in silico analysis tools showed deleterious effects of the candidate variant on the encoded protein. **TABLE 2** shows in silico analysis of the candidate variant. The prediction tools, such as BayesDel addAF, BayesDel noAF, EIGEN, EIGEN PC, FATHMM-MKL, LRT, and MutationTaster showed damaging and disease-causing effects of the variant. The CADD-SV score on the Phred scale was 40, which is categorized as potentially pathogenic. The COBALT server showed the locus of the variant was highly conserved in multiple organisms.

TABLE 1. The specific primers used for Sanger sequencing

Primer name	Sequence	Product size
SYNGAP1-F	CCATGGCAGGGTCTTCTCAA	402 bp
SYNGAP1-R	CTCACCTGCCAATGATGCTC	

FIGURE 1. **A, The pedigree of the studied family. B, Electropherograms of the Sanger sequences of the proband and his parents that show de novo occurrence of the identified variant.**

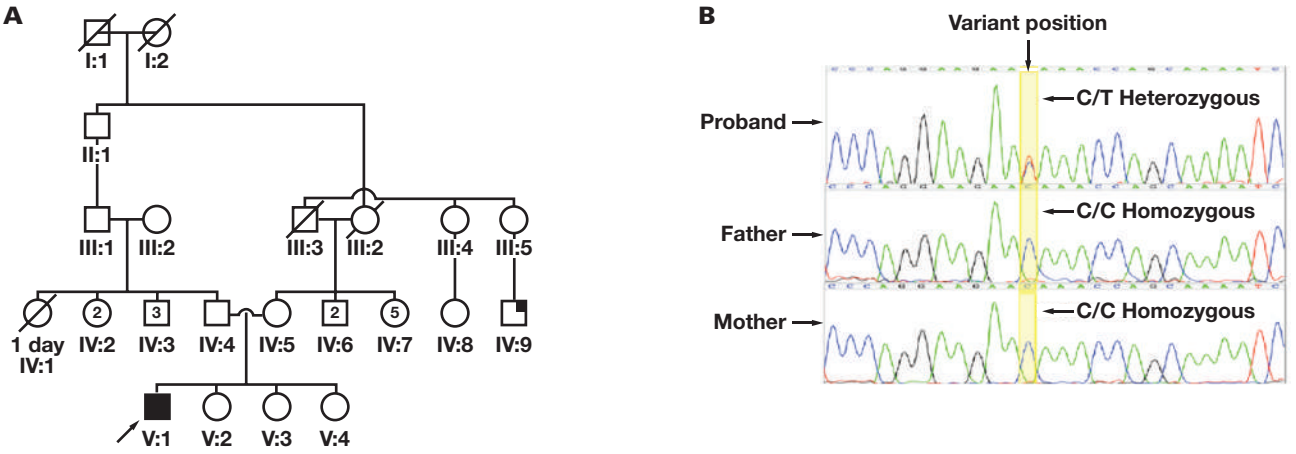

TABLE 2. **In silico data on the identified variant**

Gene	*SYNGAP1*
Variant genomic position	Chr6-33414454-C-T (GRCh37)
cDNA position	NM_006772.3:c.3685C>T
Protein change	NP_006763.2:p.Gln1229Ter
Type of mutation	Nonsense
Allele frequency in gnomAD exome	N/A
Allele frequency in gnomAD genome	N/A
Allele frequency in gnomAD (South Asian)	N/A
Iranome	N/A
CADD Phred	40
Bioinformatics tools showing damaging results	BayesDel addAF, BayesDel noAF, EIGEN, EIGEN PC, FATHMM-MKL, LRT, MutationTaster

CADD, Combined Annotation Dependent Depletion; N/A, not available.

FIGURE 2. **Proportion of different types of reported mutation in the *SYNGAP1* gene based on the nonprofessional Human Gene Mutation Database.**

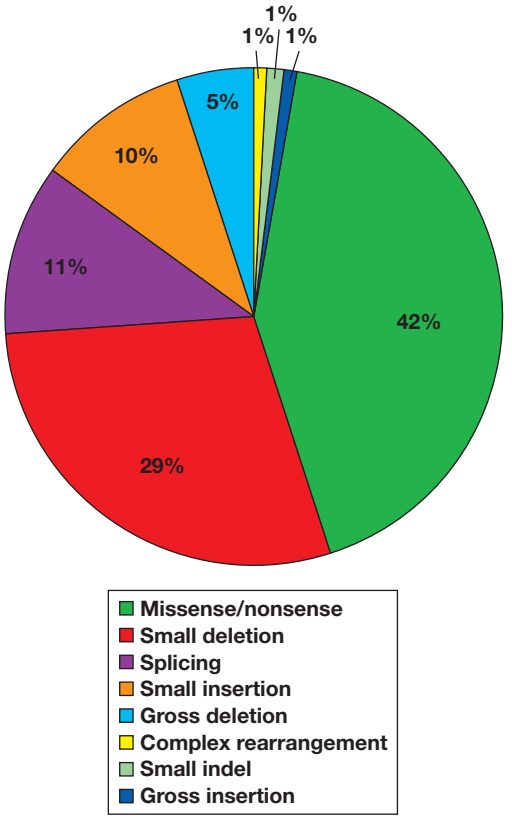

According to the ACMG guideline of variant classification,[12] the identified variant was classified as pathogenic due to these criteria for pathogenicity: PVS1(null variant), PP5 (ClinVar classifies this variant as Pathogenic), PM2 (variant not found in gnomAD), PS2 (de novo in a patient with no family history), and PM1 (located in a critical domain).

Discussion and Conclusion

MRD5 is classified as a rare nonsyndromic ID. It is a condition caused by mutations in *SYNGAP1* that affect the central nervous system, is characterized by moderate to severe ID, and presents in the first few years of life. Some patients may also experience seizures. Autism spectrum disorders may be observed in some cases. Almost all reported cases are due to de novo mutations in the *SYNGAP1* gene. Loss-of-function mutations causing haploinsufficiency have been implicated in damaging the development of the forebrain glutamatergic neurons.[16–18]

The *SYNGAP1* gene codes for a Ras GTPase activating protein, a member of the NMDA receptor complex. The *N*-terminal domain of the protein contains a Ras-GAP domain, a pleckstrin homology domain, and a C2 domain possibly involved in calcium and phospholipid binding; the *C*-terminal domain contains 10 histidine repeat regions, serine, and tyrosine phosphorylation sites and a T/SXV motif required for postsynaptic scaffold protein interaction.[19] This gene includes 9 transcripts, the largest consisting of 1343 residue and encoding 19 exons. Mutations in *SYNGAP1* were first identified in patients with nonsyndromic ID and ASD, followed by the discovery of its important role in the development and epileptic encephalopathies in 2013.[18,20,21] This study revealed a novel de novo nonsense mutation (NM_006772.3:c.3685C>T (p.Gln1229Ter)) in the *SYNGAP1* gene in

2024;55:204-208 | https://doi.org/10.1093/labmed/lmad064

FIGURE 3. **Protein sequence alignment of the SYNGAP1 protein using the National Center for Biotechnology Information Constraint-Based Multiple Alignment Tool server. Conservation analysis in 5 different organisms showed highly conserved residues in most regions of the protein; red regions downstream of the identified variant show highly conserved sequences on the SYNGAP1.**

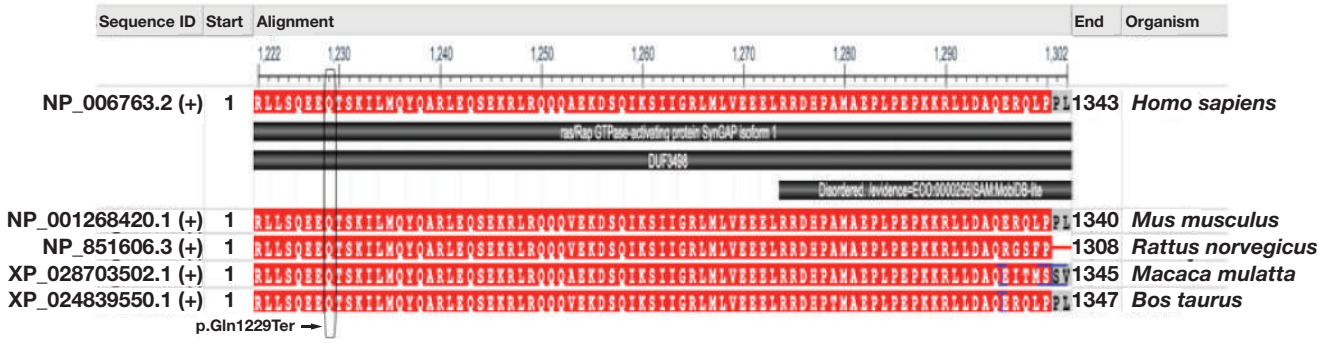

TABLE 3. **Downstream mutations of the c.3685C>T variant in the *SYNGAP1* gene and phenotypic findings**

Variant	Protein Change	Molecular consequence of mutation	Related condition	Clinical features	Reference
NM_006772.3(SYNGAP1):c.3706C>T	p.Gln1236Ter	Nonsense	Intellectual disability, autosomal dominant 5; inborn genetic diseases	Seizures, intellectual disability, global developmental delay, autistic behavior	[24]
NM_006772.3(SYNGAP1):c.3718C>T	p.Arg1240Ter	Nonsense	Intellectual disability, autosomal dominant 5; inborn genetic diseases; complex neurodevelopmental disorder	Severe cognitive impairments, seizures	[25–27]
NM_006772.3(SYNGAP1):c.3732_3735del	p.Ser1244fs	Frameshift	Intellectual disability, autosomal dominant 5	N/A	[24]
NM_006772.3(SYNGAP1):c.3788_3794del	p.Ile1263fs	Frameshift	Intellectual disability, autosomal dominant 5	Moderate intellectual disability, seizures, speech delay	[24]
NM_006772.3(SYNGAP1):c.3795-1G>A	—	Splice acceptor	Intellectual disability, autosomal dominant 5	Global developmental delay, seizure, ADHD, motor stereotypy, abnormal social behavior	[24]
NM_006772.3(SYNGAP1):c.3811G>T	p.Glu1271Ter	Nonsense	Intellectual disability, autosomal dominant 5	N/A	[24]
NM_006772.3(SYNGAP1):c.3834dup	p.Ala1279fs	Frameshift	Intellectual disability	N/A	[24]

N/A, not available.

an 11-year-old boy with severe ID, neurodevelopmental delay, speech disorder, ataxia, and aggressive behavior. To date, 228 mutations have been reported in *SYNGAP1* based on the nonprofessional version of the Human Gene Mutation Database (HGMD) that are related to ID, ASD, developmental delay, and encephalopathies. As **FIGURE 2** shows, according to the nonprofessional HGMD, most of the mutations are missense/nonsense and small deletions, but other types of mutations were reported frequently related to pathogenicity of the disorder. The identified NM_006772.3:c.3685C>T (p.Gln1229Ter) variant is located in exon 17 and caused by a premature stop codon in this exon and loss of downstream coding regions (2 later exons). It is located in encoding regions of the coiled-coil domain, which is associated with the RasGAP domain and the C2 domain.[22] According to protein alignments data in 5 organisms, almost all regions of the gene, and especially the downstream regions of the variant location, are highly conserved (**FIGURE 3**). This implies an important role for the coiled-coil domain, and downstream domains, which were highly conserved in the evolutionary process. Numerous studies had reported pathogenic mutations on downstream regions of the NM_006772.3:c.3685C>T (p.Gln1229Ter) variant (**TABLE 3** lists some downstream mutations of the variant and phenotypic findings) that confirms the critical role of the last exons in the protein function. Almost all reported downstream variants were related to ID, ASD, seizures, developmental delay, and abnormal social behavior. Thus, loss of the last exons should be considered in the pathogenicity of related disorders. As in the Vlaskamp et al[23] study, the patient in our current study also had specific facial dysmorphic features such as full slightly prominent eyebrows, hypertelorism, full nasal tip, short philtrum, cupid bow upper lip, broad mouth with diastemata of the upper teeth, and small pointed chin. Thus, these dysmorphic facial features can be considered for differential diagnosis and genetic counseling.

The findings in this study not only advance the understanding of how *SYNGAP1* variants can be implicated in phenotypes associated with ID, developmental delay, speech disorder, ataxia, and behavior problems but also allow for more diagnostic accuracy and improved quality of genetic counseling in further cases with similar variants.

Acknowledgments

We thank the family who participated in this study. We are grateful to 3Billion, Seoul, South Korea, for performing the whole exome sequencing. This study is a part of A. M.'s PhD thesis.

The research was performed in accordance with the Declaration of Helsinki and with the approval of the ethics board of the Medical University of Isfahan (Ethics code: IR.MUI.MED.REC.1400.042).

The legal guardian consented to participate after being informed of the nature of the research. The authors affirm that human research participants provided informed consent for the publication of the images in FIGURE 1.

Funding

This study was funded by the Medical University of Isfahan, Isfahan, Iran (grant No. 3991102), and research collaboration with 3Billion, Seoul, South Korea.

Data Availability

All data generated or analyzed during this study are included in this published article and the raw data that support the findings of this study are available from the corresponding author upon reasonable request. The identified variant was submitted to the ClinVar database (Accession No. SCV002573234.1).

Conflict of Interest Disclosure

The authors have nothing to disclose.

REFERENCES

1. Diagnostic and Statistical Manual of Mental Disorders. *American Psychiatric Association*; 2013:591-643.
2. Carulla LS, Reed GM, Vaez-Azizi LM, et al. Intellectual developmental disorders: towards a new name, definition and framework for "mental retardation/intellectual disability" in ICD-11. *World Psychiatry*. 2011;10(3):175.
3. Luckasson R, Reeve A. Naming, defining, and classifying in mental retardation. *Ment Retard.* 2001;39(1):47-52. doi:10.1352/0047-6765(2001)039<0047:NDACIM>2.0.CO;2
4. Shevell MI. Present conceptualization of early childhood neurodevelopmental disabilities. *J Child Neurol.* 2010;25(1):120-126. doi:10.1177/0883073809336122
5. Shevell M. Global developmental delay and mental retardation or intellectual disability: conceptualization, evaluation, and etiology. *Pediatr Clin North Am.* 2008;55(5):1071-1084, xi. doi:10.1016/j.pcl.2008.07.010
6. Rauch A, Wieczorek D, Graf E, et al. Range of genetic mutations associated with severe non-syndromic sporadic intellectual disability: an exome sequencing study. *The Lancet*. 2012;380(9854):1674-1682. doi:10.1016/s0140-6736(12)61480-9
7. Moeschler JB, ed. *Genetic Evaluation of Intellectual Disabilities. Seminars in Pediatric Neurology*. Elsevier; 2008.
8. McKusick VA. *Mendelian Inheritance in Man: Catalogs of Autosomal Dominant, Autosomal Recessive, and X-Linked Phenotypes*. Elsevier; 2014.
9. Agarwal M, Johnston MV, Stafstrom CE. SYNGAP1 mutations: Clinical, genetic, and pathophysiological features. *Int J Dev Neurosci.* 2019;78(1):65-76. doi:10.1016/j.ijdevneu.2019.08.003
10. Jeyabalan N, Clement JP. SYNGAP1: mind the gap. *Front Cell Neurosci.* 2016;10:32. doi:10.3389/fncel.2016.00032
11. Seo GH, Kim T, Choi IH, et al. Diagnostic yield and clinical utility of whole exome sequencing using an automated variant prioritization system, EVIDENCE. *Clin Genet.* 2020;98(6):562-570. doi:10.1111/cge.13848
12. Richards S, Aziz N, Bale S, et al. Standards and guidelines for the interpretation of sequence variants: a joint consensus recommendation of the American College of Medical Genetics and Genomics and the Association for Molecular Pathology. *Genet Med.* 2015;17(5):405-424. doi:10.1038/gim.2015.30
13. Ye J, Coulouris G, Zaretskaya I, Cutcutache I, Rozen S, Madden TL. Primer-BLAST: a tool to design target-specific primers for polymerase chain reaction. *BMC Bioinf.* 2012;13(1):1-11.
14. Wang K, Li H, Xu Y, et al. MFEprimer-3.0: quality control for PCR primers. *Nucleic Acids Res.* 2019;47(W1):W610-W613. doi:10.1093/nar/gkz351
15. Rentzsch P, Witten D, Cooper GM, Shendure J, Kircher M. CADD: predicting the deleteriousness of variants throughout the human genome. *Nucleic Acids Res.* 2019;47(D1):D886-D894. doi:10.1093/nar/gky1016
16. Berryer MH, Hamdan FF, Klitten LL, et al. Mutations in SYNGAP1 cause intellectual disability, autism, and a specific form of epilepsy by inducing haploinsufficiency. *Hum Mutat.* 2013;34(2):385-394. doi:10.1002/humu.22248
17. Hamdan FF, Daoud H, Piton A, et al. De novo SYNGAP1 mutations in nonsyndromic intellectual disability and autism. *Biol Psychiatry.* 2011;69(9):898-901. doi:10.1016/j.biopsych.2010.11.015
18. Hamdan FF, Gauthier J, Spiegelman D, et al. Mutations in SYNGAP1 in autosomal nonsyndromic mental retardation. *N Engl J Med.* 2009;360(6):599-605. doi:10.1056/nejmoa0805392
19. GeneCards. The Human Gene Database. www.genecards.org
20. Pinto D, Pagnamenta AT, Klei L, et al. Functional impact of global rare copy number variation in autism spectrum disorders. *Nature.* 2010;466(7304):368-372. doi:10.1038/nature09146
21. Carvill GL, Heavin SB, Yendle SC, et al. Targeted resequencing in epileptic encephalopathies identifies de novo mutations in CHD2 and SYNGAP1. *Nat Genet.* 2013;45(7):825-830. doi:10.1038/ng.2646
22. InterPro. https://www.ebi.ac.uk/interpro/about/interpro/
23. Vlaskamp DRM, Shaw BJ, Burgess R, et al. SYNGAP1 encephalopathy: a distinctive generalized developmental and epileptic encephalopathy. *Neurology.* 2019;92(2):e96-e107. doi:10.1212/WNL.0000000000006729
24. ClinVar. https://www.ncbi.nlm.nih.gov/clinvar/
25. Jang SS, Kim SY, Kim H, et al. Diagnostic yield of epilepsy panel testing in patients with seizure onset within the first year of life. *Front Neurol.* 2019;10:988. doi:10.3389/fneur.2019.00988
26. Jimenez-Gomez A, Niu S, Andujar-Perez F, et al. Phenotypic characterization of individuals with SYNGAP1 pathogenic variants reveals correlation between posterior dominant rhythm and developmental progression. *J Neurodevelop Disord*. 2019;11:1-1.
27. Rauen KA. Defining RASopathy. *Disease models & mechanisms*. 2022;15(2):dmm049344. doi:10.1242/dmm.049344

A comprehensive assessment of redox balance in small for gestational age newborns and their mothers

Almila Senat, PhD[1,], Emre Erdem Tas, MD[2], Hasan Eroglu, MD[3], Ceylan Bal, MD[4], Ayse Filiz Yavuz, MD[2], Aykan Yucel, MD[3], Ozcan Erel, MD[4], Arzu Ersoz, PhD[5]*

[1]Ankara Yildirim Beyazit University, Ankara Ataturk Training and Research Hospital, Department of Biochemistry Ankara, Turkey, [2]Ankara Yildirim Beyazit University, Faculty of Medicine, Department of Obstetrics and Gynecology, Ankara, Turkey, [3]Etlik Zubeyde Hanim Women's Health Care, Training and Research Hospital, Department of Perinatology, Ankara, Turkey, [4]Ankara Yildirim Beyazit University, Faculty of Medicine, Department of Biochemistry, Ankara, Turkey, [5]Eskisehir Technical University, Faculty of Science, Department of Chemistry, Eskisehir, Turkey. Corresponding author: Almila Senat, PhD; almilasenat@outlook.com

[*]Dr Senat is currently with the Department of Biochemistry, Istanbul Taksim Training and Research Hospital, Beyoglu/Istanbul, Turkey.

Key words: glutathione; small for gestational age; redox; thiol-disulfide homeostasis; oxidative stress; oxidized glutathione

Abbreviations: SGA, small for gestational age; ROS, reactive oxygen species; AGA, appropriate for gestational age; MPO, myeloperoxidase; TAS, total antioxidant status; TOS, total oxidant status; CAT, catalase; IMA, ischemia-modified albumin; GSH, glutathione; GSSG, oxidized GSH

Laboratory Medicine 2024;55:209-214; https://doi.org/10.1093/labmed/lmad065

ABSTRACT

Objective: The objective of this study was to assess oxidative stress in small for gestational age (SGA) newborns and their mothers by evaluating intra- and extracellular thiol homeostasis and the quantification of major oxidants and antioxidants.

Methods: A total of 75 mothers and their 75 newborns (43 SGA) were enrolled in this study. Thiol-disulfide homeostasis, serum myeloperoxidase, catalase, total oxidant, and antioxidant status were analyzed. Additionally, erythrocytic glutathione (GSH) homeostasis was measured.

Results: Although native and total thiol levels were decreased, disulfide levels were increased in SGA groups. Additionally, myeloperoxidase activity and total oxidant status levels were significantly elevated whereas total antioxidant status levels and enzymatic antioxidant systems were diminished in SGA groups. Similarly, intra-erythrocytic GSH homeostasis was shifted in favor of oxidants in SGA groups.

Conclusion: Our results demonstrate that insufficient antioxidant systems in mothers and a robust source of oxidative stress in SGA might contribute to the pathophysiology of SGA births.

Introduction

Newborns who are born with weight below the 10th percentile are defined as small for gestational age (SGA) newborns. There are various underlying factors that have been established to be causes of SGA, including nutritional, hormonal, vascular, and genetic factors.[1,2] The birth weight and length of infants are important predictors associated with health-related outcomes later in life.[3] According to recent studies, infants diagnosed with SGA may have a higher risk of experiencing various health problems later in life, including peri- and postnatal morbidity, persistent short stature, and metabolic disorders.[4] Interestingly, these risks are particularly high in healthy term SGA newborns who rapidly "catch up" to non-SGA newborns in terms of postnatal growth.[5,6]

Oxidative stress is associated with pregnancy-related disorders. During pregnancy, changes in the immune response and increased energy demands lead to elevated production of reactive oxygen species (ROS). The placenta is regarded as a major source of oxidative stress; however, under normal circumstances, maternal antioxidants are expected to counteract the elevation in ROS levels, thereby maintaining balance. Elevated oxidative stress leads to adverse outcomes for both mothers and newborns.[7,8] A recent hypothesis suggested that placental insufficiency, which is considered to be a cause of fetal growth restriction, is associated with oxidative stress originating from trophoblast invasion in the placenta as a result of high energy demands for metabolic activity, cellular growth, and proliferation.[8] Mohn et al[9] revealed that peripubertal children who were born with SGA continued to experience high levels of oxidative stress, which is a component of SGA pathophysiology. This finding suggests that oxidative stress could serve as an early indicator of metabolic and cardiovascular dysfunctions in the adulthood of individuals diagnosed with SGA at birth.[9] Our objective was to perform a comprehensive investigation of oxidative stress by evaluating intra- and extracellular oxidant-antioxidant homeostasis, as well as

major oxidant and antioxidant molecules in SGA newborns and their mothers.

Material and Methods

Study Population

A total of 75 newborns and 75 mothers were included in the study. The population consisted of 43 mothers with 43 SGA newborns and 32 mothers with appropriate for gestational age (AGA) newborns. The newborns were classified as AGA when birth weight was between the 10th and 90th percentile, whereas SGA was defined in newborns with a birth weight of <10th percentile.[2] Inclusion criteria were (1) having uncomplicated singleton gestation at full term, (2) not being diagnosed with metabolic or chronic diseases, (3) not receiving any regular treatment(s), and (4) being defined as "healthy newborns" without hypoxemia, chromosomal disorders, malformations, or acute illnesses. Additionally, those diagnosed with intrauterine growth retardation and mothers with a history of smoking were excluded. After delivery, birth weight, birth length, head circumference, 1st- and 5th-minute Apgar scores, and ponderal index (weight/[length]^3 × 100) of all newborns were recorded. The mothers provided written informed consent for the use of medical data in this research on behalf of themself and their babies. All procedures performed in studies involving human participants were in accordance with the ethical standards of the institutional and/or national research committee and with the 1964 Helsinki Declaration and its later amendments or comparable ethical standards. The present study was approved by the ethics committee of Ankara Yildirim Beyazit University, Faculty of Medicine (Approval number 26379996/220).

Blood Samples

Whole blood samples of mothers were drawn into EDTA-containing and serum separator tubes by venipuncture immediately after delivery. The whole blood of newborns was obtained from the umbilical cord vein and was drawn from the double-clamped segment of the umbilical cord. Sera of all subjects were obtained by centrifuging serum separator tubes at 1500*g* for 10 minutes. All samples were aliquoted and stored at −80°C until examination.

Measurements in Serum Samples

An automated spectrophotometric method developed by Erel and Neselioglu[10] was used to determine extracellular thiol-disulfide homeostasis. Myeloperoxidase (MPO) activity was measured according to the modified Bradley method.[11] An enzymatic method by Siotto et al[12] was used to measure ferroxidase activity. Total antioxidant status (TAS) and total oxidant status (TOS) were assessed with commercial kits (Rel Assay Diagnostics). Catalase (CAT) activity was measured by Goth's method.[13] Albumin and ischemia-modified albumin (IMA) were determined with automatized methods based on the reports by Doumas et al[14] and Bar-Or et al,[15] respectively. All parameters were measured on a Roche cobas c501 chemistry autoanalyzer (Roche Diagnostics).

Preparation of Whole Blood Samples for Intracellular Analysis

Intracellular erythrocytic glutathione (GSH) homeostasis is primarily based on GSH levels within erythrocytes, as GSH is the most abundant antioxidant molecule inside these cells. Whole blood samples drawn into EDTA tubes were used to perform erythrocyte lysis. After centrifugation to separate plasma, the plasma fraction was removed and erythrocytes were washed 3 times with a 0.9 % NaCl solution. Following the washing procedure, erythrocytes were lysed by addition of distilled water to elute the GSH content of erythrocytes. Then the supernatant fraction of lysed samples was obtained by centrifuging at 1500*g* for 10 minutes. The supernatant fraction was used for intracellular erythrocytic GSH homeostasis tests.

Intracellular Erythrocytic Glutathione Homeostasis Measurement

Intracellular erythrocytic GSH homeostasis was assessed according to the method put forth by Alisik et al.[16] In this method, the measured parameters are GSH and total GSH (GSH + oxidized GSH [GSSG]), whereas the GSSG value is calculated from these values. The GSH and total GSH (GSH + GSSG) levels were measured with an automated system using a Roche cobas c501 chemistry analyzer (Roche Diagnostics). The GSSG levels were calculated by subtracting GSH levels from total GSH (GSH + GSSG) levels and by dividing the result by 2. Hemoglobin levels were determined by using a Siemens Advia 2120i Hematology System.

Statistical Analysis

SPSS software version 20.0 was used for all statistical analyses. The Kolmogorov–Smirnov test was performed to determine the distribution characteristics of continuous variables. The variables are summarized as follows: mean ± SD were used for parametric continuous variables and medians (interquartile range) for nonparametric continuous parameters, whereas absolute and relative frequencies (n and percentage) were used for categorical variables. The independent samples *t*-test and Mann–Whitney *U* were performed to assess differences between groups, depending on parametric assumptions. Categorical variables were analyzed by the Pearson χ^2 test or the Fisher's exact test. Correlation analyses were performed with Spearman's correlation analysis. All comparisons were 2-tailed, with *P* values of <.05 considered to be statistically significant.

Results

Maternal clinical and demographic characteristics are summarized in **TABLE 1**. Gestational age was similar in the AGA and SGA groups (*P* = .328). As expected, birth weight, birth height, and head circumference were significantly different between AGA and SGA newborns (*P* < .001 for all). First and 5th minute Apgar scores were lower in SGA newborns than in AGA newborns (*P* < .001 for all) as shown in **TABLE 2**.

Native thiol, total thiol, and native thiol/total thiol index levels were higher in the maternal AGA group than in the maternal SGA group (*P* < .001, *P* = .004, and *P* < .001 respectively). In the maternal SGA group, disulfide levels, disulfide-native thiol percent, and disulfide-total thiol percent index levels were higher than the maternal AGA group (*P* < .001 for all). Whereas CAT activity and TAS levels were significantly higher in the maternal AGA group (*P* < .001 for both), IMA levels and MPO activity were significantly higher in the maternal SGA group (*P* < .001 for both), as shown in **TABLE 1**.

The AGA newborns had higher levels of native thiol, total thiol, and native-total thiol index (*P* < .001, *P* = .008, and *P* = .002, respectively), whereas disulfide levels, disulfide-native thiol percent, and disulfide-total thiol percent index levels were increased in SGA newborns (*P* <

TABLE 1. Comparison of maternal AGA and SGA groups with regard to demographic and clinical characteristics and oxidative stress parameters

	AGA (n = 32)	SGA (n = 43)	*P* value
Maternal age, y	26 (22.2-30.8)	25 (23-29)	.751
Maternal height, cm	163 (159-168)	161 (155-165)	.222
Maternal weight, kg	76 (70.2-89.8)	73 (66-80)	.043
Multiparity, n	2 (1-2.75)	3 (1-3)	.864
Caesarean section, No. (%)	14 (43.8)	24 (55.8)	.424
Native thiol, µmol/L	355 ± 55.2	289 ± 60.2	**<.001**
Total thiol, µmol/L	382 ± 53.8	339 ± 63.9	**.004**
Disulfide, µmol/L	13.6 ± 5.25	24.9 ± 7.77	**<.001**
Disulfide/native thiol, %	3.99 ± 1.97	9.08 ± 4.27	**<.001**
Disulfide/total thiol, %	3.64 ± 1.61	7.50 ± 2.70	**<.001**
Native thiol/total thiol, %	92.6 ± 3.16	84.9 ± 5.38	**<.001**
IMA, ABSU	0.50 ± 0.06	0.435 ± 0.06	**<.001**
Albumin, g/dL	3.09 (2.69-3.49)	2.78 (2.28-3.23)	**.015**
Ferroxidase, U/L	295 (271-365)	288 (232-355)	.197
Catalase, U/L	101 ± 56.1	42.8 ± 41.6	**<.001**
Myeloperoxidase, U/L	80.1 ± 29	167 ± 44.6	**<.001**
TOS, mmol H2O2 Eq/L	10.05 (8-11.6)	10.8 (9.34-16.0)	**.035**
TAS, mmol Trolox	1.32 (1.26-1.43)	1.07 (0.937-1.30)	**<.001**
GSH, µmol/L	691 ± 84.1	628 ± 69.8	**.003**
GSH + GSSG, µmol/L	963 ± 131	1010 ± 175	.268
GSSG, µmol/L	128 ± 70.2	227 ± 60.1	**<.001**
Hemoglobin, g/dL	13.5 ± 2.04	13.3 ± 1.49	.622

AGA, appropriate for gestational age; GSH, glutathione; GSH + GSSG, total GSH; GSSG, oxidized GSH; IMA, ischemia-modified albumin; SGA, small for gestational age; TAS, total antioxidant status; TOS, total oxidant status.

.001, *P* = .003, and *P* = .002, respectively). The MPO activity and TOS levels were higher in SGA newborns than AGA newborns (*P* < .001 for both), whereas, TAS levels were lower in SGA newborns (*P* < .001), as shown in **TABLE 2**.

The GSH levels in the maternal AGA group were higher than in the maternal SGA group (*P* = .003). The GSSG levels in the maternal SGA group were higher relative to the maternal AGA group (*P* < .001). Hemoglobin levels were similar in the maternal AGA and SGA groups (*P* = .622) (**TABLE 1**).

The GSH and GSH+GSSG levels were higher among AGA newborns than SGA newborns (*P* = .011 and *P* = .001, respectively). In SGA newborns, GSSG levels were significantly increased compared with AGA newborns (*P* < .001). Hemoglobin levels were similar in AGA and SGA newborns (*P* = .778) (**TABLE 2**).

The directional relationships between anthropometric measurements and oxidative parameters in newborns are summarized in **TABLE 3**. Whereas GSH levels were not associated with birth weight, height, or head circumference (*P* > .05 for all), native thiol levels were positively correlated with birth weight and gestational age (*P* = .044 and *P* = .004, respectively). Additionally, oxidant molecules were negatively correlated with all anthropometric measurements.

Discussion

Dynamic thiol-disulfide homeostasis represents the levels of thiols (-SH groups) and disulfide bonds (-S-S) and can be measured in both intra- and extracellular compartments. This crucial homeostasis is influential on several physiologic processes, including maintenance of protein structure, regulation of enzyme activity and transcription, and chaperone functions. Dysregulation of thiol homeostasis is associated with the pathophysiology of various diseases.[17]

Our results showed that SGA was associated with oxidative stress in both newborns and their mothers. To our knowledge, this study is the first to assess oxidative stress in both SGA newborns and their mothers (after delivery) by measuring intra- and extracellular thiol homeostasis. We revealed that extracellular thiol-disulfide homeostasis was dysregulated in both SGA newborns and their mothers, as illustrated by decreased native and total thiol levels and increased disulfide levels. Recently, a study evaluating SGA newborns after delivery reported significantly decreased native and total thiol levels alongside increased disulfide levels, which show a shift in oxidative balance favoring oxidative stress in these newborns.[18] In parallel with our results, impaired oxidative balance was dominant in SGA newborns.[18] There are few studies about SGA and thiol-disulfide homeostasis in newborns with SGA and their mothers. However, some studies examined thiol-disulfide homeostasis in fetal growth restriction, implying an underlying mechanism for the development of oxidative stress. These studies briefly reported that impaired thiol-disulfide homeostasis was shown in patients with intrauterine growth restriction as demonstrated by lower native thiol and total thiol levels compared with controls; however, disulfide levels were similar.[19] Additionally, it has been reported that native thiol, total thiol, and disulfide levels were decreased in patients with fetal growth restriction,

TABLE 2. Comparison of AGA and SGA newborns groups with regard to anthropometric measurements, clinical and demographic characteristics, and oxidative stress parameters

	AGA (n = 32)	SGA (n = 43)	*P* value
Birth weight, g	3390 ± 473	2435 ± 491	**<.001**
Birth height, cm	50.42 ± 1.91	45.16 ± 1.29	**<.001**
Gestational age, wk	39.1 ± 1.2	38.2 ± 1.9	.328
Apgar 1 min	8 (7-9)	6 (6-8)	**<.001**
Apgar 5 min	10 (10-10)	9 (8-10)	**<.001**
Ponderal index	2.66 ± 0.30	2.68 ± 0.511	.867
Head circumstance, cm	34.5 (33.6-35.1)	33 (31.2-34)	**<.001**
Native thiol, μmol/L	366 ± 34.7	327 ± 41	**<.001**
Total thiol, μmol/L	400 ± 32.8	376 ± 36.8	**.008**
Disulfide, μmol/L	16.6 ± 6.29	24.8 ± 7.89	**<.001**
Disulfide/native thiol, %	5.72 ± 1.51	7.96 ± 3.81	**.003**
Disulfide/total thiol, %	5.10 ± 1.21	6.71 ± 2.51	**.002**
Native thiol/total thiol, %	89.8 ± 2.43	86.6 ± 5.04	**.002**
IMA, ABSU	0.413 ± 0.041	0.411 ± 0.058	.912
Albumin, g/dL	3.48 ± 0.41	3.27 ± 0.484	.052
Ferroxidase, U/L	58.9 (54.8-63.0)	57.1 (51.2-63.4)	.488
Catalase, U/L	93.7 (75.1-150)	86.1 (55.8-122.5)	.141
Myeloperoxidase ,U/L	79.1 ± 19.5	116 ± 32.6	**<.001**
TOS, mmol H2O2 Eq/L	12.08 (9.26-15.5)	17.01 (12.2-25)	**<.001**
TAS, mmol Trolox	1.47 (1.38-1.54)	1.10 (0.78-1.40)	**<.001**
GSH, μmol/L	801 ± 139	711 ± 118	**.011**
GSH + GSSG, μmol/L	1233 ± 166	1073 ± 163	**.001**
GSSG, μmol/L	126 ± 89.1	206 ± 67.1	**<.001**
Hemoglobin, g/dL	16.9 (15.5-18.1)	16.5 (15.9-18.1)	.778

AGA, appropriate for gestational age; GSH, glutathione; GSH + GSSG, total GSH; GSSG, oxidized GSH; IMA, ischemia-modified albumin; SGA, small for gestational age; TAS, total antioxidant status; TOS, total oxidant status.

TABLE 3. Correlation analyses between anthropometric characteristics and oxidative stress parameters in newborns

	Native thiol	Disulfide	MPO	CAT	TAS	TOS	Ferrox	GSH	GSSG
BW, g	*r* = 0.245 ***P* = .044**	*r* = –0.438 ***P* < .001**	*r* = –0.372 ***P* = .002**	*r* = 0.121 *P* = .316	*r* = 0.434 ***P* < .001**	*r* = –0.292 ***P* = .015**	*r* = 0.289 ***P* = .015**	*r* = 0.227 *P* = .089	*r* = –0.302 ***P* = .025**
BH, cm	*r* = 0.231 *P* = .058	*r* = –0.351 ***P* = .004**	*r* = –0.380 ***P* = .002**	*r* = 0.142 *P* = .238	*r* = 0.338 ***P* = .003**	*r* = –0.231 *P* = .057	*r* = 0.217 *P* = .071	*r* = 0.175 *P* = .193	*r* = –0.377 ***P* = .005**
GA, wk	*r* = 0.353 ***P* = .004**	*r* = –0.336 ***P* = .006**	*r* = –0.361 ***P* = .003**	*r* = 0.385 ***P* = .001**	*r* = 0.452 ***P* < .001**	*r* = –0.098 *P* = .444	*r* = 0.148 *P* = .224	*r* = 0.114 *P* = .412	*r* = –0.390 ***P* = .007**
HC, cm	*r* = 0.189 *P* = .123	*r* = –0.343 ***P* = .004**	*r* = –0.254 ***P* = .043**	*r* = 0.079 *P* = .512	*r* = 0.406 ***P* < .001**	*r* = –0.142 *P* = .246	*r* = 0.138 *P* = .256	*r* = 0.160 *P* = .234	*r* = –0.428 ***P* = .001**

BH, birth height; BW, birth weight; CAT, catalase; Ferrox, ferroxidase; GA, gestational age; GSH, glutathione; GSSG, oxidized GSH; HC, head circumference; MPO, myeloperoxidase; TAS, total antioxidant status; TOS, total oxidant status.

suggesting that the thiol content of the placenta could be insufficient to maintain optimum thiol-disulfide homeostasis.[20] We showed that intra-erythrocytic GSH homeostasis in SGA was dysregulated in both the mothers and the SGA newborns in our study. Whereas GSH levels were decreased, GSSG levels were significantly increased. In agreement with our study, a recent report quantified GSH and GSSG levels in intrauterine growth retardation patients. The authors showed decreased GSH-GSSG ratio, lower GSH-related antioxidant enzyme activity, and decreased gene transcriptions in patients with intrauterine growth retardation compared with healthy controls.[21]

During pregnancy, physiological changes due to increased demand for energy for the growing fetus causes excessive ROS production in the placenta. Especially after the second trimester, placenta tissue can adapt to environmental circumstances and, in concert with maternal antioxidant capacity, it can neutralize free radicals and lipid peroxidation.[22] Oxidative stress has been related to various clinical courses in pregnancy.[23] Unbalanced oxidative stress may cause poor pregnancy outcomes, as fetuses and newborns are prone to oxidative hazards due to the immaturity of their antioxidant defense systems.[24] We showed that oxidative indicators, including IMA, MPO, and TOS levels, were significantly

increased in SGA newborns and their mothers, except IMA levels, which were similar in SGA and AGA newborns. Throughout pregnancy, which is a physiologically oxidative state, maternal antioxidant systems gain importance for illuminating a possible relationship between SGA pathophysiology and oxidative stress. We measured some components of the antioxidant system, including CAT, ferroxidase activity, and TAS levels in serum. The CAT activity and TAS levels were significantly lower in the maternal SGA group; however, only TAS levels were lower in SGA newborns. Similarly, Gveric-Ahmetasevic et al[25] revealed that SGA newborns and their mothers had increased malondialdehyde (MDA) levels and decreased maternal antioxidant capacity. Elevated oxidative stress in SGA newborns and their mothers was sustained on the third day after delivery, suggesting that the lipid peroxidation caused by the placenta could have been primarily responsible for oxidative stress, and therefore, could be playing a role in SGA pathophysiology. Ashina et al[26] reported that SGA infants had higher reactive oxidative molecules than control infants. We showed that disulfide, GSSG, and TOS levels were negatively correlated with birth weight, birth length, and head circumference, whereas TAS levels had positive correlations with these parameters. Therefore, it can be stated that oxidative stress may be crucial player in SGA pathophysiology and severity of oxidative stress may result in smaller birth size. Another study has reported that SGA infants had elevated TOS, IMA, and MDA levels and decreased TAS levels compared with AGA infants.[27] The SGA infants, especially those with symmetric SGA, were under significant oxidative stress compared with AGA infants. They concluded that in utero and postnatal antioxidant protection were insufficient in SGA newborns, yielding increased oxidative stress due to several factors that could not be controlled.[27] In parallel with our findings, TOS levels in that study were higher in the maternal SGA group than in the maternal AGA group. Additionally, they suggested that IMA may be a useful marker for following-up SGA infants with regard to neurological developmental delay.[27] Rossi et al[28] found elevated IMA levels during the first trimester among pregnant women who delivered SGA newborns. Also, Papageorghiou et al[29] investigated the clinical importance of IMA in the pathophysiology of SGA and found elevated IMA levels in their maternal SGA group compared with AGA. They speculated that increased IMA might be a result of pregnancy-related oxidative stress.[29] In our study, IMA levels were significantly decreased in the maternal SGA group compared with the maternal AGA group. However, there were no significant differences between SGA and AGA newborns.

Pregnancy causes alterations in the mother's antioxidant defense systems. One of the most important immune cell types is the neutrophil, for both innate and adaptive immunity. An important study reported that MPO levels were similar in pregnant and nonpregnant women; however, they found that the localization of MPO was different.[30] In pregnant women, MPO activity accumulated at the neutrophil surface, whereas in nonpregnant women, MPO activity was localized primarily in the intracellular space of neutrophils. Differences in localization might cause variations in neutrophil functions between pregnant and nonpregnant women. Ceruloplasmin is responsible for the regulation of neutrophil function and regulates ROS production capacity in neutrophils during a healthy pregnancy.[31] In our study, MPO levels were found to be significantly higher in SGA newborns and their mothers; however, there was no significant difference between the AGA and SGA groups in terms of ferroxidase activities. Elevated MPO activity supports findings showing the presence of oxidative stress in SGA newborns and their mothers. Considering our results, it might be feasible to suggest that ferroxidase activity was insufficient to neutralize MPO activity in SGA newborns and their mothers. Lee et al[32] assessed the antioxidant defense system in their study comparing AGA and SGA infants. The SGA infants showed significantly diminished antioxidant activity, including CAT activity, GSH levels, and vitamins E and A. Similarly, it was reported that CAT and GSH peroxidase activities and the levels of vitamins E, C, and A were significantly decreased in the cord blood of SGA newborns compared with AGA newborns.[33]

It should be stated that there are some limitations in our study. Our results reveal dysregulated oxidative balance in both intra- and extracellular compartments at birth. However, if the same studies had been performed at later time points, it could have been more useful and might have demonstrated variations. Also, the lack of analysis of placenta tissue might be a limitation of our study design. However, the comparison of oxidative homeostasis using a novel concept that assesses thiol-disulfide and reduced or oxidized GSH levels concurrently through the measurement of intra- and extracellular thiol-GSH homeostasis in newborns with SGA and their mothers was a primary strength of the current study. To the best of our knowledge, this is the first study of its kind in the literature.

In conclusion, SGA newborns and their mothers appear to be affected by a considerably high level of oxidative stress. The enzymatic antioxidant system was similar among SGA and AGA newborns; however, nonenzymatic antioxidants (thiols, GSH, and total antioxidant levels) were significantly decreased in SGA. Also, oxidant molecules and enzymes were significantly higher in SGA newborns and their mothers. Intra- and extracellular homeostasis of thiols is a very important indicator for the redox state, and our results demonstrate that SGA is closely associated with impaired redox state and ineffective antioxidant defense systems.

Acknowledgments

The authors thank all participants for their contributions to our study.

Conflict of Interest Disclosure

The authors have nothing to disclose.

REFERENCES

1. Netchine I, Van Der Steen M, López-Bermejo A, Koledova E, Maghnie M. New horizons in short children born small for gestational age. *Front Pediatr.* 2021;9:655931. doi:10.3389/fped.2021.655931
2. Schlaudecker EP, Munoz FM, Bardají A, et al; Brighton Collaboration Small for Gestational Age Working Group. Small for gestational age: case definition & guidelines for data collection, analysis, and presentation of maternal immunisation safety data. *Vaccine.* 2017;35(48 pt A):6518-6528. doi:10.1016/j.vaccine.2017.01.040
3. Campisi SC, Carbone SE, Zlotkin S. Catch-up growth in full-term small for gestational age infants: a systematic review. *Adv Nutr.* 2019;10(1):104-111. doi:10.1093/advances/nmy091
4. He H, Miao H, Liang Z, et al. Prevalence of small for gestational age infants in 21 cities in China, 2014–2019. *Sci Rep.* 2021;11(1):1-10.
5. Hong YH, Chung S. Small for gestational age and obesity related comorbidities. *Ann Pediatr Endocrinol Metab*. 2018;23(1):4.
6. Hwang IT. Long-term care, from neonatal period to adulthood, of children born small for gestational age. *Clin Pediatr Endocrinol*. 2019;28(4):97-103. doi:10.1297/cpe.28.97

7. Phoswa WN, Khaliq OP. The role of oxidative stress in hypertensive disorders of pregnancy (preeclampsia, gestational hypertension) and metabolic disorder of pregnancy (gestational diabetes mellitus). *Oxid Med Cell Longev.* 2021;5581570.
8. Joo EH, Kim YR, Kim N, et al. Effect of endogenic and exogenic oxidative stress triggers on adverse pregnancy outcomes: preeclampsia, fetal growth restriction, gestational diabetes mellitus and preterm birth. *Int J Mol Sci.* 2021;22(18):10122.
9. Mohn A, Chiavaroli V, Cerruto M, et al. Increased oxidative stress in prepubertal children born small for gestational age. *J Clin Endocrinol Metab.* 2007;92(4):1372-1378. doi:10.1210/jc.2006-1344
10. Erel O, Neselioglu S. A novel and automated assay for thiol/disulphide homeostasis. *Clin Biochem.* 2014;47(18):326-332. doi:10.1016/j.clinbiochem.2014.09.026
11. Bradley PP, Christensen RD, Rothstein G. Cellular and extracellular myeloperoxidase in pyogenic inflammation. *Blood.* 1982;60(3):618-622.
12. Siotto M, Pasqualetti P, Marano M, et al. Automation of o-dianisidine assay for ceruloplasmin activity analyses: usefulness of investigation in Wilson's disease and in hepatic encephalopathy. *J Neural Transm Suppl.* 2014;121(10):1281-1286.
13. Goth L. A simple method for determination of serum catalase activity and revision of reference range. *Clin Chim Acta.* 1991;196(2-3):143-151. doi:10.1016/0009-8981(91)90067-m
14. Doumas BT, Watson WA, Biggs HG. Albumin standards and the measurement of serum albumin with Bromocresol green. *Clin Chim Acta.* 1971;31(1):87-96. doi:10.1016/0009-8981(71)90365-2
15. Bar-Or D, Lau E, Winkler JV. A novel assay for cobalt-albumin binding and its potential as a marker for myocardial ischemia—a preliminary report. *J Emerg Med.* 2000;19(4):311-315. doi:10.1016/s0736-4679(00)00255-9
16. Alisik M, Neselioglu S, Erel O. A colorimetric method to measure oxidized, reduced and total glutathione levels in erythrocytes. *J Lab Med*. 2019;43(5):269-277.
17. Erel O, Erdoğan S. Thiol-disulfide homeostasis: an integrated approach with biochemical and clinical aspects. *Turk J Med Sci*. 2020;50(SI-2):1728-1738. doi:10.3906/sag-2003-64
18. Buyuk GN, Kaplan ZAO, Sert UY, et al. Is there a relationship between the umbilical cord coiling index and oxidative stress markers and SGA fetuses? Coiling index and oxidative stress. *Med Sci Dis*. 2021;8(5):310-314.
19. Cetin O, Karaman E, Boza B, et al. The maternal serum thiol/disulfide homeostasis is impaired in pregnancies complicated by idiopathic intrauterine growth restriction. *J Matern Fetal Neonatal Med.* 2018;31(5):607-613. doi:10.1080/14767058.2017.1293025
20. Eroglu H, Turgal M, Senat A, Karakoc G, Neselioglu S, Yucel A. Maternal and fetal thiol/disulfide homeostasis in fetal growth restriction. *J Matern Fetal Neonatal Med.* 2021;34(10):1658-1665. doi:10.1080/14767058.2019.1646239
21. Aljaser FS, Ghneim HK, ALshubaily MM, et al. Glutathione and oxidized nicotinamide adenine dinucleotide ([NAD. sup.+]) redox status in plasma and placental tissue of Saudi patients with intrauterine growth restriction. *Saudi Med J.* 2021;42(5):491-498. doi:10.15537/smj.2021.42.5.20200685
22. Lu J, Wang Z, Cao J, Chen Y, Dong Y. A novel and compact review on the role of oxidative stress in female reproduction. *Reprod Biol Endocrinol.* 2018;16(1):1-18.
23. Zhai W, Yang S, Cui L. Anticardiolipin IgA as a potential risk factor for pregnancy morbidity in patients with antiphospholipid syndrome. *J Lab Med*. 2022;53(5):495-499.
24. Perrone S, Laschi E, Buonocore G. Biomarkers of oxidative stress in the fetus and in the newborn. *Free Radic Biol Med.* 2019;142:23-31. doi:10.1016/j.freeradbiomed.2019.03.034
25. Gveric-Ahmetasevic S, Sunjic SB, Skala H, et al. Oxidative stress in small-for-gestational age (SGA) term newborns and their mothers. *Free Radic Res.* 2009;43(4):376-384. doi:10.1080/10715760902783285
26. Ashina M, Kido T, Kyono Y, et al. Correlation between severity of fetal growth restriction and oxidative stress in severe small-for-gestational-age infants. *Int J Environ Res*. 2021;18(20):10726.
27. Tayman C, Öztekin O, Serkant U, Yakut I, Aydemir S, Kosus A. Ischemia-modified albumin may be a novel marker for predicting neonatal neurologic injury in small-for-gestational-age infants in addition to neuron-specific enolase. *Am J Perinatol.* 2017;34(4):349-358. doi:10.1055/s-0036-1588026
28. Rossi A, Bortolotti N, Vescovo S, et al. Ischemia-modified albumin in pregnancy. *Eur J Obstet Gynecol*. 2013;170(2):348-351.
29. Papageorghiou AT, Prefumo F, Leslie K, Gaze DC, Collinson PO, Thilaganathan B. Defective endovascular trophoblast invasion in the first trimester is associated with increased maternal serum ischemia-modified albumin. *Hum Reprod.* 2008;23(4):803-806. doi:10.1093/humrep/den029
30. Kindzelskii AL, Clark AJ, Espinoza J, et al. Myeloperoxidase accumulates at the neutrophil surface and enhances cell metabolism and oxidant release during pregnancy. *Eur J Immunol.* 2006;36(6):1619-1628. doi:10.1002/eji.200535391
31. Varfolomeeva EY, Semenova EV, Sokolov AV, et al. Ceruloplasmin decreases respiratory burst reaction during pregnancy. *Free Radic Res.* 2016;50(8):909-919. doi:10.1080/10715762.2016.1197395
32. Lee Y, Chou Y. Antioxidant profiles in full term and preterm neonates. *Chang Gung Med J.* 2005;28(12):846.
33. Mirzarahimi M, Ahadi A, Bohlooli S, Namakikhalajan E, Barak M. Antioxidant levels in cord blood of term neonates and its association with birth weight. *Iran. J Child Neurol*. 2016;10(1):31-34.

Insulin receptor substrate 2 gene Gly1057Asp polymorphism is a risk factor for nonalcoholic fatty liver disease

Shadi Nouri, MD[1], Touraj Mahmoudi, MS[2], Farzaneh Hojjati, MS[2], Zeinab Nourmohammadi Najafabadi, MD[3], Radmehr Shafiee, MD[4], Shiva Sayedsalehi, MD[2], Atefeh Dehghanitafti, MD[2], Abbas Ardalani, MS[2], Kiarash Kohansal, MD[5], Gholamreza Rezamand, MD[6,7], Asadollah Asadi, PhD[8], Hossein Nobakht, MD[9], Reza Dabiri, MD[9], Hamid Farahani, PhD[10], Seidamir Pasha Tabaeian, MD[6,7], Mohammad Reza Zali, MD[2]

[1]Department of Radiology, School of Medicine, Arak University of Medical Sciences, Arak, Iran, [2]Gastroenterology and Liver Diseases Research Center, Research Institute for Gastroenterology and Liver Diseases, Shahid Beheshti University of Medical Sciences, Tehran, Iran, [3]School of Dentistry, Isfahan University of Medical Sciences, Isfahan, Iran, [4]Department of Clinical Pathology, Faculty of Veterinary Medicine, Tehran University, Tehran, Iran, [5]Physiology Research Center, [6]Department of Internal Medicine, School of Medicine, and [7]Colorectal Research Center, Iran University of Medical Sciences, Tehran, Iran, [8]Department of Biology, Faculty of Science, University of Mohaghegh Ardabili, Ardabil, Iran, [9]Internal Medicine Department, Semnan University of Medical Sciences, Semnan, Iran, [10]Department of Physiology and Pharmacology, School of Medicine, Qom University of Medical Sciences, Qom, Iran. Corresponding author: Seidamir Pasha Tabaeian; noblautoumah@gmail.com

Key words: Gly1057Asp; insulin receptor substrate 2; IRS2; NAFLD; polymorphism; rs1805097

Abbreviations: NAFLD, nonalcoholic fatty liver disease; IRS2, insulin receptor substrate 2; NASH, nonalcoholic steatohepatitis; IR, insulin resistance; T2D, type 2 diabetes; IGF, insulin-like growth factor; SNV, single nucleotide variant; BMI, body mass index; PCR, polymerase chain reaction; RFLP, restriction fragment length polymorphism; HWE, Hardy-Weinberg equilibrium; PI3K-Akt, phosphatidylinositol 3 kinase (PI3K)-protein kinase B (AKT)

Laboratory Medicine 2024;55:215-219; https://doi.org/10.1093/labmed/lmad066

ABSTRACT

Objective: Nonalcoholic fatty liver disease (NAFLD), which is an emerging global chronic liver disease, has a close association with insulin resistance. We aimed to determine whether the Gly1057Asp (rs1805097) polymorphism of the insulin receptor substrate 2 (*IRS2*) gene is associated with NAFLD.

Methods: Using the polymerase chain reaction-restriction fragment length polymorphism method, 135 patients with biopsy-proven NAFLD and 135 controls underwent *IRS2* genotype analysis.

Results: Genotype and allele distributions of the *IRS2* gene Gly1057Asp variant conformed to the Hardy-Weinberg equilibrium in both the case and control groups ($P > .05$). The Asp/Asp genotype of *IRS2* gene Gly1057Asp polymorphism compared with Gly/Gly genotype was associated with a 2.1-fold increased risk for NAFLD after adjustment for confounding factors ($P = .029$; odds ratio = 2.10, 95% CI = 1.23-3.97).

Conclusion: Our findings revealed for the first time that the Gly1057Asp Asp/Asp genotype of the *IRS2* gene is a marker of increased NAFLD susceptibility; however, studies in other populations are required to confirm the results.

Introduction

Nonalcoholic fatty liver disease (NAFLD), which has recently become a major global health problem, is typified by ectopic lipid accumulation in the liver (more than 5% of hepatocytes) without excessive drinking. NAFLD ranges in severity from simple steatosis to nonalcoholic steatohepatitis (NASH), fibrosis, and cirrhosis. In spite of the high prevalence of NAFLD worldwide (approximately 1 in 4 adults), its exact pathogenesis has still largely remained unsolved.[1] However, previous research has demonstrated that insulin resistance (IR)[2,3] and obesity[4] are the main contributors in the etiology of NAFLD. NAFLD is also linked with type 2 diabetes (T2D),[4] hyperinsulinemia,[5] impaired glucose tolerance,[6] high deposition of visceral adipose tissue,[2] dyslipidemia,[4] and high blood pressure.[4] Peripheral IR modifies lipid metabolism, and visceral and peripheral fat content facilitates the generation of IR in the hepatocytes and NAFLD development.[3] Consistently, the intensity of IR in NASH patients is higher vs subjects with simple steatosis,[7] and NAFLD patients with IR have higher circulating liver enzymes than patients without IR.[8]

During insulin signaling, insulin binds to its receptor, insulin receptor, leading to its phosphorylation, which in turn results in the

phosphorylation and activation of the substrates of the insulin receptor or insulin receptor substrates (IRSs), including IRS2. This initiates a cascade of second messengers, such as PI3K and Akt, which eventually leads to the regulation of glucose and lipid metabolism. IRS2 is a scaffolding protein that is heavily involved in the insulin signaling pathway and in pancreatic β-cell development and survival. It controls downstream signaling of insulin-like growth factor 1 (IGF1) and its receptor. At molecular levels, the impairment of the IRS2- phosphatidylinositol 3 kinase (PI3K)-protein kinase B (AKT) pathway has a key role in hepatic IR.[9–11] The *IRS2* gene appears to be implicated in the development of some metabolic disorders; significant associations have been detected between single nucleotide variants (SNVs) in the *IRS2* gene and IR,[12] T2D,[13–15] and obesity.[16,17] Finally, significant associations between NAFLD risk and some polymorphisms in the insulin pathway genes of *INSR* and *IGF1* have been found.[5,18] This study aimed to determine the possible effect of the *IRS2* gene Gly1057Asp (rs1805097) variant on the susceptibility to NAFLD. This SNV was chosen on the basis of its usage in prior genetic association studies, its position in the gene, and its high degree of heterozygosity.

Materials and Methods

Study Population

A total of 270 genetically unrelated participants including 135 patients with biopsy-proven NAFLD (age range, 31-79 years) and 135 controls (age range, 30-76 years) were enrolled in this case-control study. The study protocol was permitted by the Ethics Committee of the Research Institute for Gastroenterology and Liver Diseases of Shahid Beheshti University of Medical Sciences (Tehran, Iran), and all the subjects were informed about the study's aim and their consent was obtained before entering the study. The study adhered to the principles of the Declaration of Helsinki and subsequent amendments. Self-administered questionnaires were used to obtain general characteristics of the participants who had the same ethnic background. In this study, NAFLD patients were enrolled on the basis of the following criteria for the diagnosis of NAFLD: (1) detection of hepatic steatosis on ultrasonography; (2) considerable rise in the circulating liver enzymes levels; (3) absence of secondary causes of hepatic fat accumulation, including history of alcoholism (alcohol intake of more than 70 g/week for women or 140 g/week for men), hepatitis B or hepatitis C virus infection, Wilson's disease, autoimmune hepatitis, or medication-induced liver steatosis; and (4) liver biopsy evidence of NAFLD provided by an experienced pathologist whose analyses of the biopsy samples were in accordance with Brunt's criteria. The grades of steatosis and necroinflammation were from 0 to 3, and the stages of fibrosis were from 0 to 4. We recruited the control group from students of Shahid Beheshti University of Medical Sciences or the staff of the Research Institute for Gastroenterology and Liver Diseases. The controls consisted of individuals without abnormalities in abdominal ultrasound imaging. They all had normal serum liver enzymes levels, and none of them had a viral hepatitis infection, were addicted to alcohol, or were prescribed regular medications. Body mass index (BMI) was computed as weight divided by height squared.[19,20]

SNV Genotyping

The laboratory assistants conducted the experiments blinded to the participants' clinical data. Peripheral venous blood (5 mL) was collected in anticoagulative tubes containing EDTA and kept refrigerated at 4°C. We extracted the DNA of each individual from their blood samples using phenol chloroform extraction and ethanol precipitation protocol and stored it at −20°C until use. Genotyping of the exon 1 variant of the Gly1057Asp in the *IRS2* gene was done by the polymerase chain reaction (PCR)-restriction fragment length polymorphism (RFLP) method. In brief, genomic DNA was amplified by using the primers 5'-AGCTCCCCCAAGTCTCCTAA-3' and 5'-GGCCACACCAAAAGCCATCT-3' to discover the genotypes of the *IRS2* gene. The PCR conditions were as follows: (1) predenaturation at 95°C for 10 minutes; (2) 35 cycles for denaturation at 95°C for 45 seconds, annealing at 59°C for 35 seconds, and extension at 72°C for 40 seconds; and (3) a final extension at 72°C for 10 minutes. We used a negative control for each experiment. The PCR products (291 bp) were then analyzed by using RFLP: overnight digestion with the restriction enzyme of HhaI (Fermentas) at 37°C in a water bath. Electrophoresis was performed on 3.5% agarose gel stained with ethidium bromide and then the RFLP products (291 bp, 221 bp, and 70 bp) were visualized using ultraviolet light transillumination. The Gly allele of the *IRS2* Gly1057Asp SNV had bands of 221 bp and 70 bp, whereas its Asp allele had a band of 291 bp; thus an individual with band(s) at 221 bp and 70 bp, at 291 bp only, or at 291 bp, 221 bp, and 70 bp was defined as the Gly/Gly homozygotic genotype, Asp/Asp homozygotic genotype, and Gly/Asp heterozygotic genotype, respectively. Fifteen percent of the samples were retested randomly to check the reproducibility of the genotyping.

Statistical Analysis

Data were analyzed by SPSS software, version 25.0. For comparing continuous variables, such as age and BMI, which were expressed as mean (SD), the Student *t*-test was used. To compare categorical clinical variables of sex and smoking status, which were presented as number (%), the χ^2 test was applied. Identified genotype distributions of the *IRS2* gene Gly1057Asp variant in the case and control groups were also analyzed separately using the χ^2 test to see if they met Hardy-Weinberg equilibrium (HWE) requirements. This test was used to assess the potential differences in the allele frequencies between the 2 groups. Logistic regression analysis was performed to evaluate the possible associations between the genotype frequencies and susceptibility to NAFLD as well as for adjusting confounding factors, including age, BMI, sex, smoking history, systolic blood pressure, and diastolic blood pressure. The odds ratios (ORs) with their 95% CIs were calculated to assess the strength of the genetic associations. A significant difference was defined as $P < .05$.

Results

The characteristics of the study population are described in **TABLE 1**. The age ($P < .001$), BMI ($P < .001$), smoking rate ($P = .036$), sex ratio (male-female) ($P < .001$), systolic blood pressure ($P < .001$), and diastolic blood pressure ($P < .001$) in the NAFLD group were significantly higher than those in the control group. Compared with the control subjects, the NAFLD patients had significantly higher serum levels of aspartate aminotransferase ($P < .001$), alanine aminotransferase ($P < .001$), and γ glutamyl transferase ($P < .001$).

TABLE 2 depicts the genotype and allele frequencies of the *IRS2* gene Gly1057Asp variant in the study population. Genotype and allele

TABLE 1. General characteristics of the populations studied[a]

Characteristics	Controls (n = 135)	Patients with NAFLD (n = 135)	*P* value[b]
Age, y	31.2 (7.1)	37.5 (9.0)	<.001
Body mass index, kg/m^2	25.3 (3.4)	28.8 (5.2)	<.001
Sex			
Male	73 (54.1)	95 (70.4)	
Female	62 (45.9)	40 (29.6)	<.001
Smoking			
No	119 (88.1)	106 (78.5)	
Former	9 (6.7)	14 (10.4)	
Current	7 (5.2)	15 (11.1)	.036
Systolic blood pressure, mmHg	115.0 (12.9)	122.6 (14.2)	<.001
Diastolic blood pressure, mmHg	68.8 (8.1)	73.5 (8.9)	<.001
Aspartate aminotransferase, IU/L	20.8 (7.6)	38.5 (17.0)	<.001
Alanine aminotransferase, IU/L	19.7 (10.2)	70.8 (38.6)	<.001
Gamma glutamyl transferase, IU/L	17.8 (7.7)	57.4 (30.5)	<.001
Steatosis			
Grade 0		-	
Grade 1		31 (23.0)	
Grade 2		75 (55.5)	
Grade 3		29 (21.5)	
Necroinflammation			
Grade 0		44 (32.6)	
Grade 1		43 (31.9)	
Grade 2		45 (33.3)	
Grade 3		3 (2.2)	
Fibrosis			
Stage 0		70 (51.8)	
Stage 1		54 (40.0)	
Stage 2		9 (6.7)	
Stage 3		2 (1.5)	
Stage 4		-	

NAFLD, nonalcoholic fatty liver disease.
[a]*Variables are presented as mean (SD) or number (%).*
[b]*P value less than .05 was considered statistically significant.*

distributions of this SNV conformed to the HWE test both in the case and control groups ($P > .05$). This implies that, in this study, we used a representative sample population. Analysis of the *IRS2* gene Gly1057Asp polymorphism showed a significant difference between the patients and the controls. The Asp/Asp genotype of *IRS2* gene Gly1057Asp variant compared to the Gly/Gly genotype was significantly more frequent in the cases with NAFLD than the controls even after adjustment for confounding factors such as age and BMI ($P = .029$; OR = 2.10, 95% CI = 1.23-3.97).

Discussion

In this study, we found further evidence of the role of *IRS2* gene in NAFLD. Carrying the Gly1057Asp Asp/Asp genotype of the *IRS2* gene was associated with a 2.1-fold rise in NAFLD risk.

TABLE 2. Insulin receptor substrate 2 (*IRS2*) gene rs1805097 polymorphism in patients with nonalcoholic fatty liver disease (NAFLD) and controls and logistic regression analysis[a]

IRS2 (rs1805097)	Controls (n = 135)	NAFLD (n = 135)	OR (95% CI)	*P* value[b]
Genotype-wise comparison				
GG	57 (42.2)	46 (34.1)	1.0 (reference)	
GA	61 (45.2)	62 (45.9)	1.33 (0.75-2.90)	.617
AA	17 (12.6)	27 (20.0)	2.10 (1.23-3.97)	.029
GA and AA	78 (57.8)	89 (65.9)	1.48 (0.67-3.24)	.208
AA vs others	17 (12.6)	27 (20.0)	1.71 (0.64-3.11)	.305
Allele-wise comparison				
G	175 (64.8)	154 (57.0)	1.0 (reference)	
A	95 (35.2)	116 (43.0)	1.36 (0.70-2.47)	.175

[a]*Variables presented as number (%).*
[b]*Adjusted for age, body mass index, sex, smoking history, systolic blood pressure, and diastolic blood pressure in genotype-wise comparisons.* P *value less than .05 was considered statistically significant.*

A better comprehension of NAFLD pathogenesis will assist in the development of personalized treatments. Search for NAFLD genes has remained challenging due largely to the fact that the nature of NAFLD is supposed to be multifactorial and it derives from the interactions between multiple genes and environmental factors. Detecting the genes, however, is difficult due to, for example, the observed inconsistencies in association studies, which in turn stem from diversity in disease definition, diet, lifestyle, genetic background, or statistical analyses.[21–24] Familial clustering and ethnic diversity in NAFLD prevalence are due to genetic predisposition to the disease. Considering the fact that IR and obesity are very often among the main characteristics of NAFLD and IR is the key mechanism in the development and progression of NAFLD, the genes involved in IR are presumably candidate genes for NAFLD. The insulin signaling pathway regulates metabolism of lipids, and IR is closely linked to hepatic lipid accumulation and advanced fibrosis in NAFLD patients. IRS2 has a key role in the proximal insulin pathway, regulation of glucose homeostasis, and control of bodyweight.[25,26]

To date, there is only 1 study that investigated the role of the *IRS2* gene in susceptibility to NAFLD. Dabiri et al[27] showed that the rs2289046 3'-UTR polymorphism of the *IRS2* gene might contribute to the pathogenesis of NAFLD. In accordance with their finding, this study suggested that the Asp/Asp genotype of the *IRS2* gene Gly1057Asp variant was a risk factor for NAFLD when compared with the Gly/Gly genotype. The *IRS2* gene is located on chromosome 13q34 with numerous polymorphisms, including Gly1057Asp, which is a common nonsynonymous SNV with significant associations with various diseases. The Gly1057Asp variant causes an amino acid substitution of Gly to Asp at codon 1057 in the *IRS2* gene. Apparently, this amino acid substitution, which is in the proximity of 2 putative tyrosine phosphorylation sites at positions 1042 and 1072, may make a change to the tertiary structure and function of the IRS2 protein, which in turn leads to impaired signal transduction. Thus, this SNV, by introducing a charged amino acid (Asp) in place of a neutral one (Gly), may affect the insulin signaling pathway and alter the downstream signaling through IRS2.[14,28] Prior investigations have also indicated that subjects with the

Gly1057Asp polymorphism have a higher grade of obesity-independent IR[12] and reduced pancreatic β-cell function.[15] The Gly1057Asp variant interacts with obesity to affect pancreatic β-cell function and under conditions of obesity or high circulating levels of nonesterified fatty acids, has a detrimental effect on β-cells.[29] In comparison with the Gly/Gly+Gly/Asp genotype, the Asp/Asp genotype of the Gly1057Asp variant increases the susceptibility to T2D by interacting with obesity.[14,15] Individuals with the Asp/Asp genotype also have a higher serum C-peptide concentration, which is probably linked to lower insulin sensitivity.[13] Consistent with the above literature, we showed that the *IRS2* Gly1057Asp Asp/Asp genotype was a risk factor for NAFLD. More evidence corroborates the hypothesis that IRS2 might be involved in NAFLD pathogenesis. Insulin resistance with deficiency of IRS2-associated PI3K activity leads to a rise in intracellular fatty acid-derived metabolites. Metformin, by ameliorating the hepatic IRS2-PI3K-Akt pathway improves IR. Eugenol, which has hepatoprotective, anti-hyperglycemic, and anti-inflammatory properties, modulates insulin sensitivity and improves IR by upregulating IRS2 in rats with NAFLD. Previous reports have also demonstrated that the effects of miR-190b as a microRNA on IR is mediated via IRS2-PI3K-Akt signaling.[11,30] IRS2 also participates in preadipocyte differentiation through the upregulation of specific transcriptional factors like peroxisome proliferator-activated receptor γ.[17] Finally, the disruption of IRS2 in knockout mice results in metabolic defects in liver, hepatic IR, fatty acid accumulation in hepatic cells, steatosis, beta-cell failure, reduced β-cell mass and insulin secretion, and diabetes.[9,11,15,28,29] Consequently, there is accumulating evidence suggesting that the *IRS2* gene might contribute to NAFLD development and progression; however, the mechanism of action remains to be clarified by further research.

Some limitations of this study must be reported. A limitation is that circulating concentrations of insulin and glucose as well as sufficient genetic marker sites were not obtained; this was because of limited funding. The other limitation of this study was its modest sample size, also mostly due to budget limitations. The strengths of this report also warrant attention. The design was good and multicenter research was carried out. In addition, the gold standard method (liver biopsy) was applied and NAFLD diagnosis was not based primarily on ultrasonographic results. Finally, this study put forward some interesting and novel findings that were in accordance with prior publications.

In summary, the Gly1057Asp Asp/Asp genotype of the *IRS2* gene might predict susceptibility to NAFLD, but future larger studies are needed to confirm this finding.

Acknowledgments

The authors thank all patients and healthy blood donors for providing blood samples.

Funding

This study was funded by the Gastroenterology and Liver Diseases Research Center, Shahid Beheshti University of Medical Sciences (grant number 1425).

Conflict of Interest Disclosure

The authors have nothing to disclose.

REFERENCES

1. Lazarus JV, Mark HE, Villota-Rivas M, et al; for the NAFLD Policy Review Collaborators. The global NAFLD Policy Review and Preparedness index: are countries ready to address this silent public health challenge? *J Hepatol.* 2022;76(4):771-780. doi:10.1016/j.jhep.2021.10.025
2. Eguchi Y, Eguchi T, Mizuta T, et al. Visceral fat accumulation and insulin resistance are important factors in nonalcoholic fatty liver disease. *J Gastroenterol.* 2006;41(5):462-469. doi:10.1007/s00535-006-1790-5
3. Kosmalski M, Ziółkowska S, Czarny P, Szemraj J, Pietras T. The coexistence of nonalcoholic fatty liver disease and type 2 diabetes mellitus. *J Clin Med*. 2022;11(5):1375. doi:10.3390/jcm11051375
4. Guo X, Yin X, Liu Z, Wang J. Non-alcoholic fatty liver disease (NAFLD) pathogenesis and natural products for prevention and treatment. *Int J Mol Sci* . 2022;23(24):15489. doi:10.3390/ijms232415489
5. Nobakht H, Mahmoudi T, Sabzikarian M, et al. Insulin and insulin receptor gene polymorphisms and susceptibility to nonalcoholic fatty liver disease. *Arq Gastroenterol.* 2020;57(2):203-208. doi:10.1590/S0004-2803.202000000-39
6. Hatziagelaki E, Karageorgopoulos DE, Chounta A, Tsiavou A, Falagas ME, Dimitriadis G. Predictors of impaired glucose regulation in patients with non-alcoholic fatty liver disease. *Exp Diabetes Res.* 2012;2012:351974. doi:10.1155/2012/351974
7. Chung J, Park HS, Kim YJ, Yu M-H, Park S, Jung S-I. Association of hepatic steatosis index with nonalcoholic fatty liver disease diagnosed by non-enhanced CT in a screening population. *Diagnostics (Basel)*. 2021;11(12):2168. doi:10.3390/diagnostics11122168
8. Liu C, Shao M, Lu L, Zhao C, Qiu L, Liu Z. Obesity, insulin resistance and their interaction on liver enzymes. *PLoS One.* 2021;16(4):e0249299. doi:10.1371/journal.pone.0249299
9. Withers DJ, Gutierrez JS, Towery H, et al. Disruption of IRS-2 causes type 2 diabetes in mice. *Nature.* 1998;391(6670):900-904. doi:10.1038/36116
10. Mahmoudi T, Majidzadeh-A K, Karimi K, et al. An exon variant in insulin receptor gene is associated with susceptibility to colorectal cancer in women. *Tumour Biol.* 2015;36(5):3709-3715. doi:10.1007/s13277-014-3010-x
11. Fawzy MH, Saeed NM, El-Sherbiny DA, El-Demerdash E. Eugenol modulates insulin sensitivity by upregulating insulin receptor substrate-2 in non-alcoholic fatty liver disease in rats. *J Pharm Pharmacol.* 2021;73(6):846-854. doi:10.1093/jpp/rgab032
12. Mazzoccoli G, Dagostino MP, Fontana A, et al. Influence of the Gly1057Asp variant of the insulin receptor substrate 2 (IRS2) on insulin resistance and relationship with epicardial fat thickness in the elderly. *Exp Gerontol.* 2012;47(12):988-993. doi:10.1016/j.exger.2012.09.005
13. Mammarella S, Romano F, Di Valerio A, et al. Interaction between the G1057D variant of IRS-2 and overweight in the pathogenesis of type 2 diabetes. *Hum Mol Genet.* 2000;9(17):2517-2521. doi:10.1093/hmg/9.17.2517
14. Bodhini D, Radha V, Deepa R, et al. The G1057D polymorphism of IRS-2 gene and its relationship with obesity in conferring susceptibility to type 2 diabetes in Asian Indians. *Int J Obes (Lond).* 2007;31(1):97-102. doi:10.1038/sj.ijo.0803356
15. Barbieri M, Rizzo MR, Papa M, et al. The IRS2 Gly1057Asp variant is associated with human longevity. *J Gerontol A Biol Sci Med Sci.* 2010;65(3):282-286. doi:10.1093/gerona/glp154
16. Lautier C, El Mkadem SA, Renard E, et al. Complex haplotypes of IRS2 gene are associated with severe obesity and reveal heterogeneity in the effect of Gly1057Asp mutation. *Hum Genet.* 2003;113(1):34-43. doi:10.1007/s00439-003-0935-3
17. Muñoz AM, Velásquez CM, Agudelo GM, et al. Examining for an association between candidate gene polymorphisms in the metabolic syndrome components on excess weight and adiposity measures in

youth: a cross-sectional study. *Genes Nutr.* 2017;12:19. doi:10.1186/s12263-017-0567-1

18. Sabzikarian M, Mahmoudi T, Tabaeian SP, et al. The common variant of rs6214 in insulin like growth factor 1 (IGF1) gene: a potential protective factor for non-alcoholic fatty liver disease. *Arch Physiol Biochem*. 2023;129(1):10-15. doi:10.1080/13813455.2020.1791187
19. Brunt EM, Janney CG, Di Bisceglie AM, Neuschwander-Tetri BA, Bacon BR. Nonalcoholic steatohepatitis: a proposal for grading and staging the histological lesions. *Am J Gastroenterol.* 1999;94(9):2467-2474. doi:10.1111/j.1572-0241.1999.01377.x
20. Mahmoudi T, Karimi K, Karimi N, et al. Association of adiponectin receptor 1 gene - 106 C > T variant with susceptibility to colorectal cancer. *Meta Gene*. 2016;9:210-214. doi:10.1016/j.mgene.2016.07.008
21. Houshmand M, Mahmoudi T, Panahi MS, Seyedena Y, Saber S, Ataei M. Identification of a new human mtDNA polymorphism (A14290G) in the NADH dehydrogenase subunit 6 gene. *Braz J Med Biol Res.* 2006;39(6):725-730. doi:10.1590/s0100-879x2006000600004
22. Mahmoudi T, Arkani M, Karimi K, et al. The -4817 G>A (rs2238136) variant of the vitamin D receptor gene: a probable risk factor for colorectal cancer. *Mol Biol Rep.* 2012;39(5):5277-5282. doi:10.1007/s11033-011-1325-x
23. Nikzamir A, Esteghamati A, Hammedian AA, Mahmoudi T. The role of vascular endothelial growth factor +405 G/C polymorphism and albuminuria in patients with type 2 diabetes mellitus. *Mol Biol Rep.* 2012;39(2):881-886. doi:10.1007/s11033-011-0812-4
24. Mahmoudi T, Majidzadeh-A K, Karimi K, et al. Gly972Arg variant of insulin receptor substrate 1 gene and colorectal cancer risk in overweight/obese subjects. *Int J Biol Markers.* 2016;31(1):e68-e72. doi:10.5301/jbm.5000159
25. Fujii H, Imajo K, Yoneda M, et al; for the Japan Study Group of Non-alcoholic Fatty Liver Disease. HOMA-IR: an independent predictor of advanced liver fibrosis in nondiabetic non-alcoholic fatty liver disease. *J Gastroenterol Hepatol.* 2019;34(8):1390-1395. doi:10.1111/jgh.14595
26. Jian T, Yu C, Ding X, et al. Hepatoprotective effect of seed coat of *Euryale ferox* extract in non-alcoholic fatty liver disease induced by high-fat diet in mice by increasing IRs-1 and inhibiting CYP2E1. *J Oleo Sci.* 2019;68(6):581-589. doi:10.5650/jos.ess19018
27. Dabiri R, Mahmoudi T, Sabzikarian M, et al. A 3'-untranslated region variant (rs2289046) of insulin receptor substrate 2 gene is associated with susceptibility to nonalcoholic fatty liver disease. *Acta Gastroenterol Belg.* 2020;83(2):271-276.
28. Hu Y, Zhou M, Zhang K, et al. Lack of association between insulin receptor substrate2 rs1805097 polymorphism and the risk of colorectal and breast cancer: a meta-analysis. *PLoS One.* 2014;9(1):e86911. doi:10.1371/journal.pone.0086911
29. Stefan N, Fritsche A, Machicao F, Tschritter O, Häring HU, Stumvoll M. The Gly1057Asp polymorphism in IRS-2 interacts with obesity to affect beta cell function. *Diabetologia.* 2004;47(4):759-761. doi:10.1007/s00125-003-1302-6
30. Xu M, Zheng XM, Jiang F, Qiu W-Q. MicroRNA-190b regulates lipid metabolism and insulin sensitivity by targeting IGF-1 and ADAMTS9 in non-alcoholic fatty liver disease. *J Cell Biochem.* 2018;119(7):5864-5874. doi:10.1002/jcb.26776

The identification of diurnal variations on circulating immune cells by finger prick blood sampling in small sample sizes: a pilot study

Dayna Bushell, BMedSci[1], Jonathan Kah Huat Tan, PhD[2], Jessica Smith, BMedSci[2], Christian Moro, MBus, PhD[1,]

[1]Faculty of Health Sciences and Medicine and [2]Clem Jones Centre for Regenerative Medicine, Bond University, Robina, Australia. Corresponding author: Christian Moro; cmoro@bond.edu.au

Key words: T cells; variations; blood; lymphocytes; physiology; clinical

Abbreviations: FITC, fluorescein isothiocyanate; PBS, phosphate buffered saline; PerCp-Cy5.5, peridinin chlorophyll protein-cyanine5.5; PE, phycoerythrin

Laboratory Medicine 2024;55:220-226; https://doi.org/10.1093/labmed/lmad062

ABSTRACT

Objective: There are well-described impacts of biological rhythms on human physiology. With the increasing push for routine blood tests for preventative medical care and clinical and physiological research, optimizing effectiveness is paramount. This study aimed to determine whether it is feasible to assess diurnal variations of peripheral lymphocyte prevalence using finger prick blood in a small sample size.

Methods: Using polychromatic flow cytometry, the prevalence of lymphocytes was assessed using 25 µL fingertip blood samples at 8 AM and 5 PM from 8 participants.

Results: TH cells and B cells showed significantly higher percentages in the 5 PM samples, whereas NK cells demonstrated a significantly higher morning percentage. T cells, leukocytes, and cytotoxic T cells showed no significant changes.

Conclusion: The detection of diurnal variations demonstrates that small blood volumes can be used to detect lymphocyte variations. The lower blood volume required provides a new testing method for clinical and research settings.

Introduction

Diurnal Variation

Many physiological events, including immune responsiveness, are linked to the circadian rhythm. Diurnal changes are a form of biological rhythms that show variations synchronized with the time of day.[1,2] Diurnal variation is observed across many areas in human physiology and immunology, including hormone secretion and heart rate.[3-7] In addition to physiological responses, diurnal variation can also be observed in individual cells. Circulating blood leukocyte counts have demonstrated peak numbers in humans, mice, rats, and hamsters during the behavioral rest phases.[8-12] The diurnal pattern of leukocytes in murine models has been linked to the egress of cells from hematopoietic organs into the blood and the immigration of cells to peripheral organs.[9,13] The same molecular mechanism for the cell-intrinsic clock is present in both innate and adaptive murine, rat, and human immune cells.[14-20]

Volume of Blood Commonly Used in the Assessments of Physiological Diurnal Variation

Previous studies of physiological lymphocyte diurnal variation have predominantly used venipuncture to assess cell prevalence. An early study by Miyawaki et al[21] used 2 mL of blood drawn via syringe from the medial cubital vein for each timepoint. More recent studies by Boukelia et al[22] and Beam et al[23] used similar volumes of 8 mL and 5.5 mL, respectively, drawn using venipuncture. The studies by Lévi et al[24] and Mazzoccoli et al[25] used larger venous blood draws of 40 mL and over 100 mL, respectively. Other studies have not specified the volume drawn and used but have stated that venipuncture was used to collect peripheral blood samples.[26,27]

Blood Testing

There is an increasing use of blood testing in medical practice, extending beyond solely diagnosis, with emphasis also on preventative medicine. In normal practice, a relatively large volume of blood is drawn (usually >10 mL). However, modern machines and testing equipment have become so precise that volumes in the microliters are all that is required for widespread assessments. This means future blood testing may draw far less blood, making tests faster and with less impact on patients. In addition, small volumes of blood can be assessed from finger-prick, from

TABLE 1. Summary of reagents from the IMK Simultest Kit

Reagent	Specificity	Clone	Conjugation	Cell ID	Concentration (µg/mL)
A	CD45	2D1	FITC	Leucocytes	2.5
	CD14	MφP9	PE	Monocytes	12.5
B	IgG1	X40	FITC	Nonspecific Fc receptors	12.5
	IgG2a	X39	PE	Nonspecific Fc receptors	12.5
C	CD3	SK7	FITC	CD3/TCR	25
	CD19	4G7	PE	B cell	3.1
D	CD3	SK7	FITC	CD3/TCR	25
	CD4	SK3	PE	Helper T4 cell	1.5
E	CD3	SK7	FITC	CD3/TCR	25
	CD8	SK1	PE	Cytotoxic T8 cell	6.25
F	CD3	SK7	FITC	CD3/TCR	25
	CD16	B73.1	PE	NK cell and neutrophil	6.25
	CD56	MY31	PE	All NK cells and 5% of CD3 cells	12.5

FITC, fluorescein isothiocyanate; NK, natural killer; PE, phycoerythrin.

the ear, or other accessible points on the patient's extremities.[28] This will be less painful and a safer and easier process than the normal use of venipuncture. Furthermore, there is a possibility that time of day may affect the interpretation of peripheral lymphocytic assessments, as the prevalence of lymphocytes may vary in peripheral blood. Although both lymphocyte detection in small blood samples from large sample sizes[29] and lymphocyte diurnal variation have been established, it has not been determined whether significant variations in lymphocyte prevalence can be detected through small blood volume samples in a small sample size. As such, by determining whether a variation can be detected using small, finger prick blood samples, the methodology for clinical blood tests and physiological research can be improved, leading to better participant acceptability, a less invasive sampling technique, and an increased understanding of normal variations in lymphocytes.

Study Rationale

The time of day is often a consideration in both human population biology research and clinical assessments of allergies, autoimmune diseases, and immune-mediated inflammatory issues. However, when coupled with physiological analyses, this is often performed by drawing relatively larger volumes of serum and blood than required by the testing equipment and methods. The aim of this study was to assess whether this diurnal variation can be detected in small-volume blood draws from a small sample size and whether this is a potential future technique for the assessment of immune cells. The identification of these variations in small, finger-prick blood volumes will expand on the current literature surrounding lymphocyte diurnal variations and provide information on whether they are an important factor in finger-prick blood collections in both clinical practice and laboratory research. The outcome will be whether it is feasible for a finger-prick volume of blood to be taken and assessed in place of typical venipuncture volumes, leading to improvements in blood draw methodology and contributing to the current research into physiological diurnal variation.

Materials and Methods

Participants were recruited from a local university and all aged between 18 and 25 years. Eight healthy volunteers participated (5 males and 3 females), with blood samples being taken from each person at 2 time points, 8 AM and 5 PM, on the same day. Unlike red blood cell testing, pathology laboratories and blood test reference ranges do not take the patient's sex into account for the assessment of lymphocytes.[30] As such, males and females were grouped in this study. This number of subjects and the practice of merging sexes for white blood cell analyses are also commensurate with similar recent research in this area.[22,23,31]

Participants were not required to fast. During the collection procedure, participants had warm water applied to their fingertips to increase localized blood flow, and this was allowed to dry. A minimum of 225 µL of finger-prick blood was collected using safety lancets into two 200-µL Microvette, K3 EDTA tubes (Sarstedt Group). When possible, all collection was completed using a single fingertip. An IMK Simultest: Lymphocyte Kit (Becton Dickinson) was used for analysis with a methodology adapted from the relevant manual volume (BD Biosciences) to account for the reduced blood. Although other reagents are available, this kit is a commonly used and commercially available kit, with a long shelf life and ready-to-use reagents to conduct lymphocyte assessments. **TABLE 1** outlines the reagents provided with the kit. Additionally, 2 single stain controls were used, CD11a fluorescein isothiocyanate (FITC) mouse anti-human antibody (Ex_{max} 494 nm/Em_{max} 520 nm) and CD86 phycoerythrin (PE) mouse anti-human antibody (Ex_{max} 496 nm/Em_{max} 578 nm). To account for the lower blood volume, all volumes stated in the manual were divided by 4, resulting in 25 µL blood and 5 µL reagent. Following conjugate antibody staining for 20 minutes at room temperature, red blood cells were lysed for 10 minutes at room temperature using 500 µL 10x red blood cell lysing solution. After centrifugation (4°C at 200*g*) and discarding the supernatant, the samples were washed with 500 µL phosphate buffered saline (PBS) (Sigma Life Sciences). Following centrifugation and discarding the supernatant, samples were resuspended in 125 µL solution (PBS without calcium, chloride, or magnesium, with 2% fetal bovine serum and 0.1% sodium azide). All samples, excluding unstained, and FITC and PE were mixed with 2 µL of propidium iodide.

Flow Cytometry

Samples were analyzed on a BD FACSVerse cytometer (Becton Dickinson). Gating and compensation were conducted using FlowJo v10.8.1 software (Becton Dickinson). Lymphocyte gating was conducted individually for

FIGURE 1. **Gating method for samples. A, Lymphocytes are first selected based on forward scatter area (FSC-A) and side scatter area (SSC-A) parameters. B, Peridinin chlorophyll protein-cyanine5.5 (PerCp-Cy5.5) vs FSC-A dot plot showing gating for live cells following lymphocyte gating. Singlet gating is performed using FSC-weight (W) vs FSC-height (H) dot plots (C) and SSC-W vs SSC-H dot plots (D). E-J, Cell staining examples using fluorescein isothiocyanate (FITC) and phycoerythrin (PE) conjugated antibodies for one participant following lymphocyte, live cell, and singlet gating.**

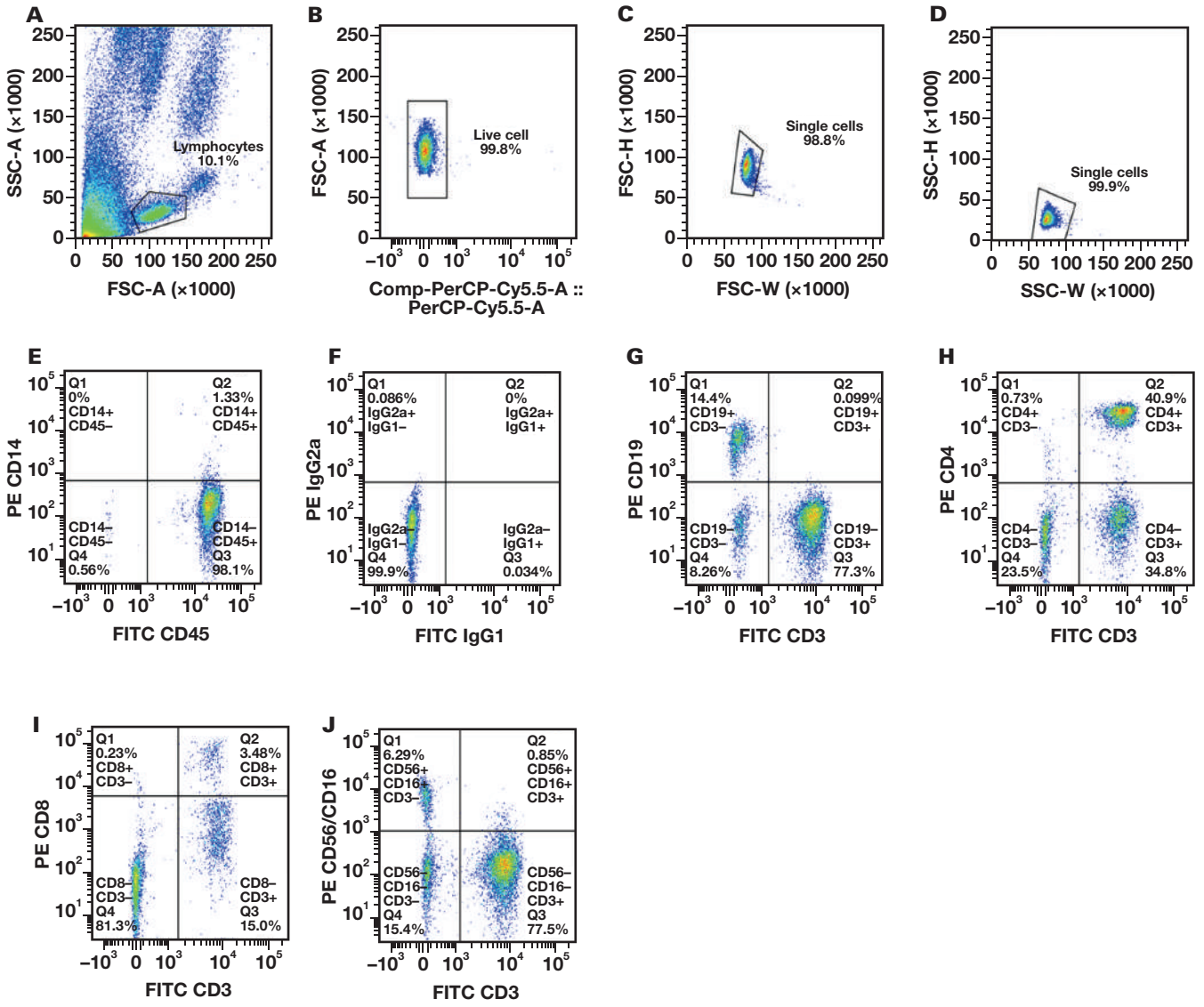

each participant with forward scatter-area (FSC-A)/side scatter-area (SSC-A) parameters. Propidium iodide live/dead cell gating using propidium iodide conjugated with peridinin chlorophyll protein-cyanine5.5 (PerCp-Cy5.5) (Ex_{max} 482 nm/Em_{max} 695 nm) was next performed with FSC-A/ PerCp-Cy5.5 parameters. Finally, singlet gating was conducted using sequential forward scatter-height/forward scatter-width and side scatter-height/side scatter-width gates. Samples were then analyzed using FITC and PE quadrants to identify surface markers and cell type.

Statistics

Data collected from this study was analyzed using Prism v9 (GraphPad Software). A paired Student 2-tailed *t*-test was used to analyze the morning and afternoon lymphocyte prevalence counts. A *P* value of less than .05 was considered significant.

Ethics

Ethics was approved by the university human research ethics committee. A written explanatory statement was provided to all participants involved, outlining the details of the project, methods of data collection, analysis confidentiality and the contact details of the study supervisor for any potential queries. Written informed consent was also obtained from all participants before the collection of the morning blood sample.

Results

Both volumes of blood, 100 µL and 25 µL were processed by the flow cytometer without error. **FIGURE 1** demonstrates an example of the gating technique used for a 25 µL sample.

TABLE 2. Comparison reference ranges (BD Biosciences IMK Simultest Lymphocyte manual) and original (100 µL) vs modified (25 µL) methodologies as percentages of total gated lymphocytes[a]

	100 µL	25 µL	95% Reference range
CD3+ (T) cell, %	62.1	60.9	72 (59-85)
$CD3^+CD4^+$ (T-helper) cell, %	35.1	35.1	46 (31-61)
$CD3^+CD8^+$ (cytotoxic) T cell, %	29.7	23.8	25 (11-38)
$CD4^+/CD8^+$ cell ratio, %	1.8	1.5	1.9 (0.9-3.6)
$CD19^+$ (B) cell, %	8.59	10.6	13 (6.4-23)
$CD16^+ 56^+$ (NK) cell, %	9.26	6.61	14 (5.6-31)

[a]*Samples taken from 1 participant. Reference ranges obtained from BD Biosciences IMK manual.*

Assessment of Low-Volume (25 µL/Reagent) Blood Compared With Standard Practice (100 µL/Reagent)

An initial assessment using a single volunteer was completed to confirm the viability of using a smaller volume of blood based on the premise outlined in the study by Moro et al.[28] Both 100 µL and 25 µL of blood reported similar results within the reference ranges (**TABLE 2**). As such, from this point, the smaller volume of blood was used to assess diurnal variation.

Assessment of Diurnal Variation

Helper T cells (CD4+) showed a significantly ($P = .0023$) higher percentage in the afternoon sample, with a mean difference between the morning and afternoon samples of 10.48% (n = 8, **FIGURE 2**). B cells (CD19+) showed a significantly ($P = .0123$) higher percentage in the afternoon sample with a mean difference of 4.62% (n = 7). NK cells (CD56+/CD16+) showed a significantly higher percentage in the morning ($P = .0462$) with a mean difference of 1.64% (n = 8). Lymphocytes (CD3+) showed no significant difference between samples (n = 8). T cells (CD3+) (n = 7) and cytotoxic T cells (CD8+) (n = 8) also showed no significant changes.

Discussion

Feasibility and Use of Low-Volume Blood Collection Methods

Typical assessment using a BD Biosciences IMK Simultest Lymphocyte Kit use 100 µL blood per reagent, totaling a minimum collection of 900 µL, excluding potential clotting, in comparison to the adapted methodology of 25 µL per reagent, totaling a minimum of 225 µL. Collecting over 900 µL of blood is not viable from a finger-prick, requiring venipuncture. In comparison, 225 µL blood can be collected from a fingertip blood sample before clotting occurs. Although this study investigated the effect of diurnal variation on lymphocytes, the successful use of fingertip blood to assess the prevalence and variation of these cells demonstrates a potential new technique for peripheral lymphocytic assessments. Furthermore, this study also demonstrates that this technique is feasible to detect significant variations in lymphocyte prevalence with a small sample size. Although previous studies are largely dated and present varying results, the significant variations detected do correlate with some previous results with 2 circadian assessments determining significant B-cell peaks in the afternoon and evening.[23,31] However, 1 of these studies attributed the changes to individual variations, rather than circadian variation,[23] requiring further research to establish the effect of diurnal variation on B-cell levels. Five of 7 studies also demonstrated that helper T cells predominantly display peaks in the afternoon and late evening.[23,31-33] The lack of significance present in T cells, cytotoxic T cells, and general lymphocyte levels may occur due to small sample sizes and as such, further research is needed to determine whether these variations can be detected accurately using this method. This demonstrates that this technique can accurately detect daily variations in B cells and helper T cells, in line with the literature, within a small sample size.

For similar applications in science and medicine, where blood draws from small groups are required, this technique can be used to identify variations in lymphocyte counts. For people adverse to venipuncture, the use of finger-prick blood sampling may present a less invasive method of analyzing immune cell levels. In addition to general fears of venipuncture, there are several reported complications with this method,[34] meaning that the use of low-volume blood collection methods presents a safer technique for blood collections, especially in situations where a person is having to undergo frequent or routine blood draws. Additionally, there are many groups of the population where venipuncture is not appropriate. For example, people who put regular strain on their arms, such as kayakers and weightlifters, may not be able to use venipuncture and as such finger-prick blood collections for immunological assessments may be far more appropriate.[28] Although there are limited opportunities for venipuncture around the body, the need to only require 25 µL of blood for each cell of interest opens far more locations for blood extraction in the body, including from fingertips, toes, and ears. Therefore, the ability for lower volumes of blood to conduct peripheral lymphocytic assessments, even in limited sample sizes, provides a new, minimally invasive method which can be used in future studies of peripheral immunological assessments or in clinical settings where blood tests are commonplace.

Potential Importance of Diurnal Variation

Although it is unclear whether diurnal variation of lymphocytes presents any biological significance, diurnal variation is a methodological problem in both population biology and clinical biology. In population biology, daily variations of immune cells can lead to variances in results, which do not relate to the topic being studied. The significant variations seen in this study from a small sample size also highlight potential impacts on some clinical tests, such as those that analyze lymphocyte prevalence to monitor HIV and lymphoma progression and treatment. As such, blood draws in a clinical setting should consider time of day in these assessments to ensure accurate interpretation of peripheral lymphocyte results. The immunological roles of lymphocytes may correspond with the variations that were observed. The increase of

FIGURE 2. Individual values and mean ± SEM (line) for morning (9 AM) and afternoon (5 PM) blood samples (A, C, E, F: n = 8; B, D: n = 7). ns, not-significant, *P < .05, ** P < .005.

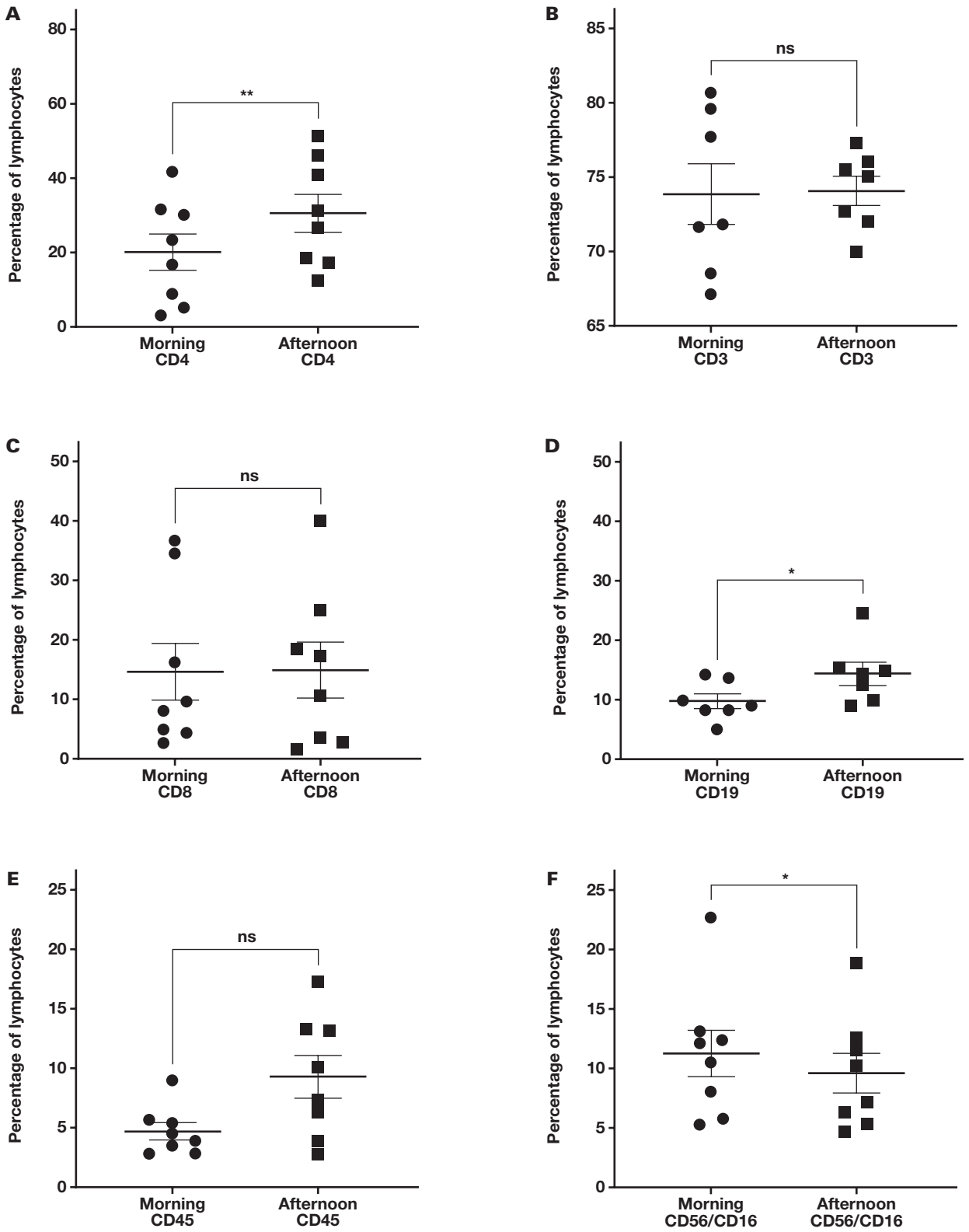

helper T cells, specifically regulatory T cells, and B cells in the afternoon may be due to their regulatory and anti-inflammatory function, with their mechanisms enhancing the environment to allow for tissue repair and regeneration during the nighttime rest phase.[35,36]

In clinical settings, the time-dependent changes of lymphocyte subsets observed may be responsible for the variation of immune responses in autoimmune diseases, allergies, and immune inflammatory conditions. Although diurnal variation in autoimmune disease

symptoms has been reported,[37-39] there is still a lack of clarity regarding the link between symptom presentation and cell variation. Due to the wide range of immune cell and lymphocyte subsets and their intertwining roles, it is currently not possible to fully establish the effect of immune diurnal variation autoimmune disease symptoms. However, it is possible that a dysregulation or disruption of circadian rhythms may lead to the presence of autoimmune disease symptoms by creating an inflammatory environment due to abnormal immune cell levels.[40] Additionally, the decreased B-cell levels in the morning sample may correspond with increased reporting of autoimmune disease allergic and asthmatic symptoms in the morning. In particular, as regulatory B cells regulate the immune response and restrict excessive inflammation, a decrease of these cells may correlate with the increased morning symptoms of immune conditions related to excessive inflammation.[41]

Limitations

This study used a small sample size, which can limit the applicability of statistical significance measured. Due to the small sample size, differences from individual factors can be shown that may not be fully attributable to diurnal variation. Additionally, when comparing with previous studies that have analyzed diurnal variation to corroborate results, most of the studies are dated and display varied times for peak lymphocyte levels. As such, future research is needed with a second cohort and larger sample sizes to further establish whether significant diurnal variations can be accurately detected when using small blood volumes.

Conclusions

Although previous studies have shown that lymphocytes can be detected in small blood samples from large sample sizes and that lymphocyte diurnal variation occurs, this study demonstrates that significant daily variations in lymphocyte counts can be determined in a small sample size from a small volume fingertip blood sample. Although it is unclear in the literature whether this variation is physiologically significant, it is possible that the physiological immune roles of the lymphocytes link to their functions. The effective use of a small fingertip blood volume in a limited sample size to detect these variations demonstrates that this technique can be applied in both physiological research, including lymphocytes and clinical practice during blood tests to identify variations present in lymphocyte prevalence. The use of this technique presents a less invasive and more acceptable technique for participants and patients. This study demonstrates small fingertip blood volumes, even when taken from small sample sizes, can detect significant lymphocyte diurnal variation, with this influencing future methodologies and considerations in clinical practice in addition to physiological and immunological research settings.

Conflict of Interest Disclosure

The authors have nothing to disclose.

REFERENCES

1. Dunlap JC, Loros JJ, DeCoursey PJ. *Chronobiology: Biological Timekeeping*. Sinauer Associates; 2004.
2. Refinetti R. *Circadian Physiology*. 3rd ed. CRC Press; 2016.
3. Cui S, Chen Y, Guo Y, Chen D. Clock genes and gastric cancer. *Biol Rhythm Res.* 2022;53(11):1720–1734. https://doi.org/10.1080/09291016.2021.2020993
4. Tsujino N, Sakurai T. Circadian rhythm of leptin, orexin and ghrelin. *Jpn J Clin Med.* 2012;70(7):1121-1125.
5. Sato T, Ida T, Kojima M. Role of biological rhythms in the performance of physical activity. *J Sports Med Phys Fitness.* 2017;6(3):125-134. https://doi.org/10.7600/jpfsm.6.125
6. Kostis JB, Moreyra A, Amendo M, Di Pietro J, Cosgrove N, Kuo P. The effect of age on heart rate in subjects free of heart disease: studies by ambulatory electrocardiography and maximal exercise stress test. *Circulation.* 1982;65(1):141-145.
7. Reynolds V, Marriott F, Shawkat F, Eggerman M, Nikolaou V. Heart-rate variation, age, and behaviour in elderly women. *Ann Hum Biol.* 1989;16(3):265-273. https://doi.org/10.1080/03014468900000382
8. Born J, Lange T, Hansen K, Mölle M, Fehm H-L. Effects of sleep and circadian rhythm on human circulating immune cells. *J Immunol*. 1997;158(9):4454-4464. https://doi.org/10.4049/jimmunol.158.9.4454
9. He W, Holtkamp S, Hergenhan SM, et al. Circadian expression of migratory factors establishes lineage-specific signatures that guide the homing of leukocyte subsets to tissues. *Immunity.* 2018;49(6):1175-1190.e7. https://doi.org/10.1016/j.immuni.2018.10.007
10. Pelegrí C, Vilaplana J, Castellote C, Rabanal M, Franch A, Castell M. Circadian rhythms in surface molecules of rat blood lymphocytes. *Am J Physiol Cell Physiol.* 2003;284(1):C67-C76.
11. Pick R, He W, Chen C-S, Scheiermann C. Time-of-day-dependent trafficking and function of leukocyte subsets. *Trends Immunol.* 2019;40(6):524-537. https://doi.org/10.1016/j.it.2019.03.010
12. Prendergast BJ, Cable EJ, Patel PN, et al. Impaired leukocyte trafficking and skin inflammatory responses in hamsters lacking a functional circadian system. *Brain Behav Immun.* 2013;32:94-104. https://doi.org/10.1016/j.bbi.2013.02.007
13. Lucas D, Battista M, Shi PA, Isola L, Frenette PS. Mobilized hematopoietic stem cell yield depends on species-specific circadian timing. *Cell Stem Cell*. 2008;3(4):364-366. https://doi.org/10.1016/j.stem.2008.09.004
14. Arjona A, Sarkar DK. Circadian oscillations of clock genes, cytolytic factors, and cytokines in rat NK cells. *J Immunol*. 2005;174(12):7618-7624. https://doi.org/10.4049/jimmunol.174.12.7618
15. Baumann A, Gönnenwein S, Bischoff SC, et al. The circadian clock is functional in eosinophils and mast cells. *Immunology.* 2013;140(4):465-474. https://doi.org/10.1111/imm.12157
16. Ella K, Csépányi-Kömi R, Káldi K. Circadian regulation of human peripheral neutrophils. *Brain Behav Immun.* 2016;57:209-221. https://doi.org/10.1016/j.bbi.2016.04.016
17. Keller M, Mazuch J, Abraham U, et al. A circadian clock in macrophages controls inflammatory immune responses. *Proc Natl Acad Sci USA.* 2009;106(50):21407-21412. https://doi.org/10.1073/pnas.0906361106
18. Nguyen KD, Fentress SJ, Qiu Y, Yun K, Cox JS, Chawla A. Circadian gene Bmal1 regulates diurnal oscillations of Ly6Chi inflammatory monocytes. *Science.* 2013;341(6153):1483-1488. https://doi.org/10.1126/science.1240636
19. Silver AC, Arjona A, Hughes ME, Nitabach MN, Fikrig E. Circadian expression of clock genes in mouse macrophages, dendritic cells, and B cells. *Brain Behav Immun.* 2012;26(3):407-413. https://doi.org/10.1016/j.bbi.2011.10.001
20. Wang X, Reece SP, Van Scott MR, Brown JM. A circadian clock in murine bone marrow-derived mast cells modulates IgE-dependent activation in vitro. *Brain Behav Immun.* 2011;25(1):127-134. https://doi.org/10.1016/j.bbi.2010.09.007
21. Miyawaki T, Taga K, Nagaoki T, Seki H, Suzuki Y, Taniguchi N. Circadian changes of T lymphocyte subsets in human peripheral blood. *Clin Exp Immunol.* 1984;55(3):618-622.
22. Boukelia B, Gomes EC, Florida-James GD. Diurnal variation in physiological and immune responses to endurance sport in highly trained

runners in a hot and humid environment. *Oxid Med Cell Longevity.* 2018;2018:3402143. https://doi.org/10.1155/2018/3402143

23. Beam CA, Wasserfall C, Woodwyk A, et al. Synchronization of the normal human peripheral immune system: a comprehensive circadian systems immunology analysis. *Sci Rep.* 2020;10(1):672. https://doi.org/10.1038/s41598-019-56951-5
24. Lévi FA, Canon C, Touitou Y, et al. Circadian rhythms in circulating T lymphocyte subtypes and plasma testosterone, total and free cortisol in five healthy men. *Clin Exp Immunol.* 1988;71(2):329-335.
25. Mazzoccoli G, De Cata A, Greco A, et al. Opposing circadian rhythms of CD3+, CD4+ and CD3+, CD8+ lymphocyte subpopulations in healthy humans. *Biol Rhythm Res.* 2011;42(2):111-118. https://doi.org/10.1080/09291011003726631
26. Mazzoccoli G, Bianco G, Correra M, et al. Circadian variation of lymphocyte subsets in health subjects. *Recenti Prog Med.* 1998;89(11):569-572.
27. Sennels HP, Jørgensen HL, Hansen AL, Goetze JP, Fahrenkrug J. Diurnal variation of hematology parameters in healthy young males: the Bispebjerg study of diurnal variations. *Scand J Clin Lab Invest.* 2011;71(7):532-541. https://doi.org/10.3109/00365513.2011.602422
28. Moro C, Bass J, Scott AM, Canetti EFD. Enhancing capillary blood collection: the influence of nicotinic acid and nonivamide. *J Clin Lab Anal.* 2017;31(6):e22142. https://doi.org/10.1002/jcla.22142
29. Srisala S, Pongsakul N, Sahakijpicharn T, Hongeng S, Chutipongtanate S, Apiwattanakul N. Capillary blood as an alternative specimen for enumeration of percentages of lymphocyte subsets. *BMC Res Notes.* 2019;12(1):633. https://doi.org/10.1186/s13104-019-4659-4
30. AACB: Australasian Association for Clinical Biochemistry and Laboratory Medicine. White Blood Cell Count. https://pathologytestsexplained.org.au/learning/test-index/wbc
31. Carmichael K, Abayomi E. Analysis of diurnal variation of lymphocyte subsets in healthy subjects in the Caribbean, and its implication in HIV monitoring and treatment. *Afr J Med Med Sci.* 2006;35:53-57.
32. Bertouch JV, Roberts-Thomson PJ, Bradley J. Diurnal variation of lymphocyte subsets identified by monoclonal antibodies. *Br Med J (Clin Res Ed).* 1983;286(6372):1171-1172. https://doi.org/10.1136/bmj.286.6372.1171
33. Ritchie AW, Oswald I, Micklem HS, et al. Circadian variation of lymphocyte subpopulations: a study with monoclonal antibodies. *Br Med J (Clin Res Ed).* 1983;286(6380):1773-1775. https://doi.org/10.1136/bmj.286.6380.1773
34. Buowari O. Complications of venepuncture. *Adv Biosci Biotechnol.* 2013;04:126-128. https://doi.org/10.4236/abb.2013.41A018
35. Li J, Tan J, Martino MM, Lui KO. Regulatory T-cells: potential regulator of tissue repair and regeneration. Review. *Front Immunol.* 2018;9(585). https://doi.org/10.3389/fimmu.2018.00585
36. Alberts B, Johnson A, Lewis J, Raff M, Roberts K, Walter P. Molecular biology of the cell. 4th ed. *Ann Bot*. 2003;91(3):401-401. https://doi.org/10.1093/aob/mcg023
37. Cutolo M. Chronobiology and the treatment of rheumatoid arthritis. *Curr Opin Rheumatol.* 2012;24(3):312-318. https://doi.org/10.1097/BOR.0b013e3283521c78
38. Reinberg A, Gervais P, Levi F, Smolensky M, Del Cerro L, Ugolini C. Circadian and circannual rhythms of allergic rhinitis: an epidemiologic study involving chronobiologic methods. *J Allergy Clin Immunol.* 1988;81(1):51-62. https://doi.org/10.1016/0091-6749(88)90220-5
39. Durrington HJ, Farrow SN, Loudon AS, Ray DW. The circadian clock and asthma. *Thorax.* 2014;69(1):90-92. https://doi.org/10.1136/thoraxjnl-2013-203482
40. Sutton CE, Finlay CM, Raverdeau M, et al. Loss of the molecular clock in myeloid cells exacerbates T cell-mediated CNS autoimmune disease. *Nat Commun.* 2017;8(1):1923. https://doi.org/10.1038/s41467-017-02111-0
41. Yang M, Rui K, Wang S, Lu L. Regulatory B cells in autoimmune diseases. *Cell Mol Immunol.* 2013;10(2):122-132. https://doi.org/10.1038/cmi.2012.60

Droplet digital polymerase chain reaction to measure heteroplasmic m.3243A>G mitochondrial mutations

Shinya Matsumoto, PhD,[1] *Takeshi Uchiumi, MD, PhD,*[1,2,3] *Nozomi Noda,*[1] *Yasushi Ueyanagi, PhD,*[1] *Taeko Hotta,*[1] *Dongchon Kang, MD, PhD*[2]

[1]Department of Clinical Chemistry and Laboratory Medicine, Kyushu University Hospital, Fukuoka, Japan, Departments of [2]Clinical Chemistry and Laboratory Medicine and [3]Health Sciences, Graduate School of Medical Sciences, Kyushu University, Fukuoka, Japan. Corresponding author: Shinya Matsumoto; matsumoto.shinya.544@m.kyushu-u.ac.jp

Key words: droplet digital PCR; mitochondrial DNA; m.3243A>G, heteroplasmy; mitochondrial disease; peripheral blood

Abbreviations: ddPCR, droplet digital polymerase chain reaction; mtDNA, mitochondrial DNA; WT, wild-type; MELAS, mitochondrial encephalomyopathy with lactic acidosis and stroke-like episodes; MIDD, maternally inherited diabetes and deafness; PCR-RFLP, PCR-restriction fragment length polymorphism; dPCR, digital PCR; LMPCR, ligation-mediated PCR; PNA, peptide nucleic acid; MERRF, myoclonic epilepsy with ragged-red fibers

Laboratory Medicine 2024;55:227-233; https://doi.org/10.1093/labmed/lmad063

ABSTRACT

Objective: Different mitochondrial DNA genotypes can coexist in a cell population as well as in a single cell, a condition known as heteroplasmy. Here, we accurately determined the heteroplasmy levels of the m.3243A>G mutation, which is the most frequently identified mutation in patients with mitochondrial diseases, using droplet digital polymerase chain reaction (ddPCR).

Methods: The m.3243A>G heteroplasmy levels in artificial heteroplasmy controls mixed with various proportions of wild-type and mutant plasmids were measured using ddPCR, PCR-restriction fragment length polymorphism, and Sanger sequencing. The m.3243A>G heteroplasmy levels in DNA, extracted from the peripheral blood of patients with suspected mitochondrial disease and healthy subjects, were determined using ddPCR.

Results: The accuracy of the ddPCR method was high. The lower limit of detection was 0.1%, which indicated its higher sensitivity compared with other methods. The m.3243A>G heteroplasmy levels in peripheral blood, measured using ddPCR, correlated inversely with age at the time of analysis. The m.3243A>G mutation may be overlooked in the peripheral blood-derived DNA of elderly people, as patients >60 years of age have heteroplasmy levels <10%, which is difficult to detect using methods other than the highly sensitive ddPCR.

Conclusion: ddPCR may be considered an accurate and sensitive method for measuring m.3243 A>G heteroplasmy levels of mitochondrial DNA.

Introduction

Mitochondria have extranuclear genomes that are common to all vertebrates. Human mitochondrial DNA (mtDNA) is circular and encodes 13 proteins, 22 tRNAs, and 2 rRNAs, all of which are essential for assembly of the mitochondrial respiratory chain, which produces most of the cellular adenosine triphosphate. The number of mtDNA mutations listed as pathogenic is currently close to 100 and is still growing.[1] A single cell may contain hundreds or thousands of mtDNA molecules. Both wild-type (WT) and mutant mtDNA can coexist in a cell population, as well as in a single cell—a condition referred to as heteroplasmy. Mitochondria are not functionally affected until the percentage of mutant mtDNA exceeds a particular value (threshold). Therefore, affected tissues often have a high percentage of heteroplasmy whereas other seemingly unaffected cells in the same individual have a very low percentage of heteroplasmy or no detectable mutation.

Mutations in mtDNA can be divided into 2 main categories: rearrangements (deletions and duplications) and point mutations. Among point mutations, the A>G mutation at m.3243 in the human mitochondrial $tRNA^{Leu(UUR)}$ gene (m.3243A>G) is the most commonly identified. This mutation is associated with a wide range of clinical manifestations, including mitochondrial encephalomyopathy with lactic acidosis and stroke-like episodes (MELAS) and maternally inherited diabetes and deafness (MIDD).[2–5]

Determination of m.3243A>G heteroplasmy levels would contribute to the knowledge of its relevance in clinical presentations, sensitivity of genetic diagnosis, and genetic counseling for disease transmission. The percentage of cells containing mtDNA with the heteroplasmic m.3243A>G mutation varies across tissues and may be the highest in affected tissues, such as muscle and brain, in cells that are postmitotic.[6,7] However, peripheral blood cells, which are noninvasively accessible and routinely used for clinical testing, usually have a low percentage

of heteroplasmy.[8] In an earlier study, the m.3243A>G mutation was detected in the blood of only 5 out of 10 patients, but in the muscle cells of all the patients.[9] Low levels of heteroplasmy in peripheral blood samples lead to false-negative results, such as when polymerase chain reaction-restriction fragment length polymorphism (PCR-RFLP) and Sanger sequencing methods are used. Therefore, a sensitive and quantitative method for accurate measurement of m.3243A>G heteroplasmic levels is very much desired.

Digital PCR (dPCR) is a third generation PCR that allows absolute quantification through partitioning the reaction. Highly sensitive and accurate in molecular detection, this technology has been used in applications such as detection of trace DNA, rare mutations, and copy number variations.[10–12] Thus, dPCR can amplify multiple DNA samples using simultaneous reactions in microspheres of several thousand nanoliters, thereby increasing reliability and sensitivity of the data. In real-time PCR, the arithmetic mean can be commonly calculated after performing a reaction multiple times. In dPCR, because thousands of reactions are performed simultaneously, highly accurate absolute quantification of nucleic acid targets can be obtained without the need for standard curves. Droplet dPCR (ddPCR) aims to amplify very small amounts of DNA and analyze the relative number of microspheres with or without the template. In the first step, the reaction mixture is separated into 20,000 droplets in a specially prepared oil solution. After amplification, a special module based on the principle of flow cytometry is used to record the fluorescence signal at the final point, and the result is expressed as the absolute number of DNA copies.[13]

This study was aimed at developing an accurate and quantitative method based on ddPCR that would allow the analysis of heteroplasmy of m.3243A>G mutation and comparing its accuracy and reliability with those of Sanger sequencing and PCR-RFLP analyses using artificial heteroplasmy controls.

Material and Methods

Patient Collection and Genomic DNA Extraction

This study was approved by the ethical review board of the Graduate School of Medical Sciences, Kyushu University. Informed consent was obtained by the attending physicians from all participants following explanations of the aim of the research and guaranteeing privacy. Peripheral blood DNA was extracted using the QIAamp DNA Blood Mini Kit (QIAGEN), following the manufacturer's instructions.

Creation of Artificial Heteroplasmy Controls

DNA samples from a patient identified with m.3243A>G mutation with approximately 30% heteroplasmy were amplified with the forward primer Mt3243F1 (5′-CGATGTTGGATCAGGACATC-3′) and the reverse primer Mt3243R1 (5′-AGTTTGATGCTCACCCTGATC-3′). The PCR was conducted with 30 cycles of denaturation at 94°C for 5 seconds, annealing at 65°C for 20 seconds, and extension at 72°C for 30 seconds.

The PCR products were cloned into the pGEM-T easy vector (Promega). Two clones, WT and the mutant, were constructed. Concentrations of the WT and mutant plasmids were measured with a Qubit dsDNA BR assay kit (Thermo Fisher Scientific) and adjusted to 1 ng/μL (approximately 2.58×10^8 copies/μL). The control plasmids were mixed to generate gradient control samples with the m.3243A>G mutation in the range of 0% to 100% mutation.

ddPCR Assay

The ddPCR mixture consisted of 1 μL DNA (containing 1 μg genomic DNA from peripheral blood sample), 10 μL 2× ddPCR Supermix for Probes (no dUTP) (Bio-Rad Laboratories), WT and mutant allele-specific probes at a concentration of 0.25 μM, primer mixtures at a concentration of 0.9 μM for the target gene, 2 U/reaction *Alu*I enzyme (New England Biolabs), and nuclease-free water in a final volume of 20 μL. All primers and probes were obtained from Bio-Rad Laboratories. Sequence and other information about primers and probes are available at www.bio-rad.com with the following Assay ID: dHsaMDS556387941. Droplets were generated using the Bio-Rad QX200 system (Bio-Rad Laboratories) following the manufacturer's instructions. The reaction mixtures were transferred to a nonskirted 96-well PCR plate (Eppendorf) for PCR using the Veriti 96-well fast thermal cycler (Thermo Fisher Scientific) under the following conditions: activation of the enzyme at 95°C for 10 min, followed by 40 cycles of a 2-step protocol consisting of incubation at 94°C for 30 seconds and then combined annealing/extension at 55°C for 1 min. The 96-well plate was next transferred to a QX200 Droplet Reader (Bio-Rad Laboratories), and fluorescence of each droplet was analyzed separately using a 2-color detection system (set to detect FAM [mutant allele] and HEX [WT allele]). The fluorescent droplets were counted to provide an absolute quantification of WT and mutant copy numbers in m.3243 in digital form using the QuantaSoft software 1.7 (Bio-Rad Laboratories).

Sanger Sequencing

Amplicons that were amplified under the same conditions as those used to create the control plasmid were subjected to direct sequencing using the Big Dye Terminator v3.1 Cycle Sequencing Kit and the 3500xL Genetic Analyzer (both from Thermo Fisher Scientific).

PCR-RFLP Assay

The 692 bp PCR products, amplified with Mt3243F1 and Mt3243R1, were digested with *Apa*I (Takara Bio, Shiga, Japan) at 37°C for 1 h and stained with ethidium bromide after electrophoresis on a 2% agarose gel. The mutated DNA was digested into 433 and 259 bp fragments whereas the WT (692 bp) remained undigested.

Results

Optimization of ddPCR Conditions

We determined the optimal PCR annealing temperature for accurate m.3243A>G heteroplasmy measurements using a 1:1 mixture of WT and mutant control plasmids. The annealing temperature was varied from 50°C to 65°C in 5°C increments (**FIGURE 1**). At 50°C and 55°C, positive droplets of both FAM and HEX were clearly separated. However, at 60°C, fluorescence intensity of the positive droplets was weak, and thus, they could not be clearly separated from the negatives. At 65°C, no DNA was amplified and no positive droplet was observed. Based on these results, we used an annealing temperature of 55°C for all our experiments.

Determination of the Accuracy of m.3243A>G Heteroplasmy Measurements in ddPCR

To confirm accuracy of ddPCR for the m.3243 A>G heteroplasmy assay, we diluted the mutant control with WT control and compared the measured values with the theoretical values of m.3243A>G heteroplasmy

FIGURE 1. **Optimization of annealing temperature for determination of mitochondrial DNA m.3243A>G heteroplasmy levels using droplet digital polymerase chain reaction (ddPCR). A 1:1 mixture of wild-type (WT) and mutant plasmids was subjected to ddPCR assay. A, 50°C. B, 55°C. C, 60°C. D, 65°C. Vertical axis shows the fluorescence intensity of FAM (channel 1) and the mutant probe and horizontal axis shows the fluorescence intensity of HEX (channel 2) and the WT probe. Blue, green, and orange dots indicate positive droplets only, for the mutant, WT, and both the probes, respectively. Black dots indicate negative droplets for both the probes.**

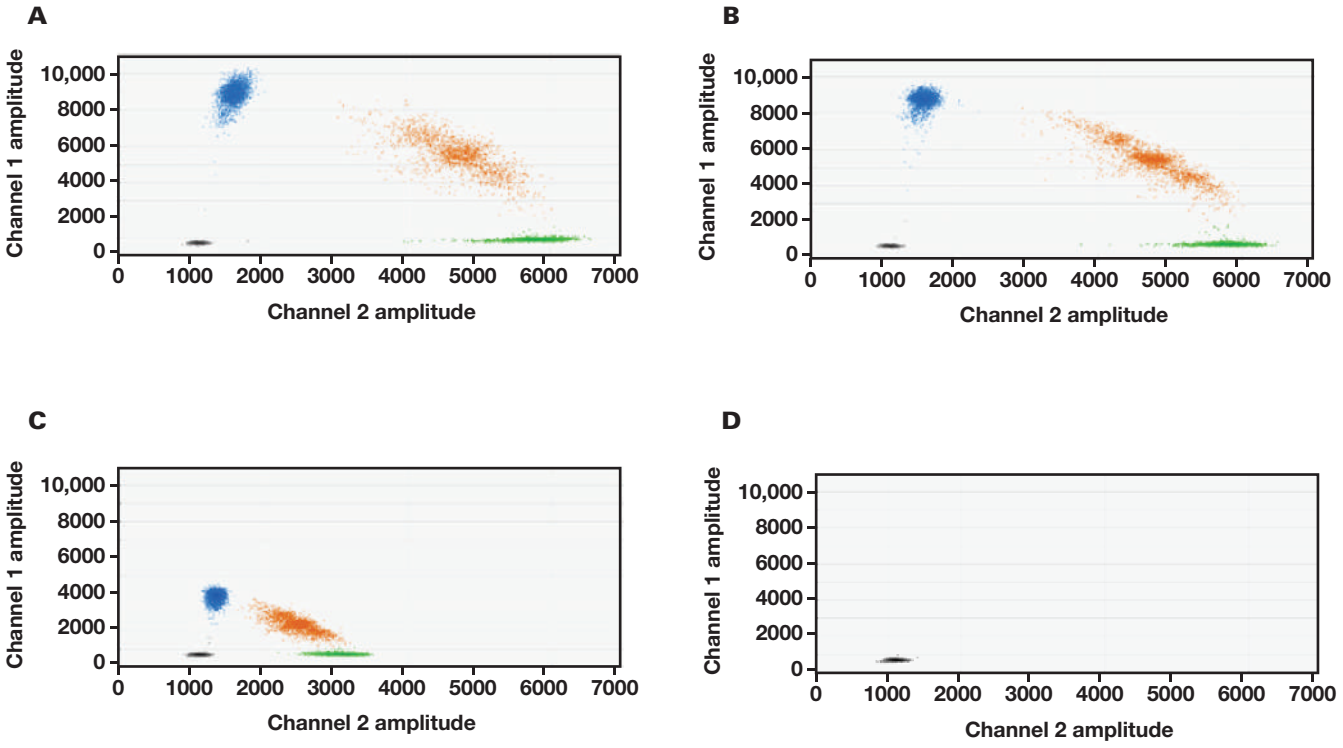

FIGURE 2. **Determination of the accuracy of droplet digital polymerase chain reaction (ddPCR). A, Wild-type and mutant control plasmids were mixed in various proportions, and the m.3243A>G heteroplasmy levels were measured using ddPCR. Theoretical and measured values were plotted thereafter (y = 0.99x – 0.079; R^2 = 0.9998). B, The averages of the theoretical and measured values are shown. All experiments were performed in triplicate.**

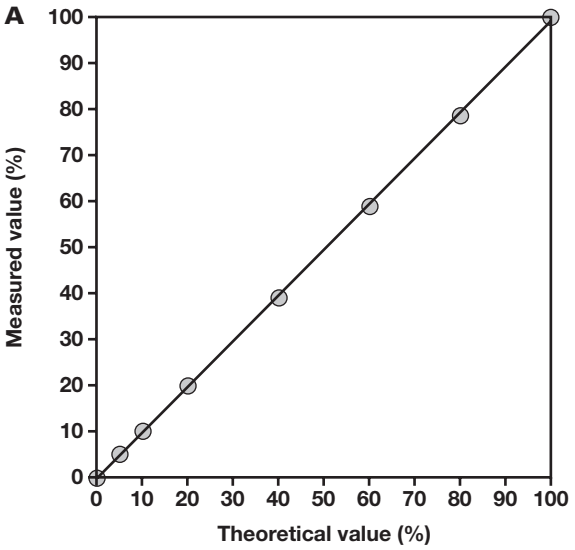

B

Theoretical value (%)	Measured value (%)
0	0.03
5	5.15
10	10.12
20	19.91
40	39.10
60	58.91
80	78.47
100	99.98

levels. For a mutation rate of 5%-100%, there was little difference between theoretical and measured values (**FIGURE 2**). This observation suggested that the ddPCR method has notably high accuracy.

Investigation of the Lower Limit of Detection

We compared the lower limit of detection of m.3243A>G heteroplasmy among ddPCR, Sanger sequencing, and PCR-RFLP using WT and

FIGURE 3. **Lower limit of detection of m.3243A>G mutation. Polymerase chain reaction (PCR) products amplified from a mixture of wild-type and mutant controls in various proportions were subjected to direct Sanger sequencing (A), PCR-restriction fragment length polymorphism (B), and drop digital PCR (C). A, Chromatograms of the sequences in various heteroplasmy levels are shown, and arrows indicate the position of m.3243. The lower limit of detection was 10%, which was the point at and before which the G-peak was not visible. B, The 692 bp PCR products were electrophoresed as described in the "Material and Methods" section. The mutated DNA was digested into 433 and 259 bp fragments. The lower limit of detection was 10%, which was the point at and before which neither of the 2 bands could be identified. M indicates a DNA ladder. Numbers on the right are the sizes (in bp) of the DNA ladder components. C, Error bars represent the mean ±2.6 SD (n = 5). The lower limit of detection was 0.08%, which is the minimum value at which +2.6 SD of the mean of the theoretical value of 0% did not overlap with -2.6 SD of the measured value.**

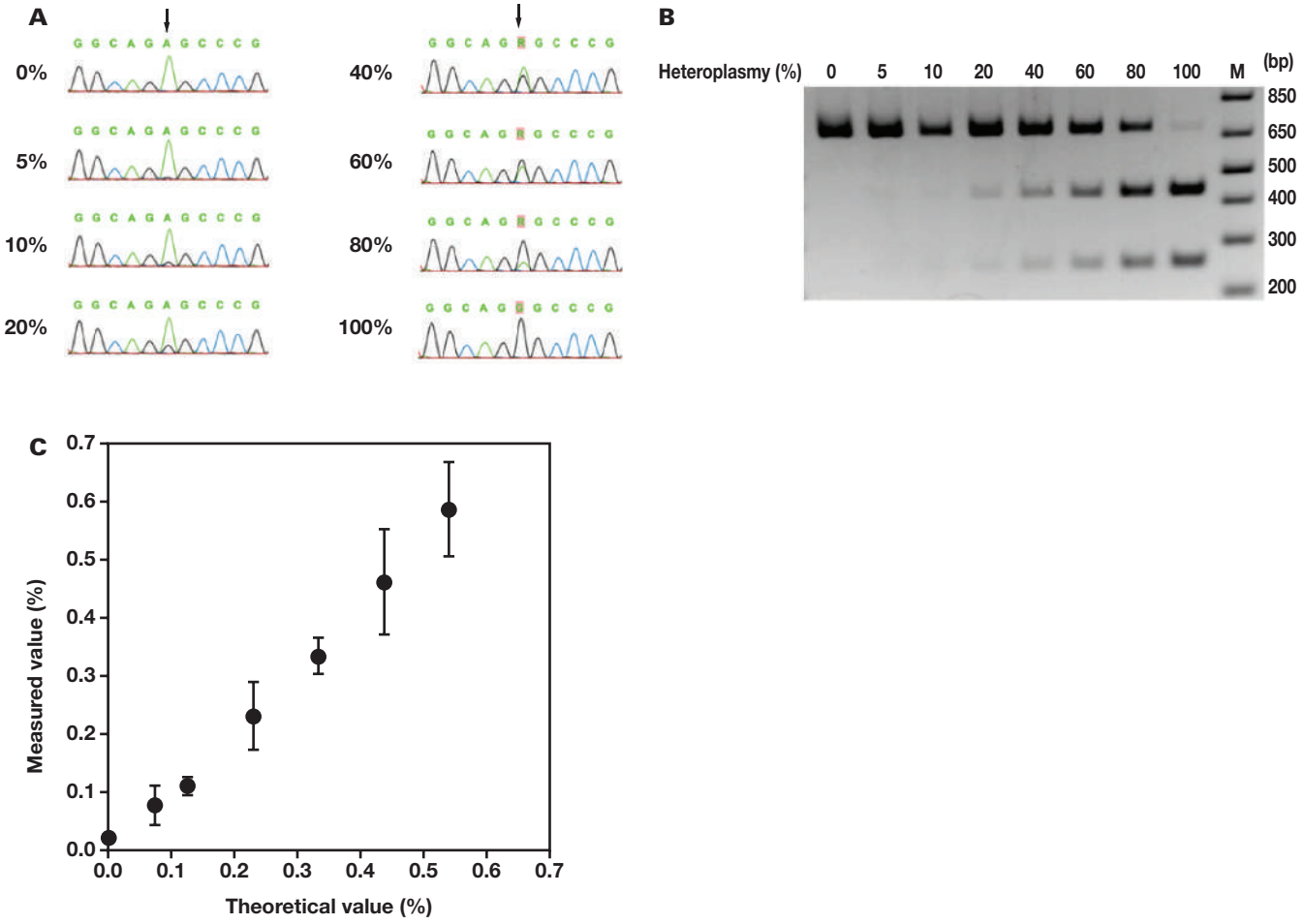

mutant controls. In Sanger sequencing, the peak of G mutation could be identified at a mutation rate of 10% but was difficult to distinguish from the background at a mutation rate of 5%; therefore, the lower limit of detection was set at 10% (**FIGURE 3A**). In PCR-RFLP, a truncated short band was visible at 10% heteroplasmy; therefore, the lower limit of detection was set at 10% (**FIGURE 3B**). In ddPCR, the minimum mutation rate that did not overlap with the average value +2.6 SD of the WT control was 0.08% (**FIGURE 3C**); therefore, the lower limit of detection was set at 0.08%. Overall, the results suggested that ddPCR could measure m.3243A>G heteroplasmy with relatively higher sensitivity than other methods.

Comparison of ddPCR with Sanger Sequencing

Next, we compared the heteroplasmy levels determined using ddPCR with those determined using Sanger sequencing for DNA extracted from the patients' peripheral blood. In Sanger sequencing, heteroplasmy levels were calculated from the ratio of the heights of A and G peaks (**FIGURE 4A**). Although the results were confirmed over a wide range of m.3243A>G heteroplasmy levels, from low to high, no significant difference was found between ddPCR and Sanger sequencing (**FIGURE 4B**). Heteroplasmy levels inferred from the ratio of peak heights in Sanger sequencing were considered accurate to some extent.

Measurement of Healthy Subject Samples

The m.3243A>G heteroplasmy levels were measured in 15 healthy donor samples using ddPCR (**TABLE 1**). All values were below 0.1%, with the highest value being 0.092%. In previous studies measuring heteroplasmy using ligation-mediated PCR (LMPCR), 0.01% heteroplasmy was detected in peripheral blood cells from approximately 50% of the

FIGURE 4. **Correlation between Sanger sequencing and drop digital polymerase chain reaction (ddPCR). A, Heteroplasmy levels in Sanger sequencing were calculated from ratio of the heights of A and G peaks. B, Heteroplasmy levels were measured using Sanger sequencing and ddPCR using DNA extracted from peripheral blood of patients harboring m.3243A>G mutation (y = 1.05x – 0.016; R^2 = 0.993).**

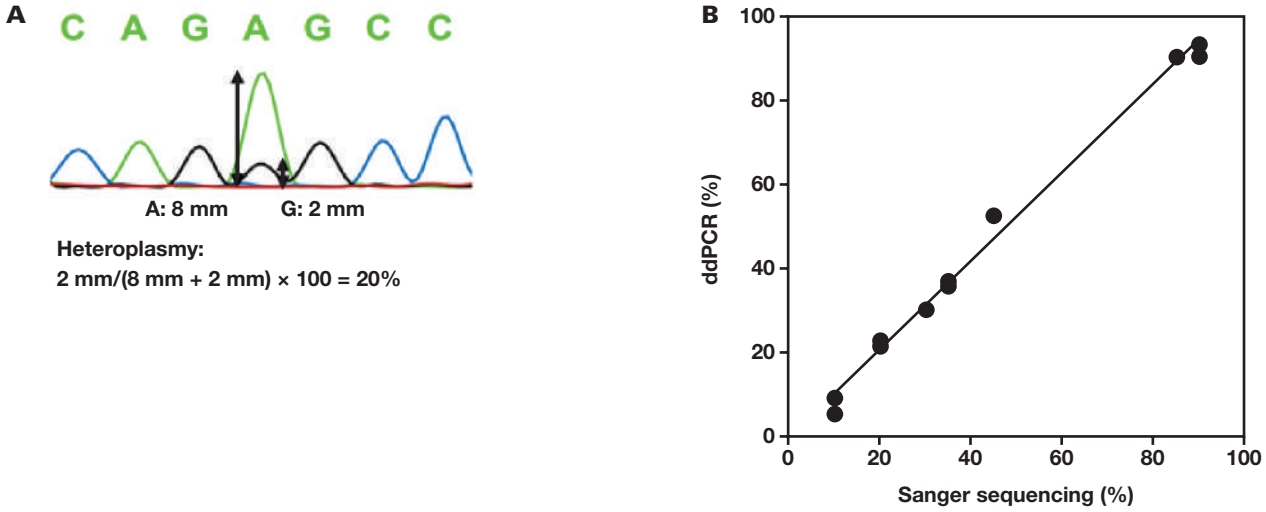

TABLE 1. **m.3243A>G heteroplasmy levels in peripheral blood of healthy subjects**

Sample No.	Heteroplasmy (%)
1	0.018
2	0.027
3	0.029
4	0.029
5	0.030
6	0.033
7	0.041
8	0.041
9	0.048
10	0.051
11	0.055
12	0.063
13	0.066
14	0.068
15	0.092

Values are the average of 2 measurements.

healthy individuals and diabetes mellitus patients; however, no healthy individual had >0.1% heteroplasmy.[14] Murdock et al[15] reported that the m.3243A>G mutation does not typically accumulate above 0.1% with age, even in muscle and brain tissues. Therefore, the presence of >0.1% heteroplasmy may be diagnostically significant, and ddPCR was found to be sensitive enough to detect it.

Heteroplasmy Levels in Peripheral Blood Samples of Patients With m.3243A>G Mutation

The m.3243A>G heteroplasmy in DNA extracted from the peripheral blood of patients with suspected mitochondrial disease was measured using ddPCR. Correlation between the heteroplasmy levels of patients who were positive for the mutation and their age was examined

FIGURE 5. **Correlation between heteroplasmy levels of the m.3243A>G mutation in peripheral blood and age during genetic analysis. Closed circles indicate affected patients and open circles indicate unaffected family members (n = 35) (y = –0.90x + 63.73; R^2 = 0.828).**

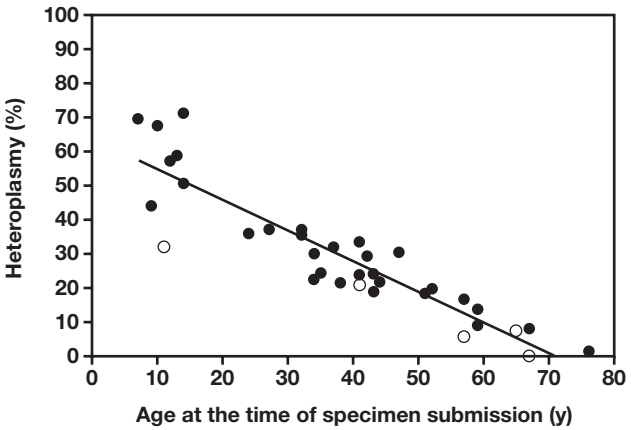

(**FIGURE 5**). An inverse correlation was observed, with heteroplasmy levels decreasing with increasing age. Family members who had not yet developed the disease were suggested to be in the same correlation equation as the patients who had already developed the disease. According to the correlation equation, heteroplasmy level was less than 10% in the 50- to 60-year-old age group, implying that it would be difficult to detect using Sanger sequencing because this method has a lower limit of detection ≥10%. In fact, some cases could only be detected using ddPCR. This suggested that the m.3243A>G mutation may have been overlooked in the peripheral blood-derived DNA of older adults.

Discussion

For many years, a sensitive method to determine heteroplasmy of the m.3243A>G mutation has been under investigation. This is

because some diabetic patients have reported to show less than 1% heteroplasmy in peripheral lymphocytes despite having more than 30% heteroplasmy in muscle,[16] and 1.3% of diabetic patients have 0.01% to 0.1% m.3243A>G heteroplasmy.[14] Previously, the RFLP assay was the most commonly used method for detecting m.3243A>G mutation in blood leukocytes. As shown in this article, the method showed only a faint band at m.3243A>G mutation load above 10%, below which it was undetectable. Although radiolabeled PCR is a highly sensitive method, it can detect <1% heteroplasmy.[17] Denaturing high-performance liquid chromatography has a limit of 3% to 10% for heteroplasmy detection.[18] The limit of heteroplasmy detection using quantitative methods based on pyrosequencing has reached 2%. Pyrosequencing showed a small difference between the measured and actual values of accuracy, from which a third-order polynomial curve was derived.[19] Quantitative real-time PCR based on TaqMan-MGB probes was used to screen a large number of samples for the m.3243A>G mutation, with heteroplasmy higher than 4%.[20] LMPCR was able to detect up to 0.01% of m.3243A>G heteroplasmy in peripheral blood samples, but the value was close to that for a qualitative method.[14] A combination of peptide nucleic acid (PNA) and allele-specific PCR had a lower limit of detection of 0.1%, the same as that in the ddPCR method used in this study, but required a calibration curve, and the calibration points had large increments (100%, 10%, 1%, 0.1%, and 0%), which were not sufficient for accurate quantification.[21] Highly sensitive methods for identifying m.3243A>G heteroplasmy are both expensive and time-consuming. Therefore, to date, there has been no method that satisfies both accuracy and detection sensitivity. In this study, ddPCR was shown to be accurate and sensitive in measuring m.3243A>G heteroplasmy, with heteroplasmy levels measured using ddPCR of artificial heteroplasmy control mixtures being almost identical to the theoretical values (**FIGURE 2**) and with a lower limit of detection of 0.08% (**FIGURE 3**).

A few reports have described the quantification of the heteroplasmy of mtDNA mutations; however, the mtDNA copy number has been quantified using ddPCR in several studies. Measurement of mtDNA copy number in cerebrospinal fluid using ddPCR confirmed that patients with symptomatic Alzheimer's disease have a significantly lower number of mtDNA copies.[22] The estimated mtDNA copy number values from ddPCR vs shotgun sequencing of the same samples were significantly correlated, and the mean mtDNA copy number values were similar.[23] The ddPCR method can quickly and reliably detect circulating cell-free mtDNA in plasma with a prior DNA extraction step.[24]

We investigated the correlation between heteroplasmy levels in peripheral blood and age using genetic analysis. In the scatter plot (**FIGURE 5**), age at the time of genetic analysis and heteroplasmy in peripheral blood showed a clear negative correlation. Although several studies have found only a weak correlation between mutation load in the blood and clinical phenotype,[25] the degree of m.3243A>G heteroplasmy has often been reported to correlate with the age of onset of MIDD and severity of hearing loss. Both blood and urine heteroplasmy levels have been suggested to be significantly negatively correlated with age, although muscle heteroplasmy is not correlated with age; age-adjusted blood m.3243A>G mutation load may be an indicator of disease burden.[26] In contrast, another study showed that m.3243A>G mutant DNA decreases with age in muscles, urine, and hair follicles.[27] The heteroplasmy levels in DNA samples from peripheral blood of 18 individuals carrying the m.3243A>G mutation showed a decrease on aging, with an average change of -0.69 ± 0.61% per year.[28] A significant negative correlation was found between body mass index and heteroplasmy, and a significant positive correlation was found between hemoglobin A1c levels and heteroplasmy.[29] A high degree of mutant heteroplasmy, male sex, and age were found to increase the severity of hearing impairment.[30] Suzuki et al[31] showed the age of onset of diabetes and deafness to be negatively correlated with heteroplasmy levels in leukocytes and the heteroplasmic concentrations of the mutation in leukocytes to be significantly higher in patients with encephalomyopathy, basal ganglia calcifications, and neuropsychiatric disturbances. In addition to m.3243A>G, other mitochondrial DNA mutations (m.3271T>C and m.14530T>C) also showed a negative correlation between blood heteroplasmy levels and age at the onset of diabetes.[32] Sunde et al[33] reported that low blood heteroplasmy rates of m.3243A>G may lead to late-onset MELAS, suggesting that accurate and sensitive measurement using ddPCR may be useful in detecting MELAS. On the contrary, the degree of heteroplasmy of mitochondrial $tRNA^{Lys}$ mutations, such as m.8344A>G identified in myoclonic epilepsy with ragged-red fibers (MERRF), was reported to be high in both symptomatic and asymptomatic cases. There was no inverse correlation with age, unlike with m.3243A>G,[34] and therefore, the sensitivity of ddPCR for heteroplasmy measurements might not be adequate in MERRF.

Similar to our results, the proportion of m.3243A>G has already been reported to decrease with age in the blood cells of unaffected familial carriers, as well as in patients with diabetes.[26] The results suggest that with early genetic testing, the likelihood of detecting mutations is greater not only in patients but also in their unaffected family members. The high sensitivity of ddPCR may be very beneficial in confirming the possibility of inheritance of the disease if the patient is affected by m.3243A>G and their family members do not have threshold heteroplasmy levels and the m.3243A>G phenotype is not absent.

Acknowledgments

We thank Editage (www.editage.com) for English language editing.

Funding

This work was supported in part by the Japan Society for the Promotion of Science (JSPS) KAKENHI (grant number JP18K15420 to S.M. and JP21K07319 to S.M.)

Conflict of Interest Disclosure

The authors have nothing to disclose.

REFERENCES

1. Wallace DC, Lott MT, Brandon MC. MITOMAP: A Human Mitochondrial Genome Database. Accessed August 30, 2022. https://www.mitomap.org/MITOMAP.
2. Goto Y, Nonaka I, Horai S. A mutation in the tRNA(Leu)(UUR) gene associated with the MELAS subgroup of mitochondrial encephalomyopathies. *Nature.* 1990;348(6302):651-653. doi:10.1038/348651a0
3. King MP, Koga Y, Davidson YM, et al. Defects in mitochondrial protein synthesis and respiratory chain activity segregate with the tRNA (Leu

(UUR)) mutation associated with mitochondrial myopathy, encephalopathy, lactic acidosis, and strokelike episodes. *Mol Cell Biol.* 1992;12(2):480-490. doi:10.1128/mcb.12.2.480-490.1992

4. Van den Ouweland JM, Lemkes HH, Trembath RC, et al. Maternally inherited diabetes and deafness is a distinct subtype of diabetes and associates with a single point mutation in the mitochondrial tRNA (Leu(UUR)) gene. *Diabetes.* 1994;43(6):746-751. doi:10.2337/diab.43.6.746
5. Newkirk JE, Taylor RW, Howell N, et al. Maternally inherited diabetes and deafness: prevalence in a hospital diabetic population. *Diabet Med.* 1997;14(6):457-460. doi:10.1002/(SICI)1096-9136(199706)14:6<457::AID-DIA372>3.0.CO;2-W
6. Ciafaloni E, Ricci E, Servidei S, et al. Widespread tissue distribution of a tRNALeu(UUR) mutation in the mitochondrial DNA of a patient with MELAS syndrome. *Neurology.* 1991;41(10):1663-1664. doi:10.1212/wnl.41.10.1663
7. Dubeau F, De Stefano N, Zifkin BG, Arnold DL, Shoubridge EA. Oxidative phosphorylation defect in the brains of carriers of the tRNAleu(UUR) A3243G mutation in a MELAS pedigree. *Ann Neurol.* 2000;47(2):179-185.
8. Hotta O, Inoue CN, Miyabayashi S, Furuta T, Takeuchi A, Taguma Y. Clinical and pathologic features of focal segmental glomerulosclerosis with mitochondrial tRNALeu(UUR) gene mutation. *Kidney Int.* 2001;59(4):1236-1243. doi:10.1046/j.1523-1755.2001.0590041236.x
9. Sue CM, Quigley A, Katsabanis S, et al. Detection of MELAS A3243G point mutation in muscle, blood and hair follicles. *J Neurol Sci.* 1998;161(1):36-39. doi:10.1016/s0022-510x(98)00179-8
10. Hudecova I. Digital PCR analysis of circulating nucleic acids. *Clin Biochem.* 2015;48(15):948-956. doi:10.1016/j.clinbiochem.2015.03.015
11. Sho S, Court CM, Kim S, et al. Digital PCR improves mutation analysis in pancreas fine needle aspiration biopsy specimens. *PLoS One.* 2017;12(1):e0170897. doi:10.1371/journal.pone.0170897
12. Whale AS, Huggett JF, Cowen S, et al. Comparison of microfluidic digital PCR and conventional quantitative PCR for measuring copy number variation. *Nucleic Acids Res*. 2012;40(11):e82. doi:10.1093/nar/gks203
13. Hindson BJ, Ness KD, Masquelier DA, et al. High-throughput droplet digital PCR system for absolute quantitation of DNA copy number. *Anal Chem.* 2011;83(22):8604-8610. doi:10.1021/ac202028g
14. Urata M, Wakiyama M, Iwase M, et al. New sensitive method for the detection of the A3243G mutation of human mitochondrial deoxyribonucleic acid in diabetes mellitus patients by ligation-mediated polymerase chain reaction. *Clin Chem.* 1998;44(10):2088-2093.
15. Murdock DG, Christacos NC, Wallace DC. The age-related accumulation of a mitochondrial DNA control region mutation in muscle, but not brain, detected by a sensitive PNA-directed PCR clamping based method. *Nucleic Acids Res.* 2000;28(21):4350-4355. doi:10.1093/nar/28.21.4350
16. Suzuki Y, Goto Y, Taniyama M, et al. Muscle histopathology in diabetes mellitus associated with mitochondrial tRNA(Leu(UUR)) mutation at position 3243. *J Neurol Sci.* 1997;145(1):49-53. doi:10.1016/s0022-510x(96)00239-0
17. Smith ML, Hua XY, Marsden DL, et al. Diabetes and mitochondrial encephalomyopathy with lactic acidosis and stroke-like episodes (MELAS): radiolabeled polymerase chain reaction is necessary for accurate detection of low percentages of mutation. *J Clin Endocrinol Metab.* 1997;82(9):2826-2831. doi:10.1210/jcem.82.9.4222
18. Biggin A, Henke R, Bennetts B, Thorburn DR, Christodoulou J. Mutation screening of the mitochondrial genome using denaturing high-performance liquid chromatography. *Mol Genet Metab.* 2005;84(1):61-74. doi:10.1016/j.ymgme.2004.09.011
19. Yan JB, Zhang R, Xiong C, et al. Pyrosequencing is an accurate and reliable method for the analysis of heteroplasmy of the A3243G mutation in patients with mitochondrial diabetes. *J Mol Diagn.* 2014;16(4):431-439. doi:10.1016/j.jmoldx.2014.03.005
20. Rong E, Wang H, Hao S, Fu Y, Ma Y, Wang T. Heteroplasmy detection of mitochondrial DNA A3243G mutation using quantitative real-time PCR assay based on TaqMan-MGB probes. *Biomed Res Int.* 2018;2018:1286480. doi:10.1155/2018/1286480
21. Urata M, Wada Y, Kim SH, et al. High-sensitivity detection of the A3243G mutation of mitochondrial DNA by a combination of allele-specific PCR and peptide nucleic acid-directed PCR clamping. *Clin Chem.* 2004;50(11):2045-2051. doi:10.1373/clinchem.2004.033761
22. Podlesniy P, Figueiro-Silva J, Llado A, et al. Low cerebrospinal fluid concentration of mitochondrial DNA in preclinical Alzheimer disease. *Ann Neurol.* 2013;74(5):655-668. doi: 10.1002/ana.23955
23. Wachsmuth M, Hübner A, Li M, Madea B, Stoneking M. Age-related and heteroplasmy-related variation in human mtDNA copy number. *PLoS Genet.* 2016;12(3):e1005939. doi:10.1371/journal.pgen.1005939
24. Ye W, Tang X, Liu C, Wen C, Li W, Lyu J. Accurate quantitation of circulating cell-free mitochondrial DNA in plasma by droplet digital PCR. *Anal Bioanal Chem.* 2017;409(10):2727-2735. doi:10.1007/s00216-017-0217-x
25. Mehrazin M, Shanske S, Kaufmann P, et al. Longitudinal changes of mtDNA A3243G mutation load and level of functioning in MELAS. *Am J Med Genet A.* 2009;149A(4):584-587. doi:10.1002/ajmg.a.32703
26. Grady JP, Pickett SJ, Ng YS, et al. mtDNA heteroplasmy level and copy number indicate disease burden in m.3243A>G mitochondrial disease. *EMBO Mol Med.* 2018;10(6):e8262. doi:10.15252/emmm.201708262
27. Liou CW, Huang CC, Wei YH. Molecular analysis of diabetes mellitus-associated A3243G mitochondrial DNA mutation in Taiwanese cases. *Diabetes Res Clin Pract.* 2001;54(suppl 2):S39-S43. doi:10.1016/s0168-8227(01)00334-5
28. 't Hart LM, Jansen JJ, Lemkes HH, de Knijff P, Maassen JA. Heteroplasmy levels of a mitochondrial gene mutation associated with diabetes mellitus decrease in leucocyte DNA upon aging. *Hum Mutat.* 1996;7(3):193-197. doi:10.1002/(SICI)1098-1004(1996)7:3<193::AID-HUMU2>3.0.CO;2-C
29. Laloi-Michelin M, Meas T, Ambonville C, et al; Mitochondrial Diabetes French Study Group. The clinical variability of maternally inherited diabetes and deafness is associated with the degree of heteroplasmy in blood leukocytes. *J Clin Endocrinol Metab.* 2009;94(8):3025-3030. doi:10.1210/jc.2008-2680
30. Uimonen S, Moilanen JS, Sorri M, Hassinen IE, Majamaa K. Hearing impairment in patients with 3243A -->G mtDNA mutation: phenotype and rate of progression. *Hum Genet.* 2001;108(4):284-289. doi:10.1007/s004390100475
31. Suzuki S, Oka Y, Kadowaki T, et al; Research Committee or Specific Types of Diabetes Mellitus with Gene Mutations of the Japan Diabetes Society. Clinical features of diabetes mellitus with the mitochondrial DNA 3243 (A-G) mutation in Japanese: maternal inheritance and mitochondria-related complications. *Diabetes Res Clin Pract.* 2003;59(3):207-217. doi:10.1016/s0168-8227(02)00246-2
32. Yang M, Xu L, Xu C, et al. The mutations and clinical variability in maternally inherited diabetes and deafness: an analysis of 161 patients. *Front Endocrinol (Lausanne)*. 2021;12:728043. doi:10.3389/fendo.2021.728043
33. Sunde K, Blackburn PR, Cheema A, et al. Case report: 5 year follow-up of adult late-onset mitochondrial encephalomyopathy with lactic acid and stroke-like episodes (MELAS). *Mol Genet Metab Rep.* 2016;9:94-97. doi:10.1016/j.ymgmr.2016.11.002
34. Ji K, Zhao B, Lin Y, et al. "Myo-neuropathy" is commonly associated with mitochondrial $tRNA^{Lysine}$ mutation. *J Neurol.* 2020;267(11):3319-3328. doi:10.1007/s00415-020-10017-z

Clinical application of a real-time polymerase chain reaction test for *CYP2C19* genotyping based on genotype distribution in a healthy Korean population

Kuenyoul Park, MD[1,*], *Soo Jin Yoo, MD*[1]

[1]Department of Laboratory Medicine, Sanggye Paik Hospital, School of Medicine, Inje University, Seoul, Republic of Korea. Corresponding author: Soo Jin Yoo; sjyoo@paik.ac.kr

Key words: CYP2C19; real-time PCR; genotype; alleles

Abbreviations: KOVA, Korean Variant Archive; CNVs, copy number variations

Laboratory Medicine 2024;55:234-237; https://doi.org/10.1093/labmed/lmad070

ABSTRACT

Objective: With the recent reports of additional alleles of the *CYP2C19* gene with decreased or no function, the clinical utility of real-time polymerase chain reaction (PCR)-based testing that detects only a small number of variant targets needs to be evaluated.

Method: We retrospectively reviewed 7-year data for real-time PCR test records from a single hospital and analyzed *CYP2C19* genotypes from publicly available whole-genome or whole-exome data from a healthy Korean population.

Results: Of the 2327 test results in this hospital, the *1 allele was most common (60.5%), followed by *2 (28.0%), *3 (10.1%), and *17 (1.4%). Among 5305 healthy Korean individuals, the frequencies of the *2, *3, and *17 alleles were 28.6%, 9.9%, and 1.0%, respectively, which were not statistically different from those of the hospital data (P = .4439, P = .6025, and P = .1142, respectively). Interestingly, the total frequency of additional nonfunctional alleles (*4, *6, *22, and *24) that could not be detected using real-time PCR was only 0.1%, with a total allele count of 8.

Conclusion: Our study shows that the clinical utility of real-time PCR for *CYP2C19* genotyping remains satisfactory. However, caution should be exercised because the test can miss patients with decreased *CYP2C19* function.

Introduction

The *CYP2C19* gene, located on chromosome 10q24, is a member of the CYP2C subfamily and plays a key role in metabolizing commonly prescribed drugs. *CYP2C19* genotyping is widely used to guide the dosage of drugs affected by *CYP2C19*, including clopidogrel, tricyclic antidepressants, selective serotonin reuptake inhibitors, proton-pump inhibitors, and voriconazole.[1–5] Only 4 alleles of the gene, *1, *2, *3, and *17, have been annotated for the *CYP2C19* phenotype, so individuals with *2 or *3 alleles have been classified as intermediate or poor metabolizers requiring consideration of alternative antiplatelet treatment, according to previous guidelines on clopidogrel and CYP2C19 published in 2013.[6] Previous studies have shown that intermediate or poor metabolizers are associated with higher rates of major adverse vascular events and significantly elevated P2Y12 reaction units in the clopidogrel platelet reactivity test.[2,7] Several real-time polymerase chain reaction (PCR) kits targeting these 4 alleles have been developed and evaluated.[8–10] However, the most recent guidelines, which were updated in 2022, include the additional decreased function allele *9 for phenotypic prediction.[2] In addition, the clinical functions of other novel alleles have also been annotated in PharmVar; the *9, *10, *16, *19, *25, and *26 alleles are annotated as decreased function alleles, and the *4, *5, *6, *7, *8, *22, *24, and *35 alleles are annotated as no function alleles (**TABLE 1**).[11] Therefore, it is necessary to confirm whether it is acceptable to continue to use the real-time PCR kits that do not contain these newly identified alleles. The genotype distribution of *CYP2C19* in Korea has been previously described in a limited number of healthy individuals (<500 individuals).[12–14] Therefore, a large number of healthy individuals must be screened for the *CYP2C19* genotype to evaluate the clinical utility of a real-time PCR method that detects only a small number of variant targets. In this study, we analyzed *CYP2C19* genotypes using publicly available whole-genome or whole-exome sequencing data from a healthy Korean population of more than 5000 individuals. In addition, we retrospectively reviewed 7-year data from real-time PCR test records from a single hospital and compared the allele frequencies with those obtained from the public data.

Methods

All results of the patients tested with *CYP2C19* genotyping were reviewed between January 2016 and December 2022 at a university-affiliated hospital in Seoul, Korea. Genomic DNA samples were extracted

using the AccuPrep Genomic DNA Extraction Kit (Bioneer), and the extracted DNA was amplified using the Real-Q CYP2C19 Genotyping Kit (Biosewoom). The allelic profile of each sample was determined based on the presence of the following variants: c.681G>A, c.636G>A, and c.806C>T. These variants were annotated as *2, *3, and *17, respectively. The predicted phenotypes of the patients were annotated according to current guidelines.[2] Clinical and demographic data were obtained from patients' electronic medical records. We also analyzed *CYP2C19* genotypes from publicly available whole-genome or whole-exome data from a healthy Korean population using the Korean Variant Archive (KOVA) for a reference database of genetic variations in the Korean population (https://www.kobic.re.kr/kova/).[15] Single-nucleotide variants of alleles with altered function according to the PharmVar scheme (https://www.pharmvar.org/gene/CYP2C19) were searched against KOVA and are depicted in **FIGURE 1**. The frequency of each allele was assumed from the frequency of signature variants of each allele in **TABLE 1**. χ^2 tests were performed to compare allele frequencies using the free MedCalc statistical calculator (https://www.medcalc.org/calc/). This study was approved by the Institutional Review Board of Sanggype Paik Hospital, which waived the need for written patient consent (2023-03-005).

TABLE 1. The signature variants of alleles with altered function annotated by PharmVar

Allele name	Signature variants (NM_000769.4)	Predicted function
CYP2C19*2	332-23A>G, 681G>A	No function
CYP2C19*3	636G>A	No function
CYP2C19*4	1A>G	No function
CYP2C19*5	1297C>T	No function
CYP2C19*6	395G>A	No function
CYP2C19*7	819 + 2T>A	No function
CYP2C19*8	358T>C	No function
CYP2C19*9	431G>A	Decreased function
CYP2C19*10	680C>T	Decreased function
CYP2C19*16	1324C>T	Decreased function
CYP2C19*17	-806C>T	Increased function
CYP2C19*19	151A>G	Decreased function
CYP2C19*22	557G>C	No function
CYP2C19*24	1004G>A	No function
CYP2C19*25	1344C>G	Decreased function
CYP2C19*26	766G>A	Decreased function
CYP2C19*35	332-23A>G	No function

Results

During the 7 years, a total of 2327 samples were submitted for *CYP2C19* testing in this hospital. The mean age of the patients tested for the *CYP2C19* genotype was 69 years, and 58.6% of the patients were men. Most of these tests were requested by the neurology department (96.2%) followed by neurosurgery (2.0%) and internal medicine (0.9%) departments. Patients referred from the neurology department were to be evaluated for antiplatelet therapy. Nineteen (86.4%) internal medicine patients were prescribed proton pump inhibitors for gastrointestinal bleeding (16 patients) or peptic ulcers (3 patients). Overall, the frequencies of the *1, *2, *3, and *17 alleles were 60.5%, 28.0%, 10.1%, and 1.4%, respectively. Of the 2327 genotype results, 46.2% and 15.0% were predicted to be intermediate and poor metabolizers, respectively. In contrast, only 1.8% and 0.1% were predicted to be rapid and ultrarapid metabolizers, respectively (**TABLE 2**).

Among 5305 healthy Korean individuals, the allele frequencies of the *2, *3, and *17 alleles were 28.6%, 9.9%, and 1.0%, respectively. Comparison of the allele frequencies of the general population with those observed in the hospital showed that the results of none of the 3 alleles were statistically different (P = .4439, .6025, and .1142, respectively). Among the other alleles with an altered function that were not detected using real-time PCR, *4 was the most common, with an allele count of 5 in the Korean population, and 5 Korean individuals had this allele as heterozygous. The others were *6, *22, and *24, with allele counts of 1. All 4 detected alleles, *4, *6, *22, and *24, were predicted to have no function. No other alleles with altered functions were found in KOVA.

FIGURE 1. The single nucleotide variants of alleles with altered function. *CYP2C19* **NM_007294.3. Upper arrows indicate variants of alleles with increased (blue arrow) and decreased function (yellow arrows) and lower arrows indicate those with no function (red arrows). All variants detected in the Korean Variant Archive (KOVA) for a reference database of genetic variations in the Korean population are displayed in a box.**

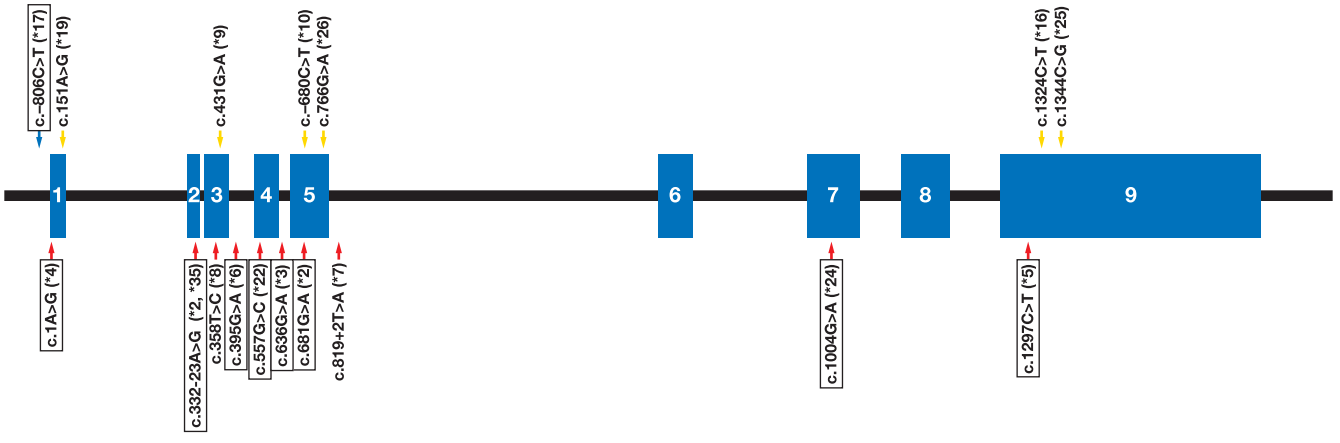

Discussion

In a retrospective review of 7 years of *CYP2C19* genotyping records, the distribution of genotypes from 2327 patients was similar to that of the KOVA data from over 5000 healthy Korean individuals. The allele frequencies from this hospital and the KOVA data were similar to those reported in other studies[12–14] of the *CYP2C19* genotype in the Korean population (**TABLE 3**). As shown in this study, the proportion of intermediate and poor metabolizers requiring adjustment of antiplatelet therapy was much higher in Asia at 45.5% and 12.2%, respectively, than that in the other regions at 23.0% and 29.1% and 1.8% and 3.1%, respectively, according to the meta-analysis.[16] Therefore, *CYP2C19* genotyping is particularly important in the Asian region.

TABLE 2. Characteristics of the patients who underwent *CYP2C19* genotype testing

Characteristic	Value
Median age (interquartile range), y	70 (61-79)
Female sex, n (%)	964 (41.4)
Department, n (%)	
Neurology	2238 (96.2)
Neurosurgery	47 (2.0)
Internal medicine	22 (0.9)
Others	20 (0.9)
CYP2C19 genotype, n (%)	
Ultrarapid metabolizer	
*17/*17	2 (0.1)
Rapid metabolizer	
*1/*17	43 (1.8)
Normal metabolizer	
*1/*1	857 (36.8)
Intermediate metabolizer	
*1/*3	266 (11.4)
*1/*2	791 (34)
*3/*17	8 (0.3)
*2/*17	10 (0.4)
Poor metabolizer	
*2/*3	134 (5.8)
*2/*2	184 (7.9)
*3/*3	32 (1.4)

The frequencies of some recently annotated rare alleles in Asians also deserve attention. Although only a few studies have been published, they suggest that these frequencies are very low. In an Indian study of 2000 individuals, rare alleles other than *2, *3, and *17 were found in only 1 case of *6 (0.05%) and 2 cases of *8 (0.1%).[17] Similarly, additional alleles affecting gene function were observed in less than 0.1% of the alleles from the KOVA data, with the highest value for the *4 allele being 0.05%. This study demonstrates the robust distribution of the *CYP2C19* genotype in the Korean population. However, larger screening studies are required to identify the rare genotypes in the Korean population.

Almost all patients with *CYP2C19* genotyping were from the neurology or neurosurgery departments. *CYP2C19* genotyping in these patients could be attributed to clopidogrel dose adjustments. Gastrointestinal bleeding and peptic ulcer were the most common diagnoses in patients in the internal medicine department. In these patients, proton pump inhibitors may have been associated with *CYP2C19* genotyping. However, *CYP2C19* genotyping also affects the recommended dosage of tricyclic antidepressants, selective serotonin reuptake inhibitors, and voriconazole.[1,4,5] Therefore, increased awareness regarding *CYP2C19* genotyping is required for services that primarily use these drugs.

Recently, several *CYP2C19* alleles have been reported to affect drug dosing in the context of *CYP2C19* metabolism. However, only a few major alleles have been observed in more than 0.1% of the healthy Korean population: *2, *3, and *17. A Chinese study showed that antiplatelet therapy guided by *CYP2C19* genotyping, targeting only the *2 and *3 alleles but with a short turnaround time of 48 hours, reduced major adverse events in patients with acute coronary syndrome.[18] The addition of some rare allelic targets may have clinical advantages. However, notably, increasing the number of primer-probe pairs in real-time PCR can be a technical challenge in the assay and may affect the accuracy of the results. Increased resource consumption may be the issue, considering the frequencies of the rare alleles. In addition, although an increased number of alleles may affect the clinical utility of real-time PCR kits, the transition to sequencing inevitably increases the burden of interpretation in clinical laboratories. Considering the genotype distribution in the Korean population, turnaround time, accessibility to devices, and convenience, real-time PCR kits are still clinically useful in Korea; however, continuous monitoring of the prevalence of novel alleles affecting *CYP2C19* function must be performed.

However, real-time PCR may fail to detect rare nontarget alleles. Clinical laboratories should inform physicians regarding the limitations

TABLE 3. Allele frequencies (%) from the previous studies of *CYP2C19* genotyping in the Korean population and this study

Alleles	Lee et al (n = 377)[13]	Lee et al (n = 463)[12]	Kim et al (n = 271)[11]	KOVA (n = 5305)
*1	64	60.6	60.0	60.4[a]
*2	28	29.9	28.4	28.6
*3	8	9.5	10.1	9.9
*17	Not tested	Not tested	1.5	1.0
Others	Not tested	Not tested	Not tested	0.1[b]

KOVA, Korean Variant Archive.
*[a]5.1% of the alleles in the KOVA (https://www.kobic.re.kr/kova/) data that do not carry c.991A>G are considered to be *38, the legacy label of which is *1A. Therefore, they were counted as *1.*
*[b]The other alleles included 5 *4 alleles, 1 *6 allele, 1 *22 allele, and 1 *24 allele.*

of real-time PCR testing and the clinical implications of undetected rare alleles, including *4, *6, *22, and *24 in the comments of test reports. The limitation of real-time PCR could be mentioned in the test report as follows: "This test may not detect rare nonfunctional alleles, which are present in approximately 0.1% of the Korean population. When using typical doses of clopidogrel, sequencing may be indicated if altered clopidogrel activity is clinically suspected." In some cases of recurrent vascular events or aberrant $P2Y_{12}$ reaction unit value on platelet reactivity monitoring, a rare allele not detected by real-time PCR may be suspected,[7,19,20] and sequencing analysis could be considered in collaboration with the clinical laboratory.

Our study was limited by its retrospective nature; no residual samples were available for sequencing to confirm the allelic profile. In addition, alleles such as *36 and *37, which are copy number variations (CNVs) of *CYP2C19* were not investigated. Therefore, further studies using CNV detection tools, such as CNV prediction using next-generation sequencing data and multiplex ligation-dependent probe amplification, are required to determine the frequency of these alleles.

In conclusion, we report that the clinical utility of real-time PCR for *CYP2C19* genotyping is still satisfactory, considering the extremely low frequency of alleles affecting *CYP2C19* gene function other than the *2, *3, and *17 alleles. However, caution should be exercised considering patients with decreased *CYP2C19* function may be missed.

Conflict of Interest Disclosure

The authors have nothing to disclose.

REFERENCES

1. Hicks JK, Sangkuhl K, Swen JJ, et al. Clinical pharmacogenetics implementation consortium guideline (CPIC) for CYP2D6 and CYP2C19 genotypes and dosing of tricyclic antidepressants: 2016 update. *Clin Pharmacol Ther.* 2017;102(1):37-44. https://doi.org/10.1002/cpt.597
2. Lee CR, Luzum JA, Sangkuhl K, et al. Clinical pharmacogenetics implementation consortium guideline for CYP2C19 genotype and clopidogrel therapy: 2022 update. *Clin Pharmacol Ther.* 2022;112(5):959-967. https://doi.org/10.1002/cpt.2526
3. Lima JJ, Thomas CD, Barbarino J, et al. Clinical pharmacogenetics implementation consortium (CPIC) guideline for CYP2C19 and proton pump inhibitor dosing. *Clin Pharmacol Ther.* 2021;109(6):1417-1423. https://doi.org/10.1002/cpt.2015
4. Moriyama B, Obeng AO, Barbarino J, et al. Clinical pharmacogenetics implementation consortium (CPIC) guidelines for CYP2C19 and voriconazole therapy. *Clin Pharmacol Ther.* 2017;102(1):45-51. https://doi.org/10.1002/cpt.583
5. Hicks JK, Bishop JR, Sangkuhl K, et al., Clinical Pharmacogenetics Implementation Consortium. Clinical pharmacogenetics implementation consortium (CPIC) guideline for CYP2D6 and CYP2C19 genotypes and dosing of selective serotonin reuptake inhibitors. *Clin Pharmacol Ther.* 2015;98(2):127-134. https://doi.org/10.1002/cpt.147
6. Scott SA, Sangkuhl K, Stein CM, et al., Clinical Pharmacogenetics Implementation Consortium. Clinical pharmacogenetics implementation consortium guidelines for CYP2C19 genotype and clopidogrel therapy: 2013 update. *Clin Pharmacol Ther.* 2013;94(3):317-323. https://doi.org/10.1038/clpt.2013.105
7. Tousoulis D, Siasos G, Zaromitidou M, et al. The impact of CYP2C19 genotype on cardiovascular events and platelet reactivity in patients with coronary artery disease receiving clopidogrel. *Int J Cardiol.* 2013;168(2):1594-1596. https://doi.org/10.1016/j.ijcard.2013.01.040
8. Kwong KM, Tam CC, Chan R, et al. Comparison of single nucleotide polymorphism genotyping of CYP2C19 by loop-mediated isothermal amplification and real-time PCR melting curve analysis. *Clin Chim Acta.* 2018;478:45-50. https://doi.org/10.1016/j.cca.2017.12.013
9. Larsen JB, Rasmussen JB. Pharmacogenetic testing revisited: 5' nuclease real-time polymerase chain reaction test panels for genotyping CYP2D6 and CYP2C19. *Pharmgenomics Pers Med*. 2017;10:115-128. https://doi.org/10.2147/PGPM.S131580
10. Kim HK, Kang HJ, Ko DH, et al. Comparison of the microarray-based assay, the real-time PCR assay, and the bidirectional sequencing method for CYP2C19 genotyping. *Clin Lab.* 2015;61(8):1109-1112. https://doi.org/10.7754/clin.lab.2015.141214
11. Botton MR, Whirl-Carrillo M, Del Tredici AL, et al. PharmVar GeneFocus: CYP2C19. *Clin Pharmacol Ther.* 2021;109(2):352-366. https://doi.org/10.1002/cpt.1973
12. Kim KA, Song WK, Kim KR, Park J-Y. Assessment of CYP2C19 genetic polymorphisms in a Korean population using a simultaneous multiplex pyrosequencing method to simultaneously detect the CYP2C19*2, CYP2C19*3, and CYP2C19*17 alleles. *J Clin Pharm Ther.* 2010;35(6):697-703. https://doi.org/10.1111/j.1365-2710.2009.01069.x
13. Lee JH, Jung HY, Choi KD, Song HJ, Lee GH, Kim J-H. The influence of CYP2C19 polymorphism on eradication of *Helicobacter pylori*: a prospective randomized study of lansoprazole and rabeprazole. *Gut Liver*. 2010;4(2):201-206. https://doi.org/10.5009/gnl.2010.4.2.201
14. Lee SS, Lee SJ, Gwak J, et al. Comparisons of CYP2C19 genetic polymorphisms between Korean and Vietnamese populations. *Ther Drug Monit.* 2007;29(4):455-459. https://doi.org/10.1097/FTD.0b013e31811f383c
15. Lee J, Lee J, Jeon S, et al. A database of 5305 healthy Korean individuals reveals genetic and clinical implications for an East Asian population. *Exp Mol Med.* 2022;54(11):1862-1871. https://doi.org/10.1038/s12276-022-00871-4
16. Klein MD, Williams AK, Lee CR, Stouffer GA. Clinical utility of CYP2C19 genotyping to guide antiplatelet therapy in patients with an acute coronary syndrome or undergoing percutaneous coronary intervention. *Arterioscler Thromb Vasc Biol.* 2019;39(4):647-652. https://doi.org/10.1161/ATVBAHA.118.311963
17. Naushad SM, Vattam KK, Devi YKD, Hussain T, Alrokayan S, Kutala VK. Mechanistic insights into the CYP2C19 genetic variants prevalent in the Indian population. *Gene.* 2021;784:145592. https://doi.org/10.1016/j.gene.2021.145592
18. Shi X, Zhang Y, Zhang Y, et al. Personalized antiplatelet therapy based on CYP2C19 genotypes in Chinese ACS patients undergoing PCI: a randomized controlled trial. *Front Cardiovasc Med*. 2021;8:676954. https://doi.org/10.3389/fcvm.2021.676954
19. Lee SH, Jeong YH, Hong D, et al., PTRG-DES Registry Investigators. Clinical impact of CYP2C19 genotype on clopidogrel-based antiplatelet therapy after percutaneous coronary intervention. *JACC Cardiovasc Interv*. 2023;16(7):829-843. https://doi.org/10.1016/j.jcin.2023.01.363
20. Wang Y, Zhao X, Lin J, et al., CHANCE investigators. Association between CYP2C19 loss-of-function allele status and efficacy of clopidogrel for risk reduction among patients with minor stroke or transient ischemic attack. *JAMA.* 2016;316(1):70-78. https://doi.org/10.1001/jama.2016.8662

A meta-analysis of the accuracy of Xpert MTB/RIF in diagnosing intestinal tuberculosis

Yuan-Lin Ding, BSMed,[1,2,], Rui-Chao Yan, BSMed,[1,2,*], Hao-Kai Chen, BM,[2,3], Xu-Guang Guo, MD,[2,3,4,5,6,7,]*

[1]Department of Medical Laboratory Science, King Med School of Laboratory Medicine, Guangzhou Medical University, Guangzhou, China; [2]Department of Clinical Laboratory Medicine, The Third Affiliated Hospital of Guangzhou Medical University, Guangzhou, China; [3]Department of Clinical Medicine, Third Clinical School of Guangzhou Medical University, Guangzhou, China; [4]Department of Medical Imageology, Second Clinical School of Guangzhou Medical University, Guangzhou, China; [5]Guangdong Provincial Key Laboratory of Major Obstetric Diseases and [6]Key Laboratory of Reproduction and Genetics of Guangdong Higher Education Institutes, Third Affiliated Hospital of Guangzhou Medical University, Guangzhou, China; [7]Guangzhou Key Laboratory for Clinical Rapid Diagnosis and Early Warning of Infectious Diseases, King Med School of Laboratory Medicine, Guangzhou Medical University, Guangzhou, China. Corresponding author: Xu-Guang Guo; gysygxg@gmail.com. *Contributed equally.

Key words: Xpert MTB/RIF; intestinal tuberculosis; meta-analysis; diagnostic; tuberculosis; *Mycobacterium tuberculosis*

Abbreviations: TB, tuberculosis; ITB, intestinal TB; EPTB, extrapulmonary TB; CD, Crohn's disease; PCR, polymerase chain reaction; MDR-TB, multidrug resistant TB; RIF, rifampicin; INH, isoniazid; CNKI, China National Knowledge Infrastructure; TP, true positive; FP, false positive; FN, false negative; TN, true negative; CRS, composite reference criteria; AUC, area under the curve; sROC, summary receiver operating characteristic; DORs, diagnostic odds ratios; PLR, positive likelihood ratio; NLR, negative likelihood ratio

Laboratory Medicine 2024;55:238-244; https://doi.org/10.1093/labmed/lmad072

ABSTRACT

Objective: A detection method with high efficiency and accuracy is urgently needed in clinical work. The purpose of our study was to determine the diagnostic accuracy of the Xpert MTB/RIF assay for intestinal tuberculosis (ITB).

Methods: We searched PubMed and 4 other databases from their establishment to July 19, 2022, for published essays of diagnostic performance in which Xpert MTB/RIF was used to test patients with clinically suspected ITB. An assessment of the quality of the selected literature was conducted using QUADAS-2. We built forest plots by MetaDiSc software.

Results: The pooled Xpert MTB/RIF sensitivity was 48%, and the specificity was 99%. Moreover, the positive likelihood ratio for ITB diagnosis was 21.61. The negative likelihood ratio was 0.54. There were substantial variations between the study estimates of sensitivity (I^2 = 87.6%) and specificity (I^2 = 82.4%).

Conclusion: Intestinal TB is detected with limited diagnostic sensitivity by Xpert MTB/RIF but with high specificity. An Xpert-positive result may facilitate the rapid identification of ITB cases. Nevertheless, a negative result has less certainty in excluding the disease.

Introduction

With HIV infection and the utilization of anti-immunosuppressive drugs, the scope of tuberculosis (TB) infection is expanding daily. As an important extrapulmonary TB (EPTB), intestinal TB (ITB) accounts for approximately 30% of extrapulmonary tuberculosis cases.[1] In India, where the burden of TB is highest, 20% of TB cases are extrapulmonary, with peritoneal TB accounting for nearly 13%.[2] Pakistan has the fifth largest burden of TB, and a study in Pakistan showed that EPTB accounted for nearly 30% of all open TB cases, with 21% of EPTB originating in the abdomen.[3] The most common cumulative site of peritoneal TB is the gastrointestinal tract, accounting for 43% to 65% of all cases of peritoneal TB.[4-17] With high incidence, ITB occurs frequently in developing countries. Intestinal TB can cause diarrhea, abdominal pain, abdominal mass, constipation, and a series of nonspecific clinical manifestations,[18] which leads to its clinical diagnosis being controversial and challenging. In addition, there are significant challenges in separating Crohn's disease (CD) from ITB, resulting in high morbidity and mortality due to misdiagnosis or delayed diagnosis.[19] As a qualitative assay, Xpert MTB/RIF is a timely polymerase chain reaction (PCR) kit that detects both *Mycobacterium tuberculosis* and rifampicin (RIF) resistance simultaneously. Furthermore, RIF resistance can be an indication for MDR-TB (multidrug resistant TB, refers to resistance to both isoniazid [INH] and RIF).[20] That is to say, this assay can assist in determining MDR-TB by detecting the presence or absence of RIF resistance, assuming that there is INH resistance. At present, although there has been widespread application of Xpert MTB/RIF for detecting pulmonary TB, it is rarely used for ITB. A meta-analysis was conducted to assess the diagnostic accuracy of Xpert MTB/RIF in ITB.

Methods

Sources of Data and Strategies for Retrieval

A total of 5 databases were used, including PubMed, Embase, Web Of Science, the Cochrane Library, and the China National Knowledge Infrastructure (CNKI), from the time they were founded to July 19, 2022. The

accuracy of Xpert MTB/RIF in ITB detection was evaluated by retrieving published articles. The search was performed by searching MeSH terms and EMTREE terms obtained by "Xpert MTB/RIF" and "intestinal tuberculosis" in PubMed and Embase. We also further explored possible candidate studies from the references to the included articles.

Inclusion Criteria

Our inclusion criteria were as follows: (1) articles that evaluated Xpert MTB/RIF detection as an ITB diagnostic tool; (2) cohort studies conducted prospectively or retrospectively; (3) reference criteria were clearly defined and suitable for our study; and (4) complete and extracted data: true positive (TP), false positive (FP), false negative (FN), and true negative (TN). Studies with too few samples (<10) conference summaries, articles without complete 2 × 2 contingency table data, and articles written in languages other than English and Chinese were excluded.

Standard of Reference

The study used composite reference criteria (CRS) or *Mycobacterium* culture as references. Composite reference criteria include clinical manifestations, histopathology, biochemical test results, smears, culture, other nucleic acid amplification tests, and treatment response to anti-TB drugs.

Filtering and Selection of Literature

Two investigators independently completed the process of searching relevant literature, reviewing the abstract, reviewing the full text of the article, and extracting data from the 2 × 2 contingency table. The 2 investigators then checked whether the extracted data were consistent, and if they were not, the above steps were repeated. Only when the data were consistent were the analysis of the data and the creation of the figures performed. A third investigator was consulted to resolve the differences between the 2 investigators. All reviewed articles in this study underwent this review process.

Data Extraction

Among the data we extracted were author, year, study design, country, specimen origin, TP, FP, FN, and TN values as well as reference criteria (mycobacterial culture and CRS) and type of specimens. In the same manner, the necessary information was independently extracted by 2 investigators from each included article and resolved through discussion with a third researcher. In the papers that we reviewed, the 3 studies from China give the complete 2 × 2 contingency table data directly in the article for us to extract. The other 5 studies from India provide partial data as well as sensitivity, specificity, positive predictive value, and negative predictive value, which allows us to calculate the 2 × 2 contingency table data.

Assessment of Study Quality

QUADAS-2, a quality assessment tool to assess the accuracy of selected articles, was used to ensure quality and avoid the possibility of bias, which was controlled by 2 investigators separately. There are 4 domains in QUADAS-2: patient selection, index tests, reference standards, and flow and timing.

Data Analysis

The TP, FP, FN, and TN values for each included article were obtained as well as the combined sensitivity, and specificity estimates and 95% CI for Xpert MTV/RIF were calculated. We graphically generated the results by mapping the sensitivity and specificity of forest figures. The area under the curve (AUC) was calculated from summary receiver operating characteristic (sROC) curves. To assess heterogeneity between studies and benchmarks, I^2 statistics were used. We used MetaDiSc software to build pooled forest figures for overall diagnostic sensitivity and specificity (95% CI) for each study.

Results

Identification of Studies

Through the retrieval strategy, 119 candidate articles were retrieved from the databases mentioned above. Thirty-one studies were included for full-text article assessment after scanning abstracts and titles and eliminating duplicate articles. Based on the inclusion criteria, 8 articles qualified for inclusion (**FIGURE 1** shows a flow diagram of study identification and inclusion), including 4 prospective studies and 4 retrospective studies.[21-28]

Characteristics of the Study

TABLE 1 summarizes the characteristics of the trials and participants included in the study. By carefully reviewing all the included literature, we concluded that "colonic biopsy" and "colonoscopic tissue samples" are essentially the same, both being biopsies taken from intestinal tissue during colonoscopy. The reason for the different presentation in **TABLE 1** is that we adopted a different presentation for each of the included studies. Similarly, "intestinal mucosal biopsy" and "intestinal tissue"

FIGURE 1. Flow diagram of study identification and inclusion.

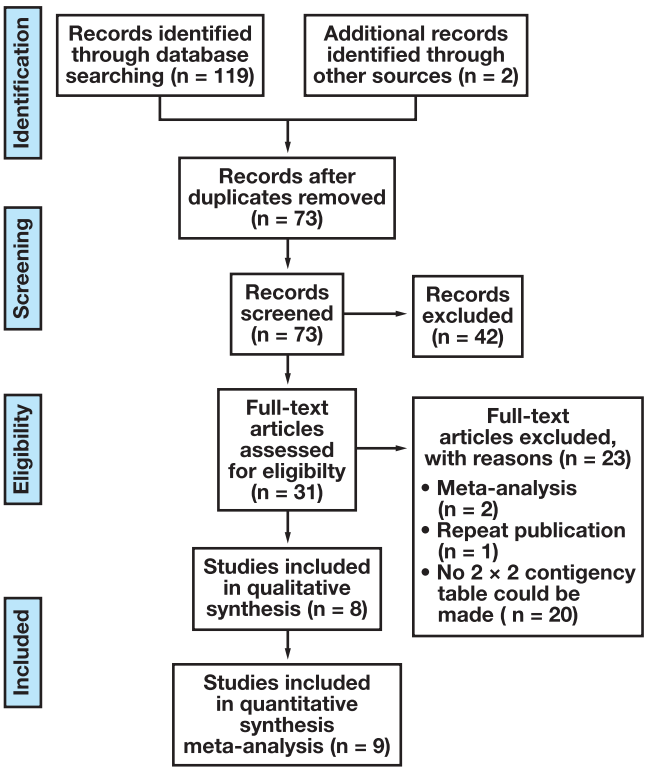

TABLE 1. Characteristics of the included studies (n = 8)

Author	Year	Study design	Country	Reference standard	Bacterial species	Type of specimens	TP	FP	FN	TN
Mei et al[23]	2016	Prospective	China	Clinical diagnosis	MTB	Intestinal mucosal biopsy	19	0	13	48
Kumar et al[28]	2017	Prospective	India	CRS	MTB	Colonic biopsy	3	0	34	61
Bellam et al[25]	2019	Retrospective	India	Histopathology	MTB	Colonic biopsy	8	0	17	15
Song et al[24]	2020	Retrospective	China	Culture	MTB	Intestinal mucosal biopsy	12	0	5	21
Xiong et al[26]	2020	Prospective	China	Clinical diagnosis	MTB	Stool	84	0	55	115
Alex et al[27]	2020	Retrospective	India	Clinical suspicion and histological	MTB	Intestinal tissue	5	7	2	25
Fei et al[21]	2021	Prospective	China	CRS/culture	MTB	Biopsy	4	0	24	43
						Surgical	10	0	4	3
Paulose et al[22]	2021	Retrospective	India	CRS	MTB	Colonoscopic tissue samples	14	0	21	391

CRS, composite reference criteria; MTB, Mycobacterium tuberculosis.

essentially both refer to biopsy on the mucosa of intestinal tissue for the same reasons as above.

Study Quality

A QUADAS-2 quality assessment was used to evaluate the included studies, and the results are presented in **FIGURE 2**. Four areas of the included articles were examined in QUADAS-2: patient selection, reference standard, index test, and flow and timing.

Diagnostic Accuracy of ITB Detected by Xpert MTB/RIF

Eight studies compared 1063 samples with the reference standard, and a range of 8% to 71% sensitivity and 78% to 100% specificity was found for Xpert MTB/RIF. The combined sensitivity and specificity of the Xpert MTB/RIF assay were 48% (95% CI, 42%-53%) with I^2 = 87.6% and 99% (95% CI, 98%-100%) with I^2 = 82.4%, respectively (**FIGURE 3**). Moreover, the positive likelihood ratio (PLR) for ITB diagnosis was 21.61 (95% CI, 4.40-106.24). The negative likelihood ratio (NLR) was 0.54 (95% CI, 0.38-0.78) (**FIGURE 4**). **FIGURE 5** shows the diagnostic odds ratios (DORs) for individual studies and the pooled DORs along with 95% CI. Compared with the reference criteria, sROC for Xpert MTB/RIF can be used to explain continuous diagnostic test results (**FIGURE 6**).

Discussion

Previous studies have noted the importance of making a rapid and accurate diagnosis for ITB because it has nonspecific clinical manifestations and is easily confused with Crohn's disease, leading to misdiagnosis and missed diagnosis. Rapid details and information on drug resistance make Xpert MTB/RIF a valuable diagnostic method. Considering that many national programs that address TB of the lungs and lymph nodes have already adopted Xpert MTB/RIF and the challenge of ITB diagnosis, we proposed the idea of using Xpert MTB/RIF to detect ITB. There have been systematic reviews and meta-analyses of Xpert MTB/RIF for the diagnosis of abdominal TB, but none are specific to ITB.

Some limitations of the study included the limited number of studies conducted on ITB in just 1 region (India or China). Another reason for the low number of studies may be related to the difficulty of obtaining materials and the need for clinical enteroscopy. In addition, there was considerable heterogeneity in our study, because some studies were prospective whereas others were retrospective. Thus, there was methodological heterogeneity. Reference standard differences can also contribute to heterogeneity in study. To determine whether the results would be considerably affected by a particular study, sensitivity analysis was also carried out, eliminating 1 study at a time and combining the other studies. We found that when Xiong et al's study[26] was excluded, the sensitivity of the combination fluctuated greatly. We considered that this was because the samples used in this study were from stool. By reviewing the original article,[21] we found that the exact location of the surgery was not specifically elaborated; we think that for the purpose of this assay, this ambiguity and potential difference in sampling location are likely not significant. The pathological changes of ITB mostly occur in the submucosa of the intestinal wall, and due to mucosal swelling, the endoscopic biopsy tissue tends to be smaller and the sampling area shallow and small, which may lead to false-negative results from Xpert MTB/RIF. In contrast, surgical pathological resection is more extensive and may reduce the possibility of missed diagnoses. Therefore, we tabulated

2024;55:238-244 | https://doi.org/10.1093/labmed/lmad072

FIGURE 2. Quality assessment of the included studies. A, Overall quality assessment of included studies. B, Quality assessment of the individual studies.

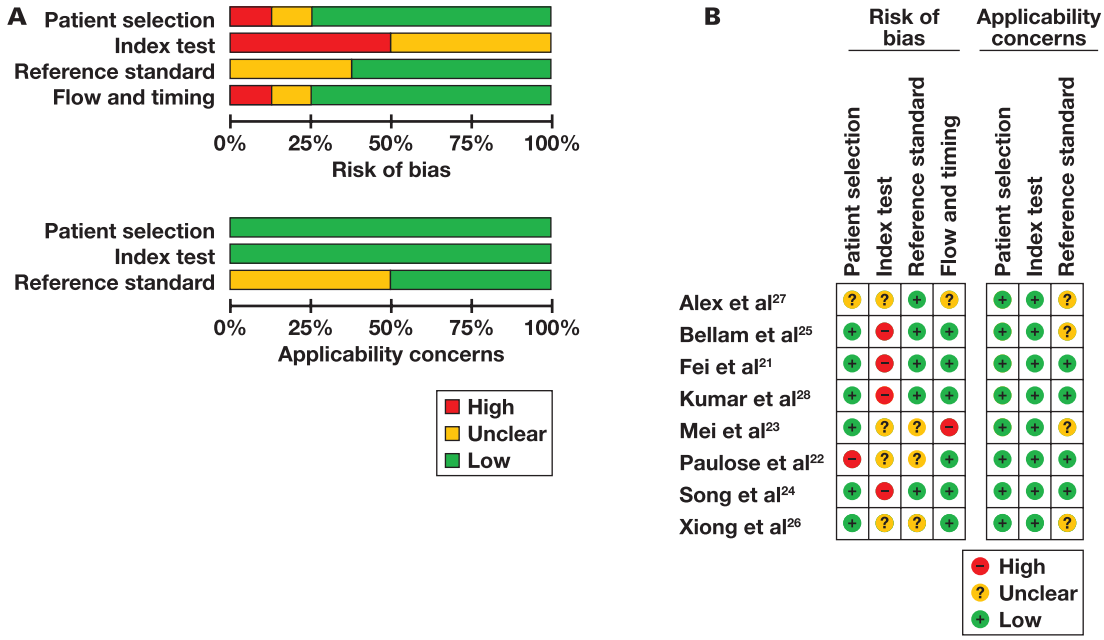

FIGURE 3. Forest plots of sensitivity (A) and specificity (B).

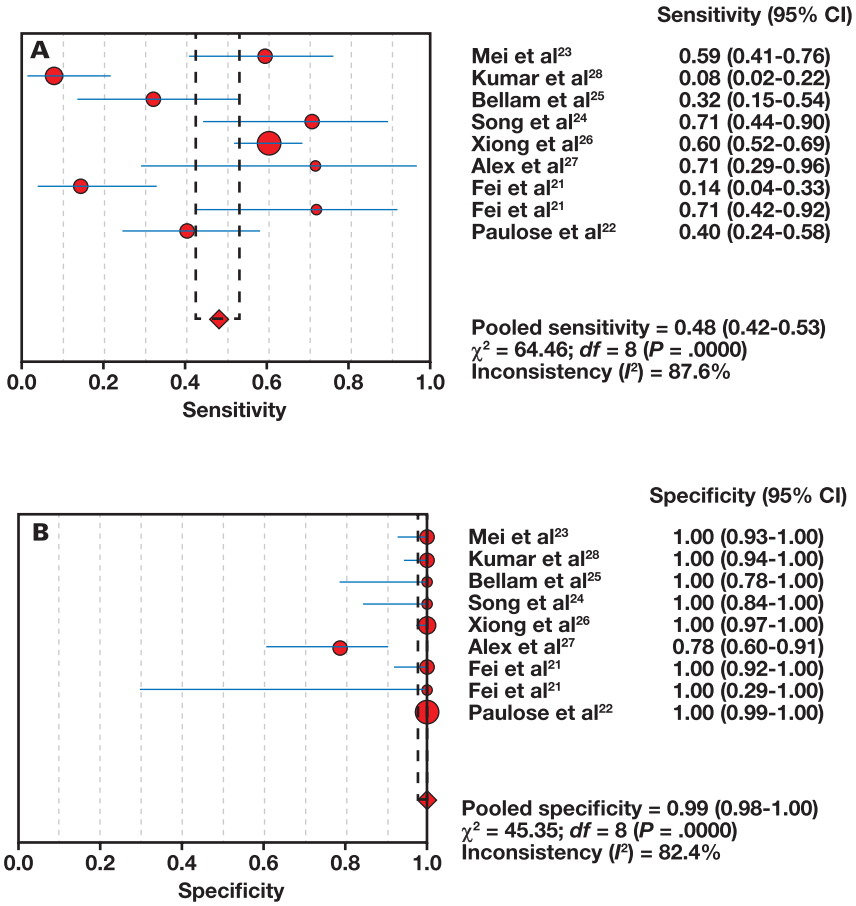

FIGURE 4. Forest plots of positive likelihood ratio (LR) (A) and negative LR (B).

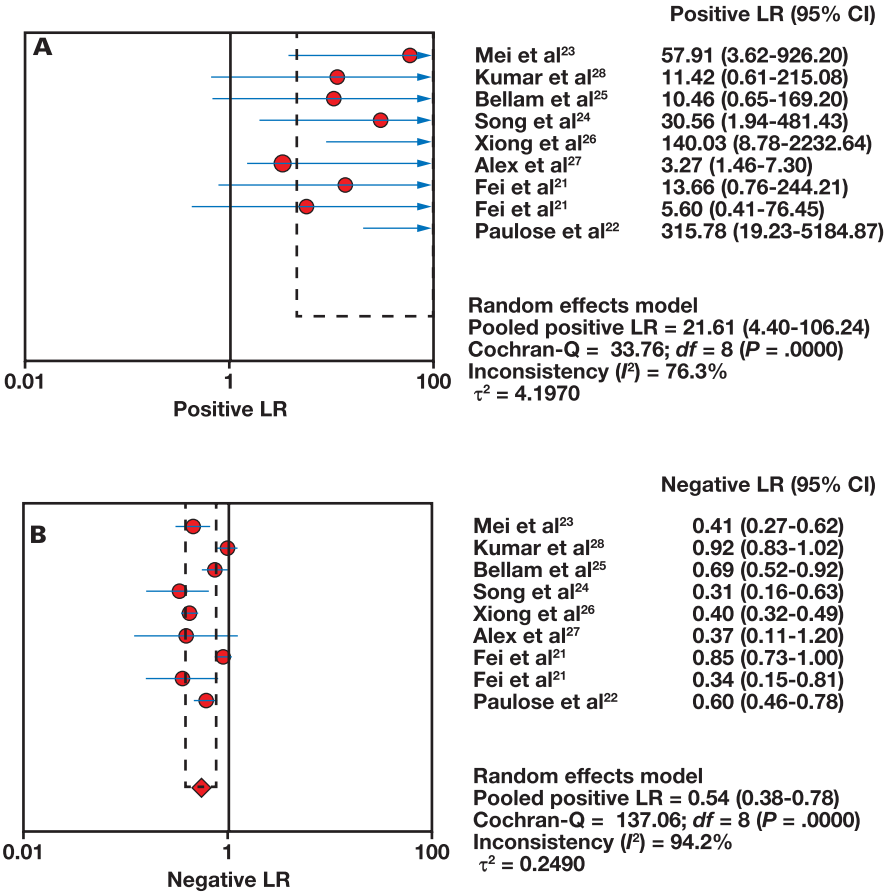

FIGURE 5. Forest plots of diagnostic odds ratio (OR) from Xpert MTB/RIF for the diagnosis of intestinal tuberculosis.

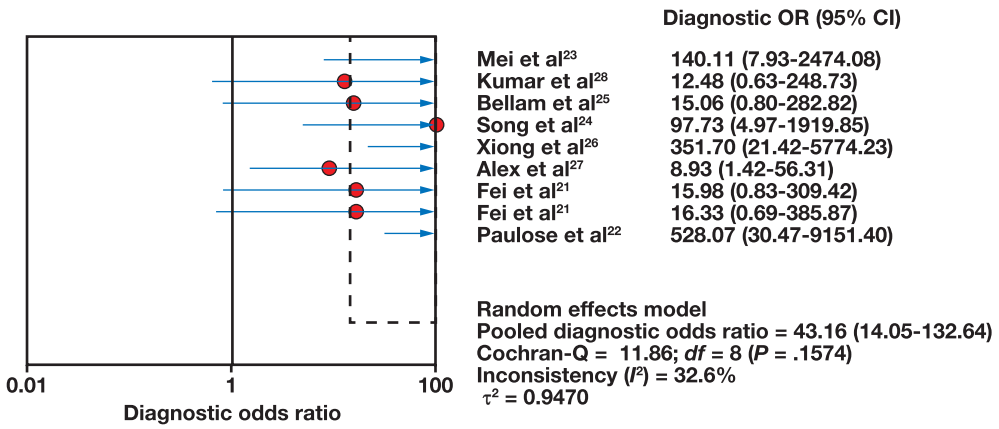

biopsy and surgery separately in the text. Regarding the distinction between "small intestine," "colon/large intestine," and "stool," we regret that we cannot elaborate on it in more detail at present because there are few studies on ITB.

According to our meta-analysis, the sensitivity of Xpert MTB/RIF for ITB detection has varied widely in different studies selected. Therefore, the pooled sensitivity (48% [95% CI, 42%-53%]) was not very high. The limited pooled sensitivity suggests that a negative Xpert assay for ITB has less certainty in excluding the disease. For better diagnosis and elimination of disease, PLR greater than 10 and NLR less than 0.1 are generally considered clinically significant.[29] We found that the PLR value and NLR value of ITB diagnosed by the Xpert MTB/RIF method were 21.61 (95% CI, 4.40-106.24; $P < .001$) and 0.54 (95% CI, 0.38-0.78; $P < .001$).

FIGURE 6. Forest plots of the summary receiver operating characteristic curve. Area under the curve (AUC) ± SE = 0.8474 ± 0.0777; Q* ± SE = 0.7787 ± 0.0731.

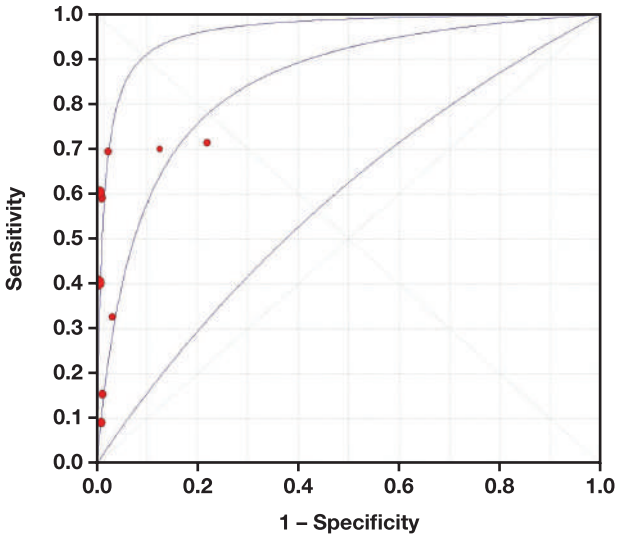

Conclusion

Overall, Xpert has limited sensitivity but high specificity for the detection of ITB. Based on the data mentioned above, Xpert MTB/RIF is promising as an earlier, faster, and more accurate method for detecting ITB than other tests.

Conflict of Interest Disclosure

The authors have nothing to declare.

REFERENCES

1. Aston NO. Abdominal tuberculosis. *World J Surg.* 1997;21(5):492-499. https://doi.org/10.1007/pl00012275
2. Cherian JJ, Lobo I, Sukhlecha A, et al. Treatment outcome of extrapulmonary tuberculosis under Revised National Tuberculosis Control Programme. *Indian J Tuberc.* 2017;64(2):104-108. https://doi.org/10.1016/j.ijtb.2016.11.028
3. Tahseen S, Khanzada FM, Baloch AQ, et al. Extrapulmonary tuberculosis in Pakistan: a nation-wide multicenter retrospective study. *PLoS One.* 2020;15(4):e0232134. https://doi.org/10.1371/journal.pone.0232134
4. Cho J-K, Choi YM, Lee SS, et al. Clinical features and outcomes of abdominal tuberculosis in southeastern Korea: 12 years of experience. *BMC Infect Dis.* 2018;18(1):699. https://doi.org/10.1186/s12879-018-3635-2
5. Chalya PL, Mchembe MD, Mshana SE, Rambau PF, Jaka H, Mabula JB. Clinicopathological profile and surgical treatment of abdominal tuberculosis: a single centre experience in northwestern Tanzania. *BMC Infect Dis.* 2013;13:270. https://doi.org/10.1186/1471-2334-13-270
6. Ramesh J, Banait GS, Ormerod LP. Abdominal tuberculosis in a district general hospital: a retrospective review of 86 cases. *QJM.* 2008;101(3):189-195. https://doi.org/10.1093/qjmed/hcm125
7. Mamo JP, Brij SO, Enoch DA. Abdominal tuberculosis: a retrospective review of cases presenting to a UK district hospital. *QJM.* 2013;106(4):347-354. https://doi.org/10.1093/qjmed/hct003
8. Singhal A, Gulati A, Frizell R, Manning AP. Abdominal tuberculosis in Bradford, UK: 1992-2002. *Eur J Gastroenterol Hepatol.* 2005;17(9):967-971. https://doi.org/10.1097/00042737-200509000-00013
9. Chien K, Seemangal J, Batt J, Vozoris NT. Abdominal tuberculosis: a descriptive case series of the experience in a Canadian tuberculosis clinic. *Int J Tuberc Lung Dis.* 2018;22(6):681-685. https://doi.org/10.5588/ijtld.17.0685
10. Tan K-K, Chen K, Sim R. The spectrum of abdominal tuberculosis in a developed country: a single institution's experience over 7 years. *J Gastrointest Surg.* 2009;13(1):142-147. https://doi.org/10.1007/s11605-008-0669-6
11. Mandavdhare HS, Singh H, Dutta U, Sharma V. A real-world experience with 6 months of antitubercular therapy in abdominal tuberculosis. *JGH Open.* 2019;3(3):201-205. https://doi.org/10.1002/jgh3.12136
12. Uygur-Bayramicli O, Dabak G, Dabak R. A clinical dilemma: abdominal tuberculosis. *World J Gastroenterol.* 2003;9(5):1098-1101. https://doi.org/10.3748/wjg.v9.i5.1098
13. Muneef MA, Memish Z, Mahmoud SA, Sadoon SA, Bannatyne R, Khan Y. Tuberculosis in the belly: a review of forty-six cases involving the gastrointestinal tract and peritoneum. *Scand J Gastroenterol.* 2001;36(5):528-532. https://doi.org/10.1080/003655201750153412
14. Urabinahatti KA, Singh AK, Nayak A, et al. Abdominal tuberculosis: an epidemiological profile and management of 40 cases in a tertiary set up. *Int Surg J*. 2016;3:1502-1508.
15. Nayagam JS, Mullender C, Cosgrove C, Poullis A. Abdominal tuberculosis: diagnosis and demographics, a 10-year retrospective review from a single centre. *World J Clin Cases.* 2016;4(8):207-212. https://doi.org/10.12998/wjcc.v4.i8.207
16. Singh A, Sahu MK, Panigrahi M, et al. Abdominal tuberculosis in Indians: still very pertinent. *J Clin Tuberc Other Mycobact Dis.* 2019;15:100097. https://doi.org/10.1016/j.jctube.2019.100097
17. Khan R, Abid S, Jafri W, Abbas Z, Hameed K, Ahmad Z. Diagnostic dilemma of abdominal tuberculosis in non-HIV patients: an ongoing challenge for physicians. *World J Gastroenterol.* 2006;12(39):6371-6375. https://doi.org/10.3748/wjg.v12.i39.6371
18. Kheyri Z, Ebadi N, Rahbari A, Ala M. Intestinal tuberculosis with Crohn's-like manifestations: a case report and a brief review of literature. *SN Compr Clin Med.* 2021;3(1):350-354. https://doi.org/10.1007/s42399-021-00739-0
19. Almadi MA, Ghosh S, Aljebreen AM. Differentiating intestinal tuberculosis from Crohn's disease: a diagnostic challenge. *Am J Gastroenterol.* 2009;104(4):1003-1012. https://doi.org/10.1038/ajg.2008.162
20. Somoskovi A, Parsons LM, Salfinger M. The molecular basis of resistance to isoniazid, rifampin, and pyrazinamide in *Mycobacterium tuberculosis*. *Respir Res.* 2001;2(3):164-168. https://doi.org/10.1186/rr54
21. Fei B, Zhou L, Zhang Y, Luo L, Chen Y. Application value of tissue tuberculosis antigen combined with Xpert MTB/RIF detection in differential diagnoses of intestinal tuberculosis and Crohn's disease. *BMC Infect Dis.* 2021;21(1):498. https://doi.org/10.1186/s12879-021-06210-8
22. Paulose RR, Kumar VA, Sharma A, et al. An outcome-based composite approach for the diagnosis of intestinal tuberculosis: a pilot study from a tertiary care centre in South India. *J R Coll Physicians Edinb.* 2021;51(4):344-350. https://doi.org/10.4997/JRCPE.2021.406
23. Mei M, Yan L, Huiling L. Application of Xpert MTB/ RIF detection in rapid diagnosis of intestinal tuberculosis. *J Pract Med*. 2016;32:3073-3075. https://doi.10.3969/j.issn.1006-5725.2016.18.037
24. Song J, Wang D, Ren S. Application of rifampicin-resistant real-time fluorescence quantitative nucleic acid amplification in diagnosis of intestinal tuberculosis. *Contemp Med*. 2020;26:89-92. https://doi.org/10.3969/j.issn.1009-4393.2020.10.033
25. Bellam BL, Mandavdhare HS, Sharma K, et al. Utility of tissue Xpert-Mtb/Rif for the diagnosis of intestinal tuberculosis in patients with ileocolonic ulcers. *Ther Adv Infect Dis.* 2019;6:2049936119863939. https://doi.org/10.1177/2049936119863939
26. Xiong Y, Gao X, Ding C, et al. The value of Gene Xpert MTB/RIF detection in feces in the early and rapid diagnosis of HIV negative

intestinal tuberculosis. *Chin J Clin Med*. 2020;27:679-683. https://doi.org/10.12025/j.issn.1008-6358.2020.20200459

27. Alex C, Sebastian B, Mathai SK, et al. Utility of GeneXpert-Mtb/Rif for the diagnosis of intestinal tuberculosis in patients with ileocolonic ulcers. *Indian J Gastroenterol.* 2020;39:S94. https://doi.org/10.1007/s12664-020-01133-9
28. Kumar S, Bopanna S, Kedia S, et al. Evaluation of Xpert MTB/RIF assay performance in the diagnosis of abdominal tuberculosis. *Intest Res.* 2017;15(2):187-194. https://doi.org/10.5217/ir.2017.15.2.187
29. Deeks JJ, Altman DG. Diagnostic tests 4: likelihood ratios. *BMJ.* 2004;329(7458):168-169. https://doi.org/10.1136/bmj.329.7458.168

CASE STUDY

The first reported case of double trisomy 10 and 20 in a product of conception

Joshua Fernandez De La Vega[1,*], *Arian Pourmehdi Lahiji*[2,*], *Caitlin Raymond*[2], *Song Han*[2], *Harshwardhan Thaker*[2], *Jianli Dong*[2]

[1]John Sealy School of Medicine and [2]Department of Pathology, University of Texas Medical Branch, Galveston, TX, US. Corresponding author: Jianli Dong; jidong@utmb.edu. *Contributed equally.

Key words: product of conception; double trisomy 10 and 20; triplosensitivity; chromosome microarray; genetics; laboratory genetics and genomics

Abbreviations: POC, product of conception; beta-hCG, beta-human chorionic gonadotropin; CMA, chromosomal microarray analysis; SNV, single nucleotide variant

Laboratory Medicine 2024;55:245-248; https://doi.org/10.1093/labmed/lmad052

ABSTRACT

Background: Double trisomies are rare findings among products of conception and are often lethal to the developing embryo or fetus.

Methods: Here we describe a double trisomy case with symptoms of threatened miscarriage at 9 weeks gestation. Ultrasound revealed an anembryonic pregnancy. Pregnancy was terminated by dilation and curettage at gestational age 11 weeks and 6 days. Histologic examination and chromosome microarray were performed on a formalin-fixed product of conception (POC) sample to identify the cause of the anembryonic pregnancy.

Results: Chromosome microarray analysis revealed a female chromosome complement with double trisomies 10 and 20, arr(10,20)x3, consistent with a karyotype of 48,XX,+10,+20.

Conclusion: To the best of our knowledge, this is the first reported case of double trisomy 10 and 20 in a POC. Due to nonspecific histopathological findings, chromosomal microarray is a powerful tool in identifying and differentiating chromosomal aneuploidies.

Greater than 50% of miscarriages have been described as having abnormalities of their chromosome complement, with single trisomy being the most common.[1,2] Double trisomies (trisomy of 2 separate chromosomes) are rare, with most studies finding incidence rates below 3% in products of conception (POC).[1-4] Only a few hundred double trisomies have been reported to date, with the most commonly reported combinations being chromosomes 2 and 16, 16 and 21, and 18 and 21.[4] Double trisomy usually results in miscarriage, although rare cases of liveborn neonates with double trisomy have been reported, including combinations of autosomes 13, 18, and 21 with sex chromosomes X and Y. This suggests the lethality of the double trisomy depends on which chromosomes are involved,[3,4] and notably, double trisomies typically involve the presence of additional copies of low gene density chromosomes. Indeed, to date there are no reports of double trisomy involving chromosome 19, which has the highest reported gene density.[4] Here, we present the first reported case of double trisomy of chromosomes 10 and 20, known to have intermediate gene densities.[5] We discuss related ultrasound and histopathologic findings, the differential diagnosis of a nonviable pregnancy, and patient follow-up after miscarriage with unique chromosome microarray result.

Clinical History

This study was approved by the University of Texas Medical Branch Institutional Review Board. A 40-year-old Hispanic G4P1203 woman at approximately 9 weeks gestation by last menstrual period presented to the emergency department (ED) with vaginal spotting and abdominal cramping. The patient had a history of pregestational diabetes and chronic hypertension. Beta-human chorionic gonadotropin (beta-hCG) level was 34,099 mUI/mL at presentation, and ultrasound revealed gestational sac diameter of 1.46 cm. Six days later, a beta-hCG level of 35,000 mUI/mL was observed. This low incremental increase prompted additional ultrasound studies in the following 2 weeks, which indicated no expansion of the gestational sac, the largest observed diameter being 1.87 cm, and no discrete yolk sac or fetal pole. A diagnosis of anembryonic pregnancy was made, and at 11 weeks and 6 days gestation, the patient underwent a dilation and curettage procedure.

Histologic examination of the POC revealed enlarged and dysmorphic chorionic villi with occasional central cisterns and syncytiotrophoblast hyperplasia (**FIGURE 1A** and **1B**). These nonspecific findings were consistent with a genetically abnormal and nonviable pregnancy.

Laboratory Role in Diagnosis

Chromosomal microarray analysis (CMA) is used to determine copy number variants in a sample and has become a first line assay for

FIGURE 1. Histologic examination and chromosome microarray analyses of the product of conception (POC) sample. A and B, Histologic examination of the POC sample. H&E stain of the sample shows hydropic chorionic villi with syncytiotrophoblast hyperplasia (A) and dysmorphic villi with central cisterns (B). C, Whole genome view of chromosome microarray analysis. The result is a female with double trisomy 10 and 20, arr(10,20)x3, consistent with a karyotype of 48,XX,+10,+20. Chromosome microarray was performed using Affymetrix OncoScan microarray (Thermo Fisher Scientific).

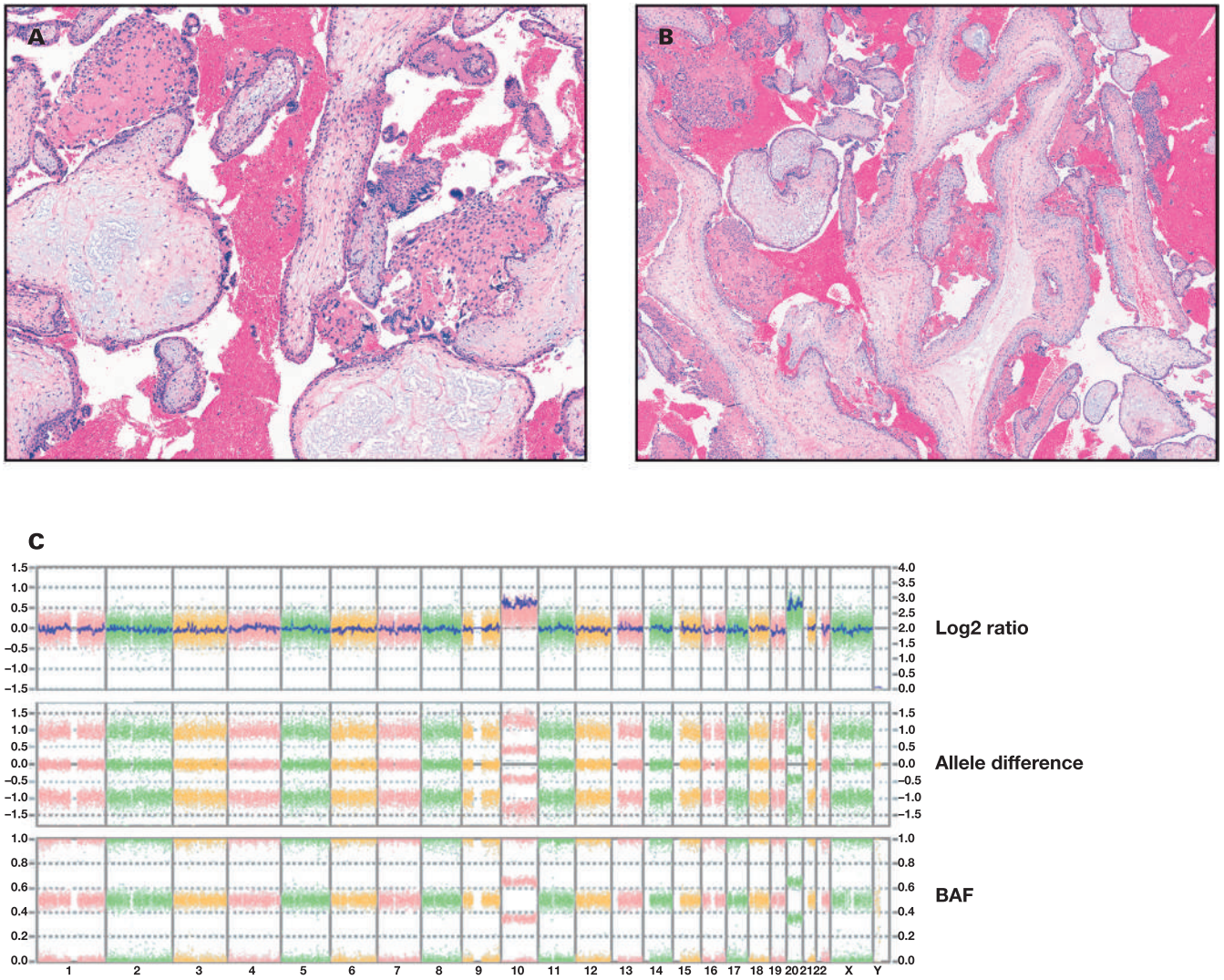

prenatal chromosomal analysis.[6,7] There are 2 major types of CMA: comparative genomic hybridization, which returns information about DNA copy numbers, and single nucleotide variant (SNV), which returns information about copy number as well as base pair genotypes using SNV probes.[8-11] In this case, CMA was performed on the formalin-fixed POC sample using Affymetrix OncoScan microarray (Thermo Fisher Scientific). The result of the SNV CMA was arr(10,20)x3, consistent with a karyotype of 48,XX,+10,+20 (**FIGURE 1C**).

Although SNV CMA can provide limited information about the unique polymorphisms presents in a sample, it is not ideal for determination of parental origin of trisomy. Parental origin is typically determined by short tandem repeat testing. Short tandem repeat testing identifies the numbers of a tandem repeat in parental samples, which can then be compared to those present in the POC sample to determine origin. Parental samples were not available in this case, and short tandem repeat testing was not performed.

Discussion

Incidence rates of double trisomy among miscarriages with chromosomal abnormalities have been found to fall between 0.21% and 2.8%, although the incidence may be higher among extremely early miscarriages that occur prior to awareness of pregnancy.[1-4,12] The mean gestational age of cases of double trisomy is lower than cases of single trisomy (8.7 ± 2.2 weeks vs 10.1 ± 2.9 weeks),[3,4] suggesting a more severe impact on viability and development. Indeed, the double trisomies that are reported typically involve chromosomes with low or low-intermediate gene density, such as chromosomes 13, 16, 18, and 21. Few cases of double trisomy involving chromosomes with intermediate or high gene density have been reported, indicating a selection bias towards lower gene doses.[3,4] The lethality of double trisomy is hypothesized to be related to the triplosensitivity of involved genes. Triplosensitivity is a term indicating whether the presence of a third copy of a gene in a diploid organism results in pathogenicity. Although

a triplosensitivity score is typically assigned to a specific gene, the density of genes across an entire chromosome can indicate the likelihood of pathogenicity in the event of aneuploidy, and chromosomes with fewer genes tend to have more favorable outcomes. Notably, rare cases of liveborn neonates with double trisomy universally involve combinations of autosomes 13, 18, and 21—all of which have low or low-intermediate gene density—with sex chromosomes X and Y.[4,5] To the best of our knowledge, our case is the first reported double trisomy of the intermediate gene density chromosomes 10 and 20 in a POC sample.

Previous studies of parental origin in double trisomy have indicated a maternal predominance and an association with advanced maternal age.[4,13] The most common mechanism implicated in trisomy is meiotic nondisjunction, in which homologous pairs of chromosomes or sister chromatids fail to separate in meiosis I or meiosis II. Mechanisms associated with meiotic nondisjunction include certain patterns of homologous chromosome recombination, which may disrupt the adhesion and separation of chromosomes and chromatids; reduced cohesion between sister chromatids due to degradation of cohesion proteins; meiotic spindle assembly dysfunction associated with decreased expression of assembly checkpoint proteins; and increased histone acetylation leading to impaired chromatin condensation.[14] Our patient's age of 40 years is associated with an increased risk for the aforementioned factors and may have played a role in the pathogenesis of this case.

Double trisomies present with a spectrum of ultrasound morphological findings, ranging from empty gestational sacs to developing embryos and fetuses, although findings trend towards empty gestational sacs.[3,15] The finding of an empty sac without an identifiable embryo may be a result of more severe gene imbalance that is incompatible with embryo and fetal development; however, given the rarity of double trisomies, there are limited data to base conclusions on. Similarly, histopathological examination of POCs with double trisomies is rarely reported in the literature. One case of 48,XXX,+18 was found to have enlarged chorionic villi with trophoblastic pseudoinclusions,[15] yet these findings are nonspecific, and there is no characteristic histomorphology or imaging finding that reliably distinguishes aneuploidy from other aberrances of chromosome complement. Therefore, further workup with genetics and genomics assays is a necessity to determine the genetic complement of the POC. Chromosomal microarray analysis is ideally suited to determine copy number differences and can provide definitive evidence of aneuploidy, although it is not sufficient to determine parental origin. In this case, CMA determined double trisomy of 10 and 20.

Determining the exact genetic abnormality present in POC is critical, as this can have significant consequences in the postpartum period for the patient. Molar pregnancies, whether complete or partial, are associated with a higher risk of gestational trophoblastic disease, in which abnormal trophoblastic cells proliferate in an uncontrolled fashion.[16] Gestational trophoblastic disease can be either benign or malignant, but successful treatment relies on early detection. Patients that carry a molar pregnancy must be followed closely in the postpartum period to ensure that levels of beta-HCG are downtrending. Thus, differentiating between a molar pregnancy and an aneuploidy such as double trisomy is critical. In our patient, the level of beta-HCG was tracked for 2 months following her miscarriage, with no evidence of gestational trophoblastic disease.

In conclusion, double trisomy is a rare finding in POC, present in a minute percentage of cases. We present the first reported case of double trisomy 10 and 20, which is notable for the relatively higher gene density of these chromosomes than is typically observed in double trisomy. Consistent with the hypothesis of greater triplosensitivity and gene density producing greater pathogenicity, this case featured an anembryonic gestation and dysmorphic chorionic villi. Although suspicious for a genetically abnormal pregnancy, these nonspecific findings were further investigated with CMA, and a diagnosis of double trisomy was made.

Case Follow-up

The patient's postoperative period was uncomplicated, with beta-hCG values gradually decreasing to normal levels over the course of 2 months. The subsequent 6 months also showed negative beta-hCG values, indicating that there were no complications.

Conflict of Interest Disclosure

The authors have nothing to disclose.

Data Availability

All data used in the preparation of this manuscript will be made available upon reasonable request to the corresponding author.

REFERENCES

1. Sahoo T, Dzidic N, Strecker MN, et al. Comprehensive genetic analysis of pregnancy loss by chromosomal microarrays: outcomes, benefits, and challenges. *Genet Med.* 2017;19:83-89. doi:10.1038/gim.2016.69
2. Menasha J, Levy B, Hirschhorn K, et al. Incidence and spectrum of chromosome abnormalities in spontaneous abortions: new insights from a 12-year study. *Genet Med.* 2005;7:251-263. doi:10.1097/01.gim.0000160075.96707.04
3. Reddy KS. Double trisomy in spontaneous abortions. *Hum Genet.* 1997;101:339-345. doi:10.1007/s004390050638
4. Diego-Alvarez D, Ramos-Corrales C, Garcia-Hoyos M, et al. Double trisomy in spontaneous miscarriages: cytogenetic and molecular approach. *Hum Reprod.* 2006;21:958-966. doi:10.1093/humrep/dei406
5. Scherer S. Guide to the Human Genome. Cold Spring Harbor Laboratory Press. Accessed March 4, 2023. http://www.cshlp.org/ghg5_all/index.shtml
6. Vora NL, Romero ST, Ralston SJ, et al. Committee opinion No.682: microarrays and next-generation sequencing technology: the use of advanced genetic diagnostic tools in obstetrics and gynecology. *Obstet Gynecol*. 2016;128:e262-e268.
7. South ST, Lee C, Lamb AN, et al. ACMG standards and guidelines for constitutional cytogenomic microarray analysis, including postnatal and prenatal applications: revision 2013. *Genet Med.* 2013;15:901-909. doi:10.1038/gim.2013.129
8. Schaaf CP, Wiszniewska J, Beaud AL, et al. Copy number and SNP arrays in clinical diagnostics. *Annu Rev Genomics Hum Genet.* 2011;12:25-51.
9. Levy B, Burnside RD. Are all chromosome microarrays the same? What clinicians need to know. *Prenat Diagn.* 2019;39:157-164. doi:10.1002/pd.5422

10. Levy B, Sigurjonsson S, Pettersen B, et al. Genomic imbalance in products of conception: single-nucleotide polymorphism chromosomal microarray analysis. *Obstet Gynecol*. 2014;124:202-209.
11. Lathi RB, Loring M, Massie JAM, et al. Informatics enhanced SNP microarray analysis of 30 miscarriage samples compared to routine cytogenetics. *PLoS One.* 2012;7:e31282. doi:10.1371/journal.pone.0031282
12. Branum AM, Ahrens KA. Trends in timing of pregnancy awareness among US women. *Matern Child Health J.* 2017;21:715-726. doi:10.1007/s10995-016-2155-1
13. Li QY, Tsukishiro S, Nakagawa C, et al. Parental origin and cell stage of non-disjunction of double trisomy in spontaneous abortion. *Congenit Anom.* 2005;45:21-25. doi:10.1111/j.1741-4520.2005.00056.x
14. Mikwar M, MacFarlane AJ, Marchetti F. Mechanisms of oocyte aneuploidy associated with advanced maternal age. *Mutat Res Rev Mutat Res.* 2020;785:108320. doi:10.1016/j.mrrev.2020.108320
15. Shah SI, Dyer L, Stanek J. Placental histomorphology in a case of double trisomy 48,XXX,+18. *Case Rep Pathol*. 2018;2018:2839765. doi:10.1155/2018/2839765
16. Pinar MH, Gibbins K, He M, Kostadinov S, Silver R. Early pregnancy losses: review of nomenclature, histopathology, and possible etiologies. *Fetal Pediatr Pathol.* 2018;37:191-209. doi:10.1080/15513815.2018.1455775

During 2023, manuscripts submitted to *Laboratory Medicine* were reviewed by a number of people other than members of the editorial board. We wish to express our gratitude to them publicly. They include:

Mohamed Abdelmonem
Gyorgy Abel
Emad S. Abood
Bodhraj Acharya
Dorothy Adcock
Reza Afrisham
Edward Ager
Apoorva Aggarwal
Pia Marie Albano
Tom Alexander
Murat Alisik
Gunay Aliyeva
Wassim Y. Almawi
Fnu Alnoor
Tc Aw
Ghufran Babar
Rasoul Baharlou
Jela Bandovic
Yousif Barzani
Umberto Basile
Ioannis Bellos
Robert Benirschke
Alexander E. Berezin
Mary Berg
Geza Bodor
Özlem. Bostan Gayret
Janetta Bryksin
Jeffrey Budd
Eileen Burd
Manca Černila
Elham Chamani
Chalisa Louicharoen Cheepsunthorn
Moutong Chen
Zhikai Chi
Anil Kiran Chokkalla
Jacky Chow
Olga Ciepiela
Aldo Clerico
Hui Cong
Adele Coriati
Aloyce Costantine
Bereczki Dániel
Riku Das
Valli De Re
Kamal Djenouhat
Michael Doubek
Wisdom Ebong
Mahmoud El-Bendary

Erica Fatica
Megan Faucett
Emmanuel Favaloro
Matthew Feldhammer
Angela Ferguson
Mariana Fragão-Marques
Natalie Frangione